Stony Brook University

African Papionin Phylogenetic History and Plio-Pleistocene Biogeography

A Dissertation Presented

By

Christopher Charles Gilbert

to

The Graduate School

in Partial Fulfillment of the

Requirements

for the Degree of

Doctor of Philosophy

in

Anthropology

Stony Brook University

May 2008

Stony Brook University

The Graduate School

Christopher Charles Gilbert

We, the dissertation committee for the above candidate for the Doctor of Philosophy degree, hereby recommend acceptance of this dissertation.

John G. Fleagle- Dissertation Advisor
Distinguished Professor, Department of Anatomical Sciences

William L. Jungers- Chairperson of Defense
Professor and Chair, Department of Anatomical Sciences

Frederick E. Grine
Professor, Department of Anthropology

Eric Delson
Professor, Department of Anthropology
CUNY- Lehman College

This dissertation is accepted by the Graduate School

Lawrence Martin
Dean of the Graduate School

Abstract of the Dissertation

African Papionin Phylogenetic History and Plio-Pleistocene Biogeography

by

Christopher Charles Gilbert

Doctor of Philosophy

in

Anthropology

Stony Brook University

2008

The cercopithecine primate tribe Papionini (Order: Primates; Family Cercopithecidae; Subfamily Cercopithecinae) are an extremely successful group of monkeys including the living macaques (*Macaca*), mangabeys (*Lophocebus, Cercocebus*), baboons (*Papio*), geladas (*Theropithecus*), mandrills, and drills (*Mandrillus*). The proliferation of the papionins is a well documented evolutionary phenomenon; in addition to the geographic and taxonomic diversity of the extant taxa, papionin monkeys are widely present and abundant members of the African Plio-Pleistocene fossil record. Despite their evolutionary success and relative abundance, the taxonomic and phylogenetic status of many Plio-Pleistocene papionins remains uncertain. Well supported phylogenetic hypotheses are essential to understanding the origins and evolution of this group: such phylogenetic trees can be used to infer the evolutionary sequence of the key characters in certain lineages as well as assess Plio-Pleistocene

biogeography. Comparative questions regarding biogeography can then be assessed and compared to contemporaneous hominin taxa.

In order to elucidate African papionin phylogenetic history, two main methods of quantitative morphological analysis were used: cladistic analysis of character data using parsimony and 3-D geometric morphometric analysis of the basicranium. In contrast to many previous phylogenetic studies of papionin craniodental data, here the effects of allometry are accounted for by applying the narrow allometric coding method to allometrically influenced morphological characters (Gilbert and Rossie, 2007). The results of the cladistic analysis (Chapter 2) strongly suggest that papionin phylogeny based on analysis of craniodental data and that based on molecular systematics are congruent and support a *Cercocebus/Mandrillus* clade as well as a *Papio/Lophocebus/Theropithecus* clade. In addition, within the *Papio/Lophocebus/Theropithecus* clade, a *Papio/Lophocebus* sister relationship is supported. If congruence between molecules and morphology is considered to be a prerequisite for accepting morphological data as being reliable, then papionin and, more broadly, primate morphology as evidenced by this data set must be considered a reliable source of phylogenetic information. When fossil taxa are added to the analysis, the two most parsimonious trees recovered suggest the following phylogenetic relationships (Chapter 3): *Parapapio*, *Pliopapio* and *Dinopithecus* are stem African papionins, *Theropithecus* is the most primitive crown African papionin taxon and the status of *T. baringensis* as a member of the genus *Theropithecus* is strongly supported, *Gorgopithecus* is closely related to *Papio* and *Lophocebus,* and *Papio quadratirostris*, as defined by Delson and Dean (1993) to include the later Omo Shungura material as well as some of the material from the Angolan Humpata Plateau, is closely related to *Mandrillus, Cercocebus*, *Procercocebus*.

To further investigate the potential signal contained within papionin cranial anatomy, I applied 3-D geometric morphometric techniques in a phylogenetic analysis of African papionin basicranial morphology (Chapter 4). Neighbor-joining and UPGMA clustering methods were used to generate phylogenetic hypotheses based on Euclidean distances between the average principal components (PC) matrices compiled by sex for each taxon. To adjust for the effects of allometry, PCs that

were significantly correlated with centroid size were excluded from the analysis. While the basicranium has been suggested to be a highly informative anatomical region in the study of other primate taxa, papionin basicranial shape, as represented by the PC matrices in this study, does not suggest the same phylogenetic relationships among taxa as the more comprehensive craniodental analyses in Chapters 2 and 3. It is difficult to properly adjust for the effects of allometry in multivariate analyses of shape, and it is likely that important phylogenetic information is contained within the information that is excluded on the size-correlated PCs. Further effort should focus on methodologies to adjust for allometric effects in multivariate morphometric analyses.

In light of the phylogenetic relationships hypothesized in Chapter 3, Chapter 5 investigates African papionin biogeography by treating biogeography as an unordered cladistic character and biogeographic regions such as South Africa, East Africa, North Africa, Central Africa, and West Africa as character states. The biogeographic character states for each fossil and extant papionin taxon are then mapped onto a cladogram derived from Chapter 3 and, using logic similar to the "progression rule" (Hennig, 1966), dispersal events are then inferred. The hypothesized biogeographic patterns of the African papionins during the Plio-Pleistocene are then compared to contemporaneous hominin biogeographic patterns. Results indicate that African papionin dispersal patterns largely mirror those of early hominins and, in at least one case, oppose general mammalian trends as well. Suggestions of unique behavioral adaptations to account for early hominin biogeography and dispersal patterns, therefore, seem unwarranted. In addition, African papionin monkeys appear to document a biogeographic connection between West and South Africa ~2.3 - 1.5 Ma.

Dedication

For my parents, Charles and Lisa, whose unconditional love and support made this dissertation possible.

Table of Contents

List of Figures

List of Tables

Acknowledgments

I must thank many people for their love, friendship, and support throughout the course of this dissertation. First and foremost, I would like to thank my parents, for whom this dissertation is dedicated. Even though they did not initially understand why I wanted to pursue a PhD in Physical Anthropology rather than a law degree or MBA, they have nonetheless always loved and supported me. Thank you, Mom and Dad.

Secondly, I would like to thank the people who first pointed me in the direction of graduate school and believed in my ability to complete a PhD, even if I was uncertain at the time. Although they might not recall, immediately following my undergraduate graduation ceremony, Elwyn Simons and Diane Brockman both independently suggested that I should consider graduate school. Sometimes it is the little things that matter most, and a few words from these two professors, whom I greatly respect and admire, was the push I needed to commit myself to a subject that I have always enjoyed. As an undergraduate, Mark Spencer, Lillian Spencer, and Rob Deaner were also instrumental in furthering my interest in Physical Anthropology. I would like to thank all of them and let them know that their teaching and enthusiasm inspired me, and I am sure that they have inspired others as well.

Next, I would like to thank all of my friends and colleagues for their unbelievable kindness and support. I thank all of my fellow IDPAS students over the years, but in particular there are a number of people who deserve mention as being especially important as friends and scientific colleagues: Andrea Baden, Matthew Banks, Doug Boyer, Mark Coleman, Abigail Derby, Andy Farke, David Fernandez, Ari Grossman, Meg Hall, Chris Heesy, Mitch Irwin, Rachel Jacobs, Jason Kamilar, Eileen Larney, Jessica Lodwick, Amy Lu, Anthony Olejniczak, Kerry Ossi, Biren Patel, Danielle Royer, Karen Samonds, Clara Scarry, Jessica Scirbona, Joe Sertich, Matthew Sisk, Tanya Smith, Liz St. Clair, Anne Su, Ian Wallace, Brandon Wheeler, and Jesse Young. Outside of IDPAS, a number of friends have assisted with places to stay, words of encouragement, and much needed recreation away from my fossil monkeys. If not for the following people, I would not have been able to complete my dissertation. I would like to thank the following people for places to stay: Michael Rosenthal and Jia Liu, Brian Gilbert, Mark

Gilbert, Sam Turvey, Eric and Jen Back, David McKenzie, Jock and Liz McKenzie, Sarah Band, Angus and Sue Band, Arnaud and Rebecca Karsenti, Lauren and Paul Van Bergen, Brian and Nicole Jones, and Jesse DeBruin. For words of encouragement and/or recreational activities outside of museums and field sites, I would particularly like to thank my brothers, Brian and Mark, as well as my good friends Jesse DeBruin, Andy Houston, Brent Johnson, Brian Jones, Arnaud Karsenti, David McKenzie, Michael Rosenthal, Mitch Rufca, Sam Turvey, Lauren Van Bergen, and Andy Woltman. Finally, one IDPAS student deserves special mention as the most important person in my life over the past few years. Andrea: Thank you, I love you, and I couldn't have done it without you.

In addition to my fellow students in IDPAS, I must thank the faculty in both the Anthropology and Anatomical Sciences departments for all their help and inspiration over the past seven years, in particular I would like to thank Carola Borries, Brigitte Demes, Diane Doran-Sheehy, John Fleagle, Fred Grine, Charlie Janson, Bill Jungers, Andreas Koenig, Dave Krause, Susan Larson, Meave Leakey, Lawrence Martin, Sharon Pochron, Jim Rohlf, Callum Ross, James Rossie, Erik Seiffert, John Shea, Jack Stern, David Strait, Randy Susman, John Wiens, and Pat Wright. Special thanks to my friends Andreas Koenig and Carola Borries, who were kind enough to give me the wonderful opportunity to conduct field research at Phu Khieo, even after I had decided to write a paleontological dissertation rather than a behavioral one. Special thanks also to my friend and colleague James Rossie, who in his short time at Stony Brook has taught me much about phylogenetic systematics. Finally, my most sincere thanks go to the administrators of the Anthropology and Anatomical Sciences departments. Linda Benson, Chris Johnson, Janet Masulo, and Jean Moreau have always had my best interests in mind, and I have always appreciated their generous assistance.

A number of people at institutions around the world were essential in allowing access to collections and generally making life much more pleasant in many cities around the world. Specifically, I would like to thank Eileen Westwig and Eric Delson (American Museum of Natural History, New York), Linda Gordon (National Museum of Natural History, Washington, DC), Bill Stanley and Michi Schulenberg (Field Museum of Natural History, Chicago), Judith Chupasko (Museum of Comparative Zoology,

Cambridge), Paula Jenkins and Daphne Hills (Natural History Museum, London), Malcolm Harman (Powell-Cotton Museum, Birchington), Wim Wendelen (Royal Museum of Central Africa, Tervuren), Graham Avery and Kerwin von Willingh (Iziko South African Museum, Cape Town), Mike Raath (University of the Witwatersrand, Department of Anatomical Sciences, Johannesburg), and Francis Thackeray and Stephany Potze (Transvaal Museum, Pretoria). In addition, thanks to Eric Delson for permission to observe and photograph the University of California Museum of Paleontology specimens on loan at the American Museum of Natural History and Randy Susman for access to extant primate specimens in his care.

Last, and certainly not least, I would like to thank my dissertation committee. Each of them has had a huge impact on me, and each deserves his own paragraph.

John Fleagle has been the best advisor I could have ever hoped for. I have always valued his tremendous insight and unbelievable gift for writing and expressing complex issues in simple terms that anyone can understand. John has not only given me great advice and encouragement through the years, but he has also bluntly informed me when my reasoning was faulty. He has taught me how to be a better scientist, editor, teacher, and public speaker. He has generously supported my dissertation research with grant money, equipment, opportunities to interact with other scientists, and a job at *Evolutionary Anthropology*. I will miss our daily conversations about *Evolutionary Anthropology* and basketball, but I am pleased that my postdoctoral appointment will not take me far from Stony Brook, if for no other reason than the fact that I will still be able to collaborate with, and learn from, John Fleagle.

Fred Grine is someone that I have always looked up to and have enormous respect for. Fred has also offered great encouragement throughout my graduate career, and his sharp and critical eye has much improved this dissertation. Fred's attention to detail and ability to frame arguments in the most effective way has been essential to developing many of the ideas expressed herein. On a personal note, I have always enjoyed Fred's zest for life and it was a particular pleasure to meet up with Fred and Sandra during my time in Cape Town, South Africa.

From the moment I met him, Bill Jungers has always been looking out for me. At my first IDPAS student meeting, Bill was immediately inquiring about an administrative

problem regarding my fellowship in order to make sure that I received all that I was promised. Whenever I have had any questions or problems with any part of my dissertation, Bill has always made time to talk and to help in any way possible. His encyclopedic knowledge of statistics is legendary, but it is his kindness and compassion that make him universally liked and respected.

Eric Delson has been an enormous help to me over the past seven years. From the beginning of my graduate career, he has always been enthusiastic about my aspirations as a fossil cercopithecoid researcher, and he has been more than generous with sharing his knowledge, fossils, casts, and equipment. Our discussions over the past few years have been some of my favorite conversations regarding the evolution of cercopithecoid monkeys; his knowledge of fossil cercopithecoid specimens around the world is unmatched. I look forward to many more productive years working with, and learning from, Eric Delson.

I would also like to express my deep gratitude to Steve Frost, who is a sort of "unofficial" committee member. Steve has been, in many ways, the most important teacher I have had in my education about extant and fossil cercopithecoid monkeys. Every time I think I have "solved" an issue surrounding fossil monkeys, a conversation with Steve soon makes me realize that I still have much to learn. It is doubtful that I will ever know as much about fossil Old World monkeys as Steve does, but if I can come anywhere close, I will truly be an expert.

Finally, I would like to thank Eric Delson, Luci Betti-Nash, and Steve Nash for their permission to use certain images contained within this document. Specifically, Stephen and Luci are responsible for the beautiful drawings presented in Chapter 1 and the maps in Chapter 5. I would also like to acknowledge that Steve Frost and David Strait are partly responsible for the character lists contained in Chapters 2 and 3; thank you to both of them for their help and permission to use these characters in this dissertation. Mark Collard generously provided the original data used in his influential studies with Bernard Wood, and they both have my sincere gratitude.

Funding for this dissertation was generously provided by the L.S.B. Leakey Foundation as well as a Graduate Council Fellowship from Stony Brook University.

Chapter 1

Introduction

The cercopithecine primate tribe Papionini (Order: Primates; Family Cercopithecidae; Subfamily Cercopithecinae) is an extremely successful group of monkeys including the living macaques (*Macaca*), mangabeys (*Lophocebus, Cercocebus*), baboons (*Papio*), geladas (*Theropithecus*), mandrills, and drills (*Mandrillus*) (Fig. 1.1). As a testament to their adaptability and evolutionary success, papionins are geographically spread throughout the Old World, from the southern tip of Africa to the snow-capped mountains of Japan and the island rainforests of Southeast Asia. The proliferation of the papionins is a well documented evolutionary phenomenon; in addition to the geographic and taxonomic diversity of the extant taxa, papionin monkeys are widely present and abundant components of the African Plio-Pleistocene fossil record.

Despite their evolutionary success and relative abundance, the taxonomic and phylogenetic status of many Plio-Pleistocene papionins remains uncertain. Questions exist over which fossil taxa are legitimate species, the phylogenetic relationships of the fossil taxa amongst themselves, and the phylogenetic relationships of the fossil taxa to extant taxa. Given the relatively rich fossil record of this group during the Plio-Pleistocene, quantitative analyses of morphological variation in a taxonomic and phylogenetic framework provide a promising way to test a series of evolutionary hypotheses. Well-supported phylogenetic hypotheses are essential to understanding the origins and evolution of this group: such phylogenetic trees can be used to infer the evolutionary sequence of the key characters in lineages as well as to determine which taxa lay within or at the base of the extant African clades. In this respect, the ancestral papionin morphotype as well as the ancestral morphotypes of the African clades can be elucidated.

For many years, molecular and morphological studies concerning the phylogenetic relationships among the extant Papionini were incongruent. Traditionally, most morphological studies concluded that the mangabeys, *Cercocebus* and *Lophocebus*, were a monophyletic group and that the mandrills and drills (*Mandrillus)* were closely related to the savannah baboons of the genus *Papio* (Fig. 1.2) (e.g., Jolly, 1972; Szalay and Delson, 1979; Strasser and Delson, 1987; Delson and Dean, 1993). By contrast, analyses of molecular data going back to the 1970's determined that the mangabeys, as traditionally constituted, were a diphyletic group (e.g., Barnicot and Wade, 1970; Barnicot and Hewett-Emmett, 1972; Cronin and Sarich, 1976; Hewett-Emmett et al., 1976). While these early studies analyzed blood proteins, more recent studies analyzed DNA directly, using both mitochondrial and Y-chromosome DNA samples (Disotell et al., 1992; Disotell, 1994; Harris and Disotell, 1998; Disotell, 2000; Harris, 2000; Tosi et al., 1999, 2003). The results of these recent molecular studies forcefully argued the following points: macaques (*Macaca*) represent the basal extant papionin taxon (a fact agreed upon by most morphological studies), *Cercocebus* and *Mandrillus* represent a monophyletic group, and finally, a clade consisting of *Papio*, *Theropithecus*, and *Lophocebus* exists but the relationships among these three genera are unresolved (Fig. 1.3). Given the power and congruence of the molecular data sets, most researchers accepted the molecular phylogeny as the best hypothesis regarding papionin phylogenetic relationships.

Acceptance of the molecular phylogeny left researchers with the realization that the Papionini, as a group, is apparently riddled with morphological homoplasy (Lockwood and Fleagle, 2000). This apparent homoplasy prevented most morphological studies from recovering trees broadly congruent with molecular data (e.g., Collard and Wood, 2000; 2001; Collard and O'Higgins, 2001; Singleton, 2002; Frost et al., 2003; Collard and Elton, 2002). The incongruence of morphological and molecular data even led some researchers to suggest that morphological data are unreliable for reconstructing phylogenetic relationships (Collard and Wood, 2000; 2001). Given the perceived unreliability of morphological data, sorting out phylogenetic relationships of fossil taxa is equally or likely more problematic. The papionin fossil record, similar to that of most mammalian groups, is composed mainly of craniodental fossils. If papionin craniodental

anatomy is truly unreliable for reconstructing phylogenetic relationships, it will be difficult to elucidate the evolutionary history of this very successful group of primates.

In contrast to the conclusion that craniodental morphology is unreliable, more recent studies suggest that closer examination of papionin craniodental and postcranial anatomy supports the same clades as molecular data (Fleagle and McGraw, 1999; 2002; McGraw and Fleagle, 2006; Gilbert, 2007; Gilbert and Rossie, 2007). In particular, recent studies have suggested that convergent allometry results the appearance of rampant homoplasy; when the effects of allometry are accounted for in phylogenetic analysis of morphological data, results suggest that morphological and molecular data offer congruent phylogenetic hypotheses (Gilbert, 2007; Gilbert and Rossie, 2007). Thus, craniodental data of these primates would appear to be no more or less reliable than molecular data for reconstructing African papionin relationships. The congruence of the two data sets provides strong support for their shared phylogenetic hypothesis, namely that *Cercocebus* and *Mandrillus* form a clade and that *Papio*, *Lophocebus*, and *Theropithecus* also form a clade among extant African papionin taxa (Fig. 1.3). Given a set of informative craniodental characters with which to evaluate the fossil record, a well-supported hypothesis of the phylogenetic relationships and evolutionary history of the African papionins should be attainable.

Given the renewed confidence in papionin craniodental anatomy, this dissertation re-examines the anatomy of extant and fossil papionins in order to understand their phylogenetic relationships and evolutionary history. In order to achieve this goal, two main methods of quantitative morphological analysis were used: cladistic analysis of character data using parsimony and 3-D geometric morphometrics of the basicranium. Thus, a direct comparison between cladistic methods and morphometric methods in the reconstruction of phylogeny can be made. With fossil taxa placed in a more firm phylogenetic framework, assessments of Plio-Pleistocene African papionin biogeography can also be made. Comparative questions regarding Plio-Pleistocene biogeography can then be assessed and patterns of dispersal can be compared with those of contemporaneous hominin taxa.

Figure Captions

Figure 1.1. Extant papionin taxa: Macaques (*Macaca*), Mangabaeys (*Lophocebus*, *Cercocebus*), Geladas (*Theropithecus*), Baboons (*Papio*), Mandrills and Drills (*Mandrillus*). Illustrations by Stephen Nash.

Figure 1.2. Traditionally hypothesized phylogenetic trees of the extant Papionini from morphological data: **a)** from Jolly (1972), Szalay and Delson (1979), Strasser and Delson (1987); **b)** from Delson and Dean (1993). Illustrations by Stephen Nash.

Figure 1.3. Hypothesized phylogenetic trees of the extant Papionini from molecular (mtDNA and Y-chromosome) data (Disotell et al., 1992; Disotell, 1994; 2000; Harris and Disotell, 1998; Tosi et al., 1999; 2003) as well as recent morphological studies (Fleagle and McGraw, 1999; 2002; McGraw and Fleagle, 2006; Gilbert, 2007; Gilbert and Rossie, 2007). Illustrations by Stephen Nash.

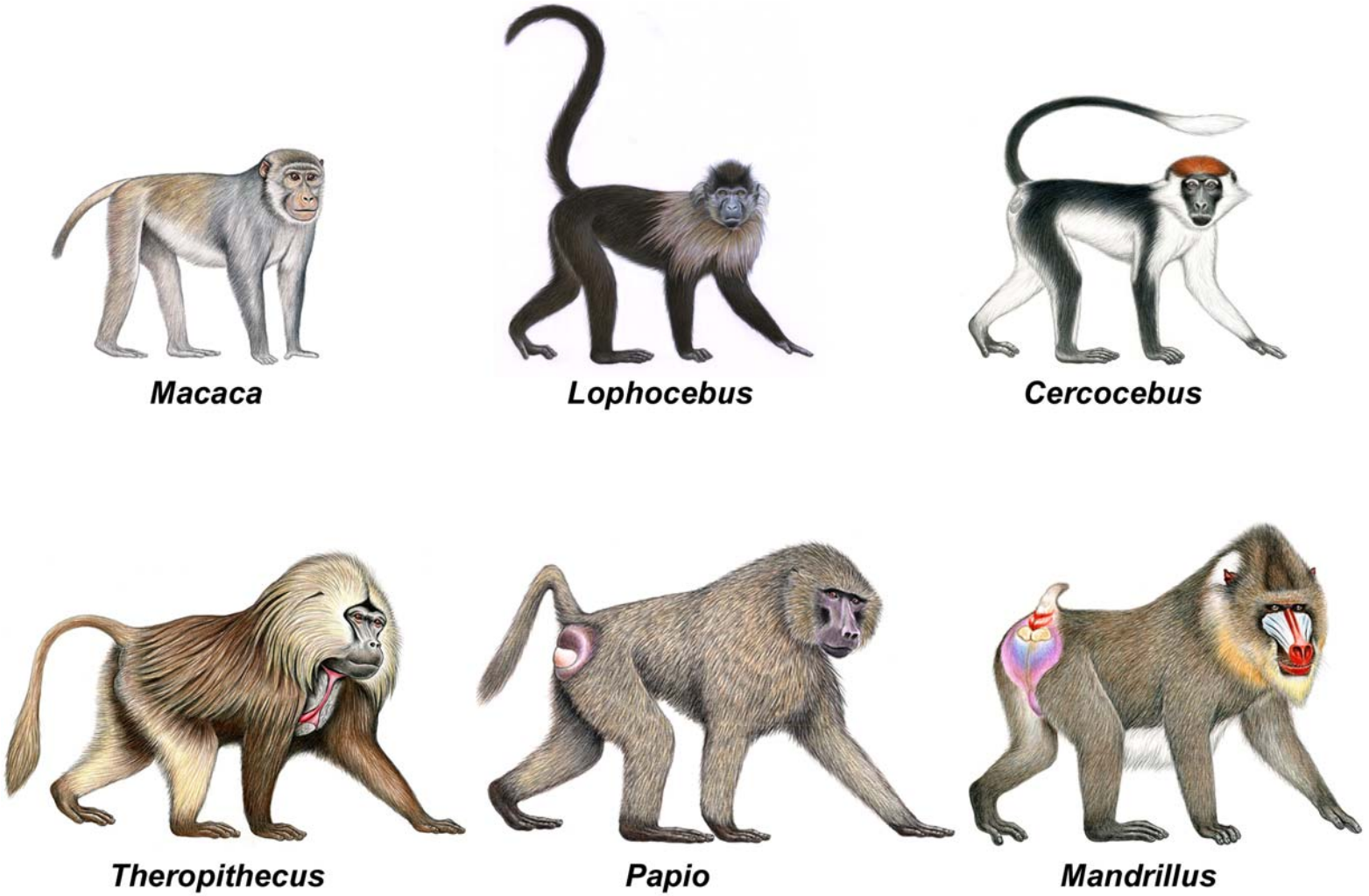
Macaca
Lophocebus
Cercocebus
Theropithecus
Papio
Mandrillus

Figure 1.1

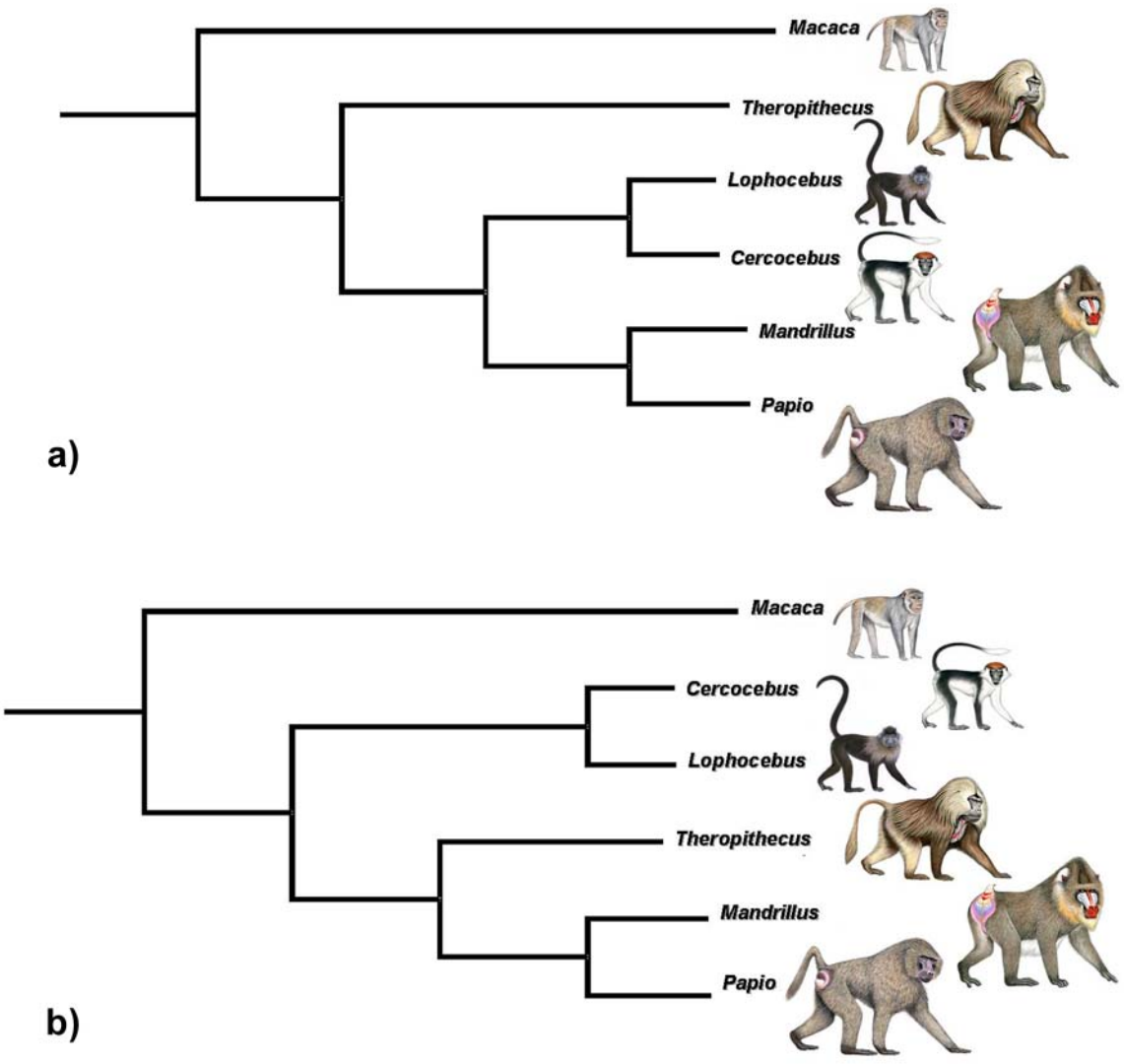
Macaca
Theropithecus
Lophocebus
Cercocebus
Mandrillus
Papio
a)
Macaca
Cercocebus
Lophocebus
Theropithecus
Mandrillus
Papio
b)

Figure 1.2

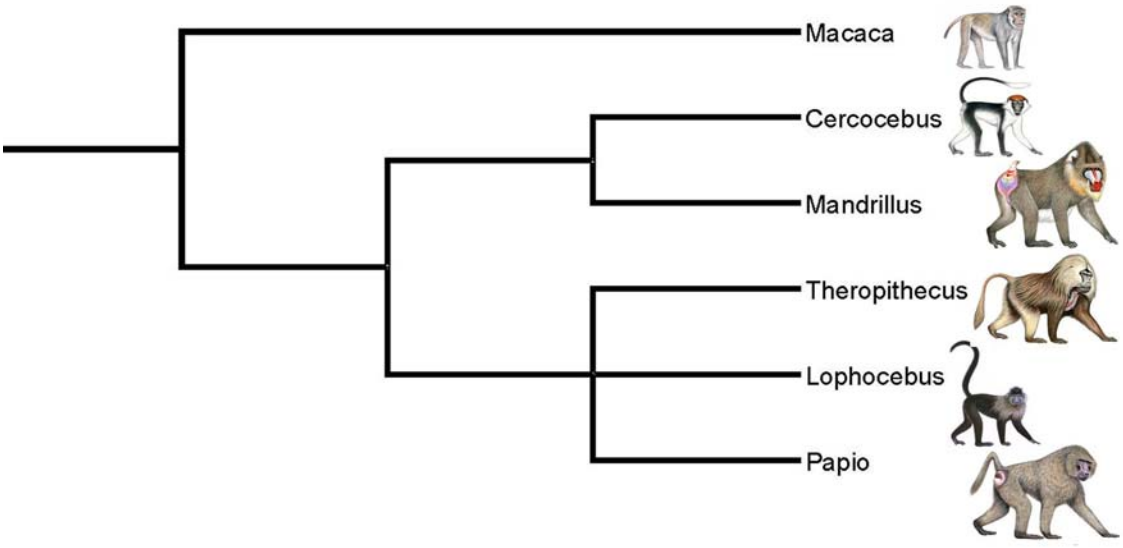
Macaca
Cercocebus
Mandrillus
Theropithecus
Lophocebus
Papio

Figure 1.3

Chapter 2

Cladistic Analysis of Extant African Papionins Using Craniodental Data

Abstract

In this study, a comprehensive phylogenetic analysis of African papionin craniodental morphology, including both quantitative and qualitative characters, is performed using the narrow allometric coding method to control for allometry. In contrast to previous studies of African papionin craniodental morphology, the results of this study strongly suggest that African papionin phylogeny based on molecular systematics and that based on morphology are congruent and support a *Cercocebus/Mandrillus* clade as well as a *Papio/Lophocebus/Theropithecus* clade. In addition, within the *Papio/Lophocebus/Theropithecus* clade, a *Papio/Lophocebus* sister relationship is supported. If congruence between molecules and morphology is considered to be a prerequisite for accepting morphological data as being reliable, then papionin and, more broadly, primate morphology as evidenced by this data set must be considered a reliable source of phylogenetic information. Among highly sexually dimorphic primates such as the papionins, male morphologies appear to be particularly good sources of phylogenetic information. This phenomenon is most likely due to sexual selection, and suggests that future analyses of highly sexually dimorphic primates should consider analyzing the sexes separately. Finally, character transformation analyses identify a series of morphological synapomorphies uniting the various papionin clades that should prove useful in future morphological analyses, especially those involving fossil taxa.

Introduction

In recent years, the reliability of primate morphological data to generate accurate phylogenetic hypotheses has been explicitly called into question (Collard and Wood, 2000; 2001). Specifically, phylogenetic analyses of extant hominoid and papionin craniodental morphology have demonstrated that homoplasy is rampant in all regions of the cranium and, more broadly, that all cranial regions are unreliable for reconstructing phylogeny (Collard and Wood, 2000; 2001). Taken at face value, these results suggest that all primate phylogenies relying on craniodental morphology are dubious (Collard and Wood, 2000; 2001). Since our understanding of primate evolution is based on a fossil record composed largely of craniodental material, the implications of Collard and Wood's (2000; 2001) studies are especially drastic.

Although the issues raised by Collard and Wood (2000; 2001) are certainly significant, and it is true that homoplasy is a widespread phenomenon with the potential to conflate the results of phylogenetic analyses (Lockwood and Fleagle, 1999), their broader claim about the inability of phylogenetic studies of skeletal and dental data to generate accurate phylogenies is far from proved (Strait and Grine, 2004; Gilbert and Rossie, 2007). The analyses that led to their results and overall conclusions are not without issue, and some of these problems have been previously identified. Thus, the choice of outgroup(s) and of which taxa to include in an analysis can have significant effects on determining character polarities, and this will influence the resulting phylogenetic trees (e.g., Strait and Grine, 2004). In fact, hominoid phylogenetic resolution improves with adjustments to allow for the assignment of multiple outgroups as well as the inclusion of fossil taxa (Strait and Grine, 2004). Fossil taxa are especially important in morphological phylogenetic analyses because they extend taxon sampling (e.g., Gauthier et al., 1988; Donaghue et al., 1989; Strait and Grine, 2004), they provide unique morphologies that help to refine assessments of character transformation (e.g., Gatesy and O'Leary, 2001; Springer et al., 2001; Gatesy et al., 2003), and consequently they increase overall phylogenetic accuracy (e.g., Wheeler, 1992; Zwickl and Hillis, 2002). In the case of hominoid phylogeny, Strait and Grine (2004) recovered the "correct" or molecular cladogram by simply expanding the outgroup and including

hominin fossils that helped to break down the "long branch" that separates *Homo* from other apes.

Additionally, as noted by Jolly (2001), the size-adjustment method employed by Collard and Wood (2000; 2001) for their quantitative characters, a geometric mean size correction, does not properly adjust for shape changes that are correlated with size (i.e., allometry). While a geometric mean method of size correction is isometric and equalizes specimen volumes while maintaining their shapes (Jungers et al., 1995), this methodology does not account for those shape differences that are correlated with size. Therefore, every allometrically influenced character is simply being grouped on the basis of body size. In effect, body size is being coded multiple times in the analysis and the influence of these size-correlated characters is reflected in the resulting trees. A subsequent study attempted to use a different method for size-correction, namely regression analysis with the retention of residuals (Nadal-Roberts and Collard, 2005). However, this method is undesirable because residuals eliminate not only size but most shape information as well (Bookstein, 1989; Jungers et al., 1995; Nadal-Roberts and Collard, 2005).

As these criticisms imply, it is difficult to adequately control for differences in body size without losing phylogenetically meaningful information. One option would be to simply exclude any allometrically influenced characters, once identified, from subsequent phylogenetic analysis, but this would surely result in a major loss of useful information because so much of form is correlated with size (see Lycett and Collard, 2005). Even when a character is significantly correlated with body size, taxa of similar sizes may have different morphologies that have real phylogenetic value. For example, when taxa form two distinct size groups, small species may have, in relative terms, long or short snouts, and large species may also have, in relative terms, long or short snouts. In such cases the relatively long snouts of small and large species may be homologous, as may be the relatively short snouts of both groups, but these homologies would be obscured by most methods of character coding that attempt to adjust for size. In such cases, a "narrow allometry" approach (Smith, 1984) would be better suited to detecting similarities in morphology (see Fig. 1). In fact, a narrow allometric coding method has been devised recently, and preliminary results suggest that it effectively adjusts for

allometry when comparing closely related animals distributed among discrete body-size groups (Gilbert and Rossie, 2007).

Herein, the narrow allometric coding method is applied to phylogenetic analyses of African papionin hard-tissue anatomy including a large set of quantitative and qualitative craniodental characters. As suggested by Gilbert and Rossie (2007), the inclusion of a large number of both quantitative and qualitative characters represents an improved data set relative to previous analyses, and this study therefore represents the most comprehensive cladistic morphological analysis of the African papionin monkeys to date. Due to the large amount of sexual dimorphism resulting in drastically different male and female papionin morphologies, three separate analyses are conducted: 1) a traditional sex-averaged analysis, 2) a male analysis, and 3) a female analysis.

In sum, the purpose of this study is threefold. First, this comprehensive data set will be used to further assess the influence of allometry on papionin craniodental morphology. Second, the results of these analyses will be compared to the results of previous molecular and morphological phylogenetic analyses of African papionin primates. If any phylogenetic hypotheses produced from this comprehensive analysis of craniodental anatomy are congruent with those produced from molecular analyses, confidence in their shared phylogenetic hypothesis will certainly be increased. In addition, for those who insist that morphological data must produce phylogenetic hypotheses congruent with molecular data in order to be considered reliable, any congruence between papionin molecules and morphology will demonstrate that hard tissue anatomy is a "reliable" source of phylogenetic information. Finally, character transformation analyses will be used to identify craniodental characters which unite the resulting African papionin clades. With a documented list of shared-derived craniodental characters supporting certain clades, a better understanding of papionin craniodental evolution will be achieved.

Methods

This study is based on published characters and character states historically deemed important in discussions of cercopithecine and papionin phylogeny combined

with my own observations (see Table 1 for the sources of individual characters). Data for the 62 quantitative characters originally used in the Collard and Wood (2000; 2001) studies were kindly provided by Mark Collard. Complete character lists with definitions and character states are presented in Tables 2.1-2.2. The taxa and sample sizes used in the phylogenetic analyses are broken down by character and presented in Table 2.3. Males and females were analyzed separately and also averaged together in a third sex-averaged analysis. Because many characters, particularly quantitative characters, were coded on the basis of narrow allometries, taxa such as *Pan* and *Colobus* are not appropriate outgroups because the allometric trajectories influencing the craniodental morphology of these primates are not comparable to those observed in African papionin monkeys; such phylogenetically and phenetically distant taxa cannot be used (Gaffney, 1979; Lockwood et al., 2004). However, Strait and Grine (2004) have also demonstrated that multiple outgroups help improve phylogenetic resolution and accuracy. To account for both of these realities, *Macaca* and *Allenopithecus* were assigned as outgroups for all analyses, but, in order to retain a relevant allometric baseline for the African papionins, only *Macaca* was coded for morphometric (quantitative) craniodental characters.

For analysis, all macaque specimens were lumped into a single taxon: *Macaca*. For quantitative characters, this included specimens of *M. fascicularis* and *M. mulatta*. For qualitative characters, this included specimens of *M. fascicularis*, *M. mulatta*, *M. nemestrina*, and *M. sylvanus*. These taxa are generally regarded by morphological and molecular studies as the relatively generalized macaques that are likely to represent the primitive morphological condition (e.g., Fooden, 1975; Szalay and Delson, 1979; Delson, 1980; Morales and Melnick, 1998; Groves, 2001). Because this analysis was conducted at the genus-level, it is appropriate to sample multiple species in an attempt to include a range of possible morphologies. For ingroup taxa, specimens of the following species and subspecies were included in their respective genera in the analysis: *Cercocebus agilis, Cercocebus torquatus, Lophocebus albigena, Lophocebus aterrimus, Mandrillus leucophaeus, Mandrillus sphinx, Papio hamadryas anubis, Papio hamadryas cynocephalus, Papio hamadryas hamadryas, Papio hamadryas kindae, Papio hamadryas papio, Papio hamadryas ursinus, Theropithecus gelada*.

In total, 157 characters were used for the analysis: 88 quantitative characters and 69 qualitative characters. Each type of character requires slightly different rules and techniques for assigning character states. For quantitative characters, an isometric size correction was first applied. For each specimen, all quantitative characters were divided by the geometric mean of all measurements for that specimen[*]. After this isometric size correction, the resulting values for each character represented some aspect of "shape" (*sensu* Mosimann, 1970; also see Darroch and Mosimann, 1985).

By definition, allometrically influenced characters are those whose shape is significantly correlated with size (Mosimann and James, 1979). To determine which characters were allometrically influenced, a correlation of all isometrically size-adjusted shape characters against the geometric mean of 62 cranial measurements was performed. Theoretically, these correlations should be calculated for each character of each specimen against the geometric mean for that specimen. This has the advantage of providing more data points to detect significance in the correlations, especially if the phylogenetic analysis in question involves a small number of taxa. However, this approach also has the serious disadvantage of being overly sensitive to characters that have a small but statistically significant size-correlated component.

The more general approach used and advocated here instead uses the average size-adjusted character value of each taxon and then correlates these to the average geometric mean of each taxon. Using an example from this analysis, Character C7 (distance between bregma and lambda) was measured on 20 male and 20 female *Cercocebus* specimens. For each specimen, a geometric mean of 62 cranial measurements was calculated and the raw measurement of C7 was divided by the geometric mean for that specimen. The new value is the size-adjusted value for C7. The average of all 20 size-adjusted values for male *Cercocebus* was calculated, as well as the average of all 20 geometric means for the *Cercocebus* males. The same procedure was carried out with females, leading to an average male value of C7, an average female value of C7, an average geometric mean for male *Cercocebus*, and an average geometric mean for female *Cercocebus*. The same calculations were performed for all taxa in the

[*] Because characters expressed as an index are already size-adjusted, they were not divided by the geometric mean. The 62 measurements used by Collard and Wood (2000; 2001) were used in the calculation of the geometric mean for each taxon.

analysis. For the correlation analysis, the average C7 values were used for males and females combined so that 12 data points were available for the correlation (i.e., 6 male values and 6 female values). These 12 values were then correlated with their corresponding 12 average geometric means. The resulting r-value for the correlation of C7 against the geometric mean was -0.908 with a p-value less than 0.001, indicating that C7 is an allometrically influenced character.

Correlation analyses were performed for all quantitative characters in the same way as outlined for character C7. The critical value for a correlation with a sample size of 12 and 10 degrees of freedom at the 0.05 significance level is 0.576 (Rohlf and Sokal, 1995). The lowest significant r-value produced from the correlation analyses performed here was 0.5987. Correlation r-values below 0.576 were considered biologically insignificant and did not warrant application of the narrow allometric coding procedure outlined here.

After the correlation analyses were performed, those shape characters that were significantly correlated with the geometric mean (size) were determined to be, by definition, significantly influenced by allometry (see Tables 2.1-2.2 for the complete list of allometrically influenced characters). Due to their correlation with body size, these characters are not independent characters and are not suitable for phylogenetic analysis without some sort of character correction. For any quantitative character determined to be allometrically influenced, the narrow allometric coding method was employed to disentangle the effects of allometry (see also Gilbert and Rossie, 2007). The papionin taxa included here were divided into two size categories: *Macaca*, *Cercocebus* and *Lophocebus* were considered to be small-bodied and *Papio*, *Theropithecus* and *Mandrillus* were considered to be large-bodied. These size groups are fairly obvious, but they can also be confirmed statistically by using gap-weighted coding for the geometric mean of each taxon and assigning two character states. These two size categories hold true for both males and females.

Again picking up with the C7 example, this character was determined to be significantly influenced by allometry due to its significant correlation with the geometric mean (see above). Therefore, the narrow allometric coding procedure was applied to character C7 in order to better reflect homologous character states in taxa of differing

body sizes (see Fig. 2.1). The values for each sex and each taxon in the small-bodied papionin taxa (*Macaca*, *Cercocebus*, and *Lophocebus*) were coded separately using gap-weighted coding and, similarly, the values for each sex and each taxon in the large-bodied papionin taxa (*Papio*, *Theropithecus*, and *Mandrillus*) were coded separately using gap-weighted coding (see Thiele, 1993 for a description of gap-weighted coding). As a result, the taxon with the lowest C7 value in the small-bodied size category (*Cercocebus*) gets assigned a character state of "0", and the taxon with the lowest C7 value in the large-bodied size category (*Mandrillus*) also gets assigned a character state of "0". If the narrow allometric procedure was not employed, *Mandrillus* would receive a value of "0" because it has the lowest C7 value among all taxa and *Cercocebus* would receive a higher character state value, depending on the number of character states chosen to be employed by the gap-weighting equation (see Fig. 2.1 and Fig. 2.2).

For all quantitative characters, gap weighted coding was used (Thiele, 1993), dividing the variation into three character states because this represents the minimum number of taxa in a given size category (see also Gilbert and Rossie, 2007). A flow chart summarizing the narrow allometric coding method for quantitative characters is presented in Figure 2.3.

Qualitative characters were scored according to the character state criteria listed in Table 2.2. To better encompass variation, intermediate character states were employed. Intermediate (polymorphic) character states for a given character were applied to any taxon displaying two or more character states in more than 20% of specimens examined. For characters with more than two discrete character states, an intermediate state was assigned if two adjacent character states totaled ≥ 80% of all observations. For example, if a character has three discrete states (0, 2, and 4), and a taxon displays states 0 or 2 combined for ≥ 80% of all observations, an intermediate state (1) was assigned for this particular taxon. If no two adjacent character states combined totaled ≥ 80% of all observations for all taxa, an additional polymorphic state was added and the character was considered unordered. In the case of multistate characters where more than two adjacent states both totaled 80%, the average of the two possible intermediate states was used. For example, if states 0 + 2 total 80% (intermediate state 1)

but states 2 + 4 also total 80% (intermediate state 3), the average of the intermediate states, in this case $(1 + 3) / 2 = 2$, was assigned.

Unless otherwise noted, qualitative characters were considered ordered. For a full description of characters, character states, and character types, see Tables 2.1 and 2.2. When possible, a similar narrow allometric coding method was employed for qualitative characters determined to be allometrically influenced. Qualitative characters were determined to be significantly influenced by allometry by taking careful note of where consistent differences exist between the morphologies of small and large taxa, similar to the analysis of Gilbert (2007). To illustrate by example, Gilbert (2007) determined that the development or extent of maxillary fossae, character F20 in this analysis, is allometrically influenced such that, where fossae are present, small taxa have greater development of this feature on average than do large taxa. Accordingly, character states were assigned separately in small and large taxa in order to restore perceived homology. The result is that large and small taxa with the greatest development of maxillary fossae relative to other taxa within their respective size categories were assigned similar character states (e.g., see Table 2.2 for character state definitions within each size category). Where data was unavailable or inapplicable for certain characters, whether they were qualitative or quantitative, the missing data ("?") code was used.

The resulting character matrices for the male, female, and sex-averaged data sets were then subjected to a series of parsimony analyses using PAUP 4.0 (Swofford, 1998), and character transformations were mapped using Mesquite 1.11 (Maddison & Maddison, 2006). Sex-averaged character states simply consisted of the average of the mean male and mean female values for each quantitative character and most of the qualitative characters. In the case of quantitative characters, the sex-averaged value for each character was then coded using gap-weighted coding with three character states. For qualitative characters, the character state value of the males and females for each taxon were averaged together. If the resulting value for any taxon ended up with a decimal of 0.5, the character states of all taxa for that character were doubled in order to work with whole number character states. If the character was unordered, the polymorphic state was one whole number higher than the highest specific character state, regardless of the doubling procedure. An exhaustive search was used to find the most parsimonious trees

and a 10,000 replication branch and bound bootstrap procedure with replacement was used to provide confidence intervals on the clades suggested by the most parsimonious trees.

Results

Almost one-third of the characters examined in this study, i.e., 51 out of 157, were significantly affected by allometry. Over two-thirds of these allometrically influenced characters (36 out of 51) were concentrated in the face, cranial vault and cranial base.

For comparison, the molecular phylogeny for the extant papionins (Disotell et al., 1992; 2000; Disotell, 1994; Harris and Disotell, 1998; Tosi et al., 1999; 2003) and the most parsimonious tree derived from the original Collard and Wood (2000) data set are presented in Figure 2.4. For a more direct comparison with the analyses presented here, the original Collard and Wood (2000) data set was reanalyzed excluding *Pan* and instead assigning *Macaca* as the outgroup, and without application of the narrow allometric coding method. The resulting cladograms from the current analyses are provided in Figure 5 and summarized with tree statistics in Table 2.4. Using the narrow allometric coding method, the most parsimonious trees resulting from the sex-averaged, male, and female analyses were congruent with the molecular phylogenetic tree (Figs. 2.4a, 2.5a, 2.5b). Therefore, the majority-rule consensus tree of the three analyses presented here is also congruent with molecular tree (Fig. 2.6). Bootstrap support values for the most parsimonious trees obtained in each individual analysis are presented in Table 2.4. The higher values here, relative to the previous analyses of Gilbert and Rossie (2007), indicate increased support for the congruence of molecular and morphological data.

The results of the character transformation analyses are presented in Table 2.5. Only those shared-derived characters supporting the clades suggested by the consensus tree are provided. Many of the characters presented in Table 2.5 are identified here, for the first time, as shared-derived characters uniting the various African papionin clades.

Discussion

As previously demonstrated, allometry has a strong influence on papionin craniodental anatomy (Freedman, 1962; Collard and O'Higgins, 2001; Singleton, 2002; Frost et al., 2003; Leigh et al., 2003; Gilbert and Rossie, 2007). The strong influence of allometry may be compensated for by using a narrow allometric approach to identify craniodental synapomorphies, and such a method must be considered a prerequisite in any attempt to conduct a meaningful phylogenetic analysis of morphological data in papionins or any other group where the included taxa show a great disparity in size. A previous analysis on a smaller number of quantitative morphological characters has demonstrated the efficacy of this type of approach (Gilbert and Rossie, 2007). The analyses conducted here confirm these findings, and extend the known utility of the narrow allometric coding method to both quantitative and qualitative characters.

Using the narrow allometric coding method, the most parsimonious phylogenetic trees produced in the sex-averaged, male, and female analyses were congruent with the consensus tree produced from molecular data. In addition, the bootstrap values associated with these trees are generally higher than those produced from quantitative morphological data alone. These tree statistics illustrate the importance of including both quantitative and qualitative characters in phylogenetic analysis (Gilbert and Rossie, 2007). Both types of characters may contain phylogenetically useful information and can help increase the accuracy of resulting trees. Future phylogenetic analyses of primate morphology should attempt to include both kinds of characters whenever possible.

In addition to the most parsimonious trees, the majority-rule consensus tree is congruent with the molecular consensus tree in suggesting a *Cercocebus/Mandrillus* clade as well as a *Papio/Lophocebus/Theropithecus* clade. While the molecular consensus tree cannot resolve the relationships among *Papio*, *Lophocebus*, and *Theropithecus*, the results from the morphological analyses presented here support the existence of a *Papio/Lophocebus* clade with *Theropithecus* placed at the base of the group. Further support of an extant sister relationship between *Papio* and *Lophocebus* may also be provided by the newly named papionin taxon *Rungwecebus kipunji*, which was originally described as *Lophocebus kipunji* but has more recently been suggested to

be more closely related to *Papio* (Jones et al., 2005; Davenport et al., 2006). No doubt further genetic and morphological analyses including *Rungwecebus* will help to resolve the genus-level relationships with the *Papio/Lophocebus/Theropithecus* group. In the meantime, as the results of this analysis suggest, the phylogenetic placement of *Theropithecus* at the base of this African papionin clade will remain the hypothesis with the most support.

The congruence achieved between the phylogenetic hypotheses produced from the morphological data presented here and the previously published molecular data indicate that there is strong support for their shared phylogenetic hypothesis. Thus, among extant African papionin taxa, there is strong support for both a *Cercocebus/Mandrillus* and a *Papio/Lophocebus/Theropithecus* clade. A more detailed and biologically meaningful interpretation of papionin craniodental morphology, taking allometry into account, clearly indicates that papionin molecules and morphology are congruent. As reliable as one considers molecular data in primate phylogenetic analysis, morphological data must be considered just as reliable. Rather than proclaiming morphological data unreliable or irrelevant (e.g., Collard and Wood, 2000; 2001; Scotland et al., 2003), it is better to understand the importance of morphological data in phylogenetic reconstruction, especially in the case of fossils, and to re-examine cases of seeming incongruence with greater scrutiny (Wiens, 2004; Smith and Turner, 2004; Gilbert and Rossie, 2007). Both molecular and morphological data are important sources of phylogenetic information, and ignoring one source or the other is not advisable if the overall goal is phylogenetic accuracy.

Similar to the findings of Gilbert and Rossie (2007), the male and female analyses presented here illustrate the dichotomous nature of African papionin craniodental anatomy. While the most parsimonious tree produced from the male analysis is congruent with the female most parsimonious tree and both suggest *Cercocebus/Mandrillus* and *Papio/Lophocebus/Theropithecus* clades, there is no bootstrap support for the *Papio/Lophocebus/Theropithecus* clade in the female analysis. In addition, analysis of male craniodental morphology results in the highest CI, RI, RC and bootstrap values, and the lowest HI values compared to all other analyses performed here (see Table 2.4). These statistics suggest that male craniodental anatomy is better at

detecting real versus apparent synapomorphies and produces more stable phylogenetic trees. The superior performance of the male craniodental data set supports previous claims about the increased utility of male morphologies relative to female morphologies among highly sexually dimorphic primates (Fleagle and McGraw, 2002; Gilbert and Rossie, 2007). It is likely that the distinctive traits of papionin males are tied to sexual selection, and these traits are phylogenetically informative because closely related taxa, by definition, must have shared a common mate recognition system more recently than distantly related taxa (Paterson, 1985; Gilbert and Rossie, 2007). In addition, sexual selection in the form of mate competition is almost exclusive to males among catarrhine taxa. Similar types and levels of contest competition over females in closely related taxa would help explain the evolution of distinctive and phylogenetically informative male craniodental characters and their potential absence in females.

Further support for sexual selection, particularly contest competition among males, as an important imprint on phylogenetic history is evident from a brief examination of two characters commonly considered closely tied to sexual selection in primates: relative male canine size and male canine size relative to female canine size. *Cercocebus* and *Mandrillus* have the largest male canines relative to body size as well as the highest levels of canine dimorphism relative to the other papionin taxa. Similarly, *Papio*, *Theropithecus*, and *Lophocebus* have the smallest male canines relative to body size and the lowest levels of canine dimorphism relative to the primitive condition expressed by *Macaca*. The distribution of these characters points to the similar patterns of sexual selection and, by extension, the shared phylogenetic history of these African papionin clades.

The performance of male craniodental morphology in the analyses presented here suggests that primate and mammalian morphological systematists should pay close attention to male morphologies among highly sexually dimorphic taxa. In fact, in addition to sex-averaged analyses, I would recommend that the sexes be analyzed separately in phylogenetic analyses of highly sexually dimorphic taxa. This is not typically done in cladistic studies, but there are good reasons to argue that it should be. While individual qualitative morphological characters can be defined in such a way to focus on male or female character states only, quantitative morphological characters

typically represent measurements that are taken on specimens of both sexes and then averaged together. These quantitative characters necessarily represent an "imaginary" morphotype; no animal exists with an intermediate male and female morphology, especially among highly sexually dimorphic and morphologically dichotomous taxa. Therefore, it may be preferable to separate the sexes and run separate phylogenetic analyses on both morphotypes. Further studies of this kind may support or refute the hypothesis that male morphologies, particularly sexually-selected characters, have increased phylogenetic value relative to female morphologies among sexually dimorphic taxa.

An alternative and more complete approach to including both male and female data in phylogenetic analysis is to combine the separate male and female matrices in a larger "combined-sex" analysis. In the case of this study, this would double the number of characters in the study, from 157 to 314. While it may be suggested that this strategy will result in the repetition and overweighting of certain characters, there are many reasons to believe that combining male and female matrices that have been coded separately is the most appropriate and accurate portrayal of morphological information about a species. First, such an approach does not create an "imaginary" morphotype; the integrity of the separate male and female morphotypes is retained. Second, male and female morphotypes in sexually dimorphic taxa are demonstrably different and these differences obviously have a genetic basis, which is included in this approach. Third, increasing the number of characters in phylogenetic analysis has been repeatedly demonstrated to increase overall phylogenetic accuracy (e.g., Wiens, 2003a; 2003b; 2006). In this case, combining characters that have been scored separately for males and females allows for both unique male and female character states that are phylogenetically informative to be sampled together during the analysis and potentially increases the strength and accuracy of the phylogenetic signal.

To demonstrate the effectiveness of a combined-sex approach, the 157 character male matrix and 157 character female matrix were combined into a 314 character matrix and then subjected to the same parsimony and bootstrap analyses. The resulting most parsimonious tree is the same as the consensus tree from the previous analyses (Fig. 2.6). In addition, the CI, RI, RC, and bootstrap values for this tree are higher than that for the

sex-averaged analysis (Table 2.4). The results of this combined-sex analysis support the hypothesis that it is a superior method for including both male and female morphological data compared to the sex-averaged analysis.

Finally, the results of the analyses here present a new and updated list of craniodental synapomorphies uniting the clades suggested by the majority-rule consensus tree. Particularly distinctive new character states identifiable in both sexes include a shorter distance between bregma and lambda, a shorter basisphenoid, a narrower posterior palate, larger male canines, and higher levels of canine dimorphism for *Cercocebus/Mandrillus* and a wider neurocranium, broader infratemporal region, relatively small canines, and lower levels of canine dimorphism for *Papio/Lophocebus/Theropithecus* (Table 2.5). These character states, in addition to those described in previous studies (e.g., Fleagle and McGraw, 1999; 2002; Groves, 2000; McGraw and Fleagle, 2006; Gilbert, 2007), should be useful in the description and identification of new fossil African papionin taxa. The more extensive list of distinctive characters for male and sex-averaged samples of papionins listed in Table 2.5 should also be helpful in the phylogenetic analysis of fossil specimens.

Conclusions

A large set of qualitative and quantitative craniodental characters for the cercopithecoid monkey tribe Papionini was subjected to phylogenetic analysis using parsimony. In order to account for the well-documented influence of allometry on the craniodental morphology of this group, the narrow allometric coding method was employed (Gilbert and Rossie, 2007). Contrary to previous analyses which have purportedly demonstrated the incongruence of papionin molecular and morphological data, the comprehensive analyses conducted here strongly suggests that, when allometry is properly accounted for in phylogenetic analysis, molecular studies of African papionin phylogeny and analyses based on craniodental morphology are congruent. Therefore, if such congruence is to be regarded as a prerequisite for assessing the reliability of morphological data, then morphological data may be regarded as just as reliable as molecular data. While molecular analyses cannot resolve the relationships among the

Papio/Lophocebus/Theropithecus clade (Disotell et al., 1992; 2000; Disotell, 1994; Harris and Disotell, 1998; Tosi et al., 1999; 2003), the morphological analyses presented here indicate that *Papio* and *Lophocebus* are sister taxa and *Theropithecus* is at the base of this grouping. As suggested by character transformation analyses, identifiable synapomorphies of *Cercocebus* and *Mandrillus* include a short distance between bregma and lambda, a short basisphenoid, a narrow posterior palate, large male canines, and high levels of canine dimorphism, while a wide neurocranium, broad infratemporal region, small male canines, and low levels of canine dimorphism unite *Papio, Lophocebus,* and *Theropithecus.* These morphologies, along with the more complete list of morphologies provided in Table 2.5, should be helpful in determining the phylogenetic position of fossil papionin taxa.

Similar to the results of Gilbert and Rossie (2007), this study found that male craniodental morphology is a particularly useful source of phylogenetic information and that the underlying reasons for this phenomenon are probably tied to sexual selection. Future studies of highly sexually dimorphic primates should pay particular attention to male morphologies and either separate the sexes in phylogenetic analysis of quantitative morphological characters or combine separate male and female matrices in a "combined-sex" analysis.

Figure Captions

Figure 2.1. Heuristic comparison of narrow allometric coding and conventional coding of size-adjusted data for hypothetical character 'relative snout length'. The study group exhibits positive allometry for the character "relative snout length", and taxa within the group fall into two basic size groups, small and large. The black lines represent ranges of relative snout length within each size group. Conventional conversion of craniometric data into phylogenetic characters (depicted in dashed lines and numbers on the Y-axis) would divide the entire range of relative snout lengths (the Y-axis) into segments horizontally, in this case producing 5 states. Narrow allometric coding (depicted by diagonally arranged prime' numbers) performs the same segmenting procedure, but applies it to the two size groups separately such that the shortest-snouted species in each group are coded as "short", and the longest-snouted species in each group are coded as "long". From Gilbert and Rossie (2007).

Figure 2.2. Flow chart outlining the difference between traditional coding methods and the narrow allometric coding procedure for allometrically influenced characters. Using the example character C7, average values for each taxon are arranged in ascending order. Traditional gap-weighted coding with three character states would assign character states among all taxa treated as one group (left-hand column). The narrow allometric coding method first divides the taxa into discrete size categories, and then uses gap-weighted coding to assign character states separately within each size category (right column). Note the difference between the character states assigned to each taxon using the different methods; the narrow allometric coding method results in a more accurate reflection of homologous character states.

Figure 2.3. Flow chart outlining the narrow allometric coding procedure for quantitative characters.

Figure 2.4. a) Hypothesized phylogenetic tree of the extant Papionini from molecular (mtDNA and Y-chromosome) data (Disotell et al., 1992; 2000; Disotell, 1994; Harris and Disotell, 1998; Tosi et al., 1999; 2003) compared with **b)** the most parsimonious tree derived from the craniodental data set of Collard and Wood (2000; 2001) using *Macaca* rather than *Pan* as the outgroup.

Figure 2.5. Most parsimonious phylogenetic trees of the extant Papionini **a)** from craniodental data in the sex-averaged and male analyses and **b)** from craniodental data in the female analysis. Note that 2.4a is congruent with the hypothesized phylogenetic tree for the extant papionins from molecular data in Figure 2.3a.

Figure 2.6. Majority-rule consensus tree of the extant Papionini from craniodental data in the male, female and sex-averaged analyses. Note that this tree is congruent with the hypothesized phylogenetic tree for the extant papionins from molecular data in Figure 2.3a. Values above the nodes correspond to the percentage of most parsimonious trees supporting a particular clade in the male, female, and sex-averaged analyses. Numbers below the nodes identify correspond to Table 2.5.

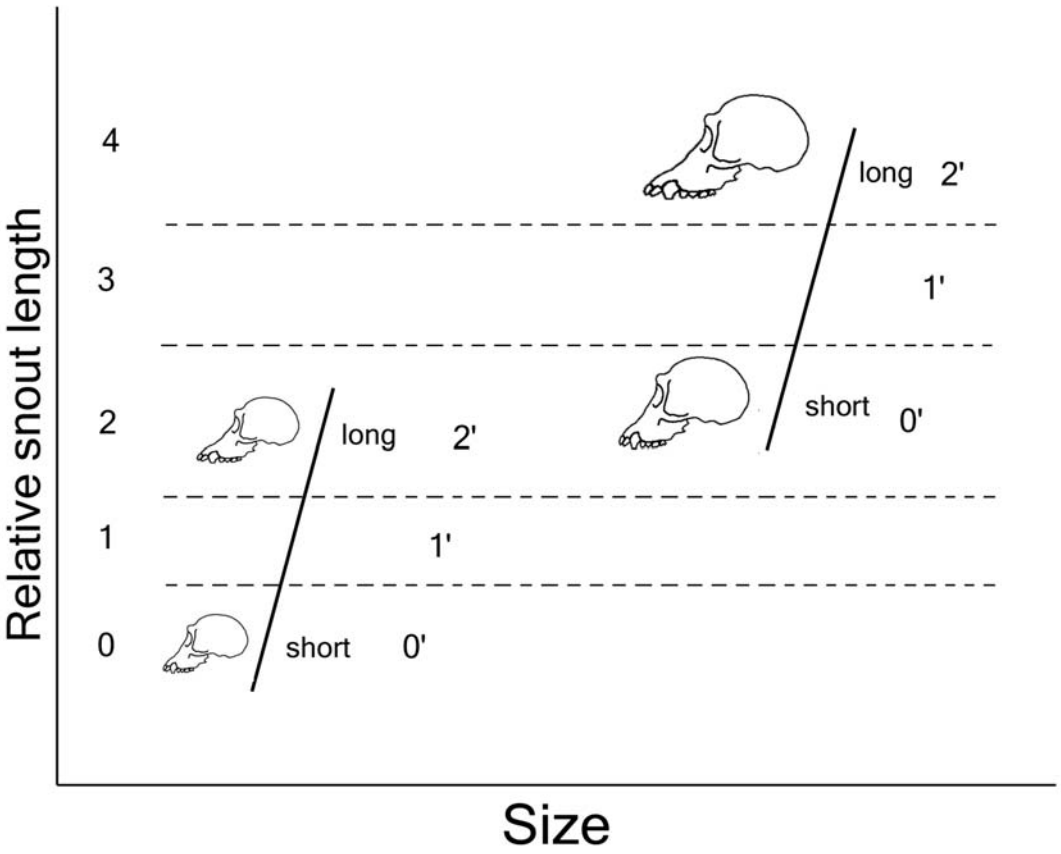
Relative snout length
4
3
2
1
0
long 2'
1'
short 0'
long 2'
1'
short 0'
Size

Figure 2.1

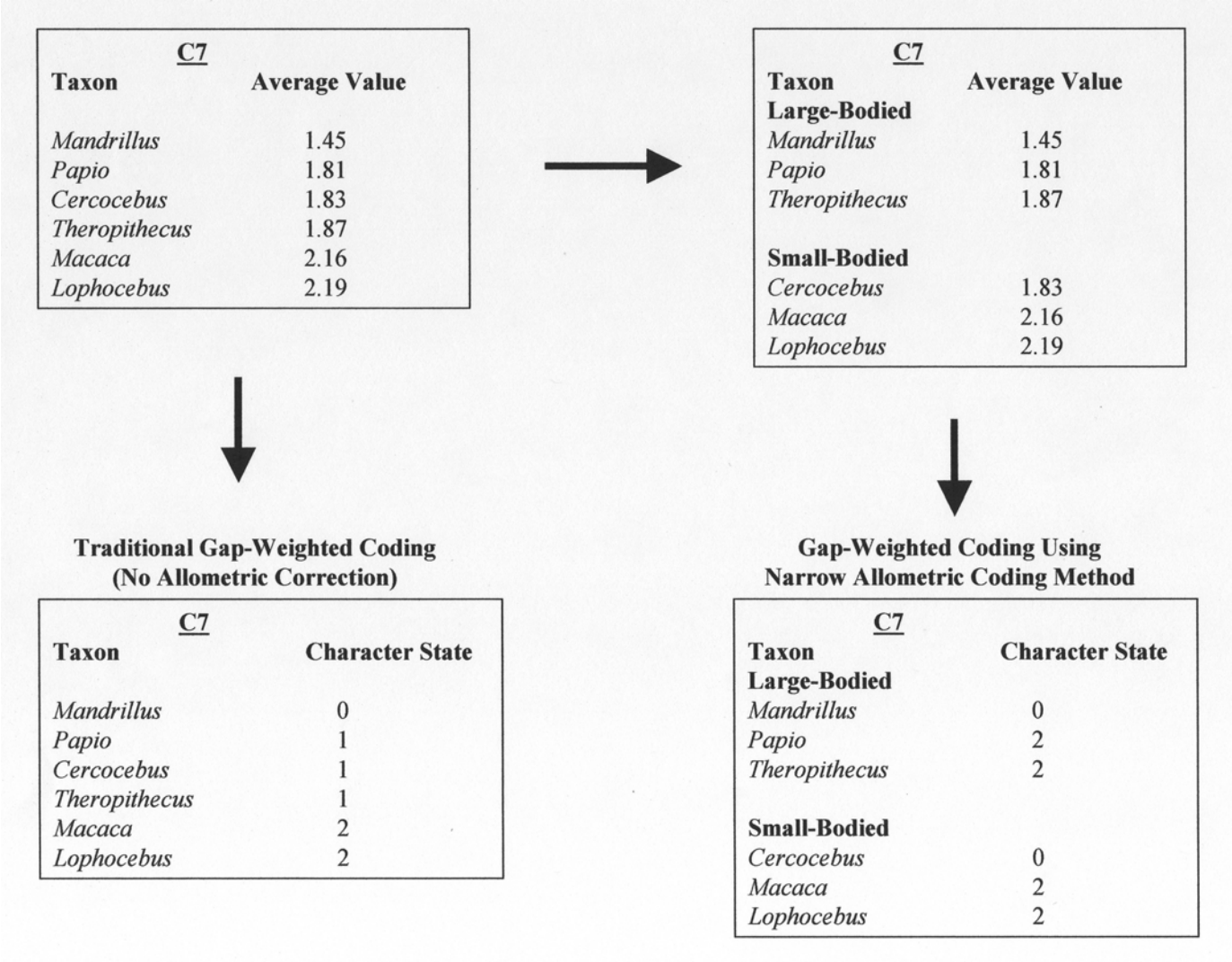
C7
Taxon
Average Value
Mandrillus 1.45
Papio 1.81
Cercocebus 1.83
Theropithecus 1.87
Macaca 2.16
Lophocebus 2.19
C7
Taxon
Average Value
Large-Bodied
Mandrillus 1.45
Papio 1.81
Theropithecus 1.87
Small-Bodied
Cercocebus 1.83
Macaca 2.16
Lophocebus 2.19
Traditional Gap-Weighted Coding
(No Allometric Correction)
C7
Taxon
Character State
Mandrillus 0
Papio 1
Cercocebus 1
Theropithecus 1
Macaca 2
Lophocebus 2
Gap-Weighted Coding Using
Narrow Allometric Coding Method
C7
Taxon
Character State
Large-Bodied
Mandrillus 0
Papio 2
Theropithecus 2
Small-Bodied
Cercocebus 0
Macaca 2
Lophocebus 2

Figure 2.2

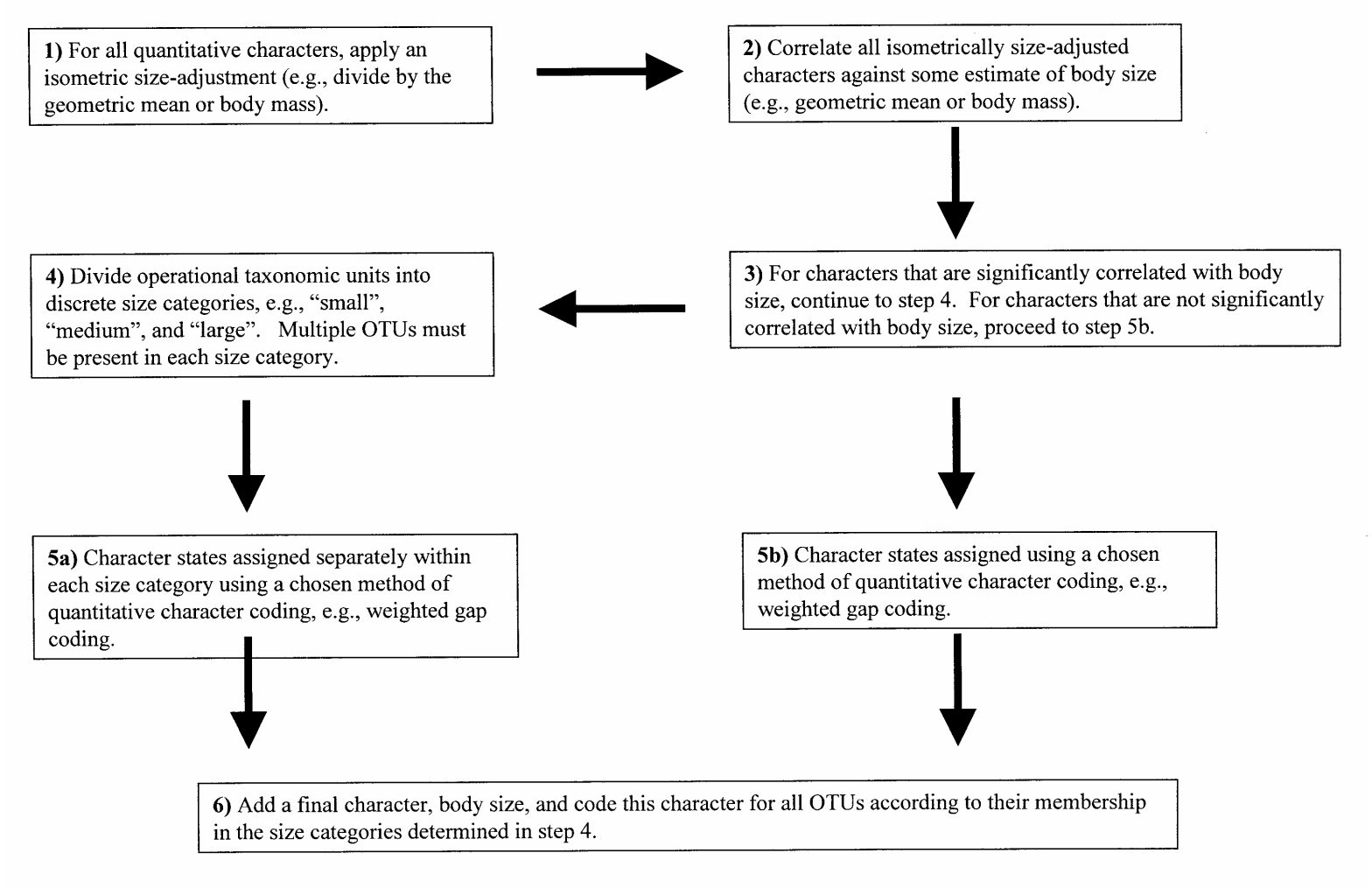
1) For all quantitative characters, apply an isometric size-adjustment (e.g., divide by the geometric mean or body mass).
2) Correlate all isometrically size-adjusted characters against some estimate of body size (e.g., geometric mean or body mass).
3) For characters that are significantly correlated with body size, continue to step 4. For characters that are not significantly correlated with body size, proceed to step 5b.
4) Divide operational taxonomic units into discrete size categories, e.g., "small", "medium", and "large". Multiple OTUs must be present in each size category.
5a) Character states assigned separately within each size category using a chosen method of quantitative character coding, e.g., weighted gap coding.
5b) Character states assigned using a chosen method of quantitative character coding, e.g., weighted gap coding.
6) Add a final character, body size, and code this character for all OTUs according to their membership in the size categories determined in step 4.

Figure 2.3

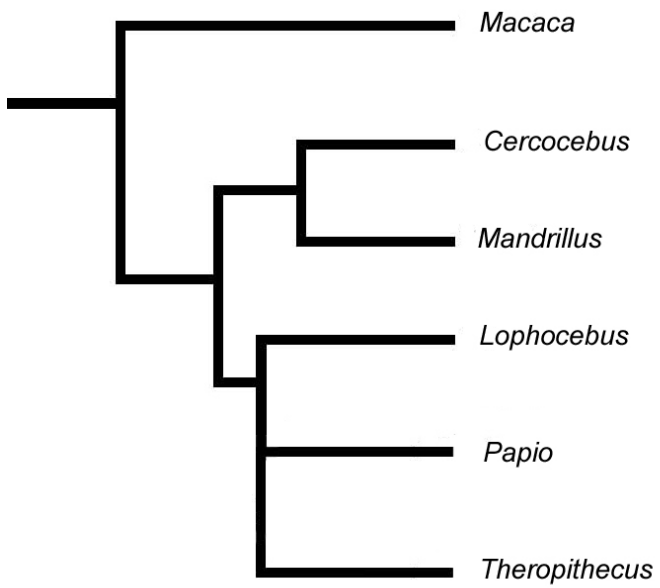
Macaca
Cercocebus
Mandrillus
Lophocebus
Papio
Theropithecus

a)

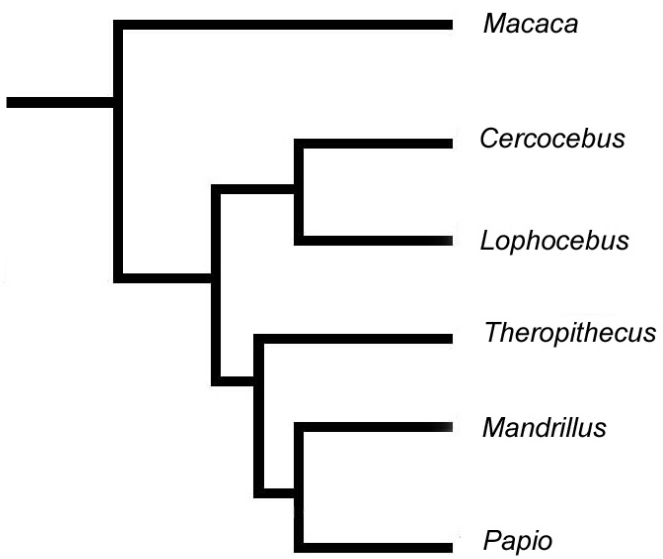
Macaca
Cercocebus
Lophocebus
Theropithecus
Mandrillus
Papio

b)

Figure 2.4

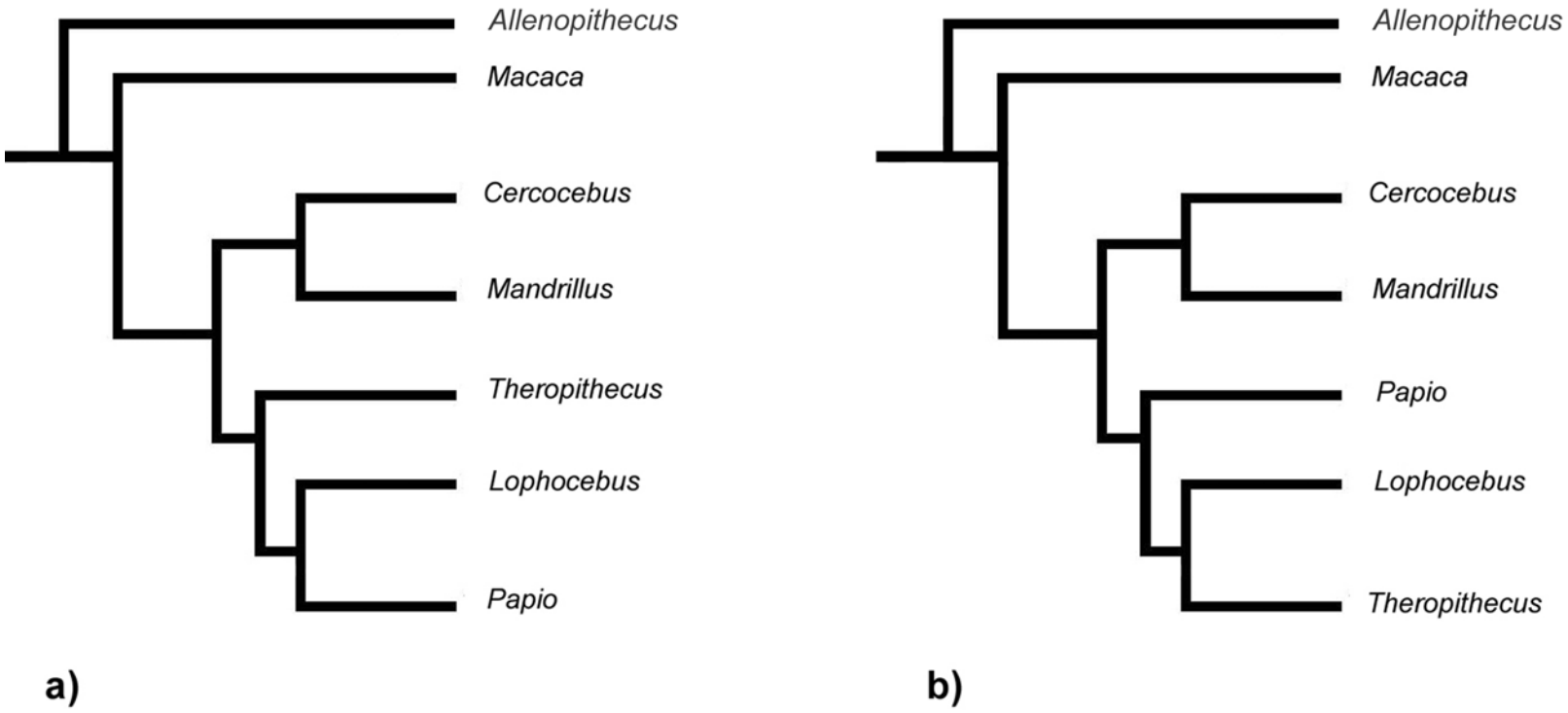
Allenopithecus
Macaca
Cercocebus
Mandrillus
Theropithecus
Lophocebus
Papio
a)
Allenopithecus
Macaca
Cercocebus
Mandrillus
Papio
Lophocebus
Theropithecus
b)

Figure 2.5

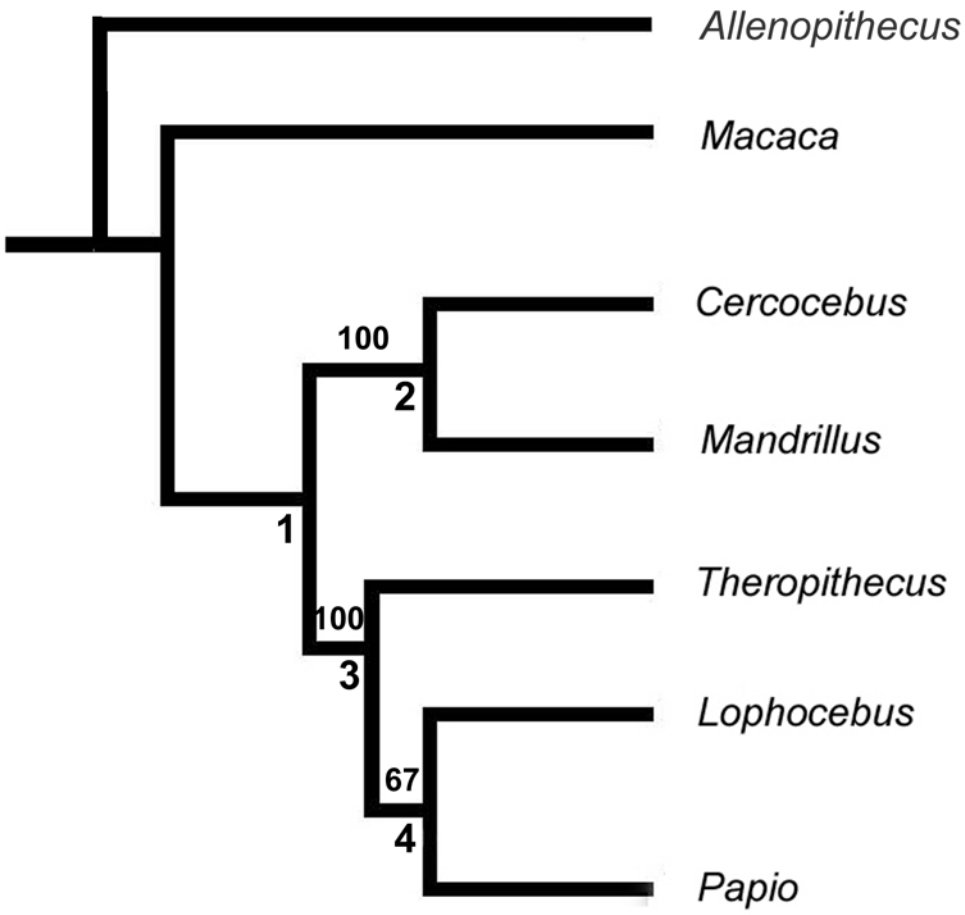
Allenopithecus
Macaca
Cercocebus
100
2
Mandrillus
1
Theropithecus
100
3
Lophocebus
67
4
Papio

Figure 2.6

Table 2.1. Characters Used in This Study.

Variable	Definition	Character Type	Reference
*C1	Glabella-inion	QN, O	Wood, 1991
*C2	Bregma-basion	QN, O	Wood, 1991
*C3	Minimum frontal breadth (minimum chord distance between frontotemporale; i.e., maximum width in the coronal plane)	QN, O	Wood, 1991
*C4	Biporionic breadth	QN, O	Wood, 1991
*C5	Glabella-bregma	QN, O	Wood, 1991
*C6	Postglabellar sulcus-bregma (distance between the deepest point of the postglabellar depression and bregma)	QN, O	Wood, 1991
*C7	Parietal-sagittal chord (bregma-lambda)	QN, O	Wood, 1991
*C8	Parietal-lambdoid chord (chord distance along the lambdoid border of the intact parietal)	QN, O	Wood, 1991
C9	Lambda-inion	QN, O	Wood, 1991
C10	Occipital-sagittal length (lambda-opisthion)	QN, O	Wood, 1991
*C11	Foramen magnum max width	QN, O	Wood, 1991
C12	Occipital condyle max length	QN, O	Wood, 1991
C13	Lambda thickness of parietal	QN, O	Wood, 1991
*C14	Breadth between carotid canals	QN, O	Chamberlain, 1987
*C15	Breadth between petrous apices	QN, O	Chamberlain, 1987
C16	Length of tympanic plate (distance from the most lateral point on the inferior surface of the tympanic plate to the carotid canal)	QN, O	Chamberlain, 1987
C17	Adult male sagittal crest position	QL, O	Eck and Jablonski, 1984; 1987
C18	Postorbital sulcus	QL, U	Szalay and Delson, 1979
*C19	Auditory meatus position	QL, O	Groves, 1978; 2000

C20	Anterior temporal line divergence	QL, O	Groves, 2000; McGraw and Fleagle, 2006; Gilbert, 2007
C21	Nuchal lines in the midline where discernable	QL, O	Gilbert, 2007
*C22	Calvarial shape (biporionic length / glabella-inion)	QN, O	General
C23	Cranial vault index (basion-bregma / glabella-inion)	QN, O	General
*C24	Postorbital constriction (min frontal breadth / max biorbital breadth)	QN, O	General
*C25	Compound temporonuchal crest	QL, O	Strait et al., 1997
C26	Definitive parietal notch	QL, O	Groves, 2000
*C27	Position of the tympanic relative to the postglenoid process	QL, O	Groves, 2000
C28	Postglenoid process height	QL, O	Groves, 2000
C29	EAM tympanic crest	QL, O	Groves, 2000
*C30	Foramen magnum max length (opisthion-basion)	QN, O	General
C31	Position of the foramen magnum relative to the biporionic line	QL, O	Dean and Wood, 1981, 1982; Strait et al., 1997
C32	EAM size	QL, O	Strait and Grine, 2004
*C33	Opisthion-inion	QN, O	General
*C34	Bieuryonic breadth	QN, O	General
*C35	Breadth between infratemporal crests (measured where spheno-temporal suture meets the infratemporal crest)	QN, O	Chamberlain, 1987; Collard and Wood, 2000; 2001
C36	Basioccipital length (basion to sphenoccipital synchondrosis in the midline)	QN, O	Chamberlain, 1987
C37	Anterior basioccipital breadth (measured across the sphenoccipital synchondrosis)	QN, O	Chamberlain, 1987
*C38	Posterior basioccipital breadth (measured across the anterior edge of the jugular foramina)	QN, O	Chamberlain, 1987
*C39	Basisphenoid length (measured from the sphenoccipital synchondrosis to the junction with the vomer in the midline)	QN, O	General
C40	Petrous apex ossified beyond spheno-occipital synchondrosis	QL, O	Collard and Wood, 2000

*C41	Shape of the choanal sides	QL, O	Groves, 2000
*C42	Shape at the posterior end of the medial pterygoid plates	QL, O	Groves, 2000
C43	Shape at the posterior edge of vomer	QL, O	Groves, 2000
C44	Vomer-presphenoid junction	QL, O	Groves, 2000
C45	Vomer/Sphenoid/Palatine contact	QL, U	General
*C46	Vomer/sphenoid contact in the midline	QL, O	General
C47	Petrous process position	QL, O	Gilbert, 2007
C48	Appearance of fossae anterior to the foramen magnum	QL, O	General
*F1	Superior facial height (nasion-prosthion)	QN, O	Wood, 1991
F2	Alveolar height (nasospinale-prosthion)	QN, O	Wood, 1991
*F3	Superior facial breadth (frontomalaretemporale-frontomalaretemporale)	QN, O	Wood, 1991
F4	Bizygomatic breadth (zygion-zygion)	QN, O	Wood, 1991
*F5	Bimaxillary breadth (zygomaxillare-zygomaxillare)	QN, O	Wood, 1991
F6	Anterior interorbital breadth (maxillofrontale-maxillofrontale)	QN, O	Wood, 1991
*F7	Orbital height (maxillofrontale-ektoconchion)	QN, O	Wood, 1991
F8	Minimum malar height (min distance from inferior orbital margin to inferior border of zygomatic process of the maxilla)	QN, O	Wood, 1991
F9	Maximum nasal aperture width (max width at whatever height it occurs)	QN, O	Wood, 1991
*F10	Nasal height (nasion-nasospinale)	QN, O	Wood, 1991
*F11	Sagittal length of nasal bones (nasion-rhinion)	QN, O	Wood, 1991
*F12	Superior breadth of nasal bones (max chord distance across the paired nasal bones at their proximal end)	QN, O	Wood, 1991
F13	Inferior breadth of nasal bones (maximum chord distance across the paired nasal bones at their distal end)	QN, O	Wood, 1991
F14	Zygomaxillare-porion	QN, O	Wood, 1991
*F15	Upper facial prognathism	QN, O	Chamberlain, 1987
*F16	Lower facial prognathism	QN, O	Chamberlain, 1987

F17	Lacrimal bone position	QL, O	Szalay and Delson, 1979; Strasser and Delson, 1987; Benefit and McCrossin, 1993
F18	Medial orbital wall composition	QL, O	Trevor-Jones, 1972
F19	Presence/Absence of maxillary fossae	QL, O	Szalay and Delson, 1979
*F20	Development of maxillary fossae	QL, O	Gilbert, 2007
F21	Maxillary ridge in males	QL, O	General
F22	Muzzle dorsum outline	QL, U	General
F23	Contact of maxillary frontal processes	QL, O	General
F24	Frontal/premaxilla contact	QL, O	General
F25	Maxillary sinus	QL, O	Rae and Koppe, 2003; Rae, 2008
F26	Positioning of the zygomatic foramina	QL, U	General
F27	Projection of nasal bones	QL, O	General
F28	Glabella prominence	QL, O	General
F29	General facial profile in lateral view	QL, O	General
F30	Nasal bone orientation in lateral view	QL, O	Gilbert, 2007
F31	Nasal bone extension over nasal aperture	QL, O	Gilbert, 2007
F32	Anteorbital drop	QL, O	General
F33	Piriform profile	QL, O	General
*F34	Relative nasal length (nasion-rhinion / nasion-prosthion)	QN, O	Szalay and Delson, 1979; Groves, 1989
F35	Maximum nasal aperture height (rhinion-nasospinale)	QN, O	General
*P1	Maxillo-alveolar length (Prosthion to a point where the line joining the posterior borders of the maxillary tuberosities crosses the median plane)	QN, O	Wood, 1991
*P2	Maxillo-alveolar breadth (ectomolare-ectomolare)	QN, O	Wood, 1991

*P3	Incisive canal-palatomaxillary suture (distance between the posterior edge of the incisive canal and the palatomaxillary suture)	QN, O	Wood, 1991
P4	Upper incisor alveolar length (distance between prosthion and the midpoint of the interalveolar septum between I^2 and C)	QN, O	Wood, 1991
P5	Palatal height at M^1 (Height in the midline between an imaginary line joining the alveolar process at the midpoint of M^1 and the roof of the palate)	QN, O	Wood, 1991
P6	Upper premolar alveolare length (min distance between the midpoints of the interalveolar septa between C/P^3 and P^4/M^1)	QN, O	Wood, 1991
P7	Upper molar length (Min distance between the midpoint of the P^4/M^1 interalveolar septum and the most posterior of the walls of the M^3 alveoli)	QN, O	Wood, 1991
P8	Canine interalveolar distance (min distance between the upper canine alveoli)	QN, O	Wood, 1991
P9	Last premolar interalveolar distance (min distance between the palatal walls of the P^4 alveoli)	QN, O	Wood, 1991
*P10	Second molar interalveolar distance (min distance between the palatal walls of the M^2 alveoli)	QN, O	Wood, 1991
*P11	I^1 MD crown diameter (max crown diameter parallel to the cervical line)	QN, O	Wood, 1991
*P12	I^1 BL crown diameter (max crown diameter perpendicular to the basal part of the labial enamel surface)	QN, O	Wood, 1991
P13	C^1 MD crown diameter (max diameter of crown perpendicular to the labiolingual axis of the tooth)	QN, O	Wood, 1991
P14	C^1 BL crown diameter (max diameter of the crown in the labiolingual axis of the tooth)	QN, O	Wood, 1991
*P15	M^3 interalveolar distance (min distance between the inner aspect of the alveolar process at the midpoint of M^3)	QN, O	Wood, 1991
P16	Palate depth at incisive fossa (the most inferior point on the posterior margin of the incisive fossa in the midline to the line between the centers of the alveolar margin on the lingual sides of C^1s)	QN, O	Chamberlain, 1987
P17	Upper premolar ratio (P^4 crown area / M^1 crown area)	QN, O	Fleagle and McGraw, 1999; 2002
P18	Mesial compressed sulcus on upper male canine	QL, O	Szalay and Delson, 1979;

			Strasser and Delson, 1987
P19	Premaxilla Length (premaxillary suture at level of alveoli to prosthion)	QN, O	General
P20	Bilophodont molars	QL, O	General
P21	P^3 protocone relative to paracone	QL, O	Szalay and Delson, 1979
P22	M^3 distal loph reduction (BL width of M^3 mesial loph / BL width of M^3 distal loph)	QN, O	Szalay and Delson, 1979
P23	Upper I^1 shape	QL, O	Szalay and Delson, 1979; Strasser and Delson, 1987
P24	Upper I^2 shape	QL, O	Szalay and Delson, 1979; Strasser and Delson, 1987
P25	Female C^1 shape	QL, U	Szalay and Delson, 1979; Napier 1981; 1985
P26	Size of I^1 relative to I^2	QL, O	General
*P27	Canine size (canine crown area)	QN, O	General
*P28	Canine size dimorphism (male relative canine crown area / female relative canine crown area)	QN, O	General
P29	Upper molariform crown shape (M^2 BL max width / M^2 MD max length)	QN, O	Szalay and Delson, 1979
P30	Molar flare	QL, O	Szalay and Delson, 1979; Frost, 2001a; 2001b
P31	M^1 shape (BL width of mesial loph / BL width of distal loph)	QN, O	Szalay and Delson, 1979
P32	M^2 shape (BL width of mesial loph / BL width of distal loph)	QN, O	Szalay and Delson, 1979
*M1	Symphyseal height (min distance between the base of the symphysis and infradentale)	QN, O	Wood, 1991
*M2	Maximum sypmhyseal depth (max depth, at right angles to symphyseal height)	QN, O	Wood, 1991

M3	Corpus height at M_1	QN, O	Wood, 1991
M4	Corpus width at M_1 (max width at right angles to corpus height at M_1, taken at the midpoint of M_1)	QN, O	Wood, 1991
M5	Corpus height at M_3	QN, O	Wood, 1991
M6	Corpus width at M_3 (max width at right angles to corpus height at M_3, taken at the midpoint of M_3)	QN, O	Wood, 1991
*M7	Lower premolar alveolar length (min distance between the midpoints of the interalveolar septa between C/P_3 and P_4/M_1)	QN, O	Wood, 1991
M8	Lower molar alveolar length (min distance between the midpoints of the interalveolar septa between P_4/M_1 and the most posterior of the walls of the M_3 alveolus)	QN, O	Wood, 1991
M9	P_4 max mesiodistal crown diameter	QN, O	Wood, 1991
M10	P_4 max buccolingual crown diameter	QN, O	Wood, 1991
M11	M_1 max mesiodistal crown diameter	QN, O	Wood, 1991
M12	M_1 max buccolingual crown diameter	QN, O	Wood, 1991
M13	M_2 max mesiodistal crown diameter	QN, O	Wood, 1991
M14	M_2 max buccolingual crown diameter	QN, O	Wood, 1991
M15	Lower premolar ratio (P_4 crown area / M_1 crown area)	QN, O	Fleagle & McGraw, 1999; 2002
M16	P_3 distal cingulum	QL, O	Szalay and Delson, 1979
M17	Buccal face of P_4 crown	QL, O	Szalay and Delson, 1979
M18	P_4 mesiobuccal flange, an extension of the enamel cap down onto the root	QL, O	Szalay and Delson, 1979
M19	Lower molar hypoconulid	QL, O	Szalay and Delson, 1979
M20	M_3 tuberculum sextum	QL, O	General
M21	Enamel folding	QL, O	Szalay and Delson, 1979
M22	Lophid orientation relative to the mandibular corpus	QL, O	Szalay and Delson, 1979
M23	Accessory cuspules in lower molar notches	QL, O	Szalay and Delson,

			1979
M24	Lower incisor lingual enamel	QL, O	Szalay and Delson, 1979
M25	Shape of lower I_2 distal surface	QL, O	Szalay and Delson, 1979
M26	Mandibular ramus angle	QL, O	Jolly, 1972; Szalay and Delson, 1979
M27	Gonial region expansion on mandibular ramus	QL, O	General
M28	Inferior portion mandibular symphysis length as scored to a specific tooth in occlusal view	QL, U	General
M29	Median mental foramen	QL, O	Szalay and Delson, 1979
M30	Mental ridges on the symphysis in males	QL, O	Szalay and Delson, 1979
M31	Development of mandibular corpus fossae	QL, O	Gilbert, 2007
M32	Width of the extramolar sulcus	QL, O	General
M33	Lingual mental foramina positioning	QL, U	Gilbert, 2007
*M34	P_4 crown shape (P_4 max BL width / P_4 max MD length)	QN, O	General
M35	M_1 crown shape (M_1 max BL width / M_1 max MD length)	QN, O	General
*M36	M_2 crown shape (M_2 max BL width / M_2 max MD length)	QN, O	General
M37	P_3 lingual "bulge", i.e., P_3 crown obliquity	QL, O	General
M38	Lower molariform tooth shape (M_1 mesial lophid / M_1 distal lophid)	QN, O	Szalay and Delson, 1979
*M39	Mandibular profile (corpus height at M_1 / corpus height at M_3)	QN, O	Szalay and Delson, 1979
M40	Curve of Spee shape	QL, O	Eck and Jablonski, 1984; Delson and Dean, 1993
M41	Symphyseal sloping	QL, O	Frost, 2001b

BS1	Body Size	QL, O	Smith and Jungers, 1997; Delson et al., 2000; Fleagle, 1999

Notes: Variables are classified by cranial region as follows: C = Cranial vault and base; F = Face; P = Palate and Upper Dentition, M = Mandible and lower dentition

QN = Quantitative character

QL = Qualitative character

O = Ordered

U = Unordered

* Character determined to be influenced by allometry

Table 2.2 Detailed Definition of Qualitative Characters Used in This Study.

Variable	Detailed Definition
C17	States: 0 = absent, 1 = intermediate, 2 = present only posteriorly, 3 = intermediate, 4 = extends anteriorly. The distinction between states 2 and 4 is determined by whether the anteriormost point of the crest is well anterior to bregma or begins at or posterior to bregma. Crest is defined here as the meeting or contact of the temporal lines.
C18	States: 0 = absent, 1 = intermediate, 2 = post-glabellar depression present, 3 = intermediate, 4 = post-orbital sulcus present, 5 = polymorphic
*C19	Small Taxa States: 0 = medial (inferior margin of the meatus is medial to porion and thus overhung by a supermeatal roof), 1 = intermediate, 2 = Extended laterally relative to the medial state, but still medial to the lateral border of the neurocranium
	Large Taxa States: 0 = Extended laterally relative to the medial state, but still medial to the lateral border of the neurocranium, 1 = intermediate, 2 = lateral (inferior margin of the meatus is lateral to porion)
C20	States: 0 = not widely divergent (i.e., pinched or slightly divergent), 1 = intermediate, 2 = widely divergent
C21	States: 0 = downturned, 1 = intermediate, 2 = upturned
*C25	Small Taxa States: 0 = absent, 1 = intermediate, 2 = partial crest confined to the lateral third of bi-asterionic breadth
	Large Taxa States: 0 = partial crest confined to the lateral third of bi-asterionic breadth, 1 = intermediate, 2 = extensive crest extending almost the entire distance between inion and the lateral margin of the supramastoid crest
C26	States: 0 = parietal/asterionic notch absent, 1 = intermediate, 2 = parietal/asterionic notch present
*C27	Small Taxa States: 0 = tympanic fused with postglenoid, 1 = intermediate, 2 = tympanic unfused and separated from the postglenoid process
	Large Taxa States: 0 = tympanic unfused and separated from the postglenoid process, 1 = intermediate, 2=tympanic unfused and widely separated from the tympanic
C28	States: 0 = very tall, 1 = intermediate, 2 = normal, 3 =intermediate, 4 = shortened
C29	States: 0 = present, 1 = intermediate, 2 = absent
C31	States: 0 = basion is well posterior to the line, 1 = intermediate, 2 = basion approximates the line, 3 = intermediate, 4 = basion is well anterior to the line

C32	States: 0 = small, 1 = intermediate, 2 = large
C40	States: 0 = absent, 1 = intermediate, 2 = present
*C41	Small Taxa States: 0 = divergent posteriorly, 1 = intermediate
	Large Taxa States: 0 = intermediate, 1 = parallel
*C42	Small Taxa States: 0 = moderately divergent, 1 = intermediate, 2 = strongly divergent
	Large Taxa States: 0 = intermediate, 1 = moderately divergent, 2 = intermediate
C43	States: 0 = not incised, 1 = intermediate, 2 = incised
C44	States: 0 = vomer non-inflated, 1 = intermediate, 2 = vomer inflated
C45	States: 0 = meet at one point, 1 = intermediate, 2 = separated by another bone, 3 = intermediate, 4 = palatine doesn't reach vomer, 5 = polymorphic
*C46	Small Taxa States: 0 = intermediate, 1 = another bone between
	Large Taxa States: 0 = clean contact, 1 = intermediate
C47	States: 0 = medially positioned, 1 = intermediate, 2 = laterally positioned
C48	States: 0 = absent or poorly defined, 1 = intermediate, 2 = present and clearly visible, 3 = intermediate, 4 = deeply excavated and sharply defined
F17	States: 0 = extends outside the orbit, 1 = intermediate, 2 = within orbit
F18	States: 0 = vomer contribution (frontal covers ethmoid), 1 = ethmoid contribution
F19	States: 0 = absent, 1 = intermediate, 2 = present
*F20	Given present in F19, Small Taxa States: 0 = extend up to the infraorbital plate, 1 = intermediate, 2 = invades infraorbital plate, 3 = intermediate, 4 = deeply invades the infraorbital plate
	Given present in F19, Large Taxa States: 0 = superior to alveolus only, 1 = intermediate, 2 = extend up to the infraorbital plate, 3 - intermediate, 4 = invades infraorbital plate
F21	States: 0 = absent, 1 = intermediate, 2 = present
F22	States: 0 = rounded, 1 = intermediate, 2 = peaked, 3 = intermediate, 4 = flat, 5 = polymorphic between states 0 and 4, 6 = polymorphic between states 0, 2, and 4
F23	States: 0 = frontal processes of maxillae do not meet in the midline, 1 = intermediate, 2 = frontal processes of maxillae meet in the midline
F24	States: 0 = absent, 1 = intermediate, 2 = present
F25	States: 0 = absent, 1 = present

F26	States: 0 = no foramina observable, 1 = intermediate, 2 = at or below plane of orbital rim, 3 = intermediate, 4 = foramina above and below the plane of the orbital rim, 5 = intermediate, 6 = above plane of orbital rim, 7 = polymorphic
F27	States: 0 = nasal bones do not project above the frontal/maxillary suture, 1 = intermediate, 2 = nasal bones project above the frontal/maxillary suture
F28	States: 0 = glabella not prominent, 1 = intermediate, 2 = glabella prominent
F29	States: 0 = straight, 1 = intermediate, 2 = concave
F30	States: 0 = straight (after anteorbital drop, if present), 1 = intermediate, 2 = slightly upturned, 3 = intermediate, 4 = upturned
F31	States: 0 = no extension, 1 = intermediate, 2 = slight extension, 3 = intermediate, 4 = significant extension, 5 = polymorphic
F32	States: 0 = absent, 1 = intermediate, 2 = present
F33	States: 0 = no anteorbital drop, distinct point at rhinion, 1 = intermediate, 2 = anteorbital drop, distinct point at rhinion, 3 = intermediate, 4 = anteorbital drop, no distinct point at rhinion
P18	States: 0 = present on the crown only, 1 = present and extends onto root
P20	States: 0 = incomplete bilophodonty, 1 = intermediate, 2 = complete bilophodonty
P21	States: 0 = protocone strongly reduced or absent, 1 = protocone present and significantly shorter than paracone, 2 = paracone present and nearly equal in height to the paracone
P23	States: 0 = rhomboidal, 1 = spatulate (defined as lingually cupped with flare, not flare by itself)
P24	States: 0 = caniniform, 1 = apically and mesially inclined
P25	States = 0 = “masculine”, 1 = intermediate, 2 = conical, 3 = intermediate, 4 = incisiform
P26	States: 0 = $I^1 \sim I^2$, 1 = intermediate, 2 = $I^1 > I^2$
P30	States: 0 = Low level of flare, 1 = intermediate level of flare, 2 = high level of flare
M16	States: 0 = absent, 1 = present
M17	States = 0 =straight as seen in occlusal view, 1 = intermediate, 2 = inflated as seen in occlusal view
M18	States: 0 = absent, 1 = present
M19	States: 0 = Hypoconulid present in all lower molariform teeth, 1 = intermediate, 2 = Hypoconulid absent in all lower molariform teeth except M_3, 3 = intermediate, 4 = Hypoconulid absent in all lower molariform teeth
M20	States: 0 = absent, 1 = intermediate, 2 = present
M21	States: 0 = non-elevated, 1 = elevated

M22	States: 0 = transverse, 1 = intermediate, 2 = oblique
M23	States: 0 = absent, 1 = intermediate, 2 = present
M24	States: 0 = absent, 1 = present
M25	States: 0 = straight, 1 = intermediate, 2 = bulge, 3 = intermediate, 4 = distinct prong
M26	States: 0 = inclined, 1 = intermediate, 2 = vertical
M27	States: 0 = absent, 1 = intermediate, 2 = present
M28	States: 0 = P_3, 1 = intermediate, 2 = P_3-P_4, 3 = intermediate, 4 = P_4, 5 = intermediate, 6 = P_4-M_1, 7 = intermediate, 8 = M_1, 9 = polymorphic
M29	States: 0 = absent, 1 = present
M30	States: 0 = absent, 1 = intermediate, 2 = present
M31	States: 0 = absent, 1 = intermediate, 2 = present
M32	States: 0 = narrow, 1 = intermediate, 2 = moderate, 3 = intermediate, 4 = wide
M33	States: 0 = present- single, 1 = intermediate, 2 = present- horizontally positioned, 3 = intermediate, 4 = present- vertically positioned, 5 = intermediate, 6 = present- variably positioned, 7 = polymorphic
M37	States: 0 = lingual bulge absent (not oblique), 1 = lingual bulge is present (oblique)
M40	States: 0 = normal, 1 = intermediate, 2 = reversed
M41	States: 0 = absent, 1 = intermediate, 2 = present (sloping), 3 = intermediate, 4 = present, extremely sloping
BS1	0 = Small Taxa, 1 = Large Taxa

Notes: Variables are classified by cranial region as follows: C = Cranial vault and base; F = Face; P = Palate and Upper Dentition, M = Mandible and lower dentition

* Character determined to be influenced by allometry

Table 2.3. Taxa and Sample Sizes For Characters Used In This Study.

Taxon	Sample Size (Males, Females)	Characters	Sources
Allenopithecus	(X, X)	C1-C16, C22-C23, F1-F16, F34, P1-P16, P27-P28, M1-M14, M34-M36, M39	Chamberlain (1987) Collard and Wood (2000; 2001)
	(X, X)	P17	Fleagle and McGraw (2002)
	(X, X)	M15	Fleagle and McGraw (2002)
	(X, X)	C33-C39, F35	This Study
	(X, X)	P19	This Study
	(X, X)	P22	Swindler, 2002
	(X, X)	P29, P33	Swindler, 2002
	(X, X)	P32	Swindler, 2002
	(X, X)	M38	Swindler, 2002
	(6, 6)	Qualitative Characters (except C47 and C48)	This Study
	(6, 6)	C47	This Study
	(6, 6)	C48	This Study
Cercocebus	(20, 20)	C1-C16, C22-C23, F1-F16, F34, P1-P16, P27-P28, M1-M14, M34-M36, M39	Chamberlain (1987) Collard and Wood (2000; 2001)
	(13, 7)	P17	Fleagle and McGraw (2002)
	(12, 7)	M15	Fleagle and McGraw (2002)
	(11, 11)	C33-C39, F35	This Study

	(6, 8)	P19	This Study
	(6, 2)	P22	Swindler, 2002
	(10, 8)	P29, P33	Swindler, 2002
	(14, 10)	P32	Swindler, 2002
	(13, 10)	M38	Swindler, 2002
	(47, 24)	Qualitative Characters (except C47 and C48)	This Study
	(16, 11)	C47	This Study
	(30, 16)	C48	This Study
Lophocebus	(20, 20)	C1-C16, C22-C23, F1-F16, F34, P1-P16, P27-P28, M1-M14, M34-M36, M39	Chamberlain (1987) Collard and Wood (2000; 2001)
	(15, 7)	P17, M15	Fleagle and McGraw (2002)
	(11, 9)	C33-C39, F35	This Study
	(6, 6)	P19	This Study
	(18, 18)	P22	Swindler, 2002
	(29, 27)	P29	Swindler, 2002
	(30, 28)	P32	Swindler, 2002
	(29, 25)	P33	Swindler, 2002
	(30, 27)	M38	Swindler, 2002
	(60, 55)	Qualitative Characters (except C47 and C48)	This Study
	(32, 25)	C47	This Study
	(31, 27)	C48	This Study

Macaca	(20, 20)	C1-C16, C22-C23, F1-F16, F34, P1-P16, P27-P28, M1-M14, M34-M36, M39	Chamberlain (1987) Collard and Wood (2000; 2001)
	(9, 13)	P17, M15	Fleagle and McGraw (2002) Gilbert (2007)
	(10, 10)	C33-C39, F35	This Study
	(6, 6)	P19	This Study
	(44, 29)	P22	Swindler, 2002
	(57, 46)	P29	Swindler, 2002
	(64, 49)	P32	Swindler, 2002
	(56, 47)	P33	Swindler, 2002
	(58, 52)	M38	Swindler, 2002
	(78, 68)	Qualitative Characters (except C47 and C48)	This Study
	(19, 20)	C47	This Study
	(10, 9)	C48	This Study
Mandrillus	(42, 20)	C1-C16, C22-C23, F1-F16, F34, P1-P16, P27-P28, M1-M14, M34-M36, M39	Chamberlain (1987) Collard and Wood (2000; 2001)
	(13, 6)	P17	Fleagle and McGraw (2002)
	(14, 6)	M15	Fleagle and McGraw (2002)
	(10, 6)	C33-C39, F35	This Study
	(6, 6)	P19	This Study

	(6, 4)	P22, P29, P32, P33, M38	This Study
	(25, 28)	Qualitative Characters (except C47 and C48)	This Study
	(10, 7)	C47	This Study
	(10, 13)	C48	This Study
Papio	(20, 19)	C1-C16, C22-C23, F1-F16, F34, P1-P16, P27-P28, M1-M14, M34-M36, M39	Chamberlain (1987) Collard and Wood (2000; 2001)
	(14, 7)	P17, M15	Fleagle and McGraw (2002)
	(8, 5)	C33-C39, F35	This Study
	(15, 5)	P19	This Study
	(24, 20)	P22	Swindler, 2002
	(37, 31)	P29	Swindler, 2002
	(38, 36)	P32	Swindler, 2002
	(36, 29)	P33	Swindler, 2002
	(37, 36)	M38	Swindler, 2002
	(118, 48)	Qualitative Characters (except C47 and C48)	This Study
	(32, 11)	C47	This Study
	(20, 5)	C48	This Study
Theropithecus	(22, 22)	C1-C16, C22-C23, F1-F16, F34, P1-P16, P27-P28, M1-M14, M34-M36, M39	Chamberlain (1987) Collard and Wood (2000; 2001)

(5, 2)	P17, M15	Fleagle and McGraw (2002)
(8, 3)	C33-C39, F35	This Study
(4, 2)	P19	This Study
(37, 20)	P22	Swindler, 2002
(18, 9)	P29	Swindler, 2002
(14, 15)	P32	Swindler, 2002
(22, 19)	P33	Swindler, 2002
(12, 11)	M38	Swindler, 2002
(14, 6)	Qualitative Characters (except C47 and C48)	This Study
(10, 5)	C47	This Study
(15, 6)	C48	This Study

Notes: Sample sizes listed for qualitative characters represent averages; individual characters vary depending on the preservation of the specimens examined.

Table 2.4. Summary of Most Parsimonious Phylogenetic Trees Produced From Exhaustive Searches In PAUP 4.10b With Bootstrap Support For Various Clades.

						Bootstrap Support, %			
Analysis	**Tree Length**	**CI**	**RI**	**RC**	**HI**	***C/M***	***P/L/T***	***P/L***	***L/T***
Sex-Averaged	494	0.636	0.39	0.248	0.364	90%	91%	64%	X
Males	410	0.661	0.448	0.296	0.339	99%	100%	82%	X
Females	424	0.62	0.356	0.221	0.38	84%	X	X	53%
Combined-Sex	836	0.639	0.398	0.254	0.361	99%	98%	74%	X

Notes: Abbreviations are as follows: C/*M = Cercocebus/Mandrillus, P/L/T = Papio/Lophocebus/Theropithecus, P/L = Papio/Lophocebus, L/T = Lophocebus/Theropithecus*. There was no bootstrap support over 50% for the *Papio/Lophocebus/Theropithecus* clade found in the female most parsimonious tree.

Table 2.5. Selected Synapomorphies Suggested By Character Transformation Analyses.

	Sex-Averaged Synapomorphies	Character Reference
NODE 1 **African Papionins**	Wide Interorbital Distance, **Maxillary Fossae Present**, **Shallow Anterior Palate**, Mandibular Corpus Fossae Present	F6, **F19**, **P16**, M31
NODE 2 ***Cercocebus/Mandrillus***	Short Neurocranium (Glabella-Inion), Low Neurocranium (Basion-Bregma), Short Distance from Glabella to Bregma, **Short Parietal-Sagittal Chord (Bregma-Lambda)**, Widely Divergent Temporal Lines, **Upturned Nuchal Crests Across the Midline**, **Narrow Calvarium Relative to Length**, High Cranial Vault Index, Short Foramen Magnum, **Short Basisphenoid**, Non-divergent Posterior Edges of the Medial Pterygoid Plates, **Medially Positioned Inferior Petrous Process**, Short Malar Height, Narrow Nasal Aperture, Low Degree of Upper Facial Prognathism, **Shallow Maxillary Fossae**, Long Upper Premolar Row, **Narrow Posterior Palate, Large Upper Premolars, Large Canines, Large Canine Sexual Dimorphism**, Long Lower Premolar Row, **Large Lower Premolars**, Straight I_2 Distal Surface, Ho**rizontally Positioned Lingual Mental Foramina**	C1, C2, C5, **C7**, C20, **C21**, **C22**, C23, C30, **C39**, C42, **C47**, F8, F9, F15, **F20**, P6, **P15**, **P17**, **P27**, **P28**, M7, **M15**, M25, **M33**
NODE 3 ***Papio/Lophocebus/ Theropithecus***	Broad Distance Between the Carotid Canals, Wide Calvarium Relative to Length, **Wide Neurocranium (Bieuryonic Breadth)**, **Broad Infratemporal Region**, Broad Posterior Basioccipital (Breadth across jugular foramina), **Deep/Extensive Maxillary Fossae**, Narrow Upper Canines (BL), Small Upper Premolars, Shallow Palate, **Small Upper Premolars, Small Canines, Small Canine Sexual Dimorphism**, Narrow Lower P_4, **Small Lower Premolars**, Deep Mandibular Corpus Fossae	C14, C22, **C34**, **C35**, C38, **F20**, P14, P16, **P17**, **P27**, **P28**, M10, **M15**, M31
NODE 4 ***Papio/Lophocebus***	Long Parietal-Lambdoid Chord, Thin Parietals, **Broad Distance Between the Petrous Apices**, Downturned Nuchal Crests Across the Midline, Long Foramen Magnum, Broad Anterior Basioccipital (distance across basioccipital synchondrosis), Wide Nasal Bones Superiorly, Broad Mid-Palate, Wide/Long Upper Canines (MD), Narrowest Upper Canines (BL), **Broad Posterior Palate, Long Premaxilla**, Shallow Mandibular Symphysis, Narrow Posterior Mandibular Corpus, **Mandibular Profile Deepens Distally from M_1-M_3**	C8, C13, **C15**, C21, C30, C37, F12, P10, P13, P14, **P15**, **P19**, M2, M6, **M39**

Male Synapomorphies		
NODE 1 **African Papionins**	Wide Interorbital Distance, **Maxillary Fossae Present**, **Shallow Anterior Palate**, Mandibular Corpus Fossae Present	F6, **F19**, **P16**, M31
NODE 2 ***Cercocebus/Mandrillus***	Short Neurocranium (Glabella-Inion), Low Neurocranium (Basion-Bregma), **Short Parietal-Sagittal Chord (Bregma-Lambda)**, Narrow Distance Between the Carotid Canals, Widely Divergent Temporal Lines, **Upturned Nuchal Crests Across the Midline, Narrow Calvarium Relative to Length**, Short Foramen Magnum, Long Occipital (Opisthion-Inion), **Short Basisphenoid**, **Medially Positioned Inferior Petrous Process**, Short Malar Height, Narrow Nasal Aperture, Low Degree of Upper Facial Prognathism, **Shallow Maxillary Fossae**, Straight Nasal Bones in Lateral Profile, Long Upper Premolar Row, **Narrow Posterior Palate, Large Upper Premolars, Large Canines, Large Canine Sexual Dimorphism**, **Long Lower Premolar Row, Large Lower Premolars**, Straight I_2 Distal Surface, **Horizontally Positioned Lingual Mental Foramina**, Broad Mesial Lophid on Lower Molars	C1, C2, **C7**, C14, C20, **C21**, **C22**, C30, C33, **C39**, **C47**, F8, F9, F15, **F20**, F30, P6, **P15**, **P17**, **P27**, **P28**, **M7**, **M15**, M25, **M33**, M38
NODE 3 ***Papio/Lophocebus/ Theropithecus***	Tall Neurocranium (Basion-Bregma), Long Distance from Glabella to Bregma, Long Parietal-Lambdoid Chord, Broad Foramen Magnum, Long Occipital Condyle, Thin Parietals, Broad Distance Between the Carotid Canals, Long Foramen Magnum, **Wide Neurocranium (Bieuryonic Breadth)**, **Broad Infratemporal Region**, Broad Posterior Basioccipital (Breadth across jugular foramina), **Deep/Extensive Maxillary Fossae**, Tall Nasal Aperture, **Small Upper Premolars, Small Canines, Small Canine Sexual Dimorphism**, Short Lower Premolar Row, **Small Lower Premolars**	C2, C5, C8, C11, C12, C13, C14, C30, **C34**, **C35**, C38, **F20**, F35, **P17**, **P27**, **P28**, M7, **M15**
NODE 4 ***Papio/Lophocebus***	Broad Anterior Neurocranium (Min. Frontal Breadth), **Broad Distance Between the Petrous Apices**, Downturned Nuchal Crests Across the Midline, Reduced Post-Orbital Constriction, Broad Anterior Basioccipital (distance across basioccipital synchondrosis), Wide Nasal Bones Superiorly, Low Degree of Lower Facial Prognathism, Long Upper Incisor Row, Broad Anterior Palate, Broad Mid-Palate, MD Long Upper Incisors, BL Broad Upper Incisors, Wide/Long Upper Canines (MD), **Broad Posterior Palate, Long Premaxilla**, Short Mandibular Symphysis,	C3, **C15**, C21, C24, C37, F12, F16, P4, P8, P10, P11, P12, P13, **P15**, **P19**, M1, M2, **M39**

Shallow Mandibular Symphysis, **Mandibular Profile Deepens Distally from M_1-M_3**

	Female Synapomorphies	
NODE 1 **African Papionins**	**Maxillary Fossae Present**, Tall Nasal Aperture, Narrow Upper Canines (BL), **Shallow Anterior Palate**	**F19**, F35, P14, **P16**
NODE 2 ***Cercocebus/Mandrillus***	**Short Parietal-Sagittal Chord (Bregma-Lambda)**, Widely Divergent Temporal Lines, **Upturned Nuchal Crests Across the Midline, Narrow Calvarium Relative to Length, High Cranial Vault Index, Short Basisphenoid,** Non-divergent Posterior Edges of the Medial Pterygoid Plates, **Medially Positioned Inferior Petrous Process, Short Malar Height, Shallow Maxillary Fossae, Narrow Posterior Palate, Large Upper Premolars, Large Canines, Large Canine Sexual Dimorphism, Long Lower Premolar Row, Large Lower Premolars, Horizontally Positioned Lingual Mental Foramina**	**C7,** C20, **C21, C22, C23, C39,** C42, **C47**, **F8, F20, P15, P17, P27, P28, M7, M15, M33**
NODE 3 ***Papio/Lophocebus/ Theropithecus***	**Wide Neurocranium (Bieuryonic Breadth), Broad Infratemporal Region, Deep/Extensive Maxillary Fossae**, Narrow Maxilla (Ectomolare-Ectomolare), Short Upper Premolar Row, **Small Upper Premolars, Small Canines, Small Canine Sexual Dimorphism, Small Lower Premolars**, Deep Mandibular Corpus Fossae	**C34, C35, F20,** P2, P6, **P17, P27, P28, M15,** M31
NODE 4 ***Papio/Lophocebus***	Broad Distance Between the Carotid Canals, **Broad Distance Between the Petrous Apices**, Long Foramen Magnum, Broad Posterior Basioccipital (Breadth across jugular foramina), Short Alveolar Region (Nasospinale-Prosthion), Broad Superior Face (Frontomalaretemporale-Frontomalaretemporale), **Broad Posterior Palate, Long Premaxilla**, Narrow Posterior Mandibular Corpus, MD Short Lower P_4s, BL Narrow Lower M_2, **Mandibular Profile Deepens Distally from M_1-M_3**	C14, **C15**, C30, C38, F2, F3, **P15, P19**, M6, M9, M14, **M39**

Notes: Characters in bold are recognized as synapomorphies in all three analyses. Only those reconstructed synapomorphies that display low degrees of homoplasy are listed here.
MD = mesiodistal
BL = buccolingual

Chapter 3

Cladistic Analysis of Extant and Fossil African Papionins Using Craniodental Data

Abstract

This chapter examines extant and fossil African papionin phylogenetic history through a comprehensive cladistic analysis of craniodental morphology using both quantitative and qualitative characters. In order to account for the well-documented influence of allometry on the papionin cranium, the narrow allometric coding method was applied to characters determined to be significantly affected by allometry. Results of the analysis suggest that *Parapapio*, *Pliopapio*, and *Dinopithecus* are stem African papionin taxa. Crown Plio-Pleistocene African papionin taxa include *Gorgopithecus*, *Lophocebus*, *Procercocebus*, and *Papio quadratirostris*. Notable phylogenetic conclusions include the following: *Papio quadratirostris*, as defined by Delson and Dean (1993), is reconstructed here as being the sister taxon to the clade containing the extant taxa *Mandrillus* and *Cercocebus*; *Theropithecus baringensis* is strongly supported as a primitive member of that genus*; Gorgopithecus* is closely related to *Papio* and *Lophocebus;* and *Theropithecus* is a primitive crown African papionin taxon. Finally, character transformation analyses identify a series of morphological transformations during the course of papionin evolution. The origin of crown African papionins is defined, at least in part, by the appearance of definitive maxillary fossae. Among crown African papionins, *Papio*, *Lophocebus*, and *Gorgopithecus* are further united by the most extensive development of this feature. The *Mandrillus/Cercocebus/Procercocebus/Papio quadratirostris* clade is defined by upturned nuchal crests (especially in males), widely divergent temporal lines (especially in males), and a tendency to enlarge the premolars as an adaptation for hard-object food processing. The adaptive origins of the genus *Theropithecus* appear associated with a diet requiring an increase in temporalis musculature, the optimal placement of occlusal forces onto the molar battery, and an

increase in the life of the posterior dentition. This shift is associated with the evolution of distinctive morphological features such as the anterior union of the temporal lines, reversed Curve of Spee, and increased enamel infoldings.

Introduction

The large African cercopithecine primates, the Papionini (Order: Primates, Tribe: Papionini), include the living macaques (*Macaca*), mangabeys (*Lophocebus and Cercocebus*), baboons (*Papio*), geladas (*Theropithecus*), mandrills, and drills (*Mandrillus*). In addition to this diversity of extant taxa, papionin monkeys are widely present and abundant members of the Plio-Pleistocene African fossil record. Questions exist over which fossil taxa are legitimate species, the phylogenetic relationships of fossil taxa amongst themselves, and the phylogenetic relationships of fossil taxa to extant taxa. Given the relatively rich fossil record of this group, an analysis of morphological variation in a phylogenetic framework would seem a promising way to test a series of evolutionary hypotheses.

While previous phylogenetic analyses of African papionin morphological data produced phylogenies incongruent with molecular data (e.g., Szalay and Delson, 1979; Strasser and Delson, 1987; Delson and Dean, 1993; Collard and Wood, 2000; 2001), more recent studies note morphological characters whose distributions support relationships similar to those suggested by molecular data (Fleagle & McGraw, 1999; 2002; McGraw and Fleagle, 2006; Gilbert, 2007a). Most recently, Gilbert and Rossie (2007) and Gilbert (Chapter 2) have demonstrated that, when allometry is accounted for in phylogenetic analysis of papionin craniodental anatomy, morphological data can produce phylogenetic trees congruent with trees produced from molecular data. If such congruence is considered to be a test of the reliability of morphological data (Collard and Wood, 2000; 2001), then craniodental data seems perfectly suitable for phylogenetic analysis.

Given the increased confidence in papionin morphological data, this study presents a comprehensive craniodental phylogenetic analysis of both extant and fossil African papionin taxa. A major goal of this analysis is to place problematic

fossil taxa in a firm phylogenetic context. In addition, it should provide clearer resolution of character state evolution as well as behavioral and ecological adaptations during the highly successful Plio-Pleistocene papionin radiation in Africa.

Taxonomic Issues

Before performing a phylogenetic analysis, operational taxonomic units (OTUs) must be defined. Table 3.1 lists the taxa recognized and used in this study. Many of these fossil taxa are universally accepted; however, the status of some fossil taxa are disputed. With regard to these disputed taxa, I will briefly justify the alpha taxonomy advocated here.

Parapapio

Traditionally, five species of *Parapapio* have been widely recognized: *Pp. jonesi*, *Pp. broomi*, *Pp. whitei*, *Pp. antiquus*, and *Pp. ado* (e.g., Szalay and Delson, 1979; Leakey and Delson, 1987; Fleagle, 1999; Jablonski, 2002). Heaton (2006) has recently argued that *Pp. whitei* is invalid, and that the specimens formerly included in this taxon are best assigned to *Pp. broomi* and *Papio izodi*. I find these arguments unconvincing for a number of reasons[1]. In contrast to Heaton's (2006) analysis, *Pp. jonesi*, *Pp. broomi*, and *Pp. whitei* are all recognized as valid taxa in this analysis (Fig. 3.1).

[1] First, Heaton's (2006) analysis was based almost solely on specimens from Sterkfontein. The most distinctive specimens of *Pp. whitei* come from Makapansgat (e.g., MP 221, MP 223) and consist of fairly complete male crania that are, in my opinion, clearly different from the most complete male crania typically assigned to *P. broomi* (e.g., STS 564, M202). While *P. broomi* males display distinctive features such as flattened muzzles, relatively straight to slightly concave nasal profiles, relatively short muzzles, and well-defined, pinched temporal lines, *P. whitei* males contrastingly display features such as peaked nasals and muzzles, slightly concave and often concavo-convex nasal profiles, a relatively long skull, a relatively long muzzle, and pinched but less well-defined temporal lines (see Fig. 3.1). Second, Heaton's (2006) taxonomic assignments were based largely on analyses of dental dimensions and five qualitative characters, and no extant sample was provided for comparison. Since dental dimensions as well as the qualitative characters used in Heaton's (2006) analysis overlap extensively among extant papionin taxa, especially at the species level, their taxonomic value is probably limited until demonstrated otherwise. Additionally, previous analyses of dental dimensions have upheld the view of *Pp. whitei* as a valid taxon at Sterkfontein (Freedman, 1957; Freedman and Stenhouse, 1972). Finally, some of the sex assignments made by Heaton (2006) are almost certainly incorrect, and these incorrect assignments appear to have distorted the analysis.

More recently, the *Parapapio* taxon at Taung, *Pp. antiquus,* has been reassigned into its own genus, *Procercocebus* (Gilbert, 2007a). This assignment is accepted here. Further support for this hypothesis will be provided if the current analysis determines *Pr. antiquus* to have a phylogenetic position distinct from *Parapapio* taxa.

In contrast to the South African *Parapapio* taxa, the status of the East African species *Pp. ado* has not been recently challenged. *Pp. ado* is therefore accepted as a valid taxon and included in this analysis.

?Theropithecus baringensis

In 1969, Leakey described a partial papionin cranium with associated mandible (KNM-BC 2) from the Chemeron Formation as *Papio baringensis* (Leakey, 1969). A second specimen, a partial mandible, was later also assigned to this taxon (Leakey and Leakey, 1976). Eck and Jablonski (1984; 1987) subsequently questioned the validity of these specimens as *Papio*, and instead argued that they represented a member of the genus *Theropithecus*, specifically an early representative of the *T. brumpti* lineage. Delson and Dean (1993) provided yet another reassessment, concluding that the assignment to *Theropithecus* was questionable.

As Delson and Dean (1993) point out, part of the problem lies in the uncertainty of grouping the cranium and associated mandible with an unassociated and relatively unworn mandibular fragment (KNM-BC 1647). While the type specimen shows little indication of the distinctive *Theropithecus* molar pattern (e.g., enamel infoldings, columnar cusps, etc.), the isolated mandibular fragment does (Delson and Dean, 1993). It is possible, however, that the isolated mandibular fragment belongs instead to *T. brumpti*, which is documented in earlier strata

---

For example, Heaton (2006) assigns STS 563, an unambiguous female mandible that Broom (1940) designated as the type specimen of *P. whitei*, as a *P. broomi* male. This is not a credible assignment because the specimen clearly displays small canines as well as P_3s with very reduced honing flanges, features that are exclusively found in female papionins (for comparison of male vs. female mandibular specimens of *P. whitei*, see Figs. 41-44 in Freedman, 1957). These incorrect sex assignments lead to problematic taxonomic conclusions. For these reasons, *Pp. jonesi*, *Pp. broomi*, and *Pp. whitei* are all recognized as valid taxa in this study (Table 3.1).

(Delson et al., 2000; Leakey, pers. comm.). In light of the uncertainty, I follow Delson and Dean (1993) and recognize KNM-BC 2 as a possible member of *Theropithecus*, *?T. baringensis*. However, in the absence of more convincing morphological evidence, I do not accept the attribution of the isolated mandible to this taxon. Instead, I provisionally assign the isolated mandibular fragment to *T.* cf. *brumpti* until otherwise demonstrated. Pending the results of the current analysis, the taxonomic and phylogenetic status of KNM-BC 2 will be reassessed.

Papio quadratirostris

In 1982, a fairly complete cranium of a large papionin from the Usno formation of the Ethiopian Omo group was described as *Papio quadratirostris* (Iwamoto, 1982). Similar to the situation with KNM-BC 2, this specimen was soon reallocated to *Theropithecus* by Eck and Jablonski (1984, 1987), and it was also suggested to be an early member of the *T. brumpti* lineage. Delson and Dean (1993) challenged this assignment and argued that the Usno specimen was best left in the genus *Papio*, and noted particular affinities to *Dinopithecus*, which they recognized as a subgenus of *Papio*. Delson and Dean (1993) also went a step further and assigned later Omo material, as well as material from the Humpata Plateau in Angola, to *P. quadratirostris*. In contrast, Jablonski (1994) recognized the later Omo and Angolan material as *Theropithecus*, grouping it with the KNM-BC 2 specimen as *T. baringensis*.

With regard to the Usno skull, I find no convincing synapomorphies to link this specimen to *Theropithecus*. Therefore, for the purposes of this analysis, I follow Delson and Dean (1993) and recognize the Usno cranium as *P. quadratirostris*. However, while Delson and Dean (1993) make a convincing argument that the later Omo material and some of the Angolan material are extremely similar to each other, I consider the assignment of the later Omo material as well as the Angolan material to *P. quadratirostris* as problematic. For example, the later Omo material and the Angolan material are dentally distinct from the type Usno specimen in displaying very enlarged premolars. In addition, there is no good

overlapping craniofacial material that allows a proper comparison between the Usno skull and the later Omo and Angolan material. The only overlapping craniofacial material is a partial male frontal from Angola (DGUNL LEBA05) that is clearly different from the frontal and temporal line morphology displayed by the Usno specimen (Fig. 3.2). While the Angolan specimen displays pinched temporal lines that appear to converge quite quickly, the Usno specimen displays widely divergent temporal lines that do not converge until the back of the cranium.

Delson and Dean (1993), as well as Jablonski (1994), recognized only one papionin taxon among the Plio-Pleistocene sites in Angola. In contrast, I believe that at least two papionin taxa are probably represented among the Angolan specimens. As mentioned above, some of the craniodental material from Angola resembles the later Omo material, particularly a few dental specimens with large premolars and a partial female cranium (see Table 3.1 for list of specimens). However, other Angolan specimens are dissimilar to those from the Omo, such as the partial male frontal DGUNL LEBA05 as well as a number of dental specimens with small premolars and a partial male mandible with a *Theropithecus*-like dentition (CAN 30 '90). In addition, a large number of the Angolan specimens are subadults, so in these cases it is not possible to be confident about their adult morphologies.

On a more theoretical level, no other Plio-Pleistocene site in South Africa contains only one papionin taxon, and it is improbable that the situation among a handful of sites on the Angolan Humpata Plateau is any different. I am also skeptical of any hypothesis arguing that two large papionin taxa are unlikely to coexist in the same region. There are many regions of Africa today where the geographical ranges of multiple papionin taxa overlap, including large-bodied species. In East Africa, the geographical ranges of *Theropithecus* and *Papio* overlap in sections of Ethiopia. In western Africa, it is likely that the ranges of *Mandrillus* and *Papio* overlap in certain regions. It is also widely recognized that populations of *Papio* baboons, traditionally recognized as separate species, intermingle and interbreed in hybrid zones all across Africa. Finally, it must be recognized that the Angolan fossils accumulated over an unknown amount of time, potentially

thousands if not hundreds of thousands of years. Given the unknown amount of time-averaging, it is entirely possible that multiple taxa are preserved in Angola that never came into contact during their lifespan in that region. Given these facts, I find it probable that multiple species are represented within the Angolan material. Given the clear affinities between some of the dental material as well as the partial adult female cranium preserved in the Angolan breccias to the late Omo material, I recognize the specimens with large premolars and other morphologies similar to the Omo material as one taxon, and the remaining material as Cercopithecidae sp. indet. (see Table 3.1).

In summary, I consider it prudent to recognize the Usno cranium, later Omo material, as well as some of the Angolan papionin material as separate taxonomic units for the purpose of this analysis. If Delson and Dean's (1993) hypothesis is correct, and all of the above material is closely related, then the Usno specimen, later Omo material, and selected Angolan material, as recognized here (see above), should be reconstructed as a clade in this analysis.

Papio izodi

Multiple species of small-bodied *Papio* have been recognized previously in the South African Plio-Pleistocene record: *P. izodi*, *P. angusticeps*, and *P. wellsi* (e.g., Gear, 1926; Broom, 1940; Freedman, 1957; 1961; 1965). Given the variability in the extant species of *Papio*, it is probably best to recognize the separate populations of small-bodied Plio-Pleistocene *Papio* as one variable taxon with multiple subspecies. Therefore, I broadly follow Szalay and Delson (1979) as well as Jablonski (2002) and recognize only one taxon, *Papio izodi,* in this analysis; I would rank the various populations of small-bodied *Papio* as subspecies (e.g., *P. i. izodi*, *P. i. wellsi*, and *P. i. angusticeps*).

Papio robinsoni

In addition to *P. izodi*, a larger *Papio* taxon has been recognized in the South African Plio-Pliestocene, namely *P. robinsoni*. Szalay and Delson (1979) and Jablonski (2002) recognize *P. robinsoni* only as a subspecies of the living *P. hamadryas* (*P. h. robinsoni*). I follow this assignment here. Given that the extant populations of *P. hamadryas* are already represented in this study, *P. h. robinsoni* is excluded from this analysis.

Theropithecus oswaldi

Nearly all authors recognize that *Theropithecus darti* and *Theropithecus oswaldi* represent an evolving lineage through time (e.g., Jolly, 1972; Dechow and Singer, 1984; Eck and Jablonski, 1987; Eck, 1993; Leakey, 1993; Delson, 1993; Frost, 2001a; 2001b; 2007; Frost and Delson, 2002; Jablonski, 2002; Gilbert, 2007b). I have previously argued that it is best to recognize the earlier and smaller-bodied populations as a separate chronospecies (*T. darti*) from the larger and morphologically distinct later populations (*T. oswaldi*) (Gilbert, 2007b). However, Leakey (1993), and most recently Frost (2007), make excellent arguments that it is best to divide the entire chronolineage into three chronosubspecies of *T. oswaldi*: *T. o. darti*, *T. o. oswaldi*, and *T. o. leakeyi*. Given the continuous nature of the morphological transformations through time, this taxonomic scheme is probably the most biologically meaningful and informative. I follow this arrangement in this study. For the analysis, I use only specimens of *T. o. darti* because these represent the most conservative specimens of the lineage and are more likely to be phylogenetically informative than the extremely large and derived later chronosubspecies *T. o. oswaldi* and *T. o. leakeyi* (see Table 3.1).

Methods

Complete character lists with definitions and character states are presented in Tables 3.2-3.3. Extant taxa and sample sizes are the same as those presented in Chapter 2. Fossil taxa and sample sizes are presented in Table 3.1.

For analysis, males and females were coded separately and then combined into a larger "combined-sex" matrix. Phylogenetic analyses involving many fossil taxa often run into problems because of large amounts of missing data. One way to combat these problems is to increase the number of characters used in the analysis (Wiens, 2003a; 2003b; 2006; Wiens et al., 2005). Increasing the number of characters in an analysis has been repeatedly demonstrated to increase overall phylogenetic accuracy and help resolve character conflict that can hamper fossil analyses with large amounts of missing data (Wiens, 2003a; 2003b; 2006; Wiens et al., 2005). In this case, combining characters that have been scored separately for males and females allows for both unique male and female character states that are phylogenetically informative to be sampled together during the analysis and potentially increase the strength and accuracy of the phylogenetic signal (see also Chapter 2). In total, 314 craniodental characters were included: 88 quantitative characters, and 69 qualitative characters coded for each sex (see Table 2 for full character list with sources). No postcranial data are included here because most of the postcranial material in the fossil record is unassociated and cannot be attributed to specific taxa.

Victoriapithecus, *Parapapio lothagamensis*, and *Macaca* were assigned as the outgroups for all analyses. While *Pp. lothagamensis* and *Macaca* were scored and used as the outgroup for both quantitative and qualitative characters, *Victoriapithecus* was scored and used as an outgroup for qualitative characters only. Because many quantitative characters were coded on the basis of narrow allometries, *Victoriapithecus* is not an appropriate outgroup for these characters since the allometric trajectory influencing the craniodental morphology of *Victoriapithecus* is not directly comparable to that observed in papionin monkeys. A phenetically distant taxon such as *Victoriapithecus* should not be used as an outgroup for these quantitative craniometric characters (Lockwood et al., 2004; Gaffney, 1979; Gilbert and Rossie, 2007). However, the inclusion of multiple outgroups has been demonstrated to increase phylogenetic accuracy, and since *Victoriapithecus* is universally recognized as a primitive cercopithecoid monkey, this taxon was scored and included as an outgroup for all qualitative characters.

While *Pp. lothagamensis* currently shares its generic name with other *Parapapio* taxa, it is clear from its published description (Leakey et al., 2003) as well as my own personal observations that this taxon is the most primitive papionin in the fossil record. *P. lothagamensis* shares a number of features with *Victoriapithecus* (including incomplete bilophodonty in some specimens, particularly subadults), and these features suggest that *Pp. lothagamensis* is probably more primitive than *Macaca*. For these reasons, *Pp. lothagamensis* is assigned as an outgroup rather than included with its congeners as an ingroup for the analysis. It is likely that *Pp. lothagamensis* is both primitive and distinct enough from later *Parapapio* taxa to deserve its own generic rank; however, I will leave this taxonomic decision up to the original authors of *Pp. lothagamensis* (Leakey et al., 2003). Given that *Macaca* is universally accepted as the sister taxon of the African papionins, it is also assigned as an outgroup for all analyses.

Values for quantitative characters were taken from original fossils, casts of original fossils, and measurements from the literature. Qualitative characters were scored on original fossils and casts. In a small number of cases, published descriptions and photographs of fossil material was used to assess qualitative states.

As described in the previous chapter, each type of character requires slightly different rules and techniques for assigning character states. For quantitative characters, an isometric size correction was first applied separately to the two separate elements of the skull (the cranium and the mandible) because these elements are rarely found associated in the fossil record. Ideally, in the current data set of 62 standard craniometric measurements for each extant specimen[*], cranial quantitative characters would be divided by the geometric mean of the 48 cranial measurements for that specimen and mandibular quantitative characters divided by the geometric mean of the 14 mandibular measurements for that specimen. However, for fossil taxa, the same set of measurements used to calculate these geometric means for extant specimens are unlikely to be preserved. To account for this reality, regression analyses of all the measurements used to calculate the geometric means for each extant specimen were performed separately for extant male and female specimens. The individual cranial measurement and mandibular

[*]The 62 measurements from Collard and Wood (2000; 2001) were used for the calculation of the geometric mean for each taxon (see Chapter 4).

measurement 1) with the highest correlation coefficient relative to the cranial and mandibular geometric means, and 2) commonly preserved in the fossil record, were then used as size corrections for each extant and fossil cranial and mandibular specimen. For the current analysis, the cranial measurement P2 (see Tables 3.2-3.3, maxillo-alveolar breadth defined as biectomolare, $r = 0.948$) and the mandibular measurement M11 (M_1 max mesiodistal crown diameter, $r = 0.935$) were used for male specimens and the measurements P2 ($r = 0.921$) and M12 (M_1 max buccolingual crown diameter, $r = 0.936$) were used as size corrections for female specimens. Regression analyses of the P2 (males and females) and M11 (males) measurements determined that these features were positively allometric. This suggests that using these measurements as size-adjustments results in a slight over-adjustment at large body sizes. However, a slight systematic over-adjustment at large body size was deemed preferable to using different measurements with much lower correlation coefficients and much lower rates of preservation in the fossil record.

After these size corrections, the resulting values for each character represented some aspect of "shape" (*sensu* Mosimann, 1970; also see Darroch and Mosimann, 1985). By definition, allometrically influenced characters are those whose shape is significantly correlated with size (Mosimann and James, 1979). Quantitative characters determined to be allometrically influenced have been identified in previous analyses of extant taxa (Gilbert and Rossie, 2007; see chapter 2), and these same characters were considered to be allometrically influenced in this analysis as well (see Tables 3.2-3.3 for the complete list of allometrically influenced characters). Due to their correlation with body size, these characters are not independent, and they are not suitable for phylogenetic analysis without some sort of character correction. For any quantitative character determined to be allometrically influenced, the narrow allometric coding method was employed to disentangle the effects of allometry (see Gilbert and Rossie, 2007). For all quantitative characters, gap weighted coding was used (Thiele, 1993), dividing the variation into three character states because this represents the minimum number of taxa in a given size category (see also Gilbert and Rossie, 2007). For all allometrically influenced characters, the 24 taxa analyzed in this study were divided into two size categories, large and small. These size groups were determined for both sexes and for each skull element (cranium

and mandible) by using gap-weighted coding on the appropriate size correction variable. Measurement P2 was coded using 2 character states (large and small) for both male and female crania; measurements M11 and M12 were used to determine size categories for male and female mandibles, respectively. Note that for some taxa, this results in crania and mandibles being classified in different size categories during coding. Size categories for cranial elements of each taxon are listed in Table 3.1. For flow charts illustrating the narrow allometric coding method for quantitative characters, see Chapter 2.

Qualitative characters were scored according to the character state criteria listed in Table 3.3. To better encompass variation, intermediate character states were employed. Due to small sample sizes, an intermediate state was assigned to any fossil taxon that exhibited more than one character state among its specimens. An extant species was considered variable for a given character if two or more character states were observed in more than 20% of specimens examined. For characters with more than two discrete character states, an intermediate state was assigned if two adjacent character states combined totaled ≥ 80% of all observations. For example, if a character has three discrete states (0, 2, and 4), and a taxon displays states 0 or 2 combined for ≥ 80% of all observations, an intermediate state (1) was assigned for this particular taxon. If no two adjacent character states combined totaled ≥ 80% of all observations, or if a fossil taxon displayed more than two adjacent character states, an additional polymorphic state was added and the character was considered unordered. In the case of multistate characters where more than two pairs of adjacent states totaled 80%, the average of the two possible intermediate states was used. For example, if states 0 + 2 total 80% (intermediate state 1) but states 2 + 4 also total 80% (intermediate state 3), the average of the intermediate states, in this case $(1 + 3) / 2 = 2$, was assigned. In an effort to reduce the amount of missing data in the analysis, any qualitative character state that was constant between male and female specimens of extant taxa was also assumed to be constant between male and female specimens of fossil taxa.

Unless otherwise noted, qualitative characters were considered ordered. For a full description of characters, character states, and character types, see Tables 3.2 and 3.3. When possible, a similar narrow allometric coding method was employed for qualitative characters determined to be allometrically influenced, as described in Chapter 2. Where

certain characters were not preserved or were inapplicable, qualitative or quantitative, the missing data ("?") code was used.

The resulting character matrices were then subjected to a parsimony analysis using PAUP 4.0 (Swofford, 2001), and character transformations were mapped using Mesquite 1.11 (Maddison & Maddison, 2006). A 10,000 replication, random addition sequence heuristic search was used to find the most parsimonious trees. To assess the stability of reconstructed clades, three analyses were performed. First, decay indices were calculated for the strict consensus tree. Second, a 1,000 replication bootstrap analysis with replacement was performed. Finally, majority-rules and strict consensus trees of all trees within 1% of the length of the most parsimonious tree were constructed (Strait et al., 1997).

Results

For comparison, the hypothesized phylogeny of the extant papionin taxa is given in Figure 3.3. Two most parsimonious trees were recovered in the analysis including fossil taxa (Fig. 3.4), and these trees differ only in the relationships among *P. quadratirostris* taxa (Fig. 3.3a, b). The majority-rule and strict consensus of these two trees is presented in Figure 3.5. Tree statistics summarizing the most parsimonious trees are provided in Table 3.4. Decay indices and the majority-rule consensus of the trees within 1% of the length of the shortest tree are presented in Figure 3.5. Given the large amount of missing data, it is perhaps not surprising that only three clades are well-supported by bootstrap values (Table 3.4). Therefore, for a better assessment of clade support and stability, I will focus attention on the decay indices and consensus of the trees within 1% length of the shortest tree (Fig. 3.5).

The most parsimonious trees in Figure 3.4 and the consensus trees in Figure 3.5 suggest that the basal African papionin taxon is *Parapapio*, represented by *Pp. whitei*, *Pp. jonesi*, and *Pp. broomi* (Fig. 3.1). These taxa form a clade at the base of the African papionin tree. The next African papionin clade to branch off is represented by *Pliopapio* and *Parapapio ado*. This grouping possibly suggests that *Pl. alemui* and *Pp. ado* are congeners; however, Frost (2001b) points out numerous

aspects of the dentition and mandible that distinguish these two taxa from each other (Fig. 3.6). In addition, no good cranial material of *Pp. ado* exists to compare with *Pliopapio*. In the current analysis, *Pp. ado* appears to group with *Pl. alemui* largely on the basis of dental dimensions (Fig. 3.6). The fact that *Pp. ado* is distinct from other *Parapapio* taxa suggests that it may be distinct enough to deserve its own genus, but I would refrain from naming a new taxon or referring the *Pp. ado* material to *Pliopapio* until better, more diagnostic material is recovered. In any case, it seems likely that *Pp. ado* and *Pliopapio*, along with the three other *Parapapio* taxa, all represent stem African papionins. This conclusion is further supported by the high decay index, relative to other clades in the most parsimonious tree, required to hypothesize these 5 taxa as crown African papionins (Fig. 3.5).

Dinopithecus is the last taxon reconstructed in the most parsimonious tree as a stem African papionin (Figs. 3.4-3.5). This result is surprising, as many authorities have argued and/or assumed *Dinopithecus* to represent a large, close relative of the living *Papio* (e.g., Freedman, 1957; Szalay and Delson, 1979; Delson and Dean, 1993; Frost, 2001a). A stem position for *D. ingens* is not strongly supported by the decay indices or bootstrap analysis (Fig. 3.5), and this may indicate that *D. ingens* is just as likely to be a crown African papionin given the available evidence. However, while it only takes one step to collapse the crown African papionin clade to include *Dinopithecus* in the strict consensus tree, it takes four steps to collapse the crown clade to include *Dinopithecus* in the majority-rule consensus tree (Fig. 3.4).

Among the crown African papionin taxa in the most parsimonious tree, it is important to note that the inclusion of fossil taxa results in the reconstruction of *Theropithecus* as the basal crown papionin taxon rather then a member of a clade also containing *Lophocebus* and *Papio* (see Figs. 3.4-3.5). *?T. baringensis* is strongly supported as a member of the *Theropithecus* clade, confirming its taxonomic status in the genus *Theropithecus*. While the trees recovered in this analysis suggest that *T. baringensis* is a basal member of the genus *Theropithecus*, they do not support a special relationship between *T. baringensis* and *T. brumpti* as hypothesized by Eck and Jablonski (1984; 1987). While a clade containing *T.*

brumpti, *T. darti*, and *T. gelada* is strongly supported (Fig. 3.4), the relationships among these taxa are unstable.

Another interesting grouping among crown papionin taxa concerns *P. izodi* and *Gorgopithecus major*. While both taxa are reconstructed as members of the clade containing *Papio* and *Lophocebus* in the most parsimonious tree, it is striking that *P. izodi* is reconstructed as the sister taxon of *Gorgopithecus* rather than extant *Papio*. Although the sister relationship between these two taxa is not strongly supported by decay indices and bootstrap values, a larger group including *Gorgopithecus*, *P. izodi*, *Papio* and *Lophocebus* is more strongly supported; it takes an additional step to collapse the clade including *Gorgopithecus, P. izodi, Papio,* and *Lophocebus* in the majority-rules consensus tree.

Finally, the most parsimonious trees in this analysis suggest that *Procercocebus antiquus* is indeed the sister taxon to *Cercocebus*, as hypothesized by Gilbert (2007a). In addition, the sister clade to *Mandrillus/Procercocebus/Cercocebus* is the group of three OTUs defined by Delson and Dean (1993) as *Papio quadratirostris*. Overall, a clade containing these six taxa (*Mandrillus*, *Cercocebus*, *Procercocebus*, and the three *P. quadratirostris* OTUs) is one of the three most strongly supported clades in the most parsimonious tree (Fig. 3.3). Contrary to the suggestions of Eck and Jablonski (1984; 1987), there is no convincing evidence to suggest that *P. quadratirostris* is closely related to *Theropithecus*, broadly, or *T. brumpti*, specifically, in any way. Instead, it is likely that a new generic nomen should be created for *P. quadratirostris* to reflect its hypothesized relationship to *Mandrillus*, *Procercocebus*, and *Cercocebus*.

Discussion

The results of the above analyses may offer some clarity regarding the evolution of the highly successful cercopithecine monkey tribe Papionini. It has long been a frustrating irony that the African papionin radiation is one of the best documented primate radiations in the fossil record, with many specimens of nearly complete crania, and yet the relationships of these fossil taxa to the extant African

papionin taxa as well to each other have remained unresolved. The increased confidence in the ability of craniodental data to accurately reflect papionin phylogenetic relationships (Chapter 2) and, more specifically, the high confidence in the phylogenetic utility of the current data set, lends significant weight to the phylogenetic hypotheses presented in Figures 3.4 and 3.5. Some of the clades reconstructed in these phylogenetic trees support previous suggestions of phylogenetic relationships, some hypothesized relationships are contrary to previous views, and other clades suggest relationships that have not previously been recognized.

Supported Phylogenetic Hypotheses

Parapapio and *Pliopapio*

Parapapio has long been recognized as a stem African papionin, if not the basal African papionin taxon (e.g., Szalay and Delson, 1979; Frost, 2001b; Jablonski, 2002). The results of this phylogenetic analysis support this view.

Frost (2001b) suggested that *Pliopapio* represented either a stem African papionin or a stem member of the *Papio/Lophocebus/Theropithecus* clade. The trees recovered in this study support the former hypothesis.

Theropithecus baringensis

Theropithecus baringensis, as represented by KNM-BC 2, is reconstructed in this analysis as a primitive member of the *Theropithecus* lineage. This phylogenetic position for *T. baringensis* is strongly supported (Fig. 3.4), although a close relationship to *T. brumpti* is uncertain. Therefore, the results of this study suggest that the question mark should be removed from the nomen for this taxon and its status as a member of *Theropithecus* should be formally recognized.

Procercocebus

The results of this phylogenetic analysis strongly support the suggestion that *Procercocebus* is a member of the extant clade containing *Cercocebus* and *Mandrillus* (Gilbert, 2007a). Furthermore, a sister relationship between *Procercocebus* and *Cercocebus* is one of the more stable groupings in this study (Fig. 3.7).

Papio and *Lophocebus*

Papio and *Lophocebus* were suggested to be sister taxa in the previous chapter (see Chapter 2). This relationship is strongly supported in the current study, even with the addition of fossil taxa.

Contrary Phylogenetic Positions

Dinopithecus

The placement of *Dinopithecus* as a stem African papionin is contrary to most authors' previous hypotheses (e.g., Freedman, 1957; Szalay and Delson, 1979; Delson and Dean, 1993; Frost, 2001a). However, this is perhaps to be expected given the large amount of missing data for this taxon, especially in the case of the male cranium (Fig. 3.8). As males are often more phylogenetically informative (see Chapter 2), the analysis here relies heavily on the less distinctive female morphologies. In addition, the highly variable extant population of *Papio* results in this taxon being coded with many intermediate states. Because only one or two *D. ingens* male cranial specimens exist, almost no characters were coded with the intermediate state, perhaps masking shared character states that would be evident with a larger sample size. Another potential issue is that the size-adjustment used in this analysis slightly over-adjusts at large body sizes, particularly for male crania. Since *Dinopithecus* is the largest taxon included in this study, it is possible that the

size-adjustment employed here slightly misrepresents certain *Dinopithecus* cranial features.

One final reason for the placement of *D. ingens* as a stem African papionin seems closely tied to the presence/absence of facial fossae (Fig. 3.8). The presence of definitive facial fossae is reconstructed as a synapomorphy of crown African papionins in this analysis, and *Dinopithecus* lacks this feature. I have argued previously that the development of facial fossae is allometrically influenced (Gilbert, 2007a), and so it is possible that *D. ingens* lacks facial fossae due to its very large size and that the narrow allometric coding method was too crude to interpret the morphology of *D. ingens* correctly. Regardless of these caveats, the most parsimonious interpretation of *D. ingens* craniodental morphology, as represented by this data set, is that *D. ingens* as a very large stem African papionin close to the origin of the crown taxa.

Gorgopithecus and *Papio izodi*

While the phylogenetic position of the enigmatic *Gorgopithecus* has always been uncertain, no previous author has suggested that *G. major* and *P. izodi* are sister taxa. Similar to the case with *Dinopithecus*, this reconstruction may be due to missing data. These taxa are linked to the exclusion of extant *Papio* and *Lophocebus* by male characters such as relatively narrow M_2s, intermediate-sized premolars, a sagittal crest at or posterior to bregma, and a definitive post-orbital sulcus. These last two characters are also often found in extant *Papio*, but due to small fossil sample size, they were scored as monomorphic in the fossils and polymorphic in the large sample of extant *Papio* crania. Larger sample sizes of *P. izodi* and *Gorgopithecus* specimens with additional morphological regions preserved would help resolve the relationships. In addition, the fact that the best preserved specimen of the male skull of *Gorgopithecus* is heavily distorted casts doubt on at least some of the quantitative male character states derived from this specimen. While the placement of both *G. major* and *P. izodi* as close relatives of extant *Papio*

and *Lophocebus* seems a likely hypothesis, it is surprising to think that *P. izodi* may be more closely related to *Gorgopithecus* than the living *Papio*.

Newly recognized relationships/clades

Gorgopithecus

As mentioned above, the phylogenetic position of *Gorgopithecus* has long been uncertain. This study suggests that *G. major* is most closely related to *Papio* and *Lophocebus* among extant taxa.

Papio quadratirostris

Delson and Dean's (1993) hypothesis regarding the close relationship between the type specimen of *P. quadratirostris* (the Usno cranium), the later Omo material, and a number of the Angolan specimens is supported by the results of this analysis. Furthermore, the analyses strongly suggest that this group of fossils is closely related to the extant clade containing *Cercocebus* and *Mandrillus*. Such a phylogenetic relationship has not been previously suggested for the Usno, Omo, or Angolan material. However, Delson and Dean (1993) hinted at the possibility of this relationship when comparing the cranial morphology of large African papionins and referring the Usno skull to the genus *Papio*. Delson and Dean (1993) also considered *Mandrillus* to be a member of the genus *Papio*, and many of the morphological similarities noted between the Usno specimen and *Papio* were, in fact, similarities more specifically with *Mandrillus* (e.g., see Figs. 3.9-3.10; see also p. 131 as well as Figs. 4.2 and 4.5 in Delson and Dean, 1993).

While the consensus tree reconstructs the type specimen of *P. quadratirostris* (Usno), later Omo material, and Angolan specimens as an unresolved trichotomy, I consider the tree in Fig. 3.3a to be the most likely given the available geological and geographical evidence. As mentioned above, the later Omo and Angolan material are united by a group of seemingly derived features, such as enlarged premolars,

that suggest them to be distinct from the earlier Usno skull. The Usno specimen is dated to approximately 3.3 Ma (Delson and Dean, 1993), and the Omo and Angolan material are perhaps 1-2 Ma younger. In the case of the Omo material, my own measurements suggest that fourth premolar size increases through time from their small size in the Usno specimen (3.3 Ma) with progressive enlargement in Members E through G (2.5-2.3 Ma; see specimens NME L 185-6, NME L 4-13b, NME Omo 42-1972-1, NME Omo 47-1970-2008; see Table 3.5 and Fig. 3.11).

If the Usno specimen and the later Shungura E-G material represents an evolving lineage, than they should probably be recognized as the same species with different chronological (anagenetic) subspecies. I would also include the Angolan material in the same subspecies as the later Omo material. In any case, it would seem that this group of fossils requires a new generic nomen to reflect their probable relationship as the sister group to the extant *Mandrillus/Cercocebus* clade.

Character Evolution and the African papionin radiation

As the low CI values in the most parsimonious trees imply, there is considerable morphological homoplasy in the African papionin radiation. This makes craniodental synapomorphies difficult to identify for many higher level clades. However, there are some characters can be identified in the transformation analyses as particularly distinctive of certain clades. Table 3.6 highlights the most distinctive synapomorphies at selected nodes.

First, two features are identified here as unique synapomorphies defining African papionin taxa apart from macaques and other early papionins. Thus, it appears that African papionins have a wider interorbital distance compared to *Macaca* as well a reduced incidence of the nasal bones projecting above the fronto-maxillary suture, particularly in females. These features are not obvious, but this is perhaps to be expected among the first African papionin taxa to diverge from an ancestral macaque-like population.

Second, the presence of definitive maxillary fossae is the one obvious cranial synapomorphy that unites all crown African papionins. *Papio, Lophocebus, Papio*

izodi, and *Gorgopithecus* are further identified by extreme development of maxillary fossae, including taxa with the deepest and most extensive fossae among all papionin taxa. *Mandrillus*, *Cercocebus* and *Papio quadratirostris* are characterized by less extensive maxillary fossae compared to *Papio, Lophocebus, Papio izodi, Gorgopithecus*, and most *Theropithecus* taxa. Another cranial feature that is seen only among crown African papionins, although not universally so, is the presence of definitive maxillary ridges and mandibular corpus fossae in males.

Third, many previous characters identified as synapomorphies of *Theropithecus* were confirmed in this study. The most distinctive characters recognized in this study include small incisors, temporal lines that meet in males to form a sagittal crest anterior to bregma, and deeply excavated fossae anterior to the foramen magnum. *Theropithecus brumpti*, the *T. oswaldi* lineage and *T. gelada* also share increased enamel infoldings, more obliquely oriented lophids on the lower molars, and a reversed Curve of Spee for the tooth row.

Finally, a series of characters can also be identified as synapomorphies defining the clade containing *Cercocebus*, *Mandrillus*, *Procercocebus*, and *Papio quadratirostris*. These taxa are all united by the appearance of widely divergent temporal lines (especially in males), upturned nuchal crests (especially in males), and less extensive development of the maxillary fossae. In addition, there is a tendency to develop very large premolars relative to the molars among these taxa. This last feature appears to have developed independently at least two times, once in the *Papio quadratirostris* group and at least once among *Mandrillus*, *Cercocebus*, and *Procercocebus*.

With a better understanding of the synapomorphies that characterize the different papionin clades, it is possible to speculate about their adaptive significance during the Plio-Pleistocene radiation of these monkeys. From the phylogenetic hypothesis presented here, it is evident that the earliest and most primitive African papionins were very macaque-like in appearance, lacking maxillary and mandibular corpus fossae, and having a generalized bilophodont dentition with relatively small premolars. Similar to macaques, *Parapapio* species came in a variety of sizes, and probably partitioned niche space in the Plio-Pleistocene by differentiation in body

size, locomotor pattern (e.g., Ciochon, 1993; Elton, 2001), and diet (e.g., Fourie et al., 2008).

In contrast to *Parapapio*, *Pliopapio*, and *Dinopithecus*, the common ancestor of all crown African papionins developed definitive maxillary fossae. The adaptive significance as well as the underlying anatomical cause of this osteological feature are unclear; however, it seems that there is an allometric component associated with the development and extent of maxillary and mandibular fossae among taxa which possess them (Gilbert, 2007a). Thus, as body and skull size decrease, the depth and extent of the maxillary fossae increases and extends into the infraorbital plate. When body size is mapped onto the phylogeny in Figures 4 and 5, it would appear that definitive maxillary fossae most likely developed in a large African papionin. This hypothesized distribution of body size also suggests that the extant mangabeys, *Lophocebus* and *Cercocebus*, are derived in their smaller size and associated cranial morphologies, as suggested by Singleton (2002).

One potential explanation for the appearance of maxillary fossae may be associated with sexual selection. Since both males and females exhibit maxillary fossae, it is unclear whether male or female preferences (or both) may have driven the evolution of this feature. However, the fact that the level of sexual dimorphism also seems to increase in crown African papionins relative to stem taxa points to the importance of sexual selection in the origin of the crown taxa.

As previously noted, (e.g., Jolly, 1970; 1972; Szalay and Delson, 1979; Eck and Jablonski, 1984; 1987; Jablonski, 1993; 2002), later members of the genus *Theropithecus* are easily identified by a number of dental synapomorphies clearly associated with adaptations to a heavily herbaceous and gramnivorous diet. While early members of the genus *Theropithecus,* as characterized by *T. baringensis*, cannot be identified on the basis of a/the derived dentition, they can be identified by the anterior union of the temporal lines (Fig. 3.12) as well as the deeply excavated fossae anterior to the foramen magnum. The anterior position of the temporal lines seems related to the increased size of the temporalis musculature as well as the optimal placement of the temporalis in order to increase occlusal forces on the molar battery (Jolly, 1970, see Fig. 3.12). This increase in musculature and chewing

emphasis probably also helped to drive selection for increased enamel infoldings, a delayed eruption pattern, and reversed Curve of Spee to lengthen the life of the molars in later *Theropithecus* taxa. The reversed Curve of Spee, associated with the delayed eruption pattern, functions to keep the posterior molar row from full occlusion as long as possible, thereby extending the life of the most posterior teeth. The adaptive and functional significance of the deeply excavated fossae anterior to the foramen magnum are unclear, although one may speculate that they are related to the orientation of the neck and skull which may be linked in modern geladas to their unique posture while foraging.

While the *Theropithecus* lineage is, in part, linked to adaptations associated with increasing the emphasis of chewing onto the posterior dentition, the *Mandrillus/Cercocebus/Papio quadratirostris* clade is defined in large part by a shift of chewing-muscle forces onto the premolars. This anterior shift most likely provides selective pressure for larger premolars. In extant *Cercocebus* and *Mandrillus,* large premolars are suggested to be adaptations for processing hard-object food items acquired while foraging on the forest floor (Fleagle and McGraw, 1999; 2002).

A similar situation probably existed in the Plio-Pleistocene *P. quadratirostris* lineage. In East Africa, the reconstructed environment of the Usno Formation includes riverine forests and woodlands (Reed, 1997). The Shungura Members E through G are also often noted as including a forest or woodland component (Eck and Jablonski, 1984, 1987; Ciochon, 1993; Reed, 1997), and a transition from well-watered riparian forests/woodlands to a river with slightly more open woodlands is documented through time (Reed, 1997). Forests and woodlands are the same types of environment that *Cercocebus* and *Mandrillus* occupy today. Therefore, similar dietary selection pressures on early members of this clade were likely, and premolar size increases through time among *P. quadratirostris* specimens in the Omo Shungura section (Table 3.5).

The reconstructed environment of the Angolan Humpata Plateau also includes more forested environments (Pickford et al., 1994), which is also consistent with the preferred habitat of extant members of this group. In the case of East Africa, a shift to a hard-object niche may have also helped to avoid direct competition with the contemporaneous

and forest-adapted *T. brumpti*. Overall, the available evidence indicates that the *Mandrillus/Cercocebus/Papio quadratirostris* clade has always been a forest-adapted lineage, which may have avoided competition with the expanding savannah-adapted *Papio* lineage. In addition, a shift to a hard-object feeding niche may have helped to avoid competition with other forest-living cercopithecines such as guenons, *Lophocebus* mangabeys, and *T. brumpti*.

Finally, the remaining crown African papionin taxa (*Papio hamadryas*, *Lophocebus*, *Gorgopithecus*, and *Papio izodi*) are not obviously grouped in any adaptively cohesive way. In fact, it seems that this group of monkeys is better defined as being unspecialized generalists than being committed to any specific type of lifestyle. The defining synapomorphy of the group is the possession of the deepest and most extensive maxillary fossae among crown African papionins (Fig. 3.13). However, as previously discussed, the adaptive significance of this feature is unclear. As is the case with most fossil papionin taxa, postcrania cannot be assigned to *Gorgopithecus* and *P. izodi*, so it is not possible to definitively assess whether or not *Lophocebus* is the only arboreal taxon among this group, although it seems likely given the available evidence.

Timing of the African papionin radiation

One final aspect of the phylogenetic hypothesis presented in this study concerns the geochronological origin of specific clades. Molecular studies suggest that the basic division between *Mandrillus/Cercocebus* and *Papio/Lophocebus/Theropithecus* took place between 6 and 10 million years ago (Ma) (Disotell and Raaum, 2002; Tosi et al., 2003; 2005). The separation of *Papio, Lophocebus,* and *Theropithecus* has been estimated to be around 4 - 5 Ma (Disotell and Raaum, 2002; Tosi et al., 2005). This date accords well with the phylogeny presented here, as no taxon reconstructed as diverging after *Theropithecus* split from the other crown African papionins is present in the fossil record before 3.3 Ma. It does, however, suggest that there was a very quick radiation of crown African papionins, as *Cercocebus* and *Mandrillus* are estimated to have diverged between 3.6 and 4.1 Ma and *P. quadratirostris,* by virtue of its earlier hypothesized branching event, is reconstructed to have diverged sometime before that. This rapid

radiation of crown African papionins at the beginning of the Pliocene may help to explain why molecular data cannot resolve the relationship between *Papio*, *Lophocebus* and *Theropithecus*. In summary, the phylogenetic hypothesis presented here is in general agreement with previous estimates of papionin divergence dates.

Conclusions

A large set of qualitative and quantitative craniodental characters for extant and fossil members of the cercopithecoid monkey tribe Papionini was subjected to phylogenetic analysis using parsimony. In order to account for the well-documented influence of allometry on the craniodental morphology of this group, the narrow allometric coding method was employed (Gilbert and Rossie, 2007). The resulting phylogenetic hypothesis reconstructs *Parapapio*, *Pliopapio* and *Dinopithecus* as stem African papionins.

The origin of crown African papionins is defined, at least in part, by the appearance of definitive facial fossae. Among crown African papionins, *Theropithecus* is reconstructed as the basal crown African papionin taxon and the status of *T. baringensis* as a member of the genus *Theropithecus* is strongly supported. The adaptive origins of the genus *Theropithecus* are associated, in part, with dietary adaptations requiring an increase in temporalis musculature and chewing emphasis onto the molars (Jolly, 1970). *Gorgopithecus* is reconstructed as having been closely related to *Papio* and *Lophocebus*, and this group is characterized by the deepest and most extensive maxillary fossae among all crown African papionins. *Lophocebus* is possibly a secondarily arboreal taxon.

Papio quadratirostris, as defined by Delson and Dean (1993) to include the later Omo Shungura material as well as some of the material from the Angolan Humpata Plateau, is reconstructed here as the sister taxon to *Cercocebus*, *Procercocebus*, and *Mandrillus*. This clade appears largely restricted to forested environments, and it is characterized by the tendency to evolve adaptations for hard-object food items, which has apparently happened in parallel at least twice. Morphological features that define this group and are linked to this ecological focus include widely divergent temporal lines that shift chewing-muscle forces towards the anterior dentition, and the consequent

enlargement of the premolars. *Papio quadratirostris* requires a new generic nomen to reflect its hypothesized position as the sister to the extant clade containing *Cercocebus* and *Mandrillus*.

Figure Captions

Figure 3.1. Comparison of three *Parapapio* taxa. From left to right, male cranial specimens of *P. jonesi* (AL 363-15), *P. broomi* (M202), and *P. whitei* (MP221). Note the peaked/raised nasals, slightly concavo-convex nasal profile, a relatively long skull, a relatively long muzzle, and pinched but less well-defined temporal lines of *P. whitei* compared to *P. broomi*.

Figure 3.2. Comparison of a) DGUNL LEBA05, a presumed adult male frontal from the Angolan Humpata Plateau with b) the Usno specimen from the Ethiopian Omo group. Note the widely divergent temporal lines and more posterior union of the temporal lines in the Usno specimen.

Figure 3.3 a) Hypothesized phylogenetic tree of the extant Papionini from molecular (mtDNA and Y-chromosome) data (Disotell et al., 1992; Disotell, 1994; 2000; Harris and Disotell, 1998; Harris, 2000; Tosi et al., 2003) and morphological data (Gilbert and Rossie, 2007; Gilbert, Chapter 2).

Figure 3.4. Most parsimonious phylogenetic trees of the extant and fossil Papionini. Tree statistics are given in Table 3.4. See Table 3.6 for list of the most distinctive synapomorphies at each of the numbered nodes.

Figure 3.5. a) Strict consensus tree of the extant and fossil Papionini. Decay indices are provided above each branch on the tree. **b)** Majority-rules consensus tree of the extant and fossil Papionini. Decay indices are provided above each branch on the tree. **c)** Majority-rules consensus tree of all trees within 1% of the length of the most parsimonious tree. Bootstrap values are provided above each branch on the tree.

Figure 3.6. Comparison of the male mandibular dentition of *Parapapio ado* from Kanapoi and *Pliopapio alemui* from Aramis. From left to right, male mandibular specimens of *P. ado* (KP-286), *P. ado* (KP 29306), and *P. alemui* (ARA-VP 1/73).

Figure 3.7. Comparison of *Procercocebus* with extant *Cercocebus*. **Top:** *Pr. antiquus* male (TP9, left) compared to *C. torquatus* male (right). **Bottom:** *Pr. antiquus* female (TP8, left) compared with *C. agilis* female (right). From Gilbert (2007a).

Figure 3.8. *Dinopithecus ingens* male (SK599, left) and female (SK553, right). Note the incompleteness of the male specimen and the lack of definitive maxillary fossae in both specimens.

Figure 3.9. Comparison, in lateral view, of a) an adult male *P. quadratirostris* (Usno) to b) an adult male *Mandrillus sphinx*. From Delson and Dean (1993).

Figure 3.10. Comparison, in dorsal view, of a) an adult male *P. quadratirostris* (Usno) to b) an adult male *Mandrillus sphinx*. From Delson and Dean (1993).

Figure 3.11. Increase in *P. quadratirostris* premolar size through time in the Omo River Basin, Ethiopia: a) Usno specimen, b) NME L 185-6, c) NME L 4013b, d) NME Omo 42-1972-1, e) NME Omo 47-1970-2008. See also Table 5.

Figure 3.12. Comparison of the four *Theropithecus* taxa recognized in this analysis. Note the anterior union of the temporal lines well-anterior to bregma, a defining feature of *Theropithecus* linked here to an increase in the size of temporalis as well as the optimal placement of temporalis in order to increase occlusal forces on the molar battery.

Figure 3.13. Development of the maxillary/suborbital fossae in the hypothesized clade including extant taxa *Papio* and *Lophocebus* as well as the fossil taxa *Gorgopithecus* and *P. izodi*. **Top:** *Gorgopithecus major* male (KA192, left) and female (KA153, right). **Bottom:** *L. albigena* female (left), *P. hamadryas kindae* female (middle), *P. h. ursinus* female (right). Note the deep and extensive maxillary/suborbital fossae found in all taxa. The results of this analysis suggest that the extensive maxillary/suborbital fossae are a defining feature of this group.

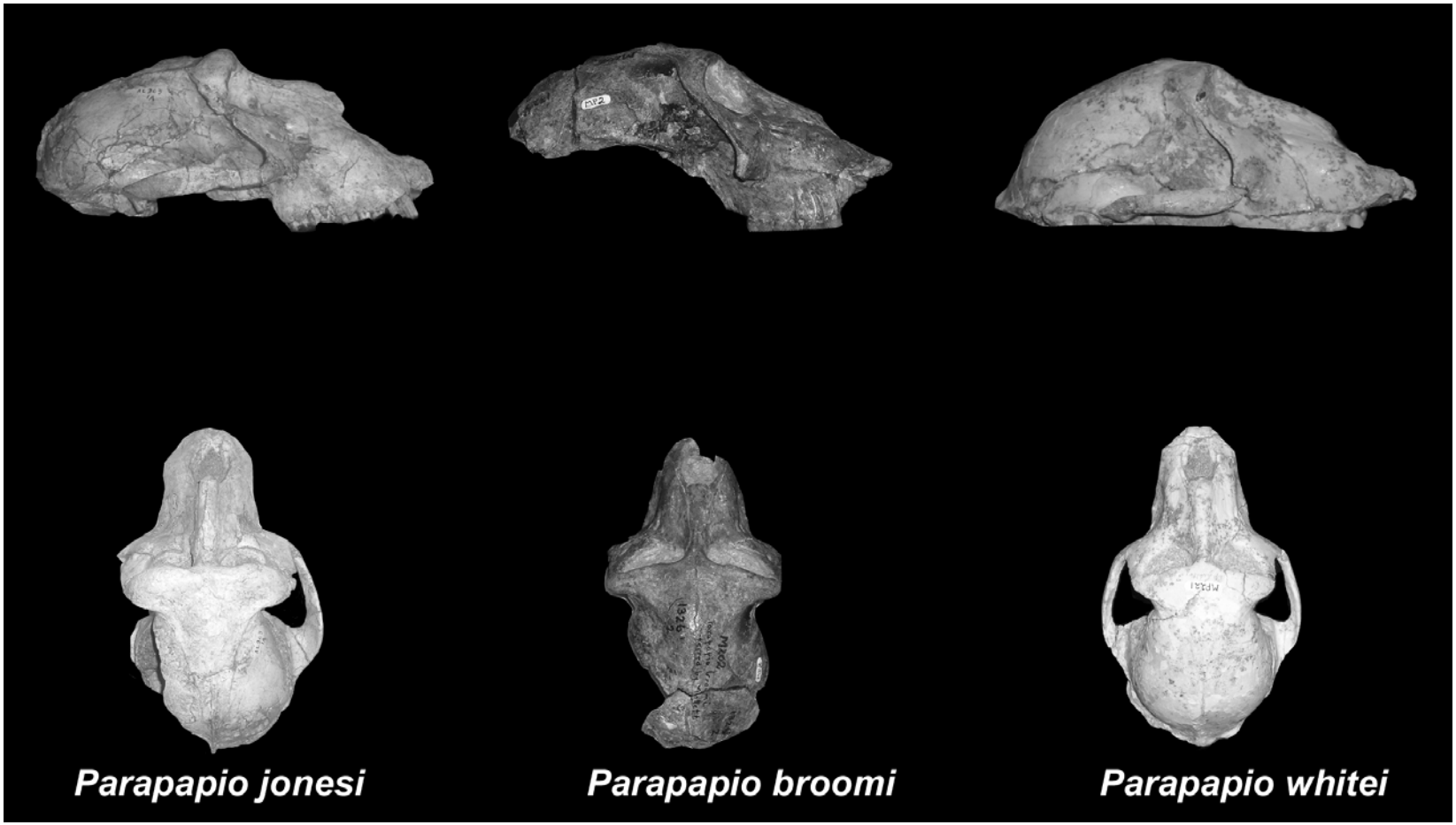

Figure 3.1

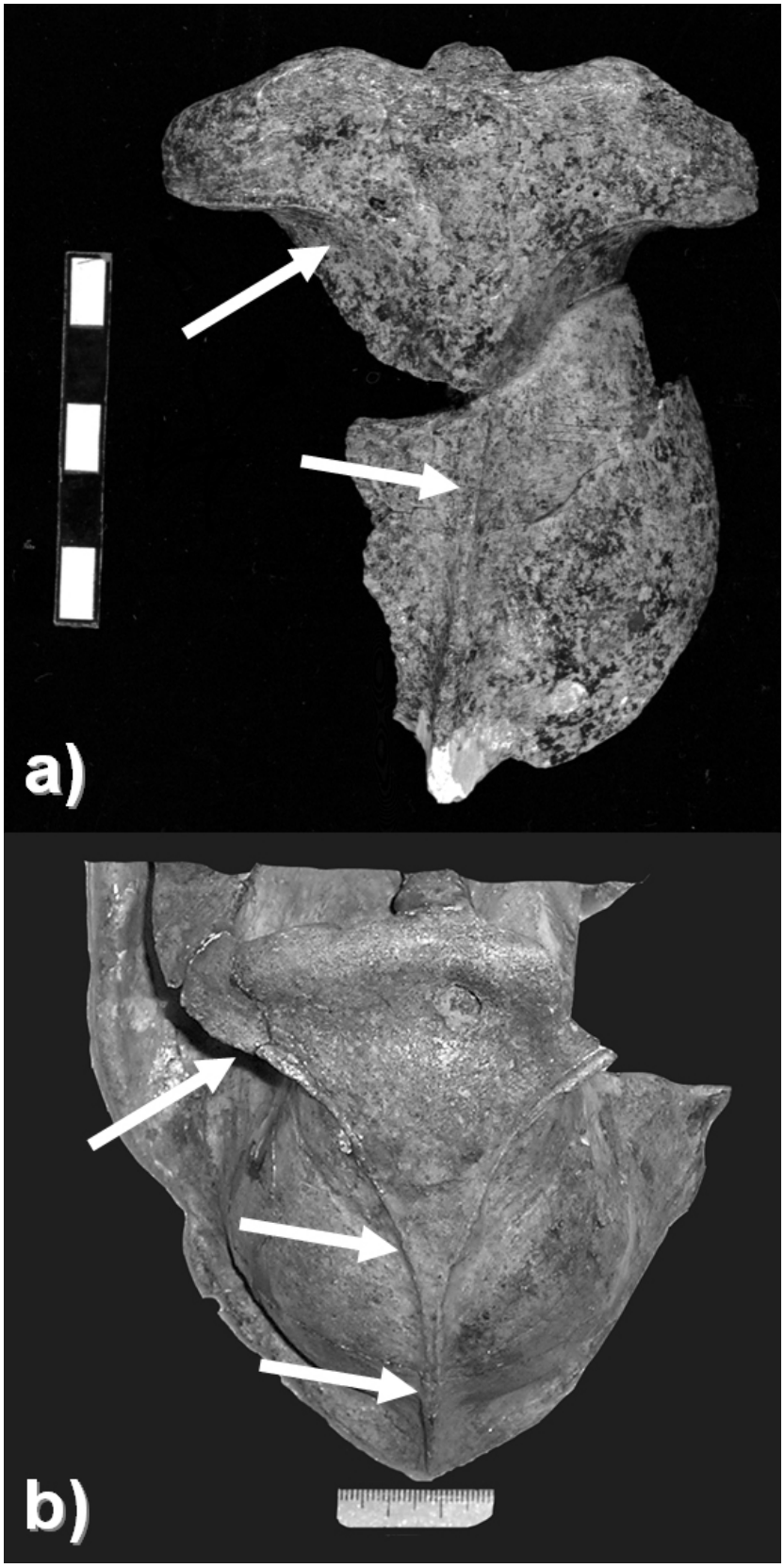

Figure 3.2

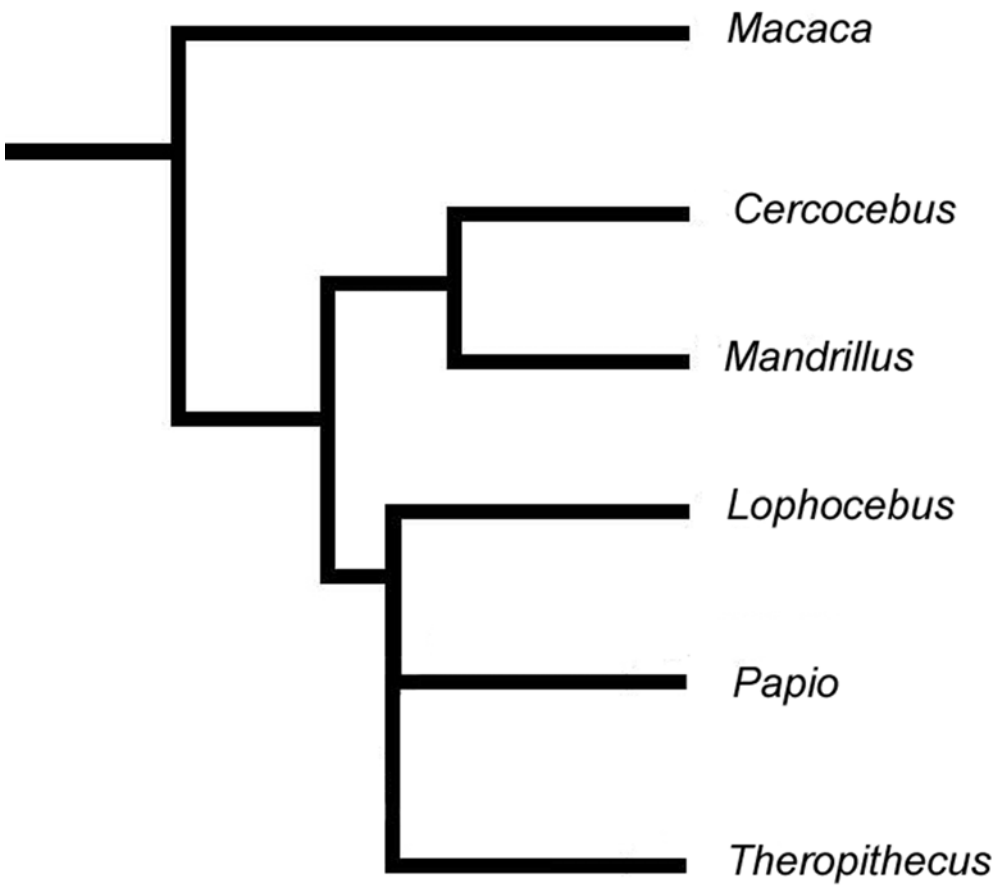
Macaca
Cercocebus
Mandrillus
Lophocebus
Papio
Theropithecus

Figure 3.3

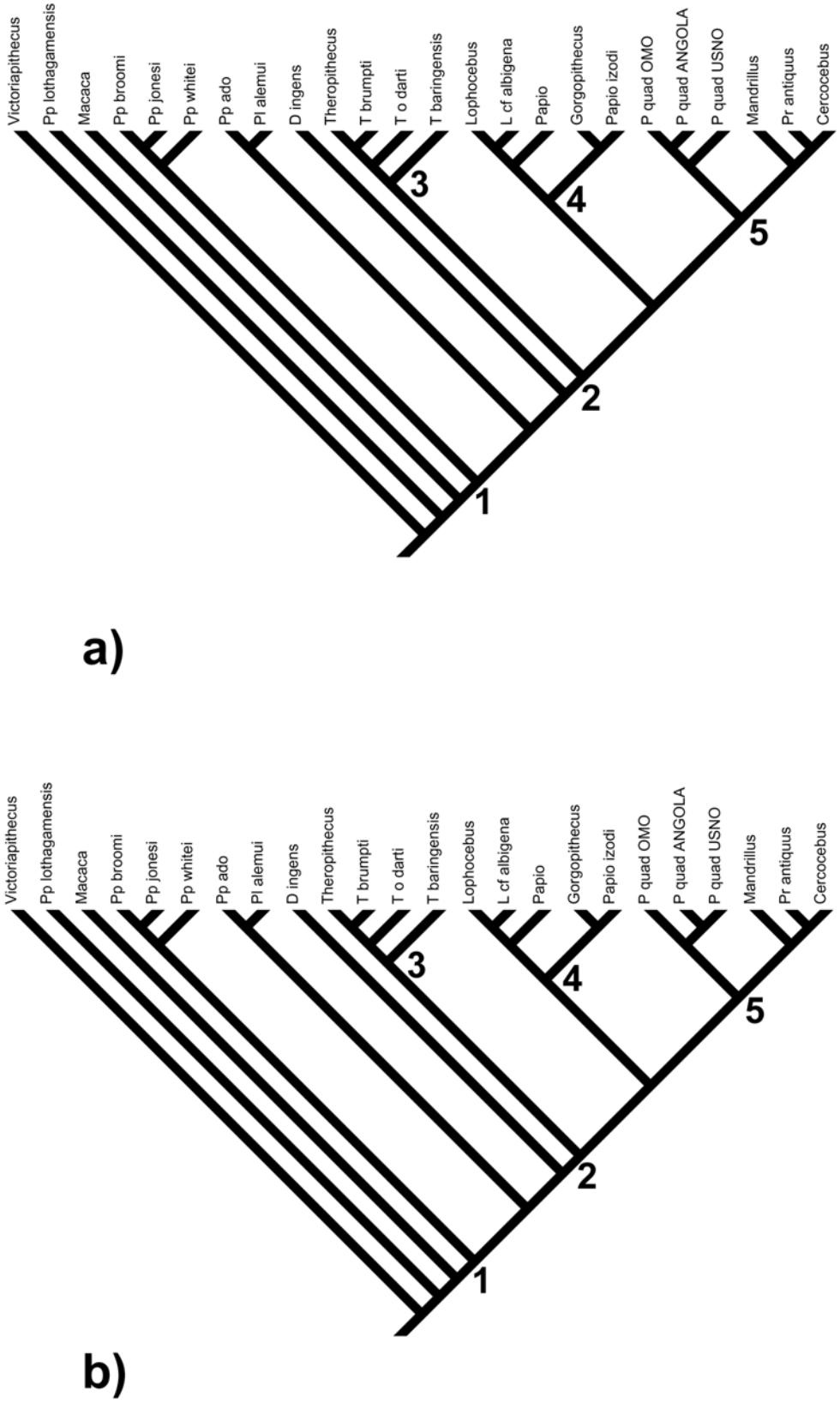
Victoriapithecus
Pp lothagamensis
Macaca
Pp broomi
Pp jonesi
Pp whitei
Pp ado
Pl alemui
D ingens
Theropithecus
T brumpti
T o darti
T baringensis
Lophocebus
L cf albigena
Papio
Gorgopithecus
Papio izodi
P quad OMO
P quad ANGOLA
P quad USNO
Mandrillus
Pr antiquus
Cercocebus
1
2
3
4
5
a)
b)

Figure 3.4

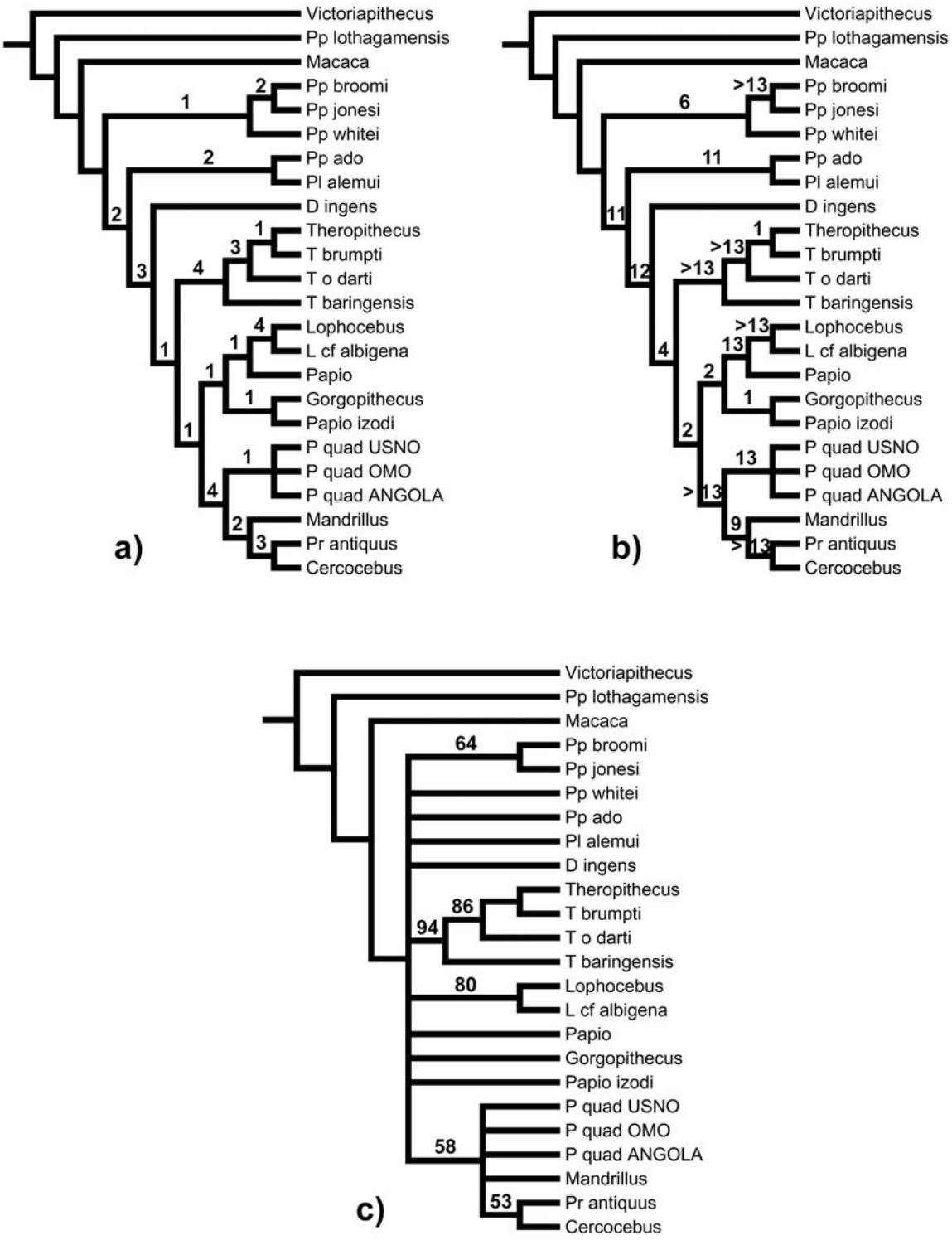
Victoriapithecus
Pp lothagamensis
Macaca
Pp broomi
Pp jonesi
Pp whitei
Pp ado
Pl alemui
D ingens
Theropithecus
T brumpti
T o darti
T baringensis
Lophocebus
L cf albigena
Papio
Gorgopithecus
Papio izodi
P quad USNO
P quad OMO
P quad ANGOLA
Mandrillus
Pr antiquus
Cercocebus
a)
b)
c)

Figure 3.5

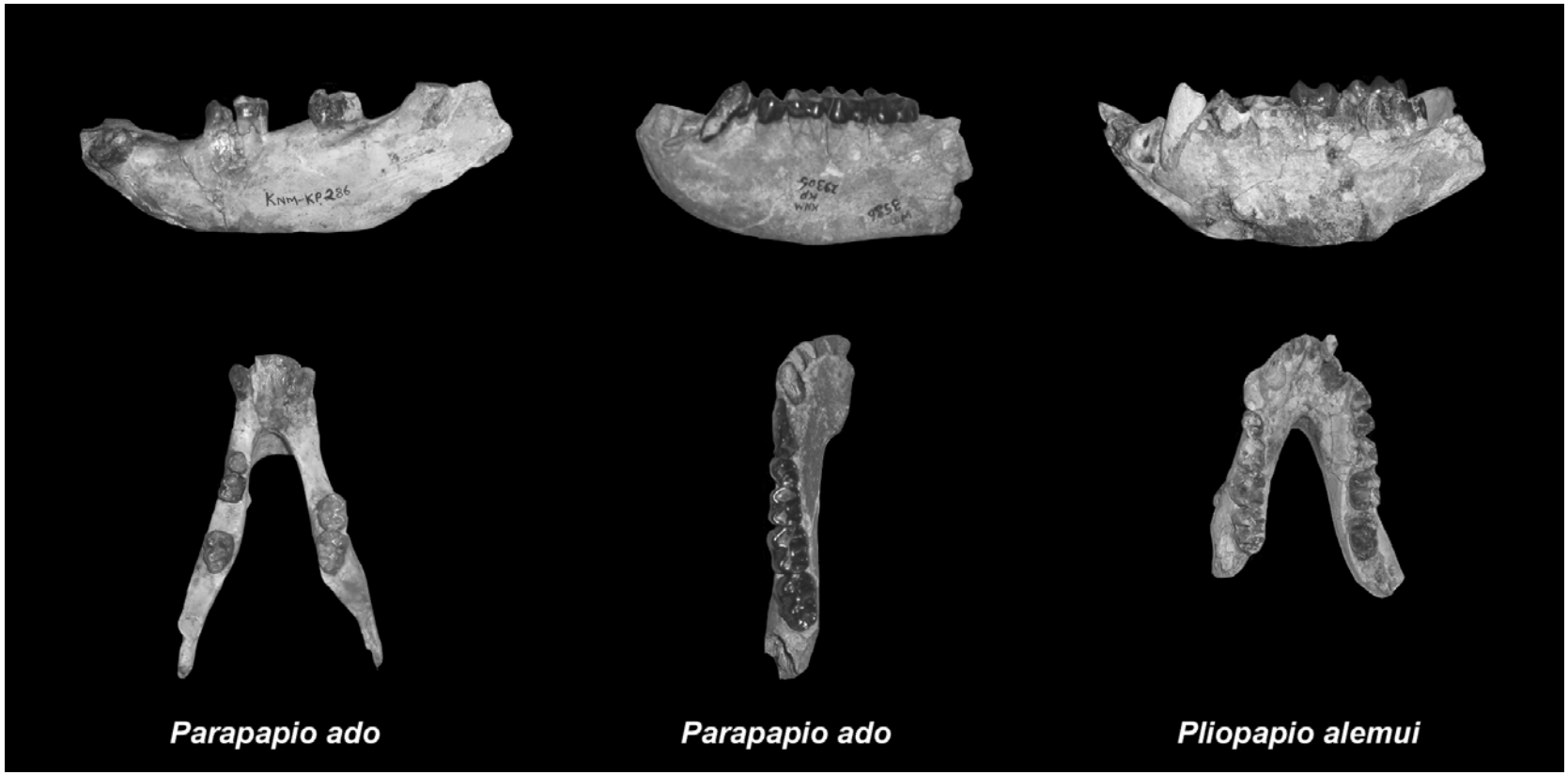

Figure 3.6

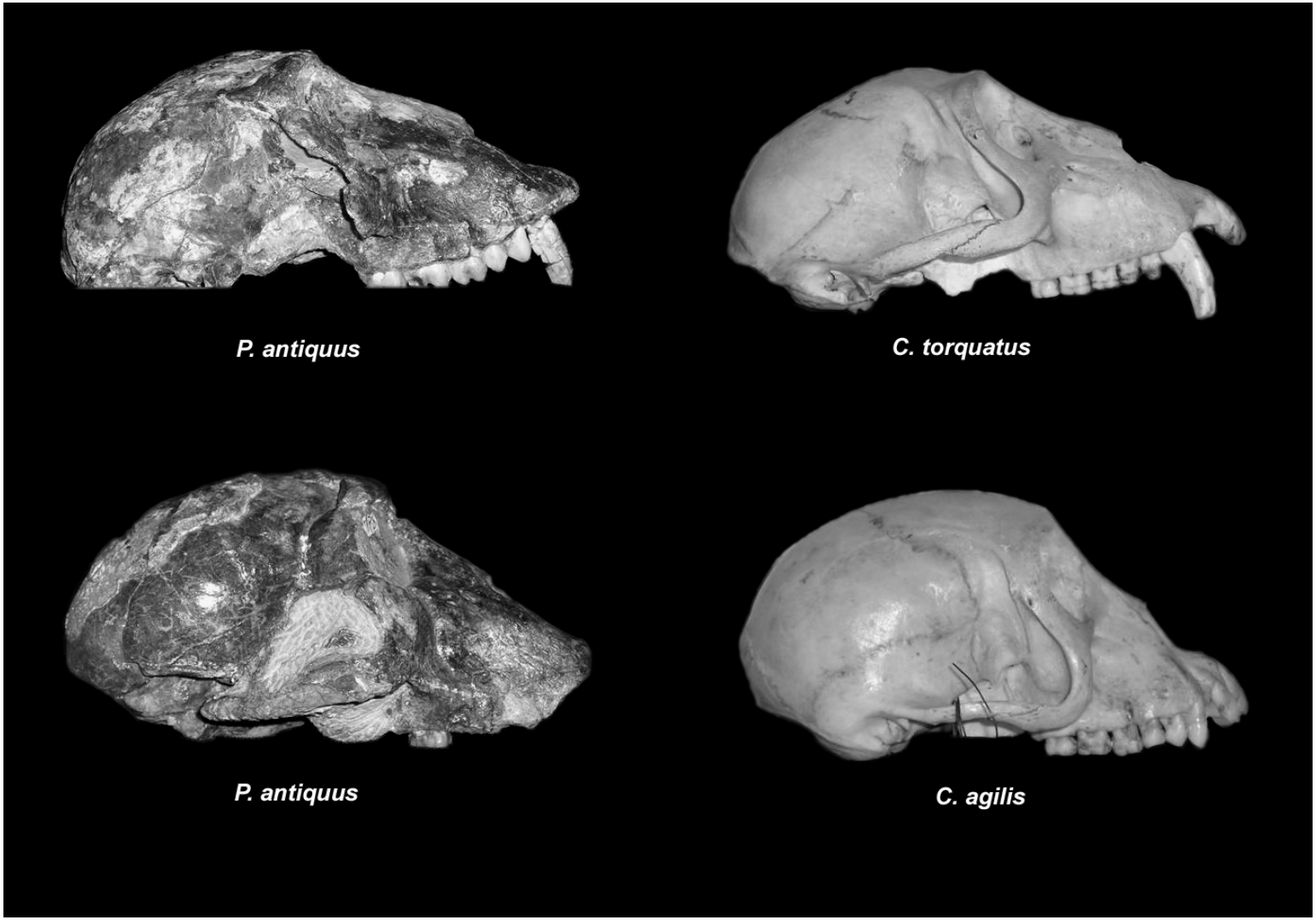

Figure 3.7

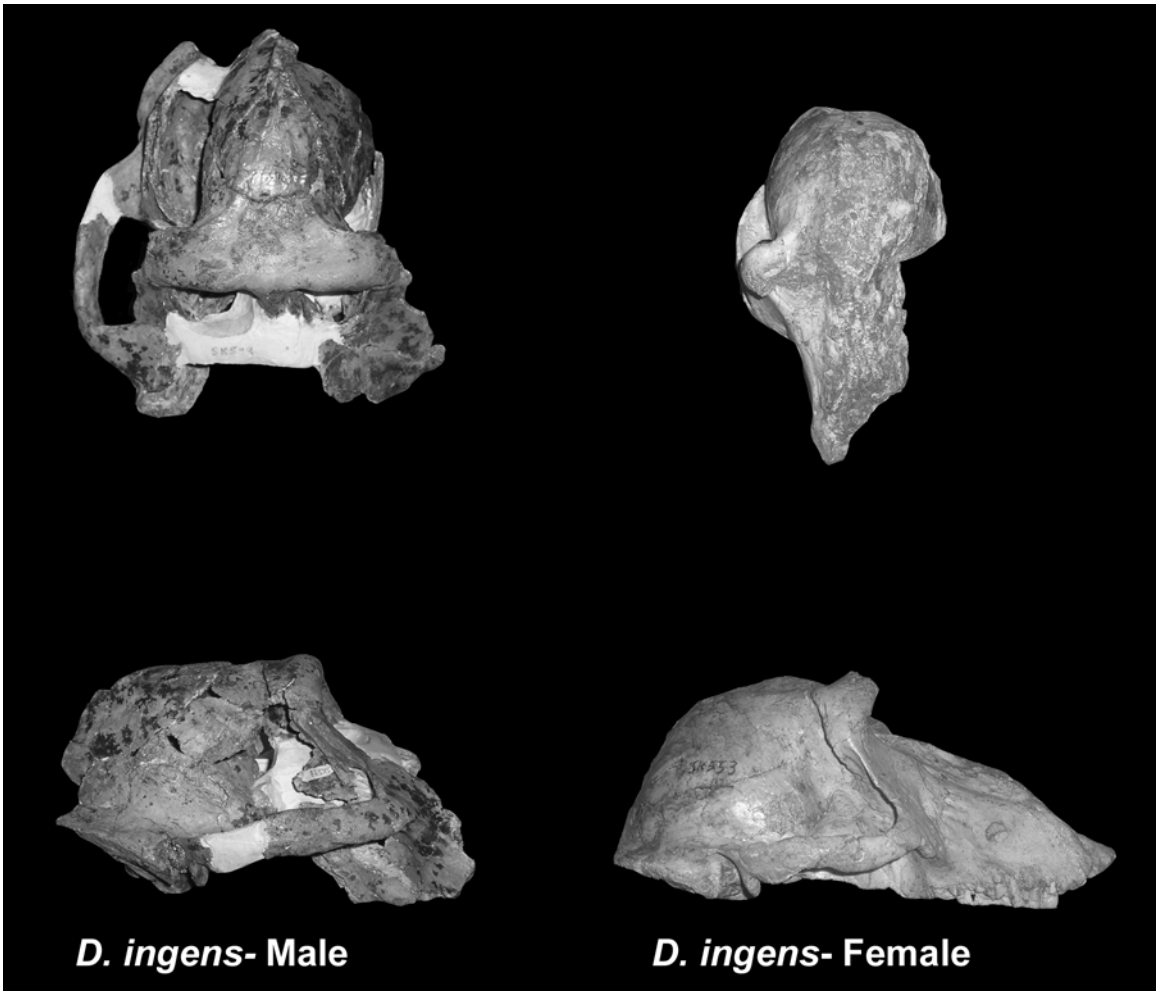

Figure 3.8

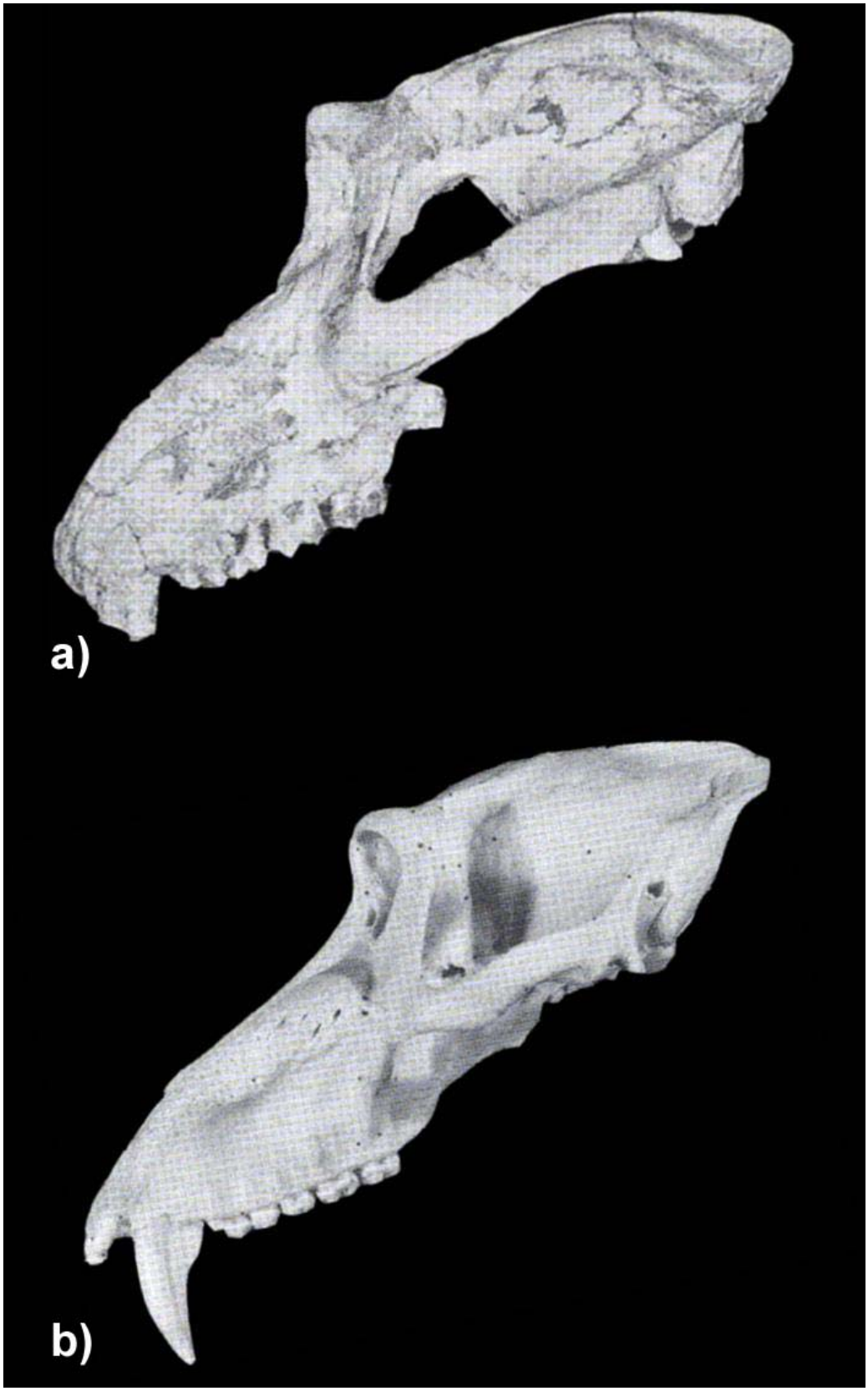

Figure 3.9

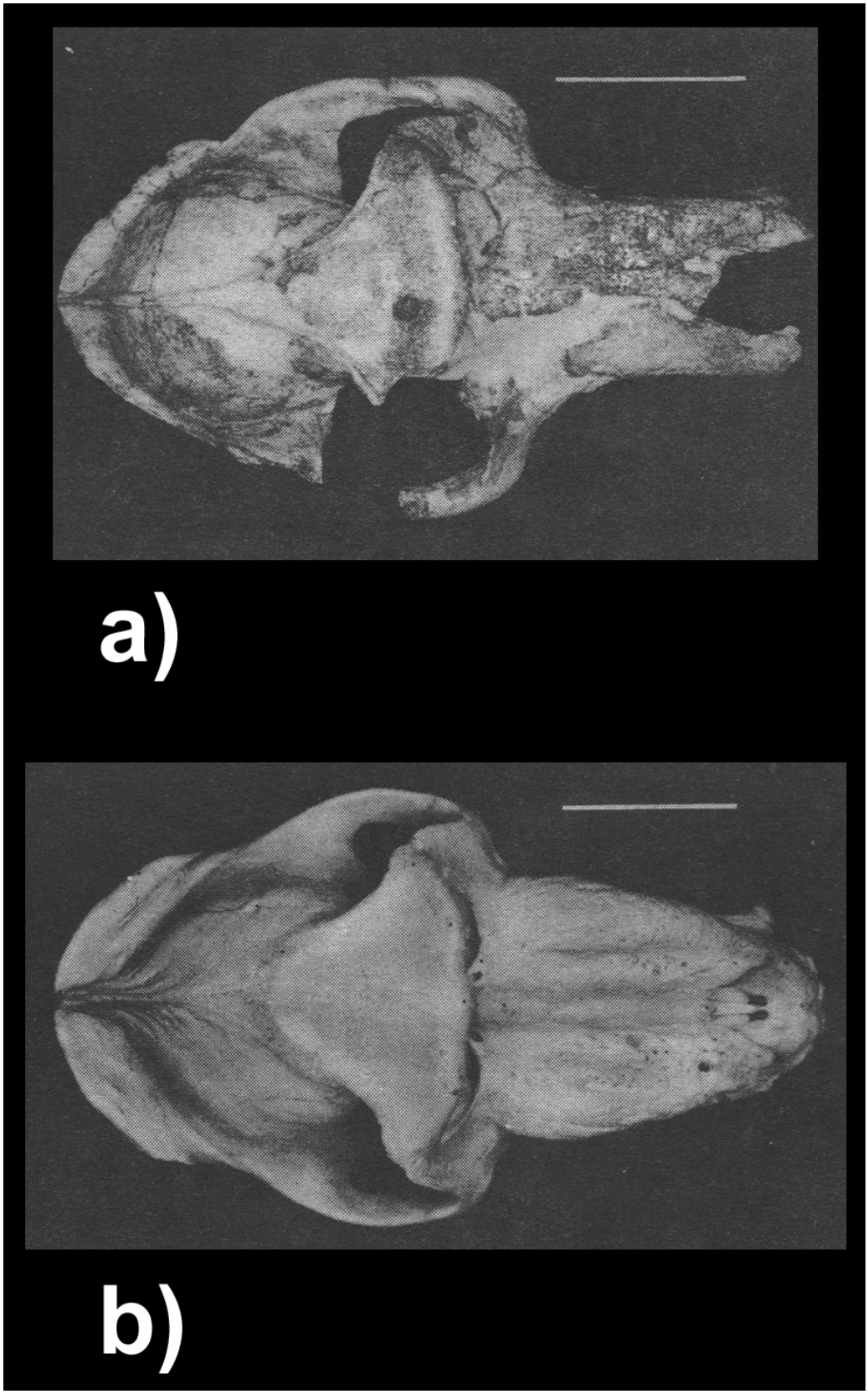

Figure 3.10

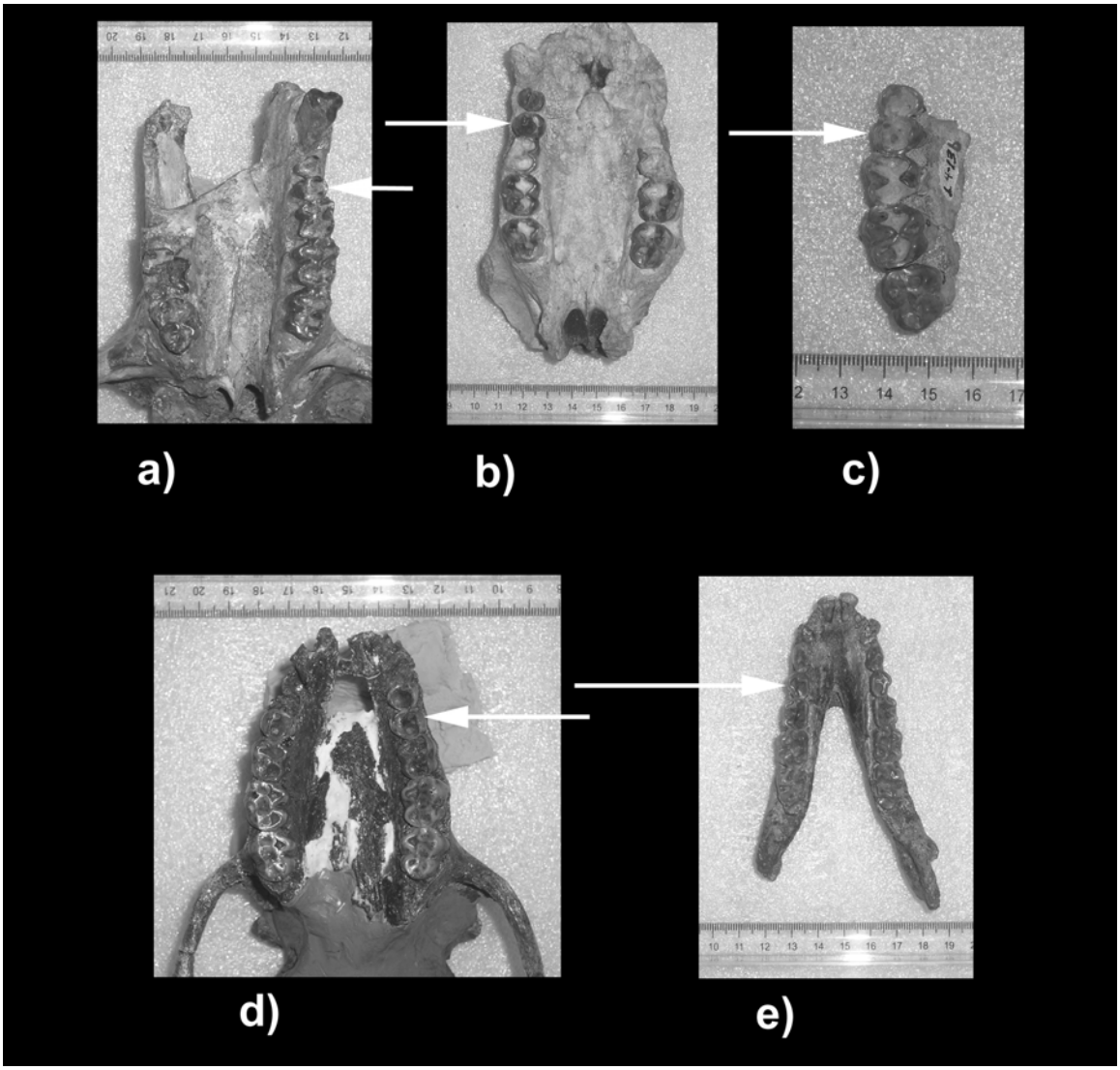

Figure 3.11

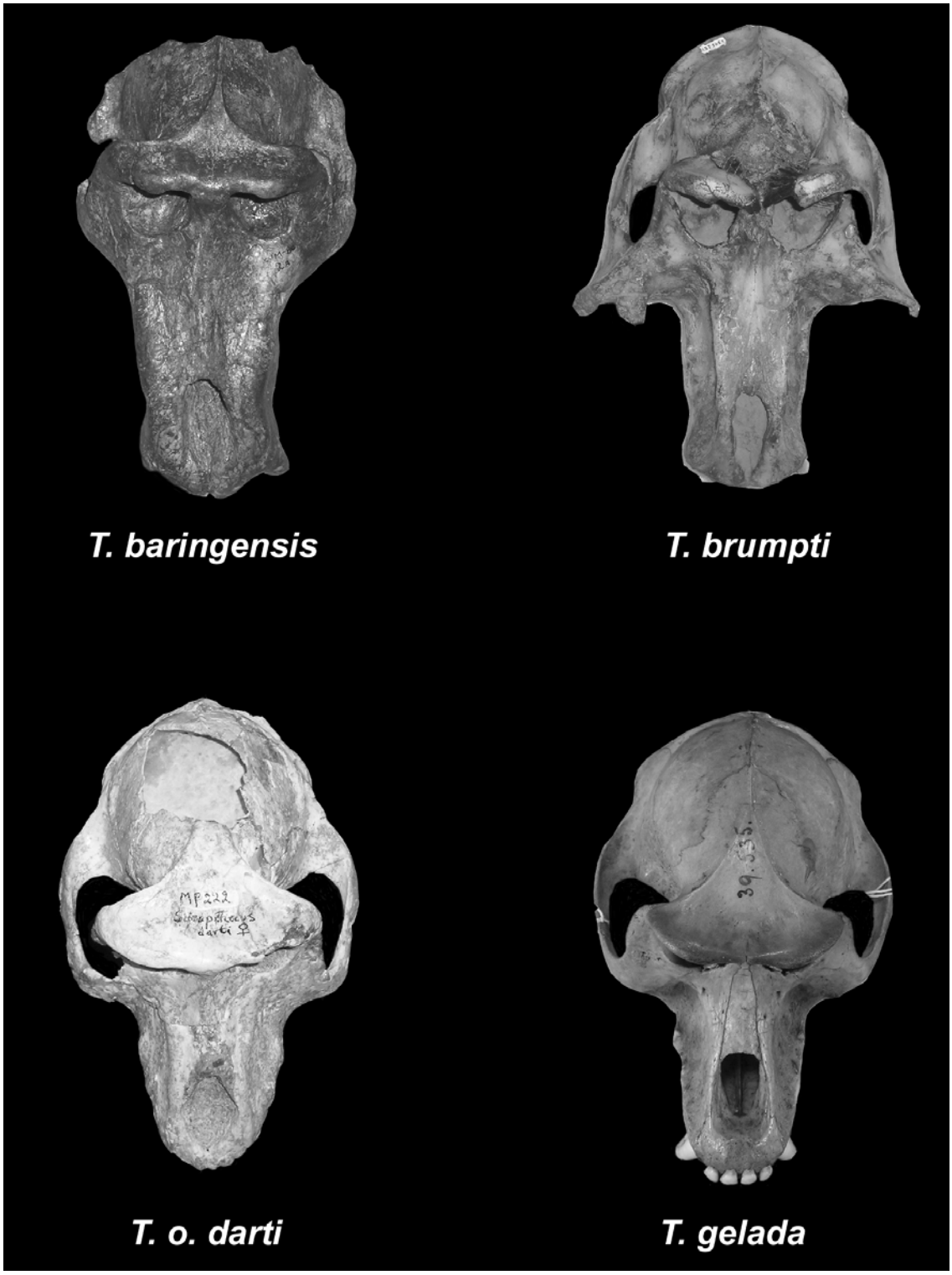

Figure 3.12

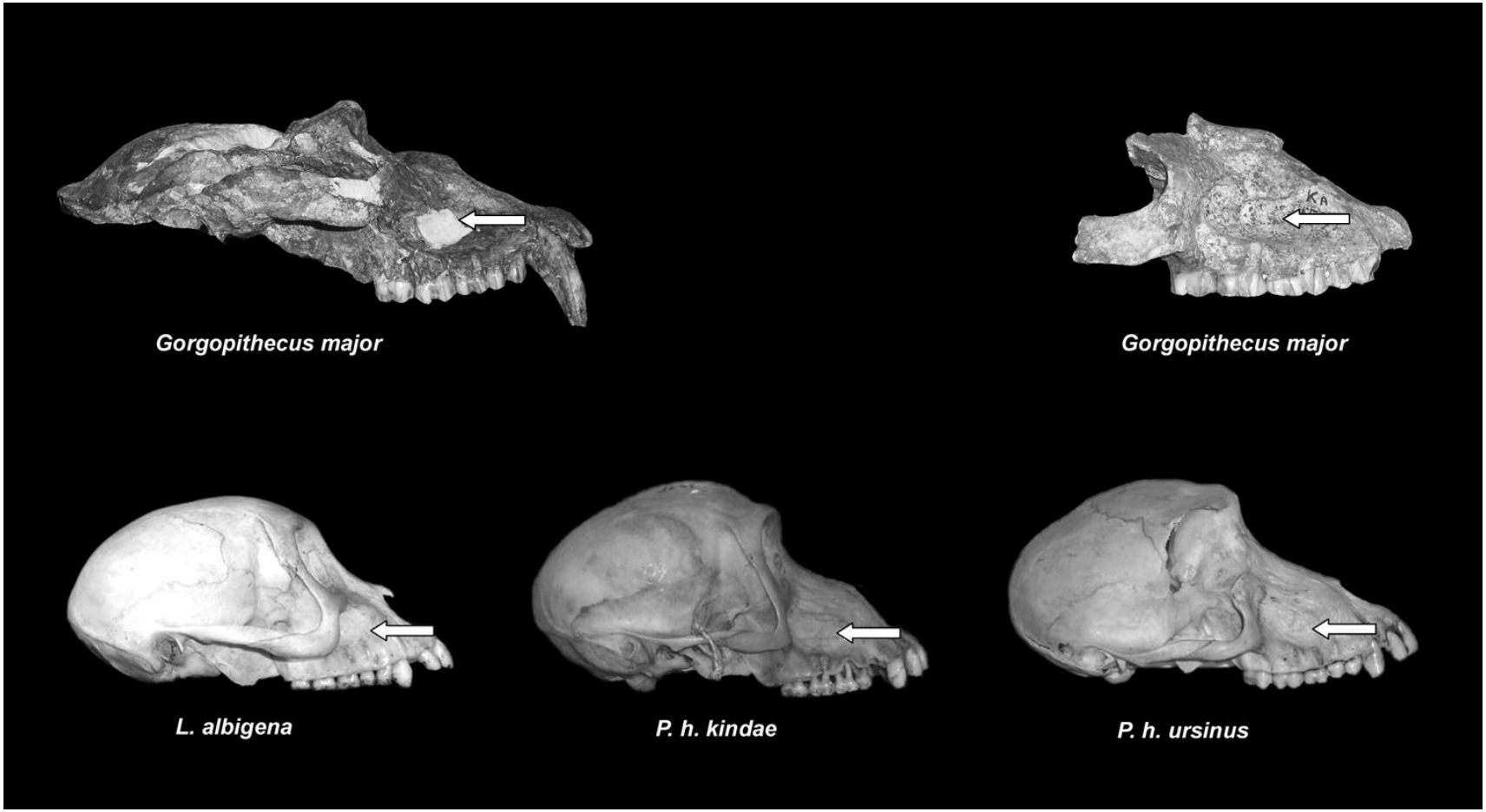
Gorgopithecus major
Gorgopithecus major
L. albigena
P. h. kindae
P. h. ursinus

Figure 3.13

Table 3.1. Fossil Taxa/OTUs recognized and used in this study.

Fossil Taxon/OTU	Size Category	Sample Size (Males, Females)	Key specimens	Source
Dinopithecus ingens	Large	(4, 8)	SB 7, SK 401, SK 542a, SK 546, SK 548, SK 553, SK 554, SK 574, SK 599, SK 600, SK 603, SK 604a	Freedman 1957; this study
Gorgopithecus major	Large	(5, 1)	KA 150, KA 153, KA 192, KA 524/676, KA 605, KA 944	Freedman 1957; this study
Lophocebus cf. albigena	Small	(4, 5)	KNM-ER 594, KNM-ER 595, KNM-ER 827, KNM-ER 898, KNM-ER 3090, KNM-ER 6014, KNM-ER 6063, KNM-ER 40476, KNM-ER 44260	this study
Papio izodi	Male Cranium = Small Male Mandible = Large Females = Large	(8, 10)	CO 100, CO 102, CO 115/103, CO 135A, KA 156, KA 161, KA 165, KA 166, KA 167C, KA 168, KA 194, KB 94, TP4/M681/AD946, TP7/M684/AD992, TP10, UCMP 12584, UCMP 12585, UCMP 125856	Freedman, 1957; Freedman, 1961; this study

Papio quadratirostris (USNO)	Large	(1, X)	NME-USNO	Iwamoto, 1982; Eck and Jablonski, 1984; Delson and Dean, 1993; this study
Papio quadratirostris (Omo)	Large	(2, 2)	NME Omo 47-1970-2008, NME Omo 42-1972-1, NME Omo L-185-6, NME Omo 75N (71)-C2	Delson and Dean, 1993 this study
Papio quadratirostris (Angola)	Large	(1, 2)	DGUNL LEBA02, DGUNL LEBA03, DGUNL LEBA06	Delson and Dean, 1993; this study
Parapapio ado	Males = Small Females = Large	(4, 1)	KNM-KP 286, KNM-KP 29306, KNM-KP 30147, KNM-KP 30538, KNM-WT 16752	Patterson, 1968; Leakey, 2003; this study
Parapapio broomi	Large	(17, 17)	M202/MP2, M211/MP11, M2961, M2962/MP76, M2978/MP92, M3037, M3067, STS 254, STS 255, STS 258, STS 264, STS 267, STS 297, STS 331, STS 332, STS 335, STS 337, STS 338, STS 339, STS 360, STS 363, STS 378A, STS 379, STS 390A, STS 393, STS 396A, STS 397, STS 409, STS 411A/B, STS 469, STS 534, STS 542, STS 562, STS 564	Freedman, 1957; Freedman, 1960; Maier, 1970; Freedman and Stenhouse, 1972; Eisenhart, 1972; this study

Parapapio jonesi	Male Cranium = Large Male Mandible = Small Females = Large	(2, 11)	AL 363-15, AL 363-1, M215/MP15, M218/MP18, M3051/MP 165, STS 250, STS 284, STS 313, STS 355, STS 372, STS 547, STS 565, SWP (STW) 27	Freedman, 1957; Freedman, 1960; Maier, 1970; Freedman, 1972 Freedman and Stenhouse, 1972; Eisenhart, 1972; Frost and Delson, 2002; this study
Parapapio lothagamensis		(5, 2)	KNM-LT 419, KNM-LT 448, KNM-LT 449, KNM-LT 23065, KNM-LT 23091, KNM-LT 24111, KNM-LT 24136	Leakey, 2003; this study
Parapapio whitei	Large	(5, 5)	M3072, MP221, MP223, STS 259, STS 266, STS 352, STS 359, STS 374, STS 389, STS 563	Freedman, 1957; Maier, 1970; Freedman, 1976 Freedman and Stenhouse, 1972; Eisenhart, 1972; this study
Pliopapio alemui	Small	(4, 5)	ARA-VP 1007, ARA-VP 1723, ARA-VP 1/73, ARA-VP 1/133, ARA-VP 1/563, ARA-VP 1/1006, ARA-VP 1/2553, ARA-VP 6/437, ARA-VP 6/933	Frost, 2001; this study

Procercocebus antiquus	Males = Small Females = Large	(4, 14)	SAM 4850, SAM 5356, SAM 5364, M3078, M3079, T11, T14, T17, T18, T20, T25, T21, TP8, TP9, TP13, UCMP 56624, UCMP 56653, UCMP 56694, UCMP 56821/125956	Gilbert, 2007; this study
?Theropithecus baringensis	Large	(1, X)	KNM-BC 2	Leakey, 1969; Eck and Jablonski, 1984 this study
Theropithecus brumpti	Large	(12, 5)	NME L17-45, NME 32-154, NME L32-155, NME L122-34, NME L338Y-2257, NME L345-3, NME L345-287, NME L576-8, KNM-WT 16749, KNM-WT 16806, KNM-WT 16808, KNM-WT 16828, KNM-WT 16888, KNM-WT 17571, KNM-WT 17555, KNM-WT 17560, KNM-WT 39368CX	Eck and Jablonski, 1987; this study
Theropithecus oswaldi darti	Large	(12, 5)	M2974, MP44, MP217, MP222, NME AL 58-23, NME AL 134-5, NME AL 142-19, NME AL 144-1, AL 153-14, NME AL 163-11, NME AL 186-17, NME AL 187-10, NME AL 196-3, NME AL 205-1, NME AL 208-10, NME AL 321-12,	Eck, 1993; Eck and Jablonski, 1987; Freedman, 1957; Maier, 1970; this study

Victoriapithecus macinnesi	X	(4, 2)	KNM-Mb 18993, KNM-MB 21027, KNM-MB 27876, KNM-MB 29100, KNM-MB 29158, KNM-MB 31281	Benefit, 1987; Benefit and McCrossin, 1993; Benefit and McCrossin, 1997; this study

Notes: Sample sizes are listed for key specimens, identifiable to sex, used in character analysis. Measurements and character state assignments were made and supplemented with additional data from the major sources listed for each taxon.

Table 3.2. Characters Used in This Study.

Variable	Definition	Character Type	Reference
*C1	Glabella-inion	QN, O	Wood, 1991
*C2	Bregma-basion	QN, O	Wood, 1991
*C3	Minimum frontal breadth (minimum chord distance between frontotemporale; i.e., maximum width in the coronal plane)	QN, O	Wood, 1991
*C4	Biporionic breadth	QN, O	Wood, 1991
*C5	Glabella-bregma	QN, O	Wood, 1991
*C6	Postglabellar sulcus-bregma (distance between the deepest point of the postglabellar depression and bregma)	QN, O	Wood, 1991
*C7	Parietal-sagittal chord (bregma-lambda)	QN, O	Wood, 1991
*C8	Parietal-lambdoid chord (chord distance along the lambdoid border of the intact parietal)	QN, O	Wood, 1991
C9	Lambda-inion	QN, O	Wood, 1991
C10	Occipital-sagittal length (lambda-opisthion)	QN, O	Wood, 1991
*C11	Foramen magnum max width	QN, O	Wood, 1991
C12	Occipital condyle max length	QN, O	Wood, 1991
C13	Lambda thickness of parietal	QN, O	Wood, 1991
*C14	Breadth between carotid canals	QN, O	Chamberlain, 1987
*C15	Breadth between petrous apices	QN, O	Chamberlain, 1987
C16	Length of tympanic plate (distance from the most lateral point on the inferior surface of the tympanic plate to the carotid canal)	QN, O	Chamberlain, 1987
C17	Adult male sagittal crest position	QL, O	Eck and Jablonski, 1984; 1987
C18	Postorbital sulcus	QL, U	Szalay and Delson, 1979
*C19	Auditory meatus position	QL, O	Groves, 1978; 2000

C20	Anterior temporal line divergence	QL, O	Groves, 2000; McGraw and Fleagle, 2006; Gilbert, 2007
C21	Nuchal lines in the midline where discernable	QL, O	Gilbert, 2007
*C22	Calvarial shape (biporionic length / glabella-inion)	QN, O	General
C23	Cranial vault index (basion-bregma / glabella-inion)	QN, O	General
*C24	Postorbital constriction (min frontal breadth / max biorbital breadth)	QN, O	General
*C25	Compound temporonuchal crest	QL, O	Strait et al., 1997
C26	Definitive parietal notch	QL, O	Groves, 2000
*C27	Position of the tympanic relative to the postglenoid process	QL, O	Groves, 2000
C28	Postglenoid process height	QL, O	Groves, 2000
C29	EAM tympanic crest	QL, O	Groves, 2000
*C30	Foramen magnum max length (opisthion-basion)	QN, O	General
C31	Position of the foramen magnum relative to the biporionic line	QL, O	Dean and Wood, 1981, 1982; Strait et al., 1997
C32	EAM size	QL, O	Strait and Grine, 2004
*C33	Opisthion-inion	QN, O	General
*C34	Bieuryonic breadth	QN, O	General
*C35	Breadth between infratemporal crests (measured where spheno-temporal suture meets the infratemporal crest)	QN, O	Chamberlain, 1987; Collard and Wood, 2000; 2001
C36	Basioccipital length (basion to sphenoccipital synchondrosis in the midline)	QN, O	Chamberlain, 1987
C37	Anterior basioccipital breadth (measured across the sphenoccipital synchondrosis)	QN, O	Chamberlain, 1987
*C38	Posterior basioccipital breadth (measured across the anterior edge of the jugular foramina)	QN, O	Chamberlain, 1987
*C39	Basisphenoid length (measured from the sphenoccipital synchondrosis to the junction with the vomer in the midline)	QN, O	General
C40	Petrous apex ossified beyond spheno-occipital synchondrosis	QL, O	Collard and Wood, 2000

*C41	Shape of the choanal sides	QL, O	Groves, 2000
*C42	Shape at the posterior end of the medial pterygoid plates	QL, O	Groves, 2000
C43	Shape at the posterior edge of vomer	QL, O	Groves, 2000
C44	Vomer-presphenoid junction	QL, O	Groves, 2000
C45	Vomer/Sphenoid/Palatine contact	QL, U	General
*C46	Vomer/sphenoid contact in the midline	QL, O	General
C47	Petrous process position	QL, O	Gilbert, 2007
C48	Appearance of fossae anterior to the foramen magnum	QL, O	General
*F1	Superior facial height (nasion-prosthion)	QN, O	Wood, 1991
F2	Alveolar height (nasospinale-prosthion)	QN, O	Wood, 1991
*F3	Superior facial breadth (frontomalaretemporale-frontomalaretemporale)	QN, O	Wood, 1991
F4	Bizygomatic breadth (zygion-zygion)	QN, O	Wood, 1991
*F5	Bimaxillary breadth (zygomaxillare-zygomaxillare)	QN, O	Wood, 1991
F6	Anterior interorbital breadth (maxillofrontale-maxillofrontale)	QN, O	Wood, 1991
*F7	Orbital height (maxillofrontale-ektoconchion)	QN, O	Wood, 1991
F8	Minimum malar height (min distance from inferior orbital margin to inferior border of zygomatic process of the maxilla)	QN, O	Wood, 1991
F9	Maximum nasal aperture width (max width at whatever height it occurs)	QN, O	Wood, 1991
*F10	Nasal height (nasion-nasospinale)	QN, O	Wood, 1991
*F11	Sagittal length of nasal bones (nasion-rhinion)	QN, O	Wood, 1991
*F12	Superior breadth of nasal bones (max chord distance across the paired nasal bones at their proximal end)	QN, O	Wood, 1991
F13	Inferior breadth of nasal bones (maximum chord distance across the paired nasal bones at their distal end)	QN, O	Wood, 1991
F14	Zygomaxillare-porion	QN, O	Wood, 1991
*F15	Upper facial prognathism	QN, O	Chamberlain, 1987
*F16	Lower facial prognathism	QN, O	Chamberlain, 1987

F17	Lacrimal bone position	QL, O	Szalay and Delson, 1979; Strasser and Delson, 1987; Benefit and McCrossin, 1993
F18	Medial orbital wall composition	QL, O	Trevor-Jones, 1972
F19	Presence/Absence of maxillary fossae	QL, O	Szalay and Delson, 1979
*F20	Development of maxillary fossae	QL, O	Gilbert, 2007
F21	Maxillary ridge in males	QL, O	General
F22	Muzzle dorsum outline	QL, U	General
F23	Contact of maxillary frontal processes	QL, O	General
F24	Frontal/premaxilla contact	QL, O	General
F25	Maxillary sinus	QL, O	General
F26	Positioning of the zygomatic foramina	QL, U	General
F27	Projection of nasal bones	QL, O	General
F28	Glabella prominence	QL, O	General
F29	General facial profile in lateral view	QL, O	General
F30	Nasal bone orientation in lateral view	QL, O	Gilbert, 2007
F31	Nasal bone extension over nasal aperture	QL, U	Gilbert, 2007
F32	Anteorbital drop	QL, O	General
F33	Piriform profile	QL, O	General
*F34	Relative nasal length (nasion-rhinion / nasion-prosthion)	QN, O	Szalay and Delson, 1979; Groves, 1989
F35	Maximum nasal aperture height (rhinion-nasospinale)	QN, O	General
*P1	Maxillo-alveolar length (Prosthion to a point where the line joining the posterior borders of the maxillary tuberosities crosses the median plane)	QN, O	Wood, 1991
*P2	Maxillo-alveolar breadth (ectomolare-ectomolare)	QN, O	Wood, 1991

*P3	Incisive canal-palatomaxillary suture (distance between the posterior edge of the incisive canal and the palatomaxillary suture)	QN, O	Wood, 1991
P4	Upper incisor alveolar length (distance between prosthion and the midpoint of the interalveolar septum between I^2 and C)	QN, O	Wood, 1991
P5	Palatal height at M^1 (Height in the midline between an imaginary line joining the alveolar process at the midpoint of M^1 and the roof of the palate)	QN, O	Wood, 1991
P6	Upper premolar alveolare length (min distance between the midpoints of the interalveolar septa between C/P^3 and P^4/M^1)	QN, O	Wood, 1991
P7	Upper molar length (Min distance between the midpoint of the P^4/M^1 interalveolar septum and the most posterior of the walls of the M^3 alveoli)	QN, O	Wood, 1991
P8	Canine interalveolar distance (min distance between the upper canine alveoli)	QN, O	Wood, 1991
P9	Last premolar interalveolar distance (min distance between the palatal walls of the P^4 alveoli)	QN, O	Wood, 1991
*P10	Second molar interalveolar distance (min distance between the palatal walls of the M^2 alveoli)	QN, O	Wood, 1991
*P11	I^1 MD crown diameter (max crown diameter parallel to the cervical line)	QN, O	Wood, 1991
*P12	I^1 BL crown diameter (max crown diameter perpendicular to the basal part of the labial enamel surface)	QN, O	Wood, 1991
P13	C^1 MD crown diameter (max diameter of crown perpendicular to the labiolingual axis of the tooth)	QN, O	Wood, 1991
P14	C^1 BL crown diameter (max diameter of the crown in the labiolingual axis of the tooth)	QN, O	Wood, 1991
*P15	M^3 interalveolar distance (min distance between the inner aspect of the alveolar process at the midpoint of M^3)	QN, O	Wood, 1991
P16	Palate depth at incisive fossa (the most inferior point on the posterior margin of the incisive fossa in the midline to the line between the centers of the alveolar margin on the lingual sides of C^1s)	QN, O	Chamberlain, 1987
P17	Upper premolar ratio (P^4 crown area / M^1 crown area)	QN, O	Fleagle and McGraw, 1999; 2002
P18	Mesial compressed sulcus on upper male canine	QL, O	Szalay and Delson, 1979;

			Strasser and Delson, 1987
P19	Premaxilla Length (premaxillary suture at level of alveoli to prosthion)	QN, O	General
P20	Bilophodont molars	QL, O	General
P21	P^3 protocone relative to paracone	QL, O	Szalay and Delson, 1979
P22	M^3 distal loph reduction (BL width of M^3 mesial loph / BL width of M^3 distal loph)	QN, O	Szalay and Delson, 1979
P23	Upper I^1 shape	QL, O	Szalay and Delson, 1979; Strasser and Delson, 1987
P24	Upper I^2 shape	QL, O	Szalay and Delson, 1979; Strasser and Delson, 1987
P25	Female C^1 shape	QL, U	Szalay and Delson, 1979; Napier 1981; 1985
P26	Size of I^1 relative to I^2	QL, O	General
*P27	Canine size (canine crown area)	QN, O	General
*P28	Canine size dimorphism (male relative canine crown area / female relative canine crown area)	QN, O	General
P29	Upper molariform crown shape (M^2 max BL width / M^2 max MD length)	QN, O	Szalay and Delson, 1979
P30	Molar flare	QL, O	Szalay and Delson, 1979; Frost, 2001a; 2001b
P31	M^1 shape (BL width of mesial loph / BL width of distal loph)	QN, O	Szalay and Delson, 1979
P32	M^2 shape (BL width of mesial loph / BL width of distal loph)	QN, O	Szalay and Delson, 1979
*M1	Symphyseal height (min distance between the base of the symphysis and infradentale)	QN, O	Wood, 1991
*M2	Maximum sypmhyseal depth (max depth, at right angles to symphyseal height)	QN, O	Wood, 1991
M3	Corpus height at M_1	QN, O	Wood, 1991
M4	Corpus width at M_1 (max width at right angles to corpus height at M_1, taken at the midpoint of M_1)	QN, O	Wood, 1991

M5	Corpus height at M_3	QN, O	Wood, 1991
M6	Corpus width at M_3 (max width at right angles to corpus height at M_3, taken at the midpoint of M_3)	QN, O	Wood, 1991
*M7	Lower premolar alveolar length (min distance between the midpoints of the interalveolar septa between C/P_3 and P_4/M_1)	QN, O	Wood, 1991
M8	Lower molar alveolar length (min distance between the midpoints of the interalveolar septa between P_4/M_1 and the most posterior of the walls of the M_3 alveolus)	QN, O	Wood, 1991
M9	P_4 max mesiodistal crown diameter	QN, O	Wood, 1991
M10	P_4 max buccolingual crown diameter	QN, O	Wood, 1991
M11	M_1 max mesiodistal crown diameter	QN, O	Wood, 1991
M12	M_1 max buccolingual crown diameter	QN, O	Wood, 1991
M13	M_2 max mesiodistal crown diameter	QN, O	Wood, 1991
M14	M_2 max buccolingual crown diameter	QN, O	Wood, 1991
M15	Lower premolar ratio (P_4 crown area / M_1 crown area)	QN, O	Fleagle & McGraw; 1999; 2002
M16	P_3 distal cingulum	QL, O	Szalay and Delson, 1979
M17	Buccal face of P_4 crown	QL, O	Szalay and Delson, 1979
M18	P_4 mesiobuccal flange, an extension of the enamel cap down onto the root	QL, O	Szalay and Delson, 1979
M19	Lower molar hypoconulid	QL, O	Szalay and Delson, 1979
M20	M_3 tuberculum sextum	QL, O	General
M21	Enamel folding	QL, O	Szalay and Delson, 1979
M22	Lophid orientation relative to the mandibular corpus	QL, O	Szalay and Delson, 1979
M23	Accessory cuspules in lower molar notches	QL, O	Szalay and Delson, 1979
M24	Lower incisor lingual enamel	QL, O	Szalay and Delson, 1979
M25	Shape of lower I_2 distal surface	QL, O	Szalay and Delson, 1979
M26	Mandibular ramus angle	QL, O	Szalay and Delson, 1979; Eck and Jablonski, 1993
M27	Gonial region expansion on mandibular ramus	QL, O	General

M28	Inferior portion mandibular symphysis length as scored to a specific tooth in occlusal view	QL, U[1]	General
M29	Median mental foramen	QL, O	Szalay and Delson, 1979
M30	Mental ridges on the symphysis in males	QL, O	Szalay and Delson, 1979
M31	Development of mandibular corpus fossae	QL, O	Gilbert, 2007
M32	Width of the extramolar sulcus	QL, O	General
M33	Lingual mental foramina positioning	QL, U	Gilbert, 2007
*M34	P_4 crown shape (P_4 max BL width / P_4 max MD length)	QN, O	General
M35	M_1 crown shape (M_1 max BL width / M_1 max MD length)	QN, O	General
*M36	M_2 crown shape (M_2 max BL width / M_2 max MD length)	QN, O	General
M37	P_3 lingual "bulge", i.e., P_3 crown obliquity	QL, O	General
M38	Lower molariform tooth shape (M_1 mesial lophid / M_1 distal lophid)	QN, O	Szalay and Delson, 1979
*M39	Mandibular profile (corpus height at M_1 / corpus height at M_3)	QN, O	Szalay and Delson, 1979
M40	Curve of Spee shape	QL, O	Eck and Jablonski, 1984; Delson and Dean, 1993
M41	Symphyseal sloping	QL, O	Frost, 2001
BS1	Body Size	QL, O	Smith and Jungers, 1997; Delson et al., 2000; Fleagle, 1999

Notes: Variables are classified by cranial region as follows: C = Cranial vault and base; F = Face; P = Palate and Upper Dentition, M = Mandible and lower dentition

QN = Quantitative character

QL = Qualitative character

O = Ordered

U = Unordered

* Character determined to be influenced by allometry

[1] Character considered ordered in female analysis

Table 3.3 Detailed Definition of Qualitative Characters Used in This Study.

Variable	Detailed Definition
C17	States: 0 = absent, 1 = intermediate, 2 = present only posteriorly, 3 = intermediate, 4 = extends anteriorly. The distinction between states 2 and 4 is determined by whether the anteriormost point of the crest is well anterior to bregma or begins at or posterior to bregma. Crest is defined here as the meeting or contact of the temporal lines.
C18	States: 0 = absent, 1 = intermediate, 2 = post-glabellar depression present, 3 = intermediate, 4 = post-orbital sulcus present, 5 = polymorphic
*C19	Small Taxa States: 0 = medial (inferior margin of the meatus is medial to porion and thus overhung by a supermeatal roof), 1 = intermediate, 2 = Extended laterally relative to the medial state, but still medial to the lateral border of the neurocranium
	Large Taxa States: 0 = Extended laterally relative to the medial state, but still medial to the lateral border of the neurocranium, 1 = intermediate, 2 = lateral (inferior margin of the meatus is lateral to porion)
C20	States: 0 = not widely divergent (i.e., pinched or slightly divergent), 1 = intermediate, 2 = widely divergent
C21	States: 0 = downturned, 1 = intermediate, 2 = upturned
*C25	Small Taxa States: 0 = absent, 1 = intermediate, 2 = partial crest confined to the lateral third of bi-asterionic breadth
	Large Taxa States: 0 = partial crest confined to the lateral third of bi-asterionic breadth, 1 = intermediate, 2 = extensive crest extending almost the entire distance between inion and the lateral margin of the supramastoid crest
C26	States: 0 = parietal/asterionic notch absent, 1 = intermediate, 2 = parietal/asterionic notch present
*C27	Small Taxa States: 0 = tympanic fused with postglenoid, 1 = intermediate, 2 = tympanic unfused and separated from the postglenoid process
	Large Taxa States: 0 = tympanic unfused and separated from the postglenoid process, 1 = intermediate, 2=tympanic unfused and widely separated from the tympanic
C28	States: 0 = very tall, 1 = intermediate, 2 = normal, 3 =intermediate, 4 = shortened
C29	States: 0 = present, 1 = intermediate, 2 = absent

C31	States: 0 = basion is well posterior to the line, 1 = intermediate, 2 = basion approximates the line, 3 = intermediate, 4 = basion is well anterior to the line
C32	States: 0 = small, 1 = intermediate, 2 = large
C40	States: 0 = absent, 1 = intermediate, 2 = present
*C41	Small Taxa States: 0 = divergent posteriorly, 1 = intermediate
	Large Taxa States: 0 = intermediate, 1 = parallel
*C42	Small Taxa States: 0 = moderately divergent, 1 = intermediate, 2 = strongly divergent
	Large Taxa States: 0 = intermediate, 1 = moderately divergent, 2 = intermediate
C43	States: 0 = not incised, 1 = intermediate, 2 = incised
C44	States: 0 = vomer non-inflated, 1 = intermediate, 2 = vomer inflated
C45	States: 0 = meet at one point, 1 = intermediate, 2 = separated by another bone, 3 = intermediate, 4 = palatine doesn't reach vomer, 5 = polymorphic
*C46	Small Taxa States: 0 = intermediate, 1 = another bone between
	Large Taxa States: 0 = clean contact, 1 = intermediate
C47	States: 0 = medially positioned, 1 = intermediate, 2 = laterally positioned
C48	States: 0 = absent or poorly defined, 1 = intermediate, 2 = present and clearly visible, 3 = intermediate, 4 = deeply excavated and sharply defined
F17	States: 0 = extends outside the orbit, 1 = intermediate, 2 = within orbit
F18	States: 0 = vomer contribution (frontal covers ethmoid), 1 = ethmoid contribution
F19	States: 0 = absent, 1 = intermediate, 2 = present
*F20	Given present in F19, Small Taxa States: 0 = extend up to the infraorbital plate, 1 = intermediate, 2 = invades infraorbital plate, 3 = intermediate, 4 = deeply invades the infraorbital plate
	Given present in F19, Large Taxa States: 0 = superior to alveolus only, 1 = intermediate, 2 = extend up to the infraorbital plate, 3 - intermediate, 4 = invades infraorbital plate
F21	States: 0 = absent, 1 = intermediate, 2 = present
F22	States: 0 = rounded, 1 = intermediate, 2 = peaked, 3 = intermediate, 4 = flat, 5 = polymorphic between states 0 and 4, 6 = polymorphic between states 0, 2, and 4
F23	States: 0 = frontal processes of maxillae do not meet in the midline, 1 = intermediate, 2 = frontal processes of maxillae meet in the midline

F24	States: 0 = absent, 1 = intermediate, 2 = present
F25	States: 0 = absent, 1 = present
F26	States: 0 = no foramina observable, , 1 = intermediate, 2 = at or below plane of orbital rim, 3 = intermediate, 4 = foramina above and below the plane of the orbital rim, 5 = intermediate, 6 = above plane of orbital rim, 7 = polymorphic
F27	States: 0 = nasal bones do not project above the frontal/maxillary suture, 1 = intermediate, 2 = nasal bones project above the frontal/maxillary suture
F28	States: 0 = glabella not prominent, 1 = intermediate, 2 = glabella prominent
F29	States: 0 = straight, 1 = intermediate, 2 = concave
F30	States: 0 = straight (after anteorbital drop, if present), 1 = intermediate, 2 = slightly upturned, 3 = intermediate, 4 = upturned
F31	States: 0 = no extension, 1 = intermediate, 2 = slight extension, 3 = intermediate, 4 = significant extension, 5 = polymorphic
F32	States: 0 = absent, 1 = intermediate, 2 = present
F33	States: 0 = no anteorbital drop, distinct point at rhinion, 1 = intermediate, 2 = anteorbital drop, distinct point at rhinion, 3 = intermediate, 4 = anteorbital drop, no distinct point at rhinion
P18	States: 0 = present on the crown only, 1 = present and extends onto root
P20	States: 0 = incomplete bilophodonty, 1 = intermediate, 2 = complete bilophodonty
P21	States: 0 = protocone strongly reduced or absent, 1 = protocone present and significantly shorter than paracone, 2 = paracone present and nearly equal in height to the paracone
P23	States: 0 = rhomboidal, 1 = spatulate (defined as lingually cupped with flare, not flare by itself)
P24	States: 0 = caniniform, 1 = apically and mesially inclined
P25	States = 0 = “masculine”, 1 = intermediate, 2 = conical, 3 = intermediate, 4 = incisiform
P26	States: 0 = $I^1 \sim I^2$, 1 = intermediate, 2 = $I^1 > I^2$
P30	States: 0 = Low level of flare, 1 = intermediate level of flare, 2 = high level of flare
M16	States: 0 = absent, 1 = present
M17	States = 0 =straight as seen in occlusal view, 1 = inflated as seen in occlusal view
M18	States: 0 = absent, 1 = present
M19	States: 0 = Hypoconulid present in all lower molariform teeth, 1 = intermediate, 2 = Hypoconulid absent in all lower molariform teeth except M_3, 3 = intermediate, 4 = Hypoconulid absent in all lower molariform teeth

M20	States: 0 = absent, 1 = intermediate, 2 = present
M21	States: 0 = non-elevated, 1 = elevated
M22	States: 0 = transverse, 1 = intermediate, 2 = oblique
M23	States: 0 = absent, 1 = intermediate, 2 = present
M24	States: 0 = absent, 1 = present
M25	States: 0 = straight, 1 = intermediate, 2 = bulge, 3 = intermediate, 4 = distinct prong
M26	States: 0 = inclined, 1 = intermediate, 2 = vertical
M27	States: 0 = absent, 1 = intermediate, 2 = present
M28	States: 0 = P_3, 1 = intermediate, 2 = P_3-P_4, 3 = intermediate, 4 = P_4, 5 = intermediate, 6 = P_4-M_1, 7 = intermediate, 8 = M_1, 9 = polymorphic
M29	States: 0 = absent, 1 = present
M30	States: 0 = absent, 1 = present
M31	States: 0 = absent, 1 = intermediate, 2 = present
M32	States: 0 = narrow, 1 = intermediate, 2 = moderate, 3 = intermediate, 4 = wide
M33	States: 0 = present- single, 1 = intermediate, 2 = present- horizontally positioned, 3 = intermediate, 4 = present- vertically positioned, 5 = intermediate, 6 = present- variably positioned, 7 = polymorphic
M37	States: 0 = lingual bulge absent (not oblique), 1 = lingual bulge is present (oblique)
M40	States: 0 = normal, 1 = intermediate, 2 = reversed
M41	States: 0 = absent, 1 = intermediate, 2 = present (sloping), 3 = intermediate, 4 = present, extremely sloping
BS1	0 = Small Taxa, 1 = Large Taxa

Notes: Variables are classified by cranial region as follows: C = Cranial vault and base; F = Face; P = Palate and Upper Dentition, M = Mandible and lower dentition. * Character determined to be influenced by allometry.

Table 3.4. Summary of Most Parsimonious Phylogenetic Tree Produced From Heuristic Search In PAUP 4.10b With Bootstrap Support For Various Clades.

Tree Length	CI	RI	RC	HI	Bootstrap Support, %		
					Lophocebus/L. cf. albigena	***T. baringensis/T. brumpti/T. darti/T. gelada***	***T. brumpti/T. darti/T. gelada***
1305	0.441	0.41	0.181	0.559	75%	66%	61%

Table 3.5. *P. quadratirostris* premolar size through time in the Omo River Basin, Ethiopia

Specimen	Omo Usno/Shungura Member	Estimated Age	P^4/M^1 ratio	P_4/M_1 ratio
Usno	U-8 or U-9	3.3 Ma	52.8	X
NME L 185-6	E	2.5 Ma	(67.4)	X
NME L 4-13b	E	2.5 Ma	67.7	X
NME Omo 42-1972-1	F	2.4 Ma	71.9	X
NME Omo 47-1970-2008	G	2.3 Ma	X	83.0

Notes: Premolar ratios = (P4 area / M1 area) x 100. Numbers in parentheses represent estimates. Estimated age values from Delson and Dean (1993) and Eck and Jablonski (1987).

Table 3.6. Selected Synapomorphies Suggested By Character Transformation Analyses.

	Sex-Averaged Synapomorphies	Character Reference
NODE 1 **African Papionins**	**Wide Interorbital Distance**, Reduced Projection of Nasal Bones Above the Fronto-Maxillary Suture in Females	F6, P14 (F)
NODE 2 **Crown African Papionins**	Broad Maxilla (Bi-Zygomaxillare) in Males, Greater Degree of Lower Facial Prognathism in Males, **Maxillary Fossae Present**, Tall Nasal Aperture in Females	F5 (M), F16 (M), F19, F35 (F)
NODE 3 ***Theropithecus***	Temporal Lines Meet to Form Sagittal Crest Well Anterior to Bregma, Low Cranial Vault Index in Females, **Deeply Excavated Fossae Anterior to Foramen Magnum**, Tall Malar Height in Females, Long Distance Between Zygomaxillare and Porion, **Small Incisors**, Short M_1 Mesial Lophs Relative to Distal Lophs in Females	C17 (M), C23 (F), C48, F8 (F), F14 (F), P26, P29 (F)
	Wide Nasal Bones Superiorly in Females, **Very Deep/Extensive Maxillary Fossae**	F12 (F), F20
NODE 4 ***Papio/Lophocebus/ Gorgopithecus***		

NODE 5 ***P. quadratirostris/*** ***Mandrillus/Cercocebus/Procercocebus***	Widely Divergent Temporal Lines, **Upturned Nuchal Crests Across the Midline**, Narrow Bi-Zygomatic Breadth in Females, Long Upper Premolar Row in Females	C20 (M), C21, F4 (F), P6 (F)

Notes: Characters in bold are recognized as synapomorphies in both males and females. Only those reconstructed synapomorphies that display low degrees of homoplasy are listed here. See Figure 3.4 for tree with corresponding nodes. (M) refers to those character states found as synapomorphies only among males; (F) refers to those character states found as synapomorphies only among females

Chapter 4

Phylogenetic Analysis of the African Papionin Basicranium using 3-D Geometric Morphometrics

Abstract

In this chapter, I apply 3-D geometric morphometric techniques in a phylogenetic analysis of African papionin basicranial morphology. The effects of allometry strongly influence papionin basicranial morphology, and unless these size effects are controlled or eliminated, phylogenetic analyses suggest traditional phylogenetic groupings of small taxa (mangabeys) and large taxa (geladas, mandrills, drills, and baboons). When the effects of allometry are eliminated by excluding size-correlated PC scores, phylogenetic analyses of papionin basicranial morphology are incongruent with recent molecular and morphological studies of African papionins. By contrast, a cladistic analysis of basicranial characters suggests the same phylogenetic relationships as recent molecular and morphological studies for the extant African papionins. The addition of fossil taxa, noted to generally increase phylogenetic accuracy, results in phylogenetic hypotheses inconsistent with recent results of molecular and morphological studies of extant and fossil African papionins. These results suggest that important phylogenetic information is contained within the size-correlated PCs, and this information is being discarded during the attempt to eliminate the effects of body size. Future 3-D morphometric studies of phylogeny should focus on the development of methodologies to adjust for allometric effects.

Introduction

In contrast to previous morphological studies (Fig. 4.1), more recent analyses have demonstrated that African papionin morphological and molecular data suggest congruent phylogenetic hypotheses (Fleagle and McGraw, 1999; 2002; Groves, 2000; Gilbert, 2007; Gilbert and Rossie, 2007; Chapter 2; Fig. 4.2). While the characters identified in these recent studies have focused on craniofacial and craniodental anatomy, it remains to be seen if other morphological regions also contain the same phylogenetic signal. One cranial region that has been suggested to be particularly informative in primate phylogenetic studies, and therefore worthy of additional scrutiny, is the basicranium.

For example, recent studies of the primate basicranium, specifically hominin and extant hominoid taxa, have proven extremely successful in identifying phylogenetic relationships from morphological data (Harvati, 2001; 2003; Lockwood et al., 2004). Lockwood et al. (2004) analyzed temporal bone morphology in a study that recovered phylogenetic trees of the extant great apes consistent with molecular phylogenies down to the subspecies level. Indeed, the basicranium has long been noted as an important region for analyzing primate phylogenetic relationships (e.g., Szalay and Delson, 1979; MacPhee and Cartmill, 1986; Ross, 1994; Kay et al., 1997; 2008; Ross et al., 1998; Ross and Covert, 2000; Bloch and Silcox, 2001; Cardini and Elton, 2008) as well as studies of hominin relationships (e.g. Strait et al., 1997; Strait, 2001; Harvati, 2001; 2003; Strait and Grine, 2004).

The results of the recent hominin and hominoid studies suggest that the basicranium may offer valuable information to place African papionin taxa in a secure phylogenetic context. This project uses a 3-D geometric morphometric analysis of the papionin basicranium in a further investigation of the phylogenetic signal contained within papionin cranial anatomy. If basicranial morphology suggests the same relationships as craniodental and molecular data (Fig. 4.2), it will strengthen the broader assertion that the basicranium is a particularly valuable source of phylogenetic information.

Methods

To assess patterns of variation in the papionin basicranium, data was collected on a large sample of over 800 extant papionin basicrania (Table 4.1). Specimens were sampled from the following collections: AMNH (American Museum of Natural History, New York), BMNH (British Museum of Natural History, London), FMNH (Field Museum of Natural History, Chicago), MCZ (Museum of Comparative Zoology, Harvard University), PCM (Powell-Cotton Museum, Birchington), RLS (Randy L. Susman personal collection, Stony Brook), RMCA (Royal Museum for Central Africa, Tervuren), TM (Transvaal Museum, South Africa), and UW-AS (Department of Anatomy, University of Witwatersrand, South Africa). A MicroScribe 3DX three-dimensional mechanical digitizer (Immersion Corp.) was used for all morphometric data collection. The 41 landmarks used to capture the shape of the basicranium are listed in Table 4.2 and illustrated in Figure 4.3; these landmarks were taken in part as a compilation of those used by Harvati (2003) and Lockwood et al. (2004). Additional basicranial landmarks deemed to be highly repeatable and potentially informative were added as well. Landmarks outside of the midline were taken on the right side of the basicranium only.

All landmark data were analyzed using 3-D geometric morphometric techniques. The data were imported into the software package Morphologika (O'Higgins and Jones, 1998), and Procrustes superimposition analyses were performed on all male basicrania, all female basicrania, and all basicrania combined. Following Procrustes superimposition, principal components analyses (PCA) were performed and a matrix of principal components (PCs) scores was produced for each specimen per analysis: males, females, and all basicrania. Generalized Procrustes Analysis adjusts only for non-allometric differences in size among specimens; thus, an adjustment for allometric size differences was required before phylogenetic analyses are performed. To account for the effects allometry, PCs significantly correlated with centroid size were excluded from further analyses involving clustering phylogenetic methods. Correlations were performed between average PC scores and average centroid sizes of each sex of each taxon for all analyses (male, female, and all basicrania). The critical r-value for a correlation with a sample size of 6 and 4 degrees of freedom at the 0.05 level is 0.811, while with a sample

size of 12 and 10 degrees of freedom the critical r-value is 0.576 (Rohlf and Sokal, 1995). Therefore, correlation r-values below 0.811 were considered insignificant in the male and female analyses, and r-values below 0.576 were considered insignificant in the analyses including all basicrania (i.e., sex-averaged analyses).

Following the exclusion of those principal components that were significantly correlated with centroid size, a mean matrix of the remaining first 52 PCs for each taxon (males, females and sex-averaged) was generated. Morphological (Euclidean) distances between taxa were then calculated in the NTSYSpc v.2.11c software package (Biostatistics, Inc.) for the male, female and sex-averaged matrices. In recognition of the improved results of combined-sex analyses for the analysis of cladistic craniodental data, male and female matrices were also combined into one large matrix in a final combined-sex analysis.

The resulting distances were then used in various neighbor-joining (NJ) and UPGMA clustering algorithms to generate phylogenetic hypotheses at the genus level. The NJ algorithm is not purely phenetic, and it has the advantage of outgroup assignment to provide a baseline polarity in terms of basicranial morphology (Lockwood et al., 2004). A composite *Macaca* as well as individual *Macaca* species were assigned as the outgroup for phylogenetic analyses in recognition that *Macaca* is a variable taxon and different species are argued to retain the primitive morphotype for the extant papionins.

Results

In all analyses, the first 52 PCs explained approximately 94% of the variance among the papionin basicrania. Eigenvalues and loadings of each of the first 52 PCs are provided in Table 4.3. Plots of the first 2 principal components in the male and female analyses are presented in Figures 4.4 and 4.5. In the male analysis, PC 1, PC 27, PC 38, and PC 42 were determined to be significantly correlated with centroid size (PC 1, r = 0.885, PC 27, r = -0.842, PC 38, r = 0.870, PC 42, r = 0.866). Among females, PC 1 and PC 48 were significantly correlated with centroid size (PC 1, r = 0.854, PC 48, r = -0.871). For the correlation analysis including all basicrania, only PC 1 was significantly correlated with centroid size (r = 0.866). Size-correlated PCs accounted for 30.7% of the

variance in the male analysis, 26.8% of the variance in the female analysis, and 29.3% in the sex-averaged (all basicrania) analysis. The effect of including size-correlated morphological shape in phylogenetic analysis is clearly demonstrated by the analyses illustrated in Figures 4.6, 4.9, and 4.12 for males, females and the sex-averaged sample. All NJ and UPGMA analyses that include size-correlated PCs result in the recovery of a tree suggesting a small-bodied group (*Cercocebus, Lophocebus*) and a large-bodied group (*Mandrillus, Papio, Theropithecus*) among African papionin taxa. These groupings are the same as those suggested by previous morphological studies (Figure 4.1b).

NJ and UPGMA trees excluding size-correlated PCs are presented in Figs. 4.7, 4.10, and 4.13 for males, females, and sex-averaged analyses, respectively. In all NJ and UPGMA trees that exclude size-correlated PCs, the mangabeys are diphyletic and *Lophocebus* is closest to *Papio*. *Theropithecus* is reconstructed as the most primitive African papionin in the NJ trees, while *Mandrillus* (males) or *Theropithecus* (females, sex-averaged) occupies this position in the UPGMA analyses.

The NJ trees that exclude size-correlated PCs and use individual *Macaca* taxa as outgroups (Figs. 4.8, 4.11, 4.14) are broadly similar to the same analyses that use an average *Macaca* (Figs. 4.7a, 4.10a, 4.13a). When *M. sylvanus*, *M. fascicularis*, and *M. mulatta* are individually used as outgroups, *Theropithecus* is suggested to be the most primitive African papionin taxon followed by successive branching of *Cercocebus* and *Mandrillus* (in some order) and finally the *Lophocebus/Papio* group. When *M. nemestrina* is used as an outgroup, however, the results are somewhat different. *Mandrillus* is the most primitive African papionin in these analyses, followed by a successive branching of *Theropithecus* and *Cercocebus* in the male analyses or a *Theropithecus/Cercocebus* and *Lophocebus/Papio* pairing in the other analyses (Figs. 4.8c, 4.11c, 4.14c). *Lophocebus* and *Papio* are reconstructed as sister taxa in all NJ analyses.

Finally, the combined-sex analyses (Fig. 4.15) suggest the same basic set of relationships as the male trees that exclude size-correlated PCs. NJ Trees suggest successive branching of *Theropithecus*, *Cercocebus*, *Mandrillus*, and then

Lophocebus/Papio. UPGMA analyses instead suggest the successive branching of *Mandrillus*, *Theropithecus*, *Cercocebus* and then *Lophocebus/Papio*.

Discussion

Results of this study illustrate the effects of allometry on the basicranial morphology of the African papionins. Including size-correlated PCs in phylogenetic analysis results in the grouping of small taxa (the mangabeys, *Cercocebus* and *Lophocebus*) and large taxa (*Theropithecus, Mandrillus* and *Papio*) (see Figs. 4.6, 4.9, 4.12). These groupings are similar to those hypothesized by previous analyses of morphological data (Fig. 4.1), and this suggests that allometry is largely responsible for the traditionally hypothesized systematic relationships of the African papionins.

Given the effect of allometry on the evolution of papionin basicranial morphology, the most informative analyses will be those that control or account for this phenomenon in some way. This study attempted to control for the effects of allometry by eliminating size-correlated PCs from phylogenetic analyses, thereby eliminating a large amount of the shape variance that is correlated with size. The results of this approach are similar to those of the early blood protein analyses (particularly Cronin and Sarich, 1976) in that they suggest the mangabeys to be diphyletic. At the very least, they imply that the traditional morphological groupings (Fig. 4.1) are incorrect (see Figs. 4.7, 4.10, 4.13). None of the analyses excluding PC 1 are congruent with the more recent molecular (e.g., Disotell et al., 1992; Disotell, 1994; 2000; Harris and Disotell, 1998; Harris, 2000; Tosi et al., 1999, 2003) and morphological analyses (e.g., Fleagle and McGraw, 1999; 2002; Gilbert, 2007; Gilbert and Rossie, 2007; Chapter 2) (Fig. 4.2). This is perhaps to be expected given that over a quarter of the shape variance is eliminated from the phylogenetic analysis. While eliminating size-correlated PCs is perhaps preferable to including the confounding effects of allometry, it is a rather crude method to attempt to control for changes in shape that are associated with changes in size. In this case, potentially useful phylogenetic information is being thrown out with the allometric bath water.

Broadly speaking, the results of this study suggest two possibilities regarding the ability of the papionin basicranium to accurately reflect phylogeny. It can be argued that basicranial shape, as represented by the PC matrices analyzed here, is not a highly informative phylogenetic region relative to other anatomical regions. This suggestion runs counter to recent 3-D geometric morphometric analyses of hominoids (Lockwood et al., 2004) and guenons (Cardini and Elton, 2008). Alternatively, it can be argued that difficulty in adjusting for the effects of allometry and other issues inherent in multivariate 3-D morphometric analyses of size-disparate taxa may help to obscure phylogenetic signals in basicranial shape.

To choose between these alternate possibilities, I conducted a direct comparison of the phylogenetic trees produced from 3-D geometric morphometrics of the basicranium to those produced from a cladistic analysis of 33 basicranial characters taken from the larger craniodental data set presented in Chapter 2 (Table 4.4). Results of the cladistic analysis demonstrate that male, female, sex-averaged, and combined-sex cladistic analyses of basicranial morphology, adjusted for allometry using the narrow allometric coding method, recover phylogenetic trees that are congruent with larger morphological data sets (Chapter 2) as well as molecular data (Fig. 4.2; Table 4.4). Furthermore, these trees have high bootstrap support (see Table 4.4). These results support other studies indicating that the basicranium is a highly informative phylogenetic region (Lockwood et al., 2004; Cardini and Elton, 2008), but suggest that the multivariate morphometric shape analyses and the PCs that contain the morphological information are not fine-grained enough, include too much "noise", or do not capture the same details as a given set of cladistic characters. The nature of principal components analyses, in particular the likely combination of many cladistic characters on individual size-correlated and size-uncorrelated PCs, effectively results in a character reduction that does not allow as fine-grained a phylogenetic analysis as cladistic studies.

While previous studies of papionin morphological data have also used sex-averaged analyses (e.g., Collard and O'Higgins, 2001; Collard and Wood, 2000; 2001; Singleton, 2002), and while this study also performed sex-averaged analyses for comparative purposes, there is little justification for such analyses in future phylogenetic studies. Papionins are highly sexually dimorphic taxa. Averaging highly dimorphic male

and female morphotypes results in the creation of an "imaginary" morphotype. While any average of morphological data is an imaginary morphotype, averaging multiple individuals of two shape dimorphic sexes results in a morphotype that is, from a phylogenetic perspective, a biologically irrelevant entity. Therefore, the sex-averaged analysis will not be discussed further in this study.

In another attempt to analyze both sexes simultaneously in phylogenetic analysis, the individual male and female matrices were combined into one large PC matrix, similar to the methodology described in Chapter 2. In terms of tree topology, the results of these combined-sex analyses were virtually identical to the sex-averaged analyses, and incongruent with recent molecular and morphological analyses (e.g., Disotell et al., 1992; Disotell, 1994; 2000; Harris and Disotell, 1998; Tosi et al., 1999, 2003; Fleagle and McGraw, 1999; 2002; Harris, 2000; Gilbert, 2007; Gilbert and Rossie, 2007; Chapter 2). One of the major reasons the combined-sex character matrices were effective in cladistic analyses is that they increased the number of characters analyzed and investigated phylogeny on a finer scale. As mentioned above, it would appear that multivariate data reduction methods such as PCAs result in many of these separate characters being "lumped" into various PCs, particularly PC 1 in both male and female matrices. This data reduction and, in effect, character reduction may also help to explain the relatively poor performance of the combined-sex analyses of 3D morphometric data relative to those reported in Chapter 2.

While phylogenetic trees generated from extant papionin basicranial anatomy are incongruent with trees generated from molecular data (Disotell et al., 1992; Disotell, 1994; 2000; Harris and Disotell, 1998; Harris, 2000; Tosi et al., 1999, 2003) and craniodental data (Gilbert and Rossie, 2007; Chapter 2), phylogenetic resolution may well improve with the inclusion of fossil taxa. Fossil taxa are especially important in phylogenetic analyses because they extend taxon sampling (e.g., Gauthier et al., 1988; Strait & Grine, 2004), provide unique morphologies that help to refine assessments of polarity (e.g., Gatesy & O'Leary, 2001; Springer et al., 2001; Gatesy et al., 2003), and increase overall phylogenetic accuracy (e.g., Wheeler, 1992; Zwickl & Hillis, 2002; Strait and Grine, 2004). Therefore, an analysis using the same methodology as described above including fossil taxa for both males and

females was performed. The maximum number of shared landmarks between the largest number of taxa was used in an effort to maximize landmark and taxon inclusion (29 landmarks among five fossil taxa for males and 25 landmarks among 5 taxa for females; see Table 4.5), resulting in reduced landmark lists for each sex compared to the extant analyses. Due to the differing number of landmarks and taxa between male and female analyses including fossil taxa, sex-averaged and combined-sex analyses were not performed. The results of the analyses excluding size-correlated PCs are presented in Figures 4.16 and 4.17.

While the inclusion of fossil taxa in phylogenetic analysis has the potential to increase phylogenetic accuracy (Wheeler, 1992; Zwickl & Hillis, 2002; Strait and Grine, 2004), the results of this study do not appear to support this notion for the reduced landmark data set. If the congruent phylogenetic relationships suggested by recent molecular (Disotell et al., 1992; Disotell, 1994; 2000; Harris and Disotell, 1998; Harris, 2000; Tosi et al., 1999, 2003) and morphological (Fleagle and McGraw, 1999; 2002; Gilbert, 2007; Gilbert and Rossie, 2007; Chapter 2) studies are considered to be accurate, then the phylogenetic relationships suggested by the current study, even with the inclusion of fossil taxa, are likely to be incorrect. For example, a clade containing *Cercocebus* and *Mandrillus* is strongly supported by both molecular and craniodental data (Disotell et al., 1992; Disotell, 1994; 2000; Harris and Disotell, 1998; Harris, 2000; Tosi et al., 1999, 2003; Fleagle and McGraw, 1999; 2002; Gilbert, 2007; Gilbert and Rossie, 2007; Chapter 2), but such a grouping is not found in any of the phylogenetic trees produced here, even when fossil taxa are included. In addition, while a clade containing extant and fossil *Theropithecus* taxa is strongly supported in the phylogenetic hypothesis presented earlier in Chapter 3, *Theropithecus* taxa in the current analysis of extant and fossil papionins are found to be paraphyletic. For these reasons many researchers, including myself, would find the groupings in the reduced landmark analyses to be difficult to accept and, in fact, highly unlikely.

There are several potential explanations for the reduced accuracy of the phylogenetic hypotheses produced in the current analyses. The most obvious is that the morphological regions represented by the excluded landmarks include a large amount of phylogenetically informative anatomy. These regions include portions of the zygomatic,

the inferior petrous process, the basioccipital including the region between the external occipital protuberance (EOP) and opisthion, and most of the sphenoid bone among males, and the zygomatic, the articular tubercle, the stylomastoid foramen, the carotid canal, the inferior petrous process, the basioccipital including the region between EOP and opisthion, the inferior portion of the occipital condyle, and most of the sphenoid bone among females. Another potential reason for the incongruent results produced in this study has to do with the fossil specimens themselves. Almost every fossil specimen is subject to some distortion through the process of fossilization. This distortion may have a strong effect on multivariate shape analyses such as this one whereas cladistic studies relying on more discrete character states may be able to circumvent this problem to some degree. Along with distortion inherent in fossil specimens, my own attempts at estimating certain landmarks may have also added slight inaccuracies to the representation of morphology. The fact that many of the fossil specimens and taxa are grouped together in the phylogenetic analyses suggests that there is some common factor that may account for their placement in the various trees. It is possible that the small sample size of fossil taxa and individuals makes it difficult to sample key fossil morphologies that drive polarity and increase phylogenetic accuracy. Finally, it is again probable that eliminating size-correlated PCs is too blunt an instrument to effectively adjust for allometry in the current analyses.

While 3D morphometric data from the basicranium may be appropriate for phenetic and other assessments of papionin morphology, the evidence presented here suggests that, perhaps in contrast to other primate groups, they are not optimal for phylogeny reconstruction in papionins. As suggested above, it appears that allometry and other issues inherent in multivariate 3-D morphometric analyses of size-disparate taxa may help to obscure phylogenetic signals in basicranial shape. Unfortunately, a narrow allometric adjustment similar to the one outlined in the cladistic analyses (Chapters 2 and 3) was inappropriate in this study because such a procedure would involve adjusting PC scores, thereby fundamentally altering basicranial shape. Future phylogenetic analyses of 3-D morphometric data should focus on improved techniques for detecting phylogenetic information within allometrically influenced datasets. In the meantime, the phylogenetic hypotheses of extant and fossil African papionin taxa produced from cladistic analysis of

quantitative and qualitative craniodental data (Chapters 2 and 3) will be preferable to the hypotheses suggested by this study.

Conclusions

Papionin basicranial morphology is highly influenced by allometry. When this allometry was controlled for by excluding size-correlated PC scores in a 3-D geometric morphometric analysis of extant papionin basicranial shape, phylogenetic trees were incongruent with recent molecular and morphological studies of extant African papionins. A reduced-landmark 3-D geometric morphometric analysis of extant and fossil papionin basicranial morphology was also inconsistent with previous results of molecular and morphological studies of extant and fossil African papionin phylogeny. There are a number of possible reasons for the inconsistent and seemingly inaccurate results presented here, the most important being the inability of current multivariate morphometric methods to adjust for the effects of allometry in phylogenetic analyses of shape. Because of these problems, cladistic analyses of more traditional morphological data may offer a more fine-grained and superior approach to understanding phylogenetic relationships (see Chapters 2 and 3), at least for the case of the African papionin monkeys. Future 3-D morphometric studies of phylogeny should focus on the development of methodologies to adjust for allometric effects.

Figure Legends

Figure 4.1. Traditionally hypothesized phylogenetic trees of the extant Papionini from morphological data. **a)** Szalay and Delson (1979), Strasser and Delson (1987), **b)** Delson and Dean (1993). Figure from Gilbert, 2007.

Figure 4.2. Hypothesized phylogenetic tree of the extant Papionini from recent molecular (Disotell et al., 1992; Disotell, 1994; 2000; Harris and Disotell, 1998; Tosi et al., 1999) and morphological (Gilbert and Rossie, 2007; Chapter 2) studies.

Figure 4.3. 41 landmarks used in this study, as illustrated on the basicranium of *Papio hamadryas ursinus*. Adapted from Freedman (1957).

Figure 4.4. Plot of PC 1 vs. PC 2 for male basicranial shape. Wireframe images illustrating the changes in basicranial shape across each axis are indicated at the ends of each axis. Minimum convex polygons surround the distributions of each extant papionin genus. C = *Cercocebus* (green), L = *Lophocebus* (red), Mc = *Macaca* (blue), Mn = *Mandrillus* (yellow), P = *Papio* (orange), T = *Theropithecus* (purple).

Figure 4.5. Plot of PC 1 vs. PC 2 for male basicranial shape. Wireframe images illustrating the changes in basicranial shape across each axis are indicated at the ends of each axis. Minimum convex polygons surround the distributions of each extant papionin genus. C = *Cercocebus* (green), L = *Lophocebus* (red), Mc = *Macaca* (blue), Mn = *Mandrillus* (yellow), P = *Papio* (orange), T = *Theropithecus* (purple).

Figure 4.6. Hypothesized phylogenetic trees from 3-D geometric morphometric analysis of male basicranial data including size-correlated PCs: **a)** Phylogenetic tree produced from neighbor-joining (NJ) analysis, and **b)** Phylogenetic tree produced from UPGMA analysis.

Figure 4.7. Hypothesized phylogenetic trees from 3-D geometric morphometric analysis of male basicranial data excluding size-correlated PCs: **a)** Phylogenetic tree produced from NJ analysis, and **b)** Phylogenetic tree produced from UPGMA analysis.

Figure 4.8. Hypothesized phylogenetic trees from 3-D geometric morphometric analysis of male basicranial data excluding size-correlated PCs and using individual macaque taxa as outgroups: **a)** Phylogenetic tree produced from NJ analysis using *M. fascicularis* as the outgroup, **b)** Phylogenetic tree produced from NJ analysis using *M. mulatta* as the outgroup, **c)** Phylogenetic tree produced from NJ analysis using *M. nemestrina* as the outgroup, and **d)** Phylogenetic tree produced from NJ analysis using *M. sylvanus* as the outgroup.

Figure 4.9. Hypothesized phylogenetic trees from 3-D geometric morphometric analysis of female basicranial data including size-correlated PCs: **a)** Phylogenetic tree produced from NJ analysis, and **b)** Phylogenetic tree produced from UPGMA analysis.

Figure 4.10. Hypothesized phylogenetic trees from 3-D geometric morphometric analysis of female basicranial data excluding size-correlated PCs: **a)** Phylogenetic tree produced from NJ analysis, and **b)** Phylogenetic tree produced from UPGMA analysis.

Figure 4.11. Hypothesized phylogenetic trees from 3-D geometric morphometric analysis of female basicranial data excluding size-correlated PCs and using individual macaque taxa as outgroups: **a)** Phylogenetic tree produced from NJ analysis using *M. fascicularis* as the outgroup, **b)** Phylogenetic tree produced from NJ analysis using *M. mulatta* as the outgroup, **c)** Phylogenetic tree produced from NJ analysis using *M. nemestrina* as the outgroup, and **d)** Phylogenetic tree produced from NJ analysis using *M. sylvanus* as the outgroup.

Figure 4.12. Hypothesized phylogenetic trees from 3-D geometric morphometric analysis of sex-averaged basicranial data including size-correlated PCs: **a)** Phylogenetic tree produced from NJ analysis, and **b)** Phylogenetic tree produced from UPGMA analysis.

Figure 4.13. Hypothesized phylogenetic trees from 3-D geometric morphometric analysis of sex-averaged basicranial data excluding size-correlated PCs: **a)** Phylogenetic tree produced from NJ analysis, and **b)** Phylogenetic tree produced from UPGMA analysis.

Figure 4.14. Hypothesized phylogenetic trees from 3-D geometric morphometric analysis of sex-averaged basicranial data excluding size-correlated PCs and using individual macaque taxa as outgroups: **a)** Phylogenetic tree produced from NJ analysis using *M. fascicularis* as the outgroup, **b)** Phylogenetic tree produced from NJ analysis using *M. mulatta* as the outgroup, **c)** Phylogenetic tree produced from NJ analysis using *M. nemestrina* as the outgroup, and **d)** Phylogenetic tree produced from NJ analysis using *M. sylvanus* as the outgroup.

Figure 4.15. Hypothesized phylogenetic trees from 3-D geometric morphometric analysis of combined-sex basicranial data excluding size-correlated PCs: **a)** Phylogenetic tree produced from NJ analysis, and **b)** Phylogenetic tree produced from UPGMA analysis.

Figure 4.16. Hypothesized phylogenetic trees from 3-D geometric morphometric analysis of extant and fossil male basicranial data excluding size-correlated PCs: **a)** Phylogenetic tree produced from NJ analysis, and **b)** Phylogenetic tree produced from UPGMA analysis. Excluded PCs = PC4, PC6, PC11, PC26, and PC35.

Figure 4.17. Hypothesized phylogenetic trees from 3-D geometric morphometric analysis of extant and fossil female basicranial data excluding size-correlated PCs: **a)** Phylogenetic tree produced from NJ analysis, and **b)** Phylogenetic tree produced from UPGMA analysis. Excluded PCs = PC1, PC8, PC15, PC21, PC29, PC38, PC41, PC43, and PC44.

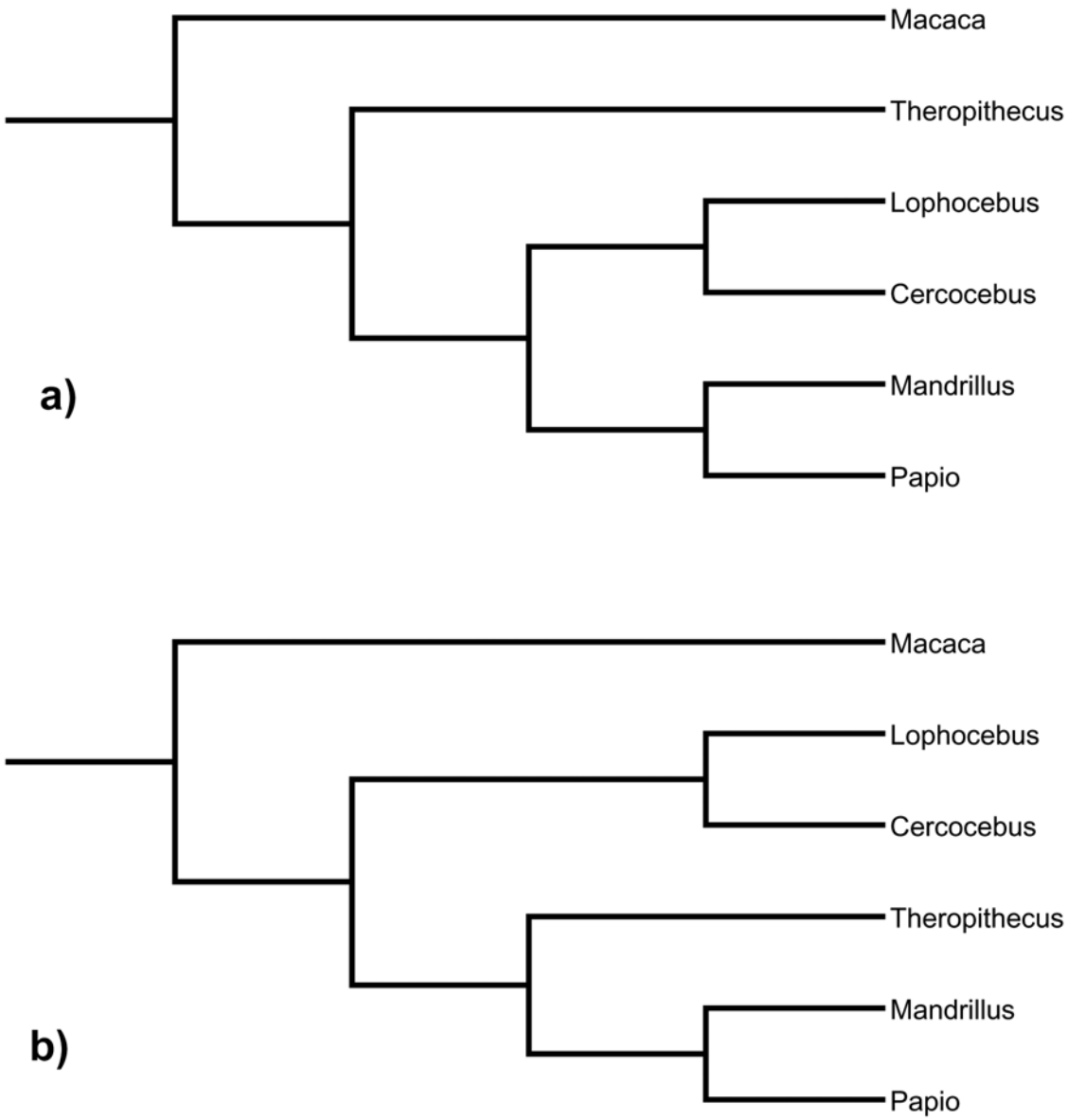
Macaca
Theropithecus
Lophocebus
Cercocebus
Mandrillus
Papio
a)
Macaca
Lophocebus
Cercocebus
Theropithecus
Mandrillus
Papio
b)

Figure 4.1

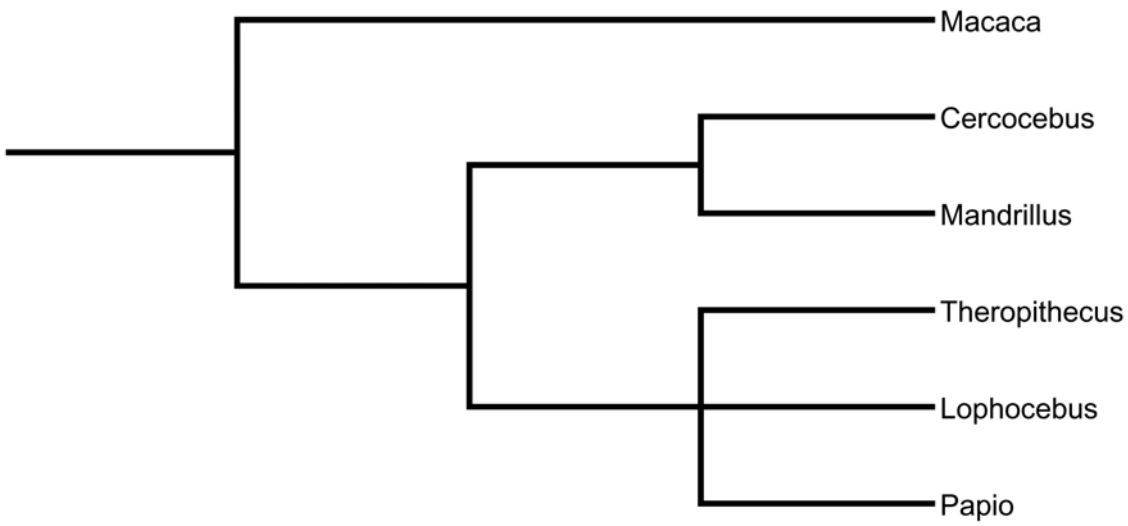
Macaca
Cercocebus
Mandrillus
Theropithecus
Lophocebus
Papio

Figure 4.2

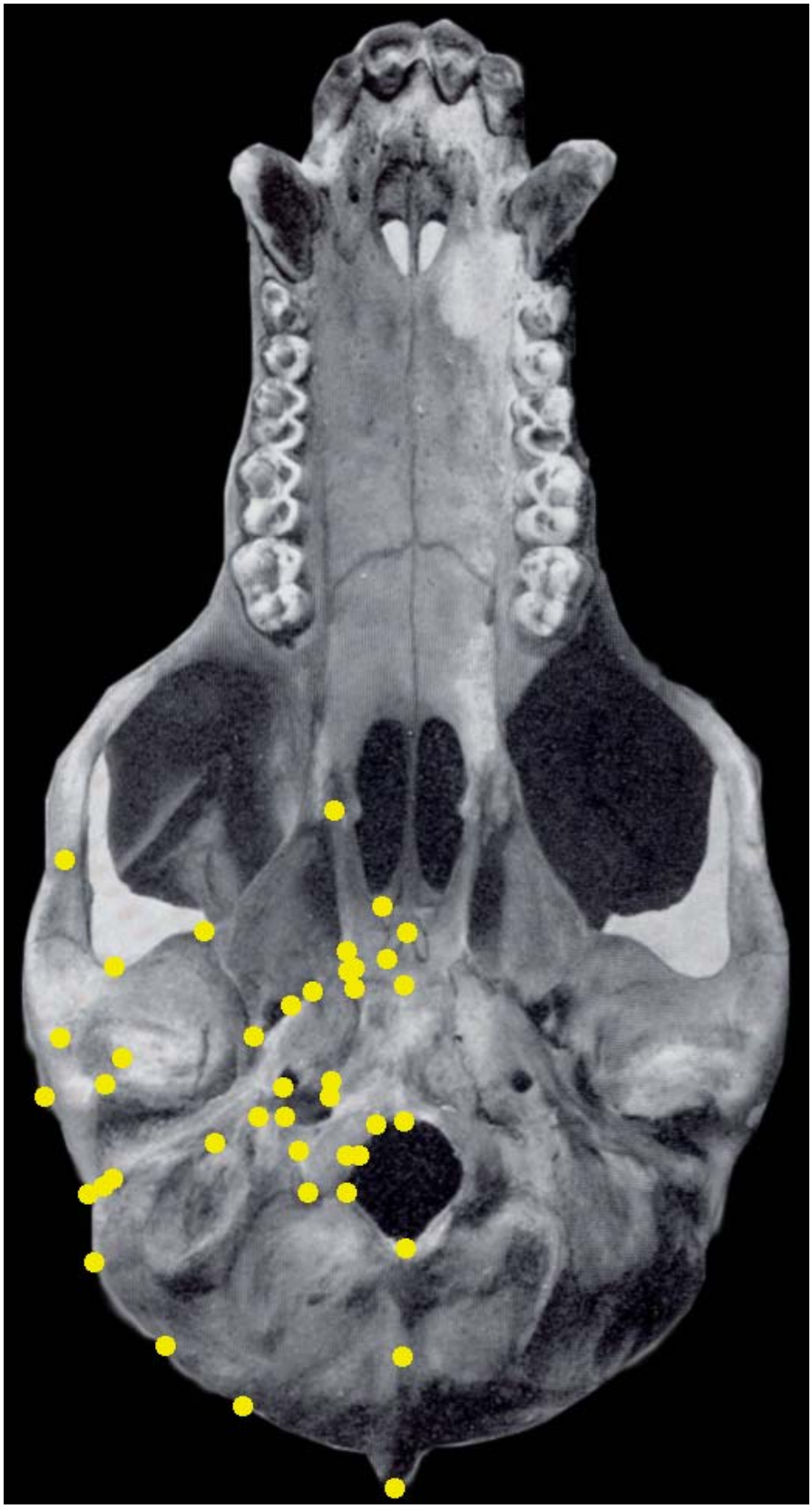

Figure 4.3

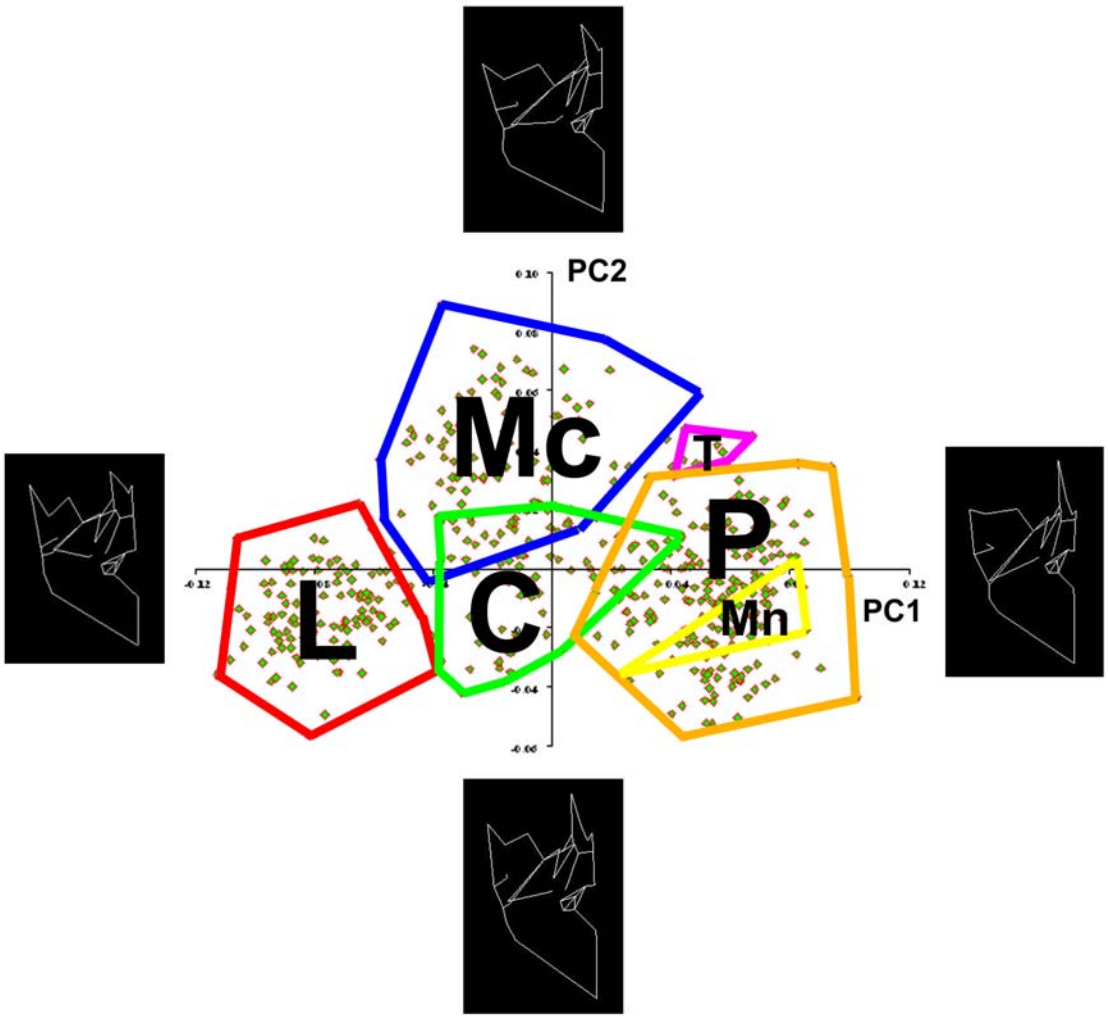

Figure 4.4

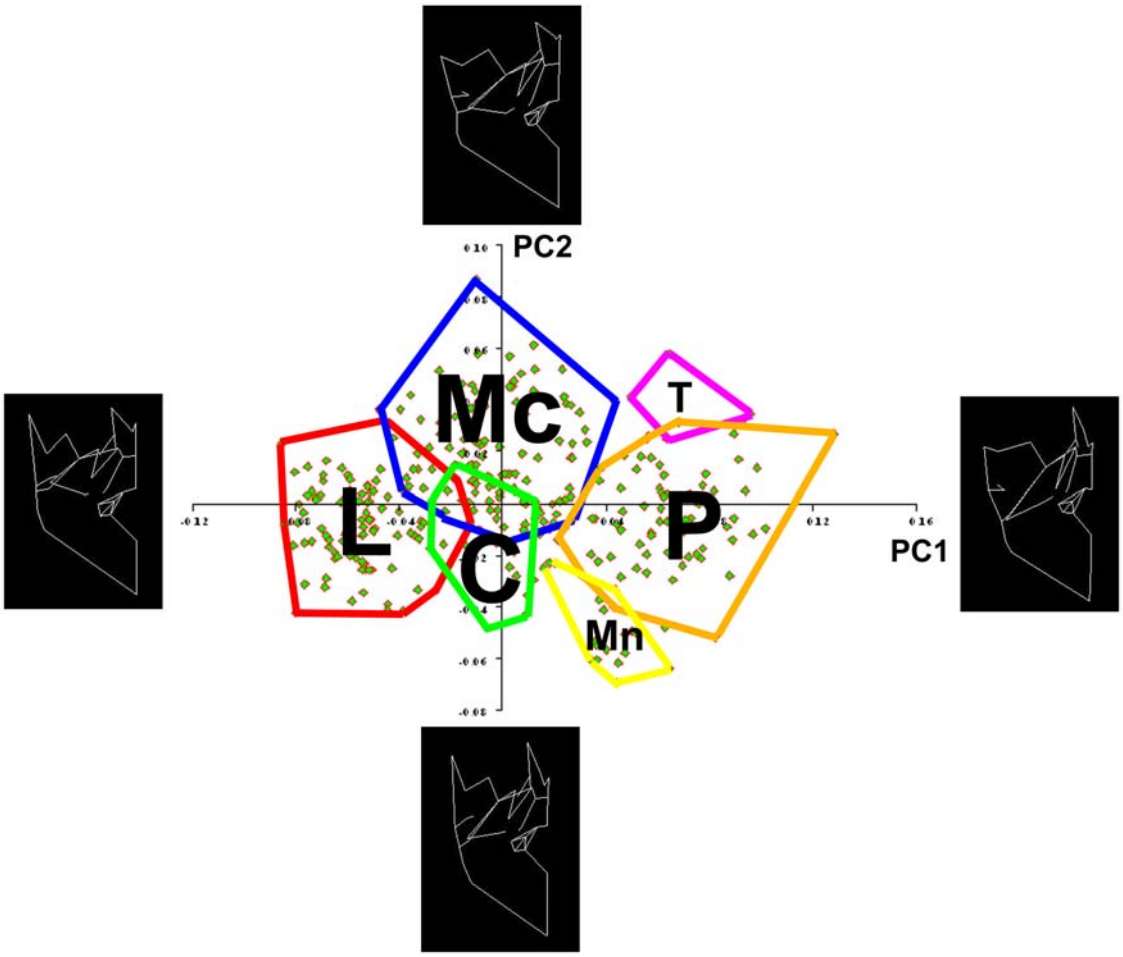

Figure 4.5

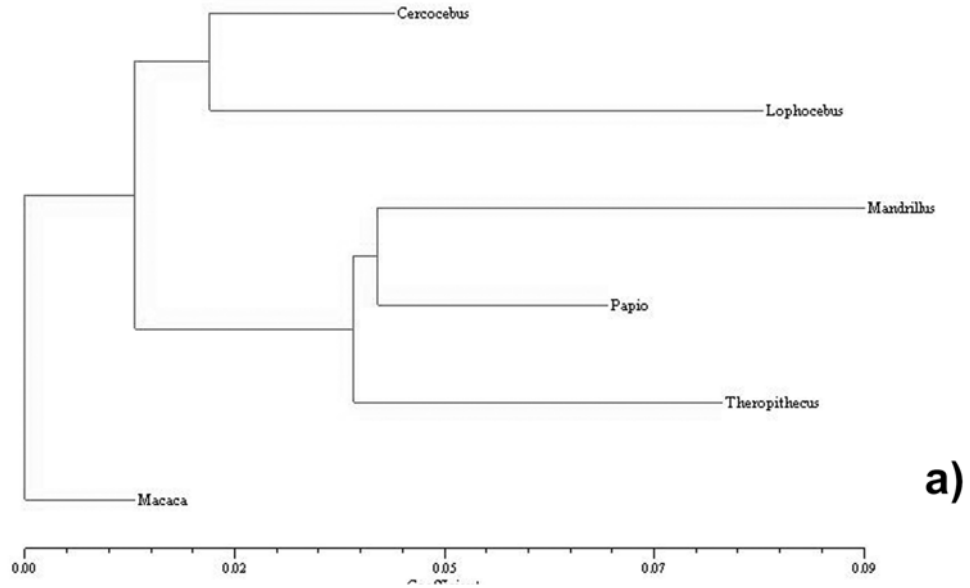
Cercocebus
Lophocebus
Mandrillus
Papio
Theropithecus
Macaca
a)
0.00
0.02
0.05
0.07
0.09

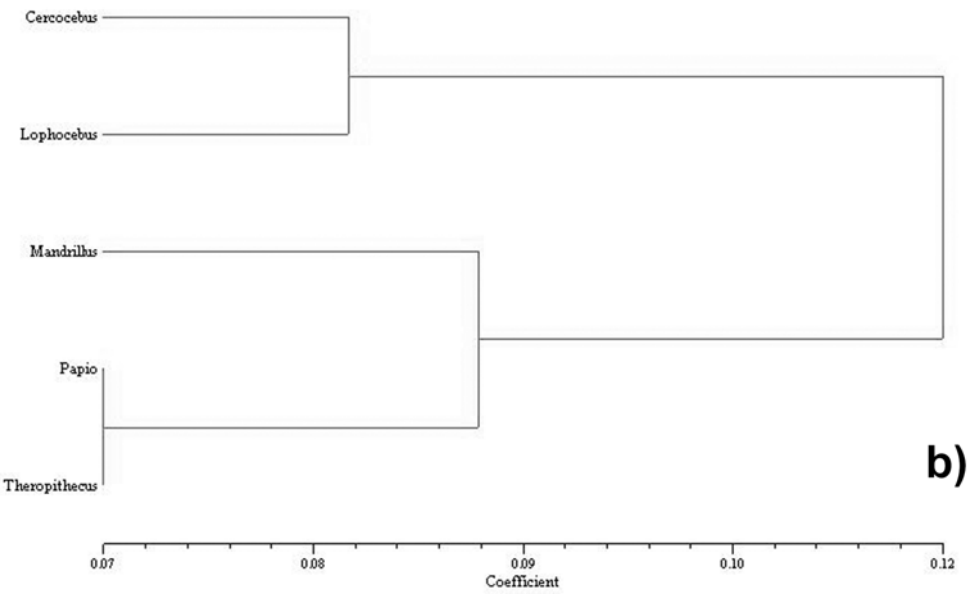
Cercocebus
Lophocebus
Mandrillus
Papio
Theropithecus
b)
0.07
0.08
0.09
0.10
0.12
Coefficient

Figure 4.6

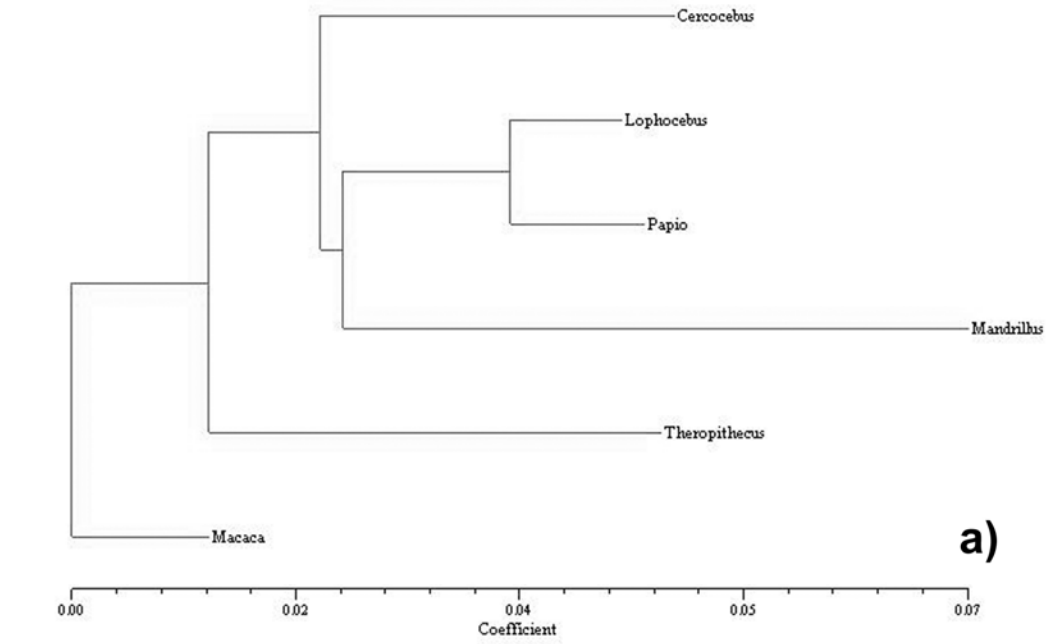
Cercocebus
Lophocebus
Papio
Mandrillus
Theropithecus
Macaca
a)
0.00
0.02
0.04
0.05
0.07
Coefficient

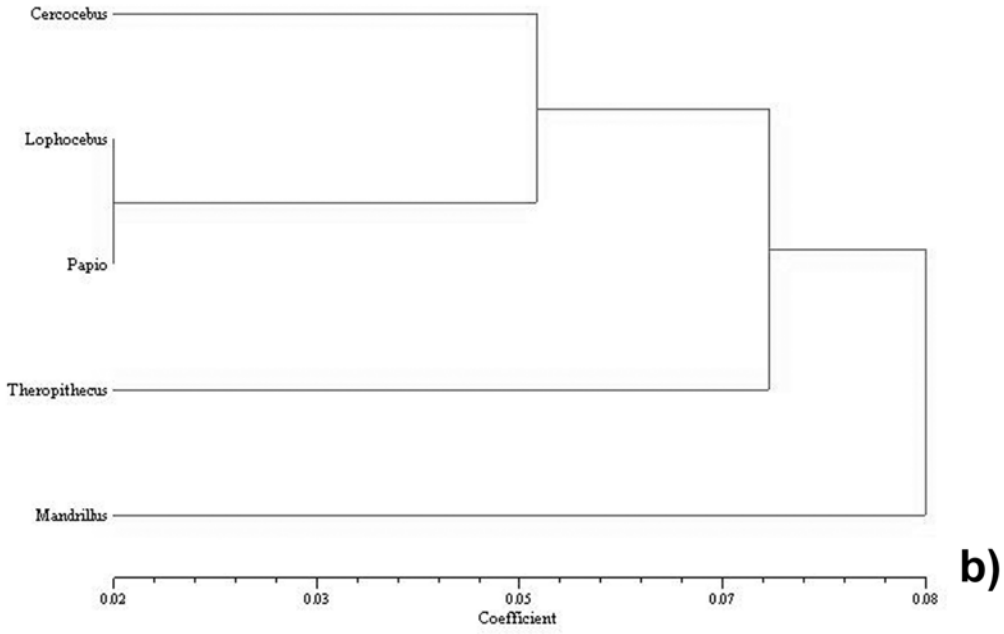
Cercocebus
Lophocebus
Papio
Theropithecus
Mandrillus
b)
0.02
0.03
0.05
0.07
0.08
Coefficient

Figure 4.7

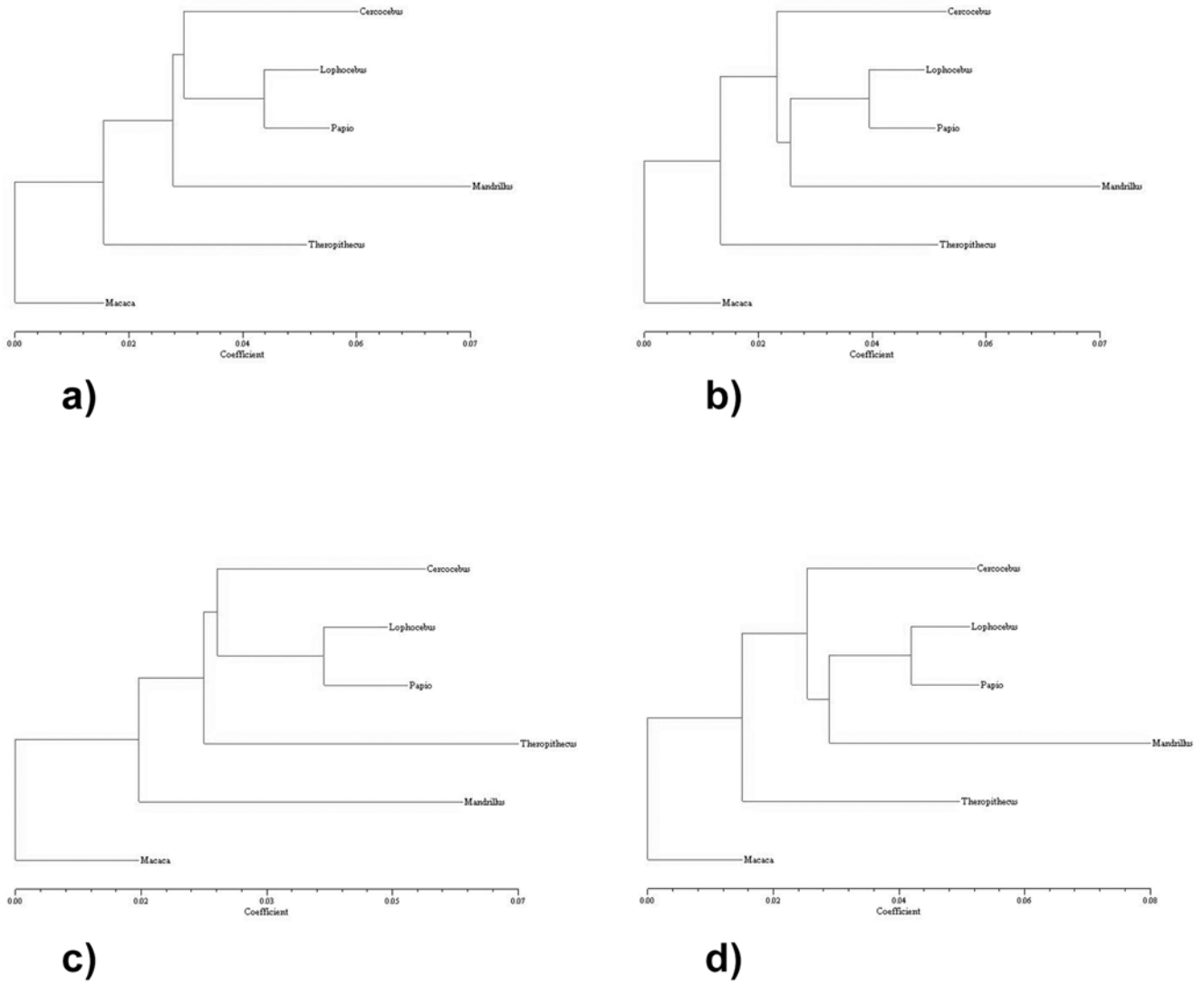
Cercocebus
Lophocebus
Papio
Mandrillus
Theropithecus
Macaca
0.00
0.02
0.04
0.06
0.07
Coefficient
a)
Cercocebus
Lophocebus
Papio
Mandrillus
Theropithecus
Macaca
0.00
0.02
0.04
0.06
0.07
Coefficient
b)
Cercocebus
Lophocebus
Papio
Theropithecus
Mandrillus
Macaca
0.00
0.02
0.03
0.05
0.07
Coefficient
c)
Cercocebus
Lophocebus
Papio
Mandrillus
Theropithecus
Macaca
0.00
0.02
0.04
0.06
0.08
Coefficient
d)

Figure 4.8

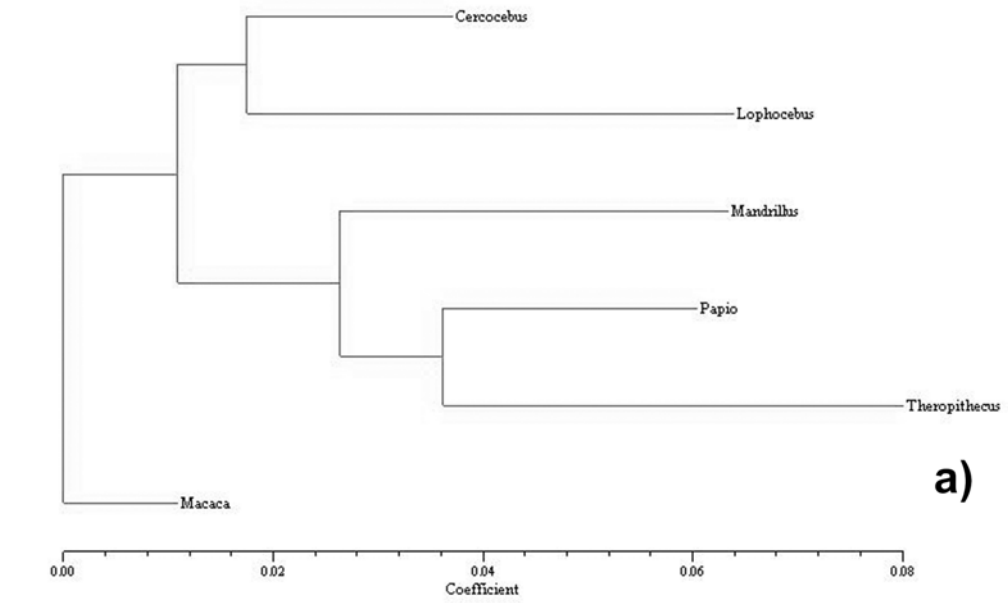
Cercocebus
Lophocebus
Mandrillus
Papio
Theropithecus
Macaca
a)
0.00
0.02
0.04
0.06
0.08
Coefficient

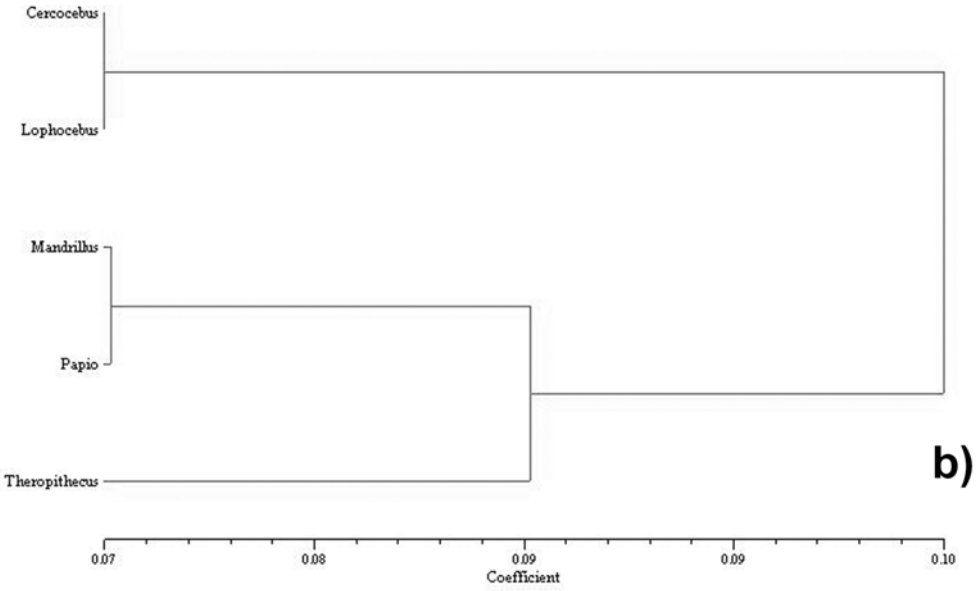
Cercocebus
Lophocebus
Mandrillus
Papio
Theropithecus
b)
0.07
0.08
0.09
0.09
0.10
Coefficient

Figure 4.9

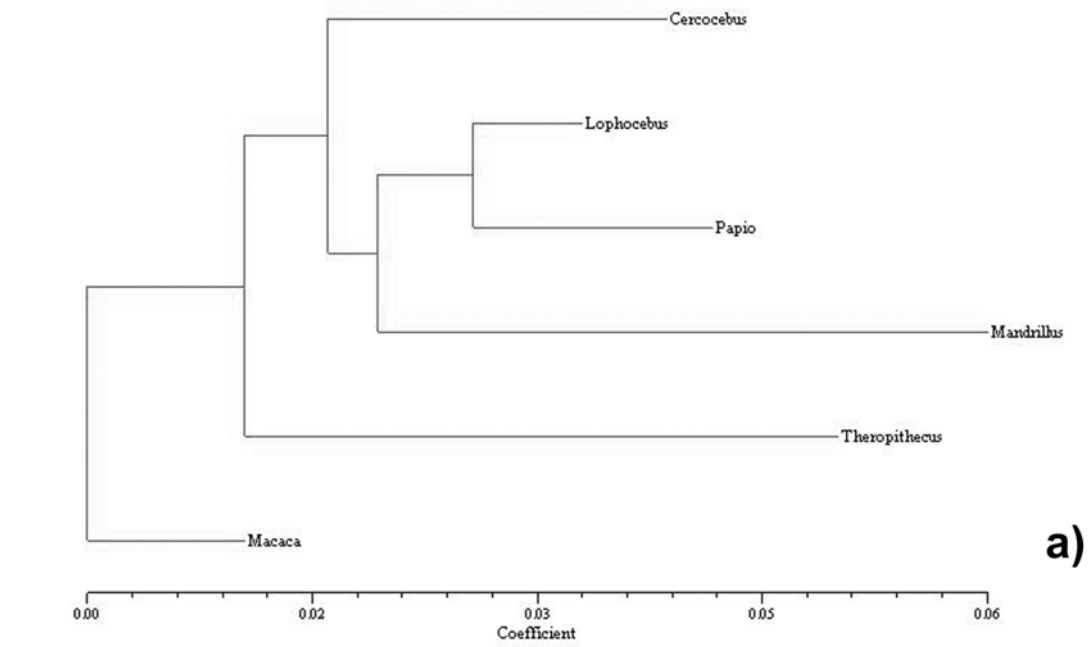

a)

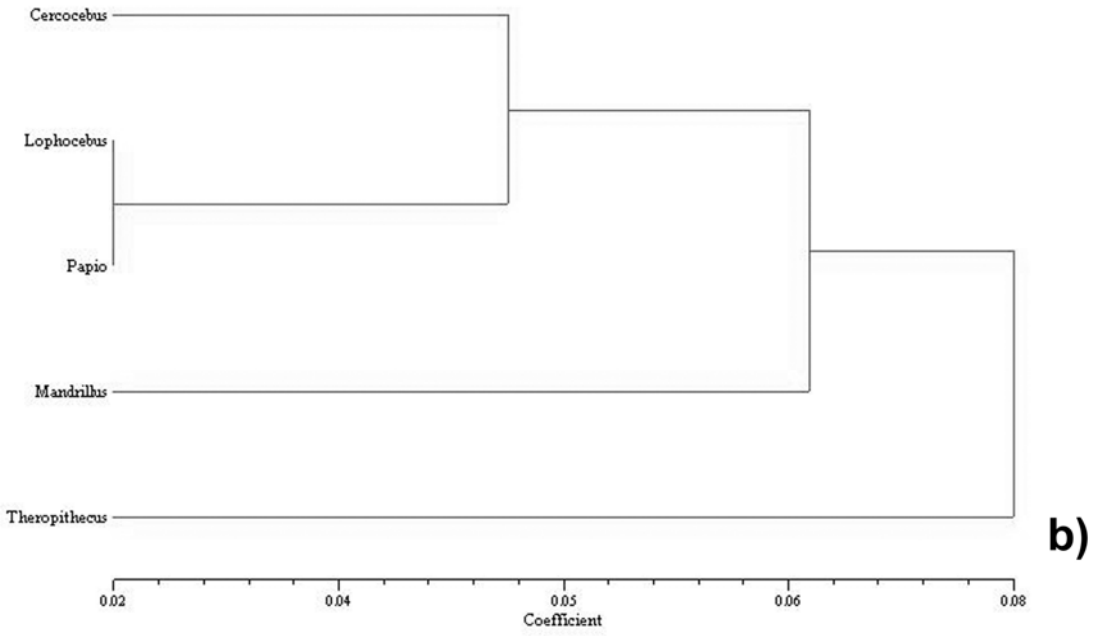

b)

Figure 4.10

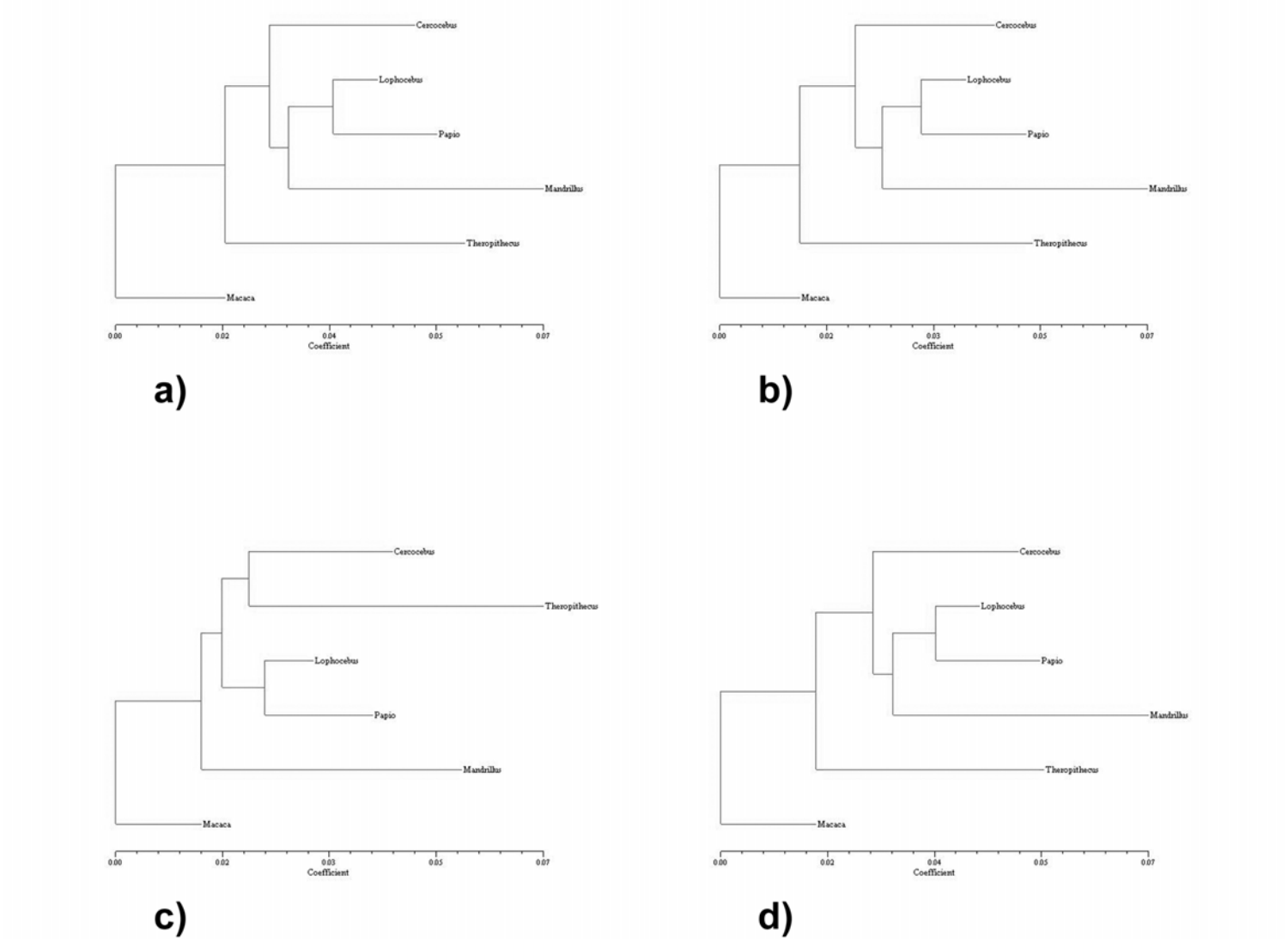
Cercocebus
Lophocebus
Papio
Mandrillus
Theropithecus
Macaca
0.00
0.02
0.04
0.05
0.07
Coefficient
a)
Cercocebus
Lophocebus
Papio
Mandrillus
Theropithecus
Macaca
0.00
0.02
0.03
0.05
0.07
Coefficient
b)
Cercocebus
Theropithecus
Lophocebus
Papio
Mandrillus
Macaca
0.00
0.02
0.03
0.05
0.07
Coefficient
c)
Cercocebus
Lophocebus
Papio
Mandrillus
Theropithecus
Macaca
0.00
0.02
0.04
0.05
0.07
Coefficient
d)

Figure 4.11

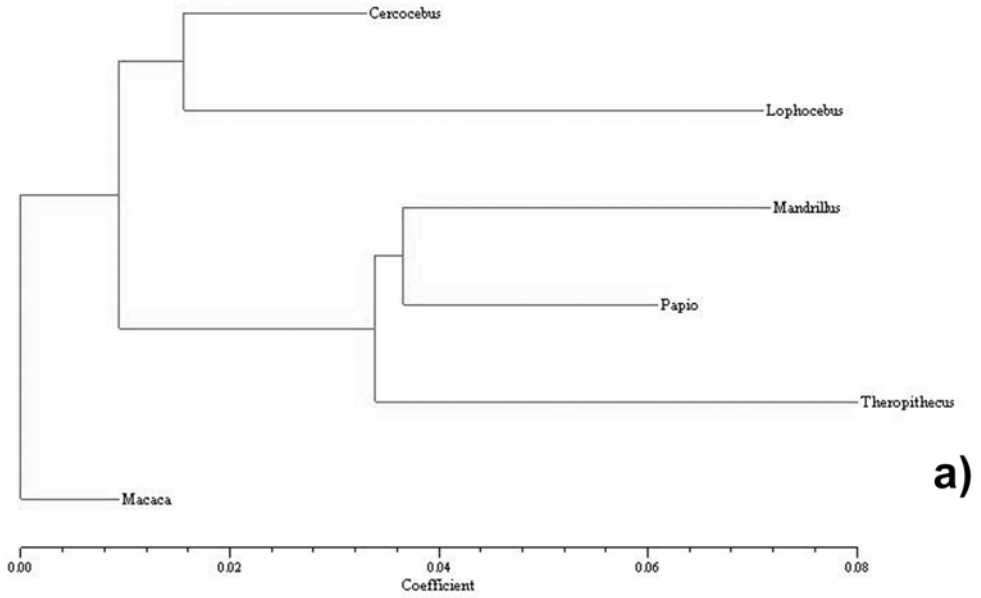
Cercocebus
Lophocebus
Mandrillus
Papio
Theropithecus
Macaca
a)
0.00
0.02
0.04
0.06
0.08
Coefficient

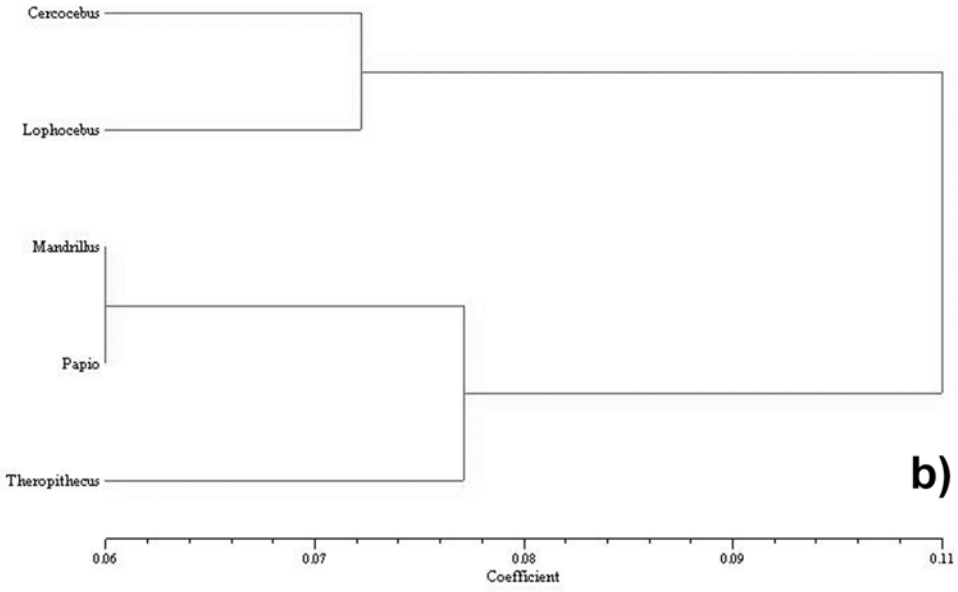
Cercocebus
Lophocebus
Mandrillus
Papio
Theropithecus
b)
0.06
0.07
0.08
0.09
0.11
Coefficient

Figure 4.12

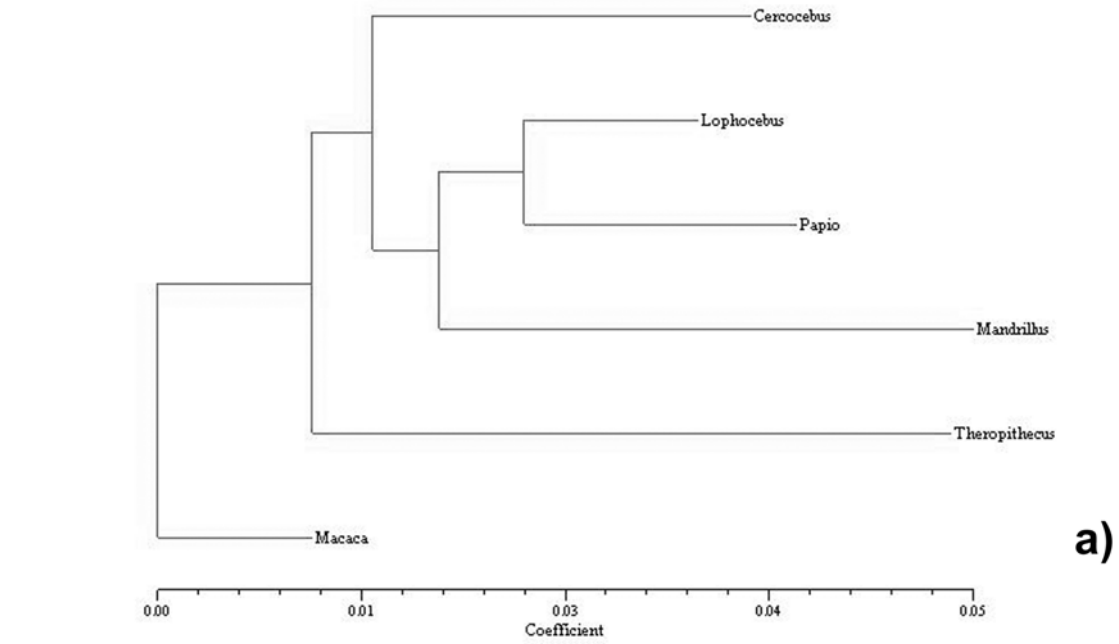

a)

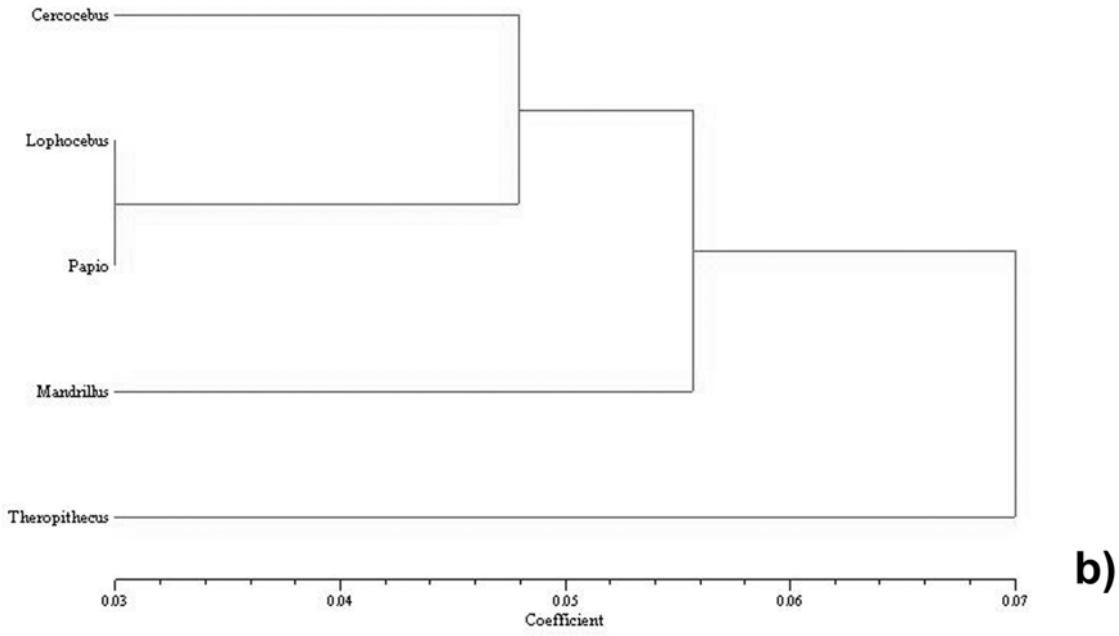

b)

Figure 4.13

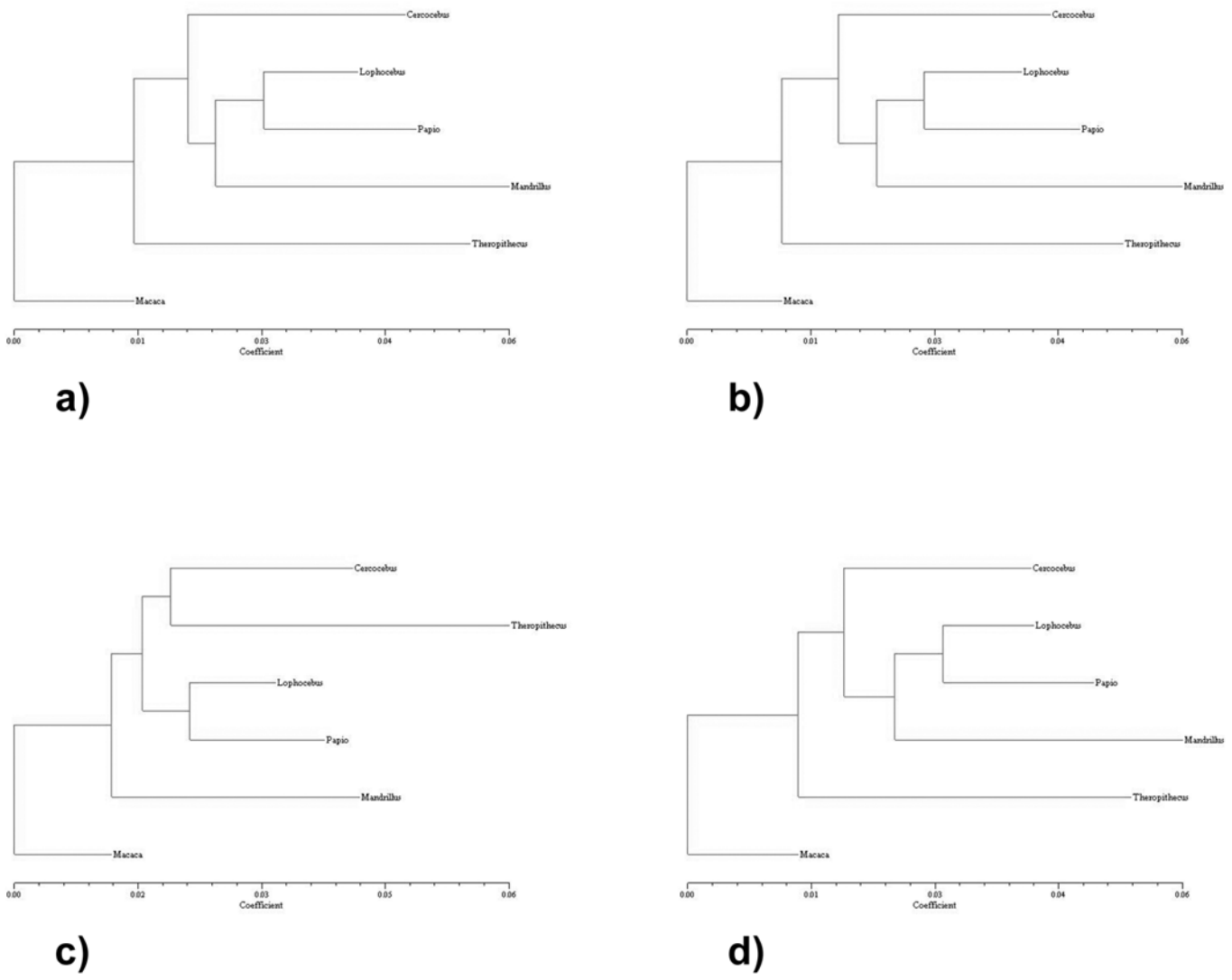
Cercocebus
Lophocebus
Papio
Mandrillus
Theropithecus
Macaca
0.00
0.01
0.03
0.04
0.06
Coefficient
a)
b)
0.02
0.05
c)
d)

Figure 4.14

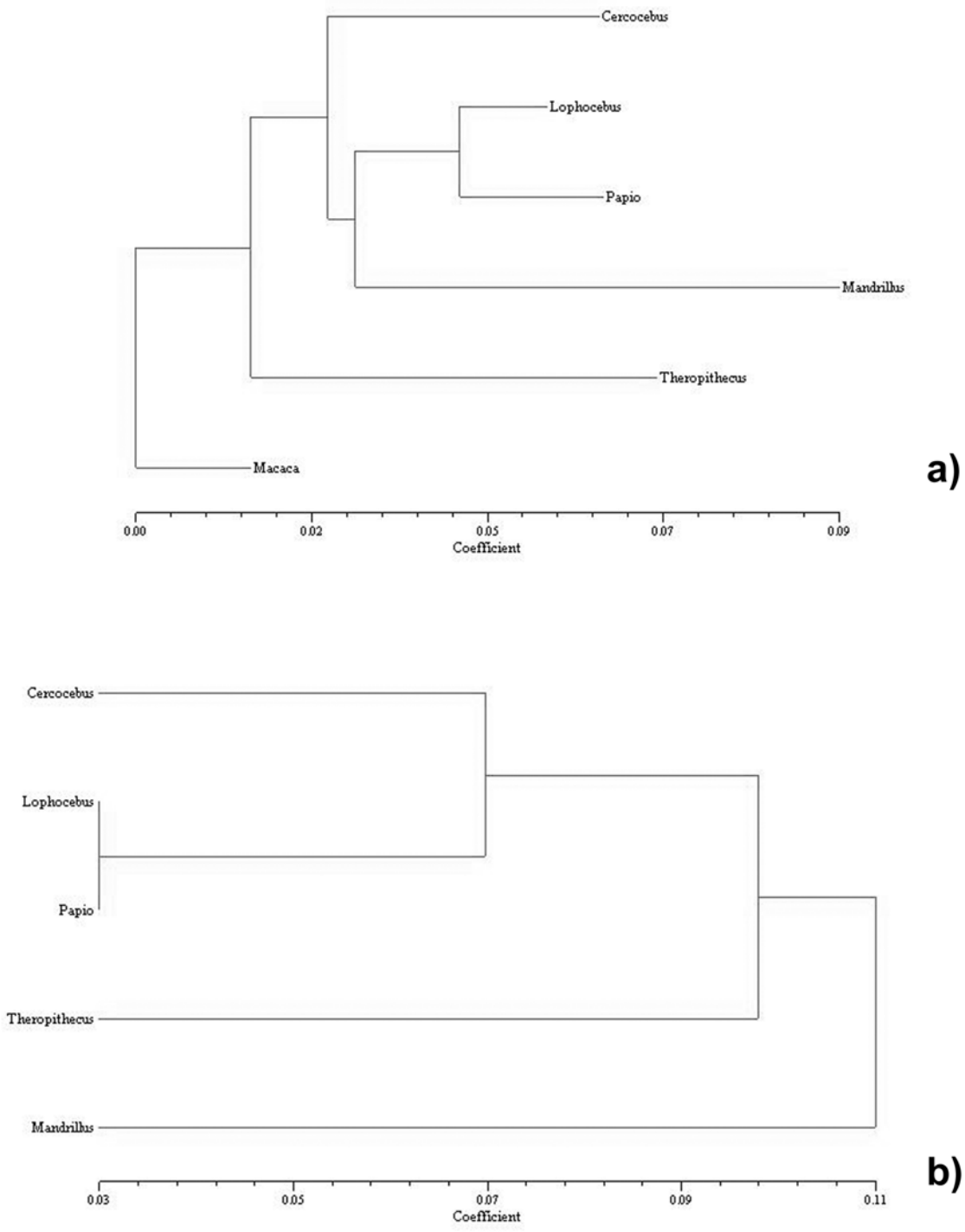
Cercocebus
Lophocebus
Papio
Mandrillus
Theropithecus
Macaca
0.00
0.02
0.05
0.07
0.09
Coefficient
a)
Cercocebus
Lophocebus
Papio
Theropithecus
Mandrillus
0.03
0.05
0.07
0.09
0.11
Coefficient
b)

Figure 4.15

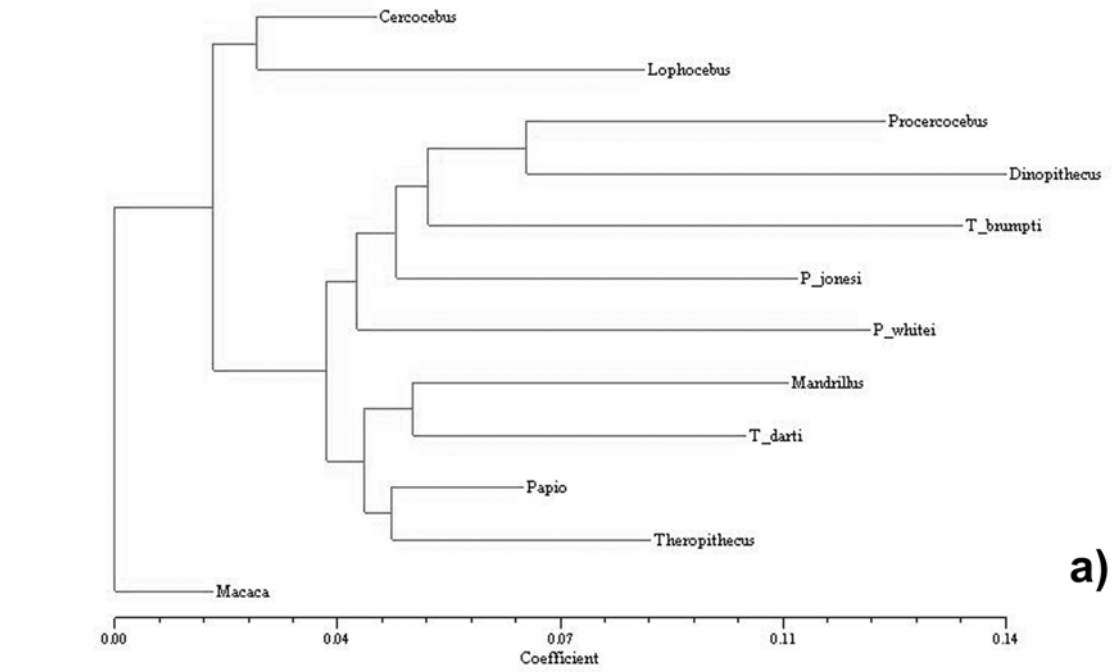
Cercocebus
Lophocebus
Procercocebus
Dinopithecus
T_brumpti
P_jonesi
P_whitei
Mandrillus
T_darti
Papio
Theropithecus
Macaca
0.00
0.04
0.07
0.11
0.14
Coefficient
a)

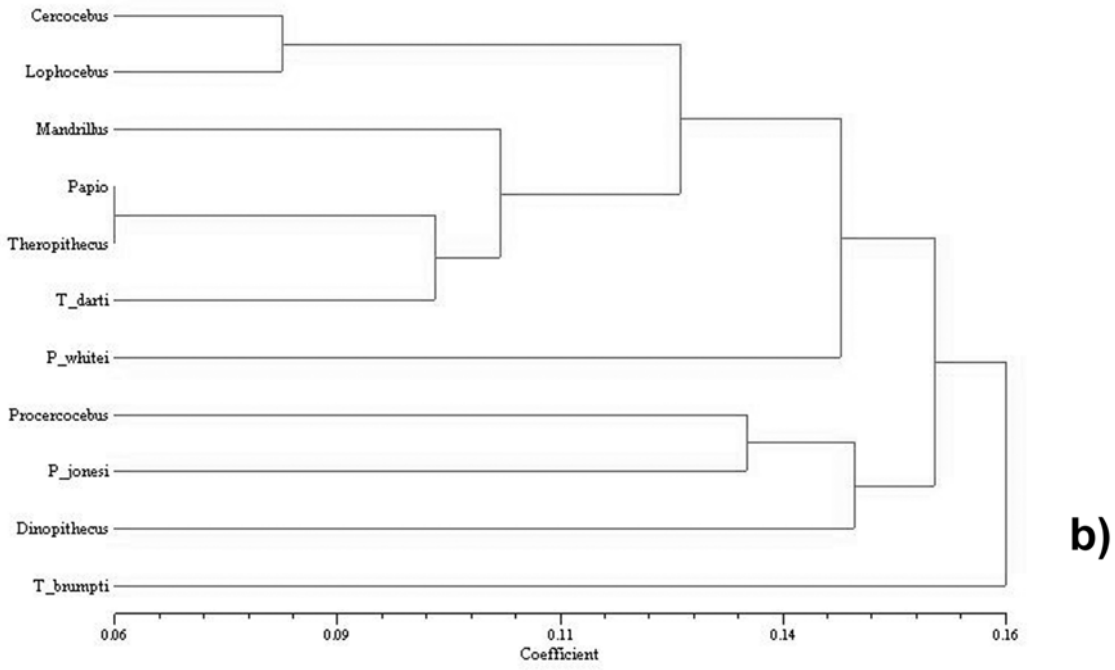
Cercocebus
Lophocebus
Mandrillus
Papio
Theropithecus
T_darti
P_whitei
Procercocebus
P_jonesi
Dinopithecus
T_brumpti
0.06
0.09
0.11
0.14
0.16
Coefficient
b)

Figure 4.16

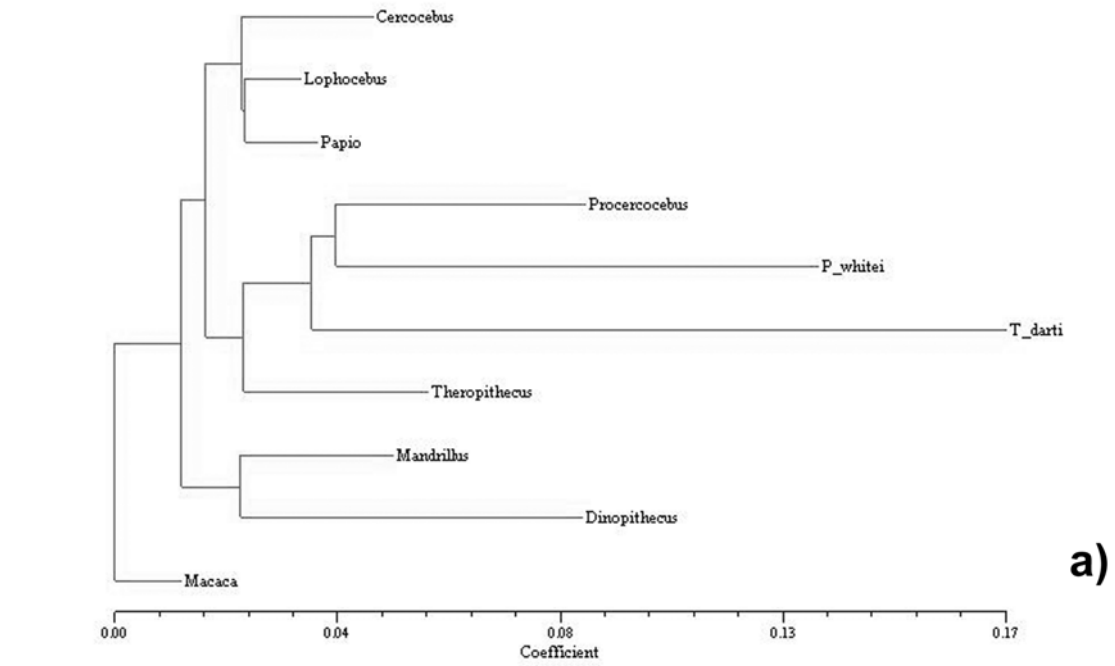
Cercocebus
Lophocebus
Papio
Procercocebus
P_whitei
T_darti
Theropithecus
Mandrillus
Dinopithecus
Macaca
0.00
0.04
0.08
0.13
0.17
Coefficient
a)

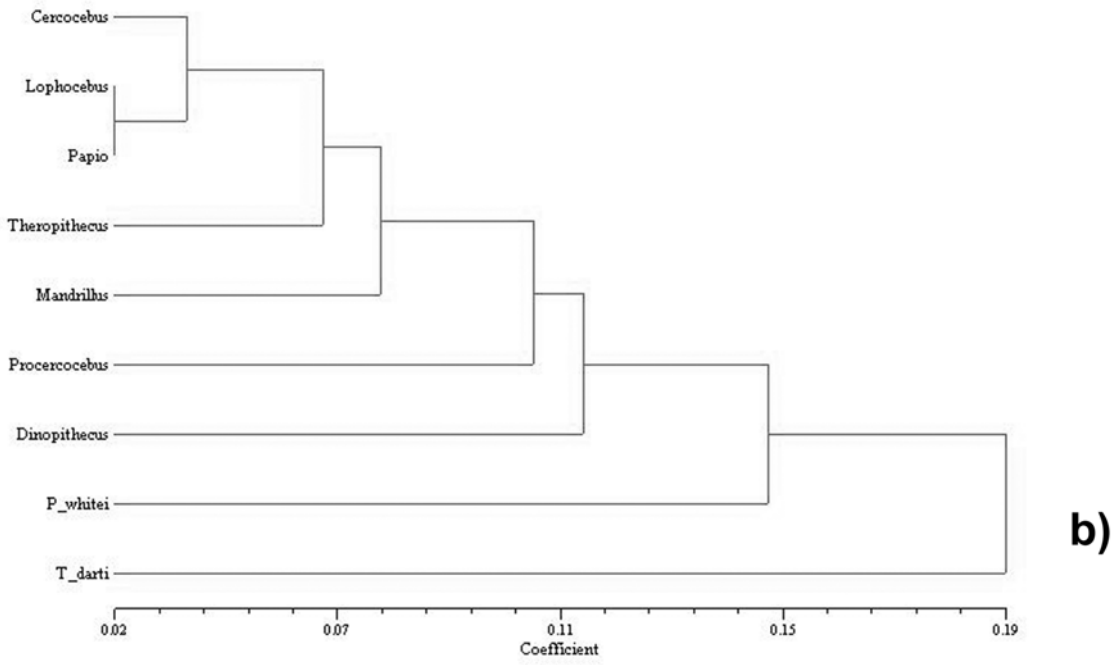
Cercocebus
Lophocebus
Papio
Theropithecus
Mandrillus
Procercocebus
Dinopithecus
P_whitei
T_darti
0.02
0.07
0.11
0.15
0.19
Coefficient
b)

Figure 4.17.

Table 4.1. Sample of extant papionin basicrania used in this study.

Taxon	Male sample size	Female sample size
Cercocebus agilis	26	16
Cercocebus atys	15	24
Cercocebus torquatus	26	7
Lophocebus albigena	70	62
Lophocebus aterrimus	48	39
Macaca fascicularis	54	31
Macaca mulatta	17	27
Macaca nemestrina	18	16
Macaca sylvanus	8	9
Mandrillus leucophaeus	17	17
Mandrillus sphinx	15	9
Papio hamadryas anubis	84	34
Papio hamadryas cynocephalus	18	9
Papio hamadryas hamadryas	7	2
Papio hamadryas kindae	8	6
Papio hamadryas papio	11	1
Papio hamadryas ursinus	44	8
Theropithecus gelada	14	6

Table 4.2. Basicranial landmarks used in this study.

Landmark	Landmark #
Intersection of the infratemporal crest and sphenosquamosal suture	1
Most posterior point on zygomatic "U" with temporal	2
Most medial point on sphenosquamosal suture	3
Point on the center of the articular tubercle	4
Deepest point within the mandibular fossa	5
Most inferior point on the postglenoid process	6
Apex of the petrous part of the temporal bone	7
Most posterolateral point on the margin of the carotid canal entrance	8
Most lateral point on the margin of the stylomastoid foramen	9
Most medial point on the jugular fossa	10
Most lateral point on the jugular fossa	11
Most inferior point on the external auditory meatus	12
Point on lateral margin of zygomatic process of the temporal bone at the position of the postglenoid process	13
Auriculare	14
Porion	15

Euryon	16
Most anterior tip of the petrous process	17
Suture between temporal and zygomatic bones on inferior aspect of zygomatic process	18
Parietal notch	19
Asterion	20
External occipital protuberance (EOP)	21
Point on the medial nuchal line halfway between the EOP and foramen magnum	22
Opisthion	23
Basion	24
Most posterolateral point on the occipital condyle	25
Most posterior point on the occipital condyle along the margin of the foramen magnum	26
Most lateral point on the occipital condyle (point on the middle of the lateral edge of the condyle)	27
Most anterior point on the occipital condyle along the margin of the foramen magnum	28
Point on the center of the occipital condyle (inferior aspect)	29
Hypoglossal foramen	30
Point where the occipital, tympanic temporal, and petrous temporal meet	31
Most posterior point where the occipital meets the anterior edge of the jugular	32
Most anterior point where the occipital meets the petrous temporal and sphenoid	33
Most anterior point on the basioccipital in the midline (sphenobasion)	34
Most posterior point (lateral to midline) where the sphenoid meets the vomer	35

Point on the sphenoid in the midline in contact with the vomer (vomer notch)	36
Point where medial pterygoid plate meets sphenoid body (branching point)	37
Point where the apex of the petrous temporal and basisphenoid meet	38
Most posterolateral point on the medial pterygoid plate (anteromedial point on foramen ovale)	39
Point where sphenoid and palatine first meet (superiorly)	40
Most anterolateral (inferior) point on the medial pterygoid plate where the sphenoid meets the palatine	41

Table 4.3. Eigenvalues for the 1st 52 principal components in the male, female, and all basicrania (sex-averaged) analyses.									
	Males			**Females**			**All Basicrania**		
Principal Component	Eigenvalue	Proportion of Variance	Cumulative Variance	Eigenvalue	Proportion of Variance	Cumulative Variance	Eigenvalue	Proportion of Variance	Cumulative Variance
1	3.14E-03	2.94E-01	2.94E-01	2.34E-03	2.65E-01	2.65E-01	3.09E-03	2.93E-01	2.93E-01
2	7.36E-04	6.90E-02	3.63E-01	6.33E-04	7.18E-02	3.37E-01	7.06E-04	6.68E-02	3.60E-01
3	7.01E-04	6.58E-02	4.29E-01	5.73E-04	6.50E-02	4.02E-01	6.61E-04	6.26E-02	4.22E-01
4	5.81E-04	5.45E-02	4.83E-01	4.93E-04	5.59E-02	4.58E-01	5.91E-04	5.60E-02	4.78E-01
5	5.06E-04	4.74E-02	5.31E-01	3.88E-04	4.40E-02	5.02E-01	4.98E-04	4.71E-02	5.25E-01
6	4.17E-04	3.91E-02	5.70E-01	3.09E-04	3.51E-02	5.37E-01	3.96E-04	3.75E-02	5.63E-01
7	3.49E-04	3.28E-02	6.03E-01	2.83E-04	3.21E-02	5.69E-01	3.73E-04	3.53E-02	5.98E-01
8	2.89E-04	2.71E-02	6.30E-01	2.43E-04	2.75E-02	5.97E-01	2.83E-04	2.67E-02	6.25E-01
9	2.44E-04	2.29E-02	6.53E-01	2.24E-04	2.54E-02	6.22E-01	2.53E-04	2.40E-02	6.49E-01
10	2.20E-04	2.06E-02	6.73E-01	1.75E-04	1.98E-02	6.42E-01	2.13E-04	2.02E-02	6.69E-01
11	1.85E-04	1.73E-02	6.91E-01	1.68E-04	1.91E-02	6.61E-01	1.68E-04	1.59E-02	6.85E-01
12	1.66E-04	1.56E-02	7.06E-01	1.60E-04	1.81E-02	6.79E-01	1.60E-04	1.51E-02	7.00E-01
13	1.60E-04	1.50E-02	7.21E-01	1.38E-04	1.56E-02	6.95E-01	1.54E-04	1.46E-02	7.14E-01
14	1.43E-04	1.34E-02	7.35E-01	1.35E-04	1.53E-02	7.10E-01	1.46E-04	1.38E-02	7.28E-01
15	1.33E-04	1.25E-02	7.47E-01	1.27E-04	1.44E-02	7.24E-01	1.34E-04	1.27E-02	7.41E-01
16	1.26E-04	1.19E-02	7.59E-01	1.14E-04	1.30E-02	7.37E-01	1.19E-04	1.13E-02	7.52E-01
17	1.11E-04	1.05E-02	7.69E-01	1.13E-04	1.29E-02	7.50E-01	1.16E-04	1.10E-02	7.63E-01
18	1.04E-04	9.73E-03	7.79E-01	1.05E-04	1.19E-02	7.62E-01	1.04E-04	9.82E-03	7.73E-01
19	1.00E-04	9.38E-03	7.88E-01	8.80E-05	9.98E-03	7.72E-01	9.70E-05	9.18E-03	7.82E-01
20	9.35E-05	8.77E-03	7.97E-01	8.47E-05	9.61E-03	7.82E-01	9.38E-05	8.88E-03	7.91E-01
21	8.78E-05	8.23E-03	8.05E-01	8.33E-05	9.45E-03	7.91E-01	9.04E-05	8.56E-03	8.00E-01
22	8.67E-05	8.13E-03	8.14E-01	8.01E-05	9.08E-03	8.00E-01	8.29E-05	7.85E-03	8.08E-01
23	8.46E-05	7.93E-03	8.21E-01	7.22E-05	8.19E-03	8.08E-01	7.66E-05	7.25E-03	8.15E-01
24	8.06E-05	7.56E-03	8.29E-01	6.95E-05	7.88E-03	8.16E-01	7.42E-05	7.02E-03	8.22E-01
25	7.58E-05	7.10E-03	8.36E-01	6.74E-05	7.65E-03	8.24E-01	7.32E-05	6.93E-03	8.29E-01
26	7.02E-05	6.58E-03	8.43E-01	6.53E-05	7.41E-03	8.31E-01	6.99E-05	6.62E-03	8.35E-01
27	6.75E-05	6.33E-03	8.49E-01	6.15E-05	6.98E-03	8.38E-01	6.58E-05	6.22E-03	8.42E-01

28	6.21E-05	5.82E-03	8.55E-01	5.78E-05	6.55E-03	8.45E-01	6.34E-05	6.00E-03	8.48E-01
29	6.02E-05	5.65E-03	8.61E-01	5.37E-05	6.09E-03	8.51E-01	5.86E-05	5.54E-03	8.53E-01
30	5.79E-05	5.43E-03	8.66E-01	5.12E-05	5.80E-03	8.57E-01	5.74E-05	5.43E-03	8.59E-01
31	5.67E-05	5.32E-03	8.71E-01	5.02E-05	5.69E-03	8.63E-01	5.58E-05	5.28E-03	8.64E-01
32	5.30E-05	4.97E-03	8.76E-01	4.69E-05	5.32E-03	8.68E-01	5.29E-05	5.00E-03	8.69E-01
33	4.97E-05	4.66E-03	8.81E-01	4.56E-05	5.17E-03	8.73E-01	5.20E-05	4.92E-03	8.74E-01
34	4.89E-05	4.59E-03	8.85E-01	4.51E-05	5.12E-03	8.78E-01	4.86E-05	4.60E-03	8.78E-01
35	4.55E-05	4.27E-03	8.90E-01	4.28E-05	4.85E-03	8.83E-01	4.62E-05	4.38E-03	8.83E-01
36	4.27E-05	4.00E-03	8.94E-01	4.03E-05	4.57E-03	8.88E-01	4.35E-05	4.11E-03	8.87E-01
37	4.21E-05	3.95E-03	8.98E-01	3.86E-05	4.38E-03	8.92E-01	4.17E-05	3.94E-03	8.91E-01
38	3.89E-05	3.65E-03	9.01E-01	3.69E-05	4.18E-03	8.96E-01	4.10E-05	3.88E-03	8.95E-01
39	3.67E-05	3.44E-03	9.05E-01	3.61E-05	4.09E-03	9.00E-01	3.95E-05	3.74E-03	8.98E-01
40	3.49E-05	3.28E-03	9.08E-01	3.46E-05	3.92E-03	9.04E-01	3.63E-05	3.44E-03	9.02E-01
41	3.44E-05	3.23E-03	9.11E-01	3.37E-05	3.82E-03	9.08E-01	3.55E-05	3.36E-03	9.05E-01
42	3.43E-05	3.22E-03	9.15E-01	3.21E-05	3.64E-03	9.12E-01	3.51E-05	3.32E-03	9.09E-01
43	3.38E-05	3.17E-03	9.18E-01	3.02E-05	3.42E-03	9.15E-01	3.40E-05	3.21E-03	9.12E-01
44	3.18E-05	2.98E-03	9.21E-01	2.91E-05	3.30E-03	9.18E-01	3.26E-05	3.09E-03	9.15E-01
45	3.09E-05	2.90E-03	9.24E-01	2.85E-05	3.23E-03	9.22E-01	3.16E-05	2.99E-03	9.18E-01
46	2.94E-05	2.76E-03	9.26E-01	2.79E-05	3.16E-03	9.25E-01	3.11E-05	2.94E-03	9.21E-01
47	2.91E-05	2.73E-03	9.29E-01	2.70E-05	3.06E-03	9.28E-01	2.94E-05	2.79E-03	9.24E-01
48	2.88E-05	2.70E-03	9.32E-01	2.52E-05	2.86E-03	9.31E-01	2.83E-05	2.68E-03	9.26E-01
49	2.67E-05	2.50E-03	9.34E-01	2.41E-05	2.73E-03	9.33E-01	2.78E-05	2.63E-03	9.29E-01
50	2.61E-05	2.45E-03	9.37E-01	2.37E-05	2.69E-03	9.36E-01	2.67E-05	2.53E-03	9.31E-01
51	2.57E-05	2.41E-03	9.39E-01	2.29E-05	2.60E-03	9.39E-01	2.61E-05	2.47E-03	9.34E-01
52	2.41E-05	2.26E-03	9.41E-01	2.25E-05	2.55E-03	9.41E-01	2.52E-05	2.38E-03	9.36E-01

Table 4.4. Summary of Most Parsimonious Phylogenetic Trees Produced From Exhaustive Searches In PAUP 4.10b With Bootstrap Support For Various Clades.

						Bootstrap Support, %	
Analysis	**Tree Length**	**CI**	**RI**	**RC**	**HI**	***Cercocebus Mandrillus***	***Papio/Lophocebus/Theropithecus***
Sex-Averaged	115	0.6261	0.4416	0.2765	0.3739	80%	90%
Males	79	0.6709	0.5439	0.3649	0.3291	82%	98%
Females	86	0.6279	0.4182	0.2626	0.3721	76%	71%
Combined-Sex	165	0.6485	0.4821	0.3127	0.3515	90%	99%

Notes: Study based on 33 basicranial characters. Characters included: C4, C10-C12, C14-C16, C19, C21, C25-C48. See Tables 2.1-2.2 in Chapter 2 for full description of these characters and character states.

Table 4.5. Basicranial landmarks used in this study.

Landmark	Landmark #	Male/Female
Intersection of the infratemporal crest and sphenosquamosal suture	1	M, F
Most posterior point on zygomatic "U" with temporal	2	M
Most medial point on sphenosquamosal suture	3	M, F
Point on the center of the articular tubercle	4	M
Deepest point within the mandibular fossa	5	M, F
Most inferior point on the postglenoid process	6	M, F
Apex of the petrous part of the temporal bone	7	M, F
Most posterolateral point on the margin of the carotid canal entrance	8	M
Most lateral point on the margin of the stylomastoid foramen	9	M
Most medial point on the jugular fossa	10	M, F
Most lateral point on the jugular fossa	11	M, F
Most inferior point on the external auditory meatus	12	M, F
Point on lateral margin of zygomatic process of the temporal bone at the position of the postglenoid process	13	M, F
Auriculare	14	M, F
Porion	15	M, F
Most lateral point on the mastoid process	16	M, F
Most anterior tip of the petrous process	17	
Suture between temporal and zygomatic bones on inferior aspect of zygomatic process	18	
Parietal notch	19	M, F

Asterion	20	M, F
External occipital protuberance (EOP)	21	
Point on the medial nuchal line halfway between the EOP and foramen magnum	22	
Most posterior point on foramen magnum in the midline (opisthion)	23	F
Most anterior point on foramen magnum in the midline	24	M, F
Most posterolateral point on the occipital condyle	25	M, F
Most posterior point on the occipital condyle along the margin of the foramen magnum	26	M, F
Most lateral point on the occipital condyle (point on the middle of the lateral edge of the condyle)	27	M, F
Most anterior point on the occipital condyle along the margin of the foramen magnum	28	M, F
Point on the center of the occipital condyle (inferior aspect)	29	M
Hypoglossal foramen	30	
Point where the occipital, tympanic temporal, and petrous temporal meet	31	M, F
Most posterior point where the occipital meets the anterior edge of the jugular	32	M, F
Most anterior point where the occipital meets the petrous temporal and sphenoid	33	M, F
Most anterior point on the basioccipital in the midline	34	M, F
Most posterior point (lateral to midline) where the sphenoid meets the vomer	35	
Point on the sphenoid in the midline in contact with the vomer (vomer notch)	36	
Point where medial pterygoid plate meets sphenoid body (branching point)	37	
Point where the apex of the petrous temporal and basisphenoid meet	38	F
Most posterolateral point on the medial pterygoid plate (anteromedial point on foramen ovale)	39	
Point where sphenoid and palatine first meet (superiorly)	40	
Most anterolateral (inferior) point on the medial pterygoid plate where the sphenoid meets the palatine	41	M

Notes: Males/Females column refers to landmarks that are included in the male and female reduced-landmark analyses. M indicates those

landmarks used in male analyses, F indicates those landmarks used in female analyses, and M, F indicates those landmarks used in both male and female analyses.

Chapter 5

Plio-Pleistocene Biogeography of the African Papionins and Its Relationship to Hominin Biogeography

Abstract

Early hominin biogeography is contested and poorly understood. Depending on the analysis, two to seven dispersals between East and South Africa have been hypothesized during the Plio-Pleistocene. To better understand hominin evolutionary history and biogeography, the evolutionary history and biogeography of contemporaneous mammals, especially primates, can be used to test alternative hypotheses.

Papionins have long been argued to be good adaptive and phylogenetic models for human evolution (e.g., Jolly, 1970; 2001). Plio-Pleistocene African papionin monkeys are found at nearly all East and South African hominin sites, and yet similar to the situation with hominins, the evolutionary biogeography of this group remains unresolved. The current study investigates African papionin biogeography by treating biogeography as an unordered cladistic character and biogeographic regions such as South Africa, East Africa, North Africa, Central Africa, and West Africa as character states. The biogeographic character states for each fossil and extant African papionin taxon are then mapped onto a recently hypothesized cladogram derived from craniodental data (see Chapter 3) and dispersal events are then inferred. The hypothesized biogeographic patterns of the African papionins during the Plio-Pleistocene are then compared to contemporaneous hominin biogeographic patterns. Results indicate that papionin dispersal patterns largely mirror those of early hominins and, in at least one case, oppose general mammalian trends as well. Suggestions of unique behavioral adaptations to account for early hominin biogeography and dispersal patterns, therefore, seem unwarranted.

Introduction

An understanding of the common and unique aspects of human evolution is best achieved through comparative methods in which hominin morphology and behavior are compared with the morphological and behavioral adaptations of other organisms. African papionin monkeys have historically been used as important models for early hominin adaptations because of their hypothesized similar ecological niche on the Plio-Pleistocene African savannah or woodland mosaic environments. Fossil African papionins are reported at nearly all early hominin sites and many other non-hominin-bearing sites during the Plio-Pleistocene. Furthermore, as large, omnivorous Old World primates, African papionin monkeys represent a group of mammals that are closely related to early hominins in size and are in many cases found in the same habitats. As large anthropoid primates surviving in similar habitats, African papionins may have also shared similar behavioral adaptations compared to early hominin species (e.g., Jolly, 1970; 2001). Therefore, Plio-Pleistocene African papionin biogeography might offer a particularly informative test of early hominin dispersal patterns and behavioral adaptations (e.g., Strait & Wood, 1999).

In a recent study, Strait & Wood (1999) inferred four to seven hominin dispersal events between East and South Africa during the Plio-Pleistocene. Earlier views hypothesized only two or three dispersal events between these biogeographic regions (e.g., Turner & Wood, 1993; Bromage et al., 1995). Strait & Wood (1999) also observed that *Paranthropus robustus*, and possibly *Homo habilis*, appeared to disperse in the opposite direction of most mammalian taxa. These early hominins were reconstructed as dispersing southward from East to South Africa around 2.5 million years ago (Ma), a period of time during which most other mammalian taxa apparently moved northward from South to East Africa (Vrba, 1992; Turner & Wood, 1993; Strait & Wood, 1999). Strait & Wood (1999) hypothesized that unique behavioral or anatomical adaptations possessed by early hominins were probably responsible for their departure from typical African mammalian dispersal patterns.

This study attempts to use African papionin biogeography to assess patterns of early hominid dispersal during the Plio-Pleistocene. In order to do so, a reasonable

phylogenetic hypothesis of extant and fossil African papionin taxa is needed. Since the fossil record is largely composed of craniodental material, any phylogenetic hypothesis must rely largely on craniodental characters. Some studies have argued that primate phylogenetic hypotheses derived from craniodental data are unreliable; however, more recent studies have demonstrated that primate craniodental data is perfectly suitable for phylogenetic analysis and can produce phylogenetic hypotheses that are congruent with molecular data (Strait and Grine, 2004; Gilbert and Rossie, 2007; see Chapters 2 and 3). In this study, a recently hypothesized cladogram derived from craniodental data (see Chapter 3) is used to infer African papionin biogeographic patterns during the Plio-Pleistocene and then compared to those of hominins and other African mammals. The perceived uniqueness of hominin dispersal events can then be independently tested with an ecologically similar group of anthropoid primates.

Methods

To analyze dispersal patterns, methodology similar to the traditional "progression rule" (Hennig, 1966) was used. The progression rule argues that a cladogram of species-relationships is sufficient by itself to indicate centers of origin and directions of dispersal (Nelson & Platnick, 1981). For this study the most parsimonious trees derived from craniodental data in Chapter 3 were used.

Following the methods of Strait and Wood (1999), biogeographic patterns implied by the cladograms were determined by treating biogeography as an unordered cladistic character with biogeographic regions of Africa corresponding to separate character states. Five regions of Africa were recognized: 0 = East Africa, 1 = North Africa, 2 = South Africa, 3 = Central Africa, and 4 = West Africa. The taxonomy used for the analysis is the same as that presented in Chapter 3 (Table 5.1; see also Chapter 3, Table 3.1 for a list of specimens). The geographic location(s) and temporal duration of each extant and fossil taxon used in the analysis were taken from data reported in the literature as well as my own personal observations (Table 5.1). The time period sampled by the fossil sites encompasses the Late Miocene through the Plio-Pleistocene.

By tracing geographic character state changes using parsimony in the "trace character history" option of Mesquite 1.11 (Maddison and Maddison, 2006), African papionin biogeographic patterns and dispersal events were reconstructed. By using known fossil dates of the taxa analyzed, dispersal dates for particular taxa or a hypothetical ancestor could be inferred. Hypothetical ancestors were located at the internal nodes of the cladogram, and each character state change in the cladogram theoretically represented a dispersal event (Strait & Wood, 1999). Taxa known from multiple geographic regions were assigned multiple character states. These multiple assignments sometimes resulted in equivocal nodes, stems, and branches. *Victoriapithecus* from the Middle Miocene of East Africa, *Parapapio lothagamensis* from the Late Miocene of East Africa, and *Macaca* from the Late Miocene to present of North Africa were considered the outgroups in the analysis; this arrangement set East Africa as the "primitive" geographic character state. For the final character state coding of the biogeographic character by taxon, see Table 5.1.

Results

Figure 5.1 presents the phylogenetic trees, reconstructed biogeographic character state changes, and the estimated timing of dispersal events for each extant and fossil papionin taxon in the analysis. The key to the color-coding system is presented in Table 5.2. According to these phylogenies, the first reconstructed dispersal event involved *Parapapio* or its immediate ancestor (IA), *Theropithecus oswaldi* (or IA), and possibly *Dinopithecus ingens* (or IA). This earliest dispersal event took place between ~5.0 – 3.0 Ma. Grine and Hendey (1981) tentatively assigned isolated teeth from the South African site of Langebaanweg to *Pp. jonesi*, but these specimens are so fragmentary that no definitive assignment is possible. If the generic assignment is proven to be correct, then *Parapapio* or the ancestor of *Parapapio* must have dispersed to South Africa before ~5.0 Ma. Regardless of the assignment of the Langebaanweg specimens, *Parapapio* (or IA) along with *T. o. darti* (or IA) are reconstructed as dispersing to South Africa sometime before ~3.0 Ma when they are first documented at Makapansgat. In addition, *Pp. jonesi* (or IA) is hypothesized to have migrated from South Africa to East Africa ~3.5 Ma when

it tentatively appears at Ahmado and Hadar (Frost, 2001a; Frost and Delson, 2002), making it most likely that the genus arrived in South Africa before ~3.5 Ma.

The next dispersal event from East to South Africa appears to have taken place between 2.5 and 1.5 Ma, and involved *Dinopithecus ingens* (or IA), *Papio hamadryas robinsoni* (or IA), the ancestor of the *Gorgopithecus/P. izodi* clade, and possibly *Papio quadratirostris*. A subset of this event corresponding to the dispersal of other mammalian taxa between East and South Africa between 1.8 and 1.5 Ma may have involved *Papio quadratirostris*. Sometime after ~2.5 Ma, *Papio hamadryas* is also hypothesized to have dispersed to East Africa, Central Africa, and West Africa as well. Given the earliest occurrence of fossil *P. hamadryas* specimens in South Africa (*P. h. robinsoni*), it seems likely that *P. hamadryas* dispersed from South Africa to other biogeographic regions (see Discussion below). Extant *Lophocebus* (or IA) migrated from East to Central Africa during this time period (sometime after 2.5 Ma).

Three other major dispersal events are implied by the cladograms used by this study. Sometime between 3.4 and 2.3 Ma, the ancestor of the *Cercocebus/Procercocebus/Mandrillus* group, and possibly *P. quadratirostris* (as represented in the Humpata Plateau of Angola), are hypothesized to have dispersed from East to West Africa. Furthermore, between 2.3 and 1.5 Ma, there was a dispersal event from West Africa to South Africa involving *Procercocebus* (or IA) and possibly the aforementioned Angolan *P. quadratirostris*, supporting recent suggestions by Gilbert (2007) of a faunal connection between West Africa and South Africa during the Plio-Pleistocene. Finally, between 2.3 Ma and the present, *Cercocebus* (or IA) is hypothesized to have dispersed from West to Central Africa.

Table 5.3 and Figures 5.2-5.3 illustrate the hypothesized dispersal events in this study compared to the hominin dispersal events hypothesized by Strait and Wood (1999), and the non-primate mammalian dispersal events inferred by other authors (e.g., Vrba, 1992; Turner and Wood, 1993). Similar to taxa including *Australopithecus africanus*, African papionin monkeys such as *Parapapio* and *Theropithecus* are hypothesized to have dispersed from East to South Africa between ~3.5 – 3.0 Ma (Fig. 5.2). Similar to early hominins and distinct from most other mammalian taxa, African papionin monkeys are also hypothesized to have dispersed from East to South Africa between 2.5 and 1.5

Ma (Fig. 5.2b). During this time period, most other mammalian taxa appear to have been dispersing northward from South to East Africa (Vrba, 1992; Turner and Wood, 1993; Strait and Wood, 1999). Potentially diverging from the patterns seen among hominins and other mammals, there is weak evidence for an African papionin dispersal event from East to South Africa ~ 1.8 Ma. However, only one taxon is reconstructed as possibly migrating from East to South Africa between 2.3 and 1.5 Ma (*P. quadratirostris*), and given the location of this taxon in Angola, it is probably more likely to have reached South Africa from West Africa. In fact, African papionin monkeys appear to be unique in that they are hypothesized to have dispersed from West to South Africa during this time interval (~2.3 – 1.5 Ma; see Figure 5.3).

Discussion

Similar to early hominin dispersal patterns, the results of this study suggest that the African papionin monkeys did not always follow typical mammalian migration patterns during the Plio-Pleistocene. For every early hominin dispersal event, there is at least one African papionin taxon potentially dispersing in the same direction at the same time. Specifically, while many mammalian taxa appear to migrate north between 2.7 and 2.0 Ma, both papionins and early hominins appear to migrate south from East Africa around ~2.5 Ma (see Fig. 5.1; Fig. 5.2b; Table 5.3). Any behavioral adaptation invoked to explain early hominin biogeographic patterns, then, should also be common to papionin species such as *Dinopithecus ingens*, *Gorgopithecus major, Papio izodi* and *Papio hamadryas*.

If this is, indeed, the case, it may then be asked: What do *Dinopithecus ingens*, *Gorgopithecus major*, *Papio* sp., *Paranthropus robustus* and *Homo habilis* all have in common behaviorally? *Dinopithecus ingens*, *Gorgopithecus major*, and early *Papio* taxa were all probably terrestrial generalists most similar to modern savanna baboons (e.g., Szalay & Delson, 1979; Fleagle, 1999). Did *Paranthropus robustus* or *Homo habilis* engage in similar activities? This remains an open question. I would speculate, however, that primates are a more generalist or eurybiomic group than has previously been studied in a detailed biogeographic context. Other mammalian groups typically cited are usually

characterized by more specialist or stenobiomic species such as bovids and micromammals (e.g., for other mammals see Vrba, 1992; Turner & Wood, 1993; Wesselman, 1985). As a more eurybiomic group, primates may be more geographically flexible and able to tolerate conditions or exploit resources across a larger range of habitats than more stenobiomic mammalian taxa. Detailed biogeographical studies of other eurybiomic and stenobiomic taxa are needed to support this claim.

A unique series of dispersal events is suggested by the analysis here that, to my knowledge, has not been previously documented in studies of mammalian biogeography during the African Plio-Pleistocene. The proposed biogeographic connection between West and South Africa, specifically, appears to be a unique event confined to the *Papio quadratirostris/Cercocebus/Mandrillus* clade. However, the presumed connection between these two geographic regions, as documented by these monkeys, suggests that other African mammals, including hominins, may have shared a similar biogeographic connection as well. Future field work in the Plio-Pleistocene deposits between West and South Africa may confirm or refute this hypothesis. As is always the case with interpreting biogeography from fossils, all assumptions and conclusions are subject to change with the collection of additional fossil specimens or different interpretations of phylogenetic relationships among taxa from different biogeographical regions (Fleagle and Gilbert, 2006).

Previous reconstructions of *Cercocebus* evolutionary biogeography have argued for a dispersal east and west from the low latitudes of Central Africa (Grubb, 1978; 1982; McGraw and Fleagle, 2006). In contrast, the current study suggests that *Cercocebus* or its immediate ancestor arose in West Africa and subsequently migrated to Central Africa. This hypothesis suggests that the populations of extant *Cercocebus torquatus* in West Africa represent the ancestral *Cercocebus* populations (Figure 5.3). This scenario further supports the suggestion that *C. torquatus* retains the primitive craniodental morphology for the genus, a morphology that is also generally similar to that of its sister genus *Procercocebus* (Gilbert, 2007).

Similar to *Cercocebus* and *Procercocebus*, the presence of *P. quadratirostris* fossils in East and southwestern Africa also suggest a wider distribution for the *Papio quadratirostris/Cercocebus/Mandrillus* clade than its current limited distribution in West

and Central Africa. In East Africa, the Shungura Formation Members E-G are often noted as containing forested/woodland components in the environment (e.g., Eck and Jablonski, 1984; 1987; Reed, 1997; Chapter 3), and so the extension or origination of *Cercocebus/Mandrillus* relatives in the same type of environment that the extant taxa occupy is reasonable. In large part, the extended distribution of *Papio quadratirostris* is linked with a Plio-Pleistocene extension of forested environments into East Africa and southern Angola. The available evidence therefore indicates that *Papio quadratirostris/Cercocebus/Mandrillus* has always been a forest-adapted lineage. This probably helped to avoid competition with the expanding savannah-adapted *Papio* lineage (see also Chapter 3). Unlike *Cercocebus*, however, the fact that the earliest and most primitive fossils potentially attributable to *P. quadratirostris* exist in East Africa suggests a potential East African origin and subsequent dispersal into West Africa for mandrills and drills (Figure 5.3).

Another interesting taxon in this analysis is *Papio hamadryas*. The cladogram here suggests that this species or its immediate ancestor originated in East Africa and dispersed to South Africa and elsewhere after ~2.5 Ma. Molecular studies suggest that the extant *P. h. ursinus* population in South Africa is the most genetically diverse, implying that the South African population is the oldest (e.g., Newman et al., 2004). The occurrence of the first recognized subspecies of *P. hamadryas* in the fossil record, *P. h. robinsoni*, in South Africa seems to corroborate this scenario. The simplest explanation is that the immediate ancestor of *P. h. robinsoni* dispersed from East to South African prior to 2.5 Ma, *P. h. robinsoni* then evolved in South Africa, and finally the extant populations of *P. hamadryas* diverged from the early South African *P. h. robinsoni* population.

One final noteworthy observation from this analysis is the implied biogeographic history of the mangabeys: *Lophocebus* appears to have distributed from East Africa into Central Africa, while *Cercocebus* appears to have dispersed from West Africa to Central Africa. This scenario suggests a basic geographic division between these taxa and that subsequent dispersal events resulted in the overlapping geographic ranges seen today.

Conclusions

In light of the biogeographic patterns detected in Plio-Pleistocene African papionins, explanations of early hominin dispersal patterns involving unique behavioral adaptations seem unwarranted. It is more likely that general behavioral adaptations common to multiple primate species at this time allowed for dispersal patterns that were independent of other mammalian groups. It is suggested here that papionin and early hominin species are eurybiomic compared to the mammalian groups (for example bovids and micromammals) typically cited in studies of major dispersal events.

In addition to hypothesized dispersal events between East and South Africa, African papionins appear to document a biogeographic connection between West and South Africa ~2.3 - 1.5 Ma (Figure 5.3). Future paleontological work may help determine if this faunal connection may have involved other mammalian taxa, including hominins. Given the available evidence, it would appear that the *Cercocebus/Mandrillus* lineage is linked with a Plio-Pleistocene extension of forested environments from East Africa to West Africa and southward to Angola and South Africa. The living mangabey taxa, *Cercocebus* and *Lophocebus*, were most likely geographically separated during their origins, with the oldest and most primitive *Cercocebus* populations evolving in West Africa and the oldest and most primitive populations of *Lophocebus* evolving in East Africa. Subsequent to their origins, both mangabey groups dispersed in Central Africa where they now cohabitate in extant forests.

Figure Legends

Figure 5.1. Most parsimonious phylogenetic trees of the extant and fossil Papionini derived from craniodental data. The only difference between the two trees is that a) hypothesizes *P. quadratirostris* populations from the Omo Shungura Formation and Angola are sister taxa, while b) hypothesizes that the USNO specimen and *P. quadratirostris* from Angola are sister taxa. Biogeographic character states are mapped onto the cladograms and color changes along branches indicate changes in character states representing hypothesized dispersal events (see Table 5.1 for assigned states and Table 5.2 for color key). The timing of dispersal events is indicated for selected nodes and branches and derived from the temporal data presented in Table 5.1.

Figure 5.2. Hypothesized mammalian and hominin dispersal events in the African Plio-Pleistocene (see also Table 5.3). **a)** Three main mammalian dispersal events, **1:** ~3.0 Ma, *Australopithecus, Canis*, *Cercopithecoides, Diceros*, *Dinopithecus*, *Metridiochoerus*, *Parapapio, Theropithecus,* **2:** ~ 2.7-2.0 Ma, *Homo*, *Paranthropus*, *Cercopithecoides*, *Connochaetes*, *Parmularius*, *Tragelaphus*, *Antidorcus*, **3:** ~ 1.8 Ma – 1.5 Ma, *Homo*, *Equus*, *Hipparion, Hippotragus*, *Kobus*, *Metridiochoerus*, *Nyctereutes*, *Tragelaphus*; **b)** Four main hominin dispersal events. Dispersals 1 – 3 are the same as those in 2a, however there is an additional event, **4:** ~ 2.5 – 1.7 Ma, potentially involving the hominin taxa *P. robustus* and *H. habilis* (see also Strait and Wood, 1999). This implied dispersal may have included the papionin taxa *Dinopithecus ingens*, the ancestor of *Gorgopithecus major*/*Papio izodi*, *Papio hamadryas robinsoni*, and/or *Papio quadratirostris* as well.

Figure 5.3. Additional papionin dispersal events implied by this study compared to early hominin dispersals (see also Table 5.3). The four main hominin and cercopithecoid dispersal waves are indicated by the faded arrows between East and South Africa (see also Fig. 5.2b). In addition to these 4 events, members of the *Cercocebus/Mandrillus* clade are hypothesized to have dispersed between East and West Africa, West and South Africa, and West and Central Africa. The extant distribution of the *Cercocebus/Mandrillus* clade is illustrated by the shaded regions on the map. Key fossil taxa and their hypothesized dispersal events are also indicated as **5:** ~3.4 – 2.3 Ma, *Papio quadratirostris*, the ancestor of *Mandrillus/Procercocebus/Cercocebus*, **6:** ~2.3 – 1.5 Ma, *Procercocebus*, *Papio quadratirostris,* **7:** ~ 2.3 Ma – present, *Cercocebus*.

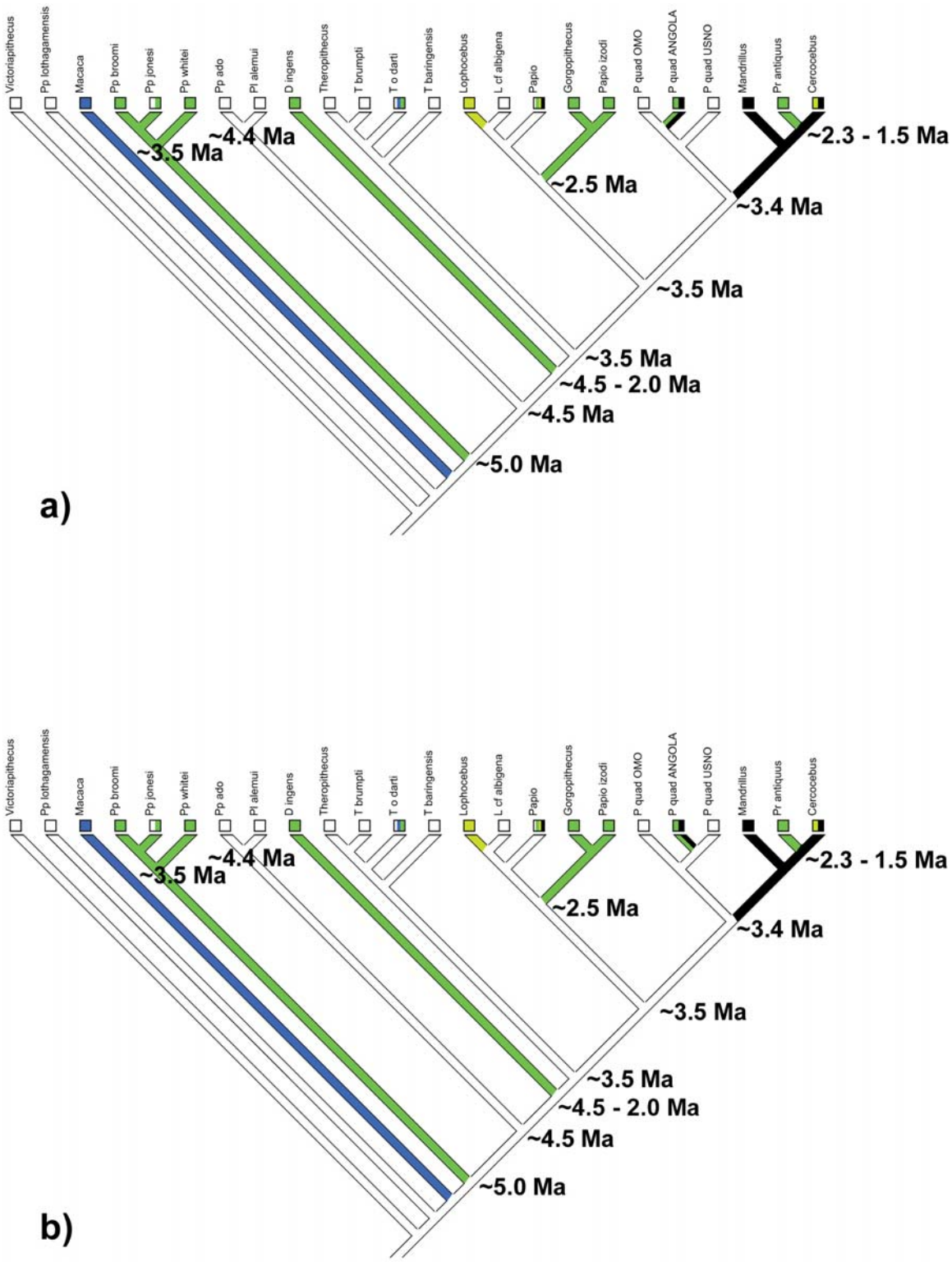
Victoriapithecus
Pp lothagamensis
Macaca
Pp broomi
Pp jonesi
Pp whitei
Pp ado
Pl alemui
D ingens
Theropithecus
T brumpti
T o darti
T baringensis
Lophocebus
L cf albigena
Papio
Gorgopithecus
Papio izodi
P quad OMO
P quad ANGOLA
P quad USNO
Mandrillus
Pr antiquus
Cercocebus
~4.4 Ma
~3.5 Ma
~2.3 - 1.5 Ma
~2.5 Ma
~3.4 Ma
~3.5 Ma
~3.5 Ma
~4.5 - 2.0 Ma
~4.5 Ma
~5.0 Ma
a)
b)

Figure 5.1

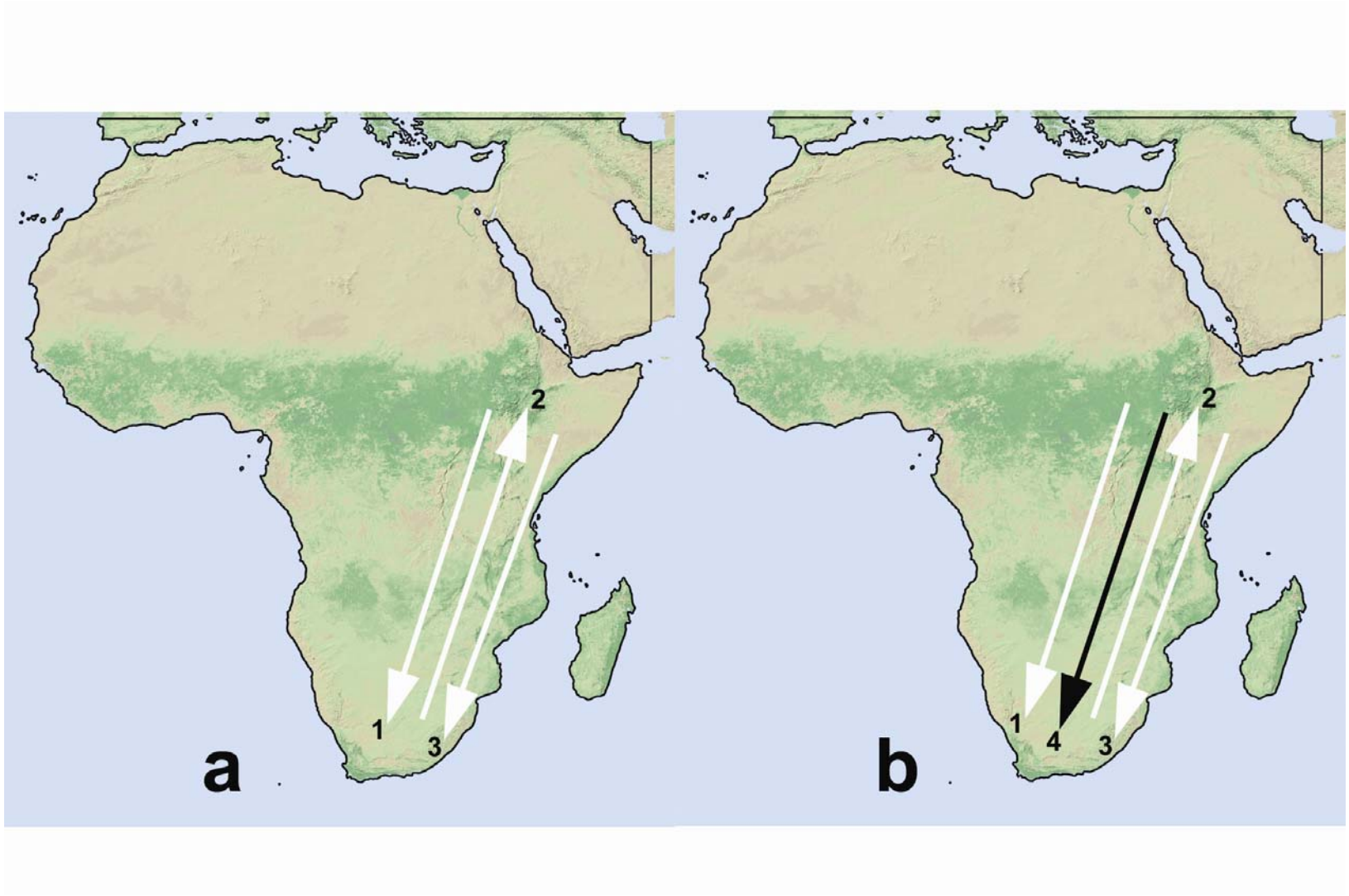

Figure 5.2

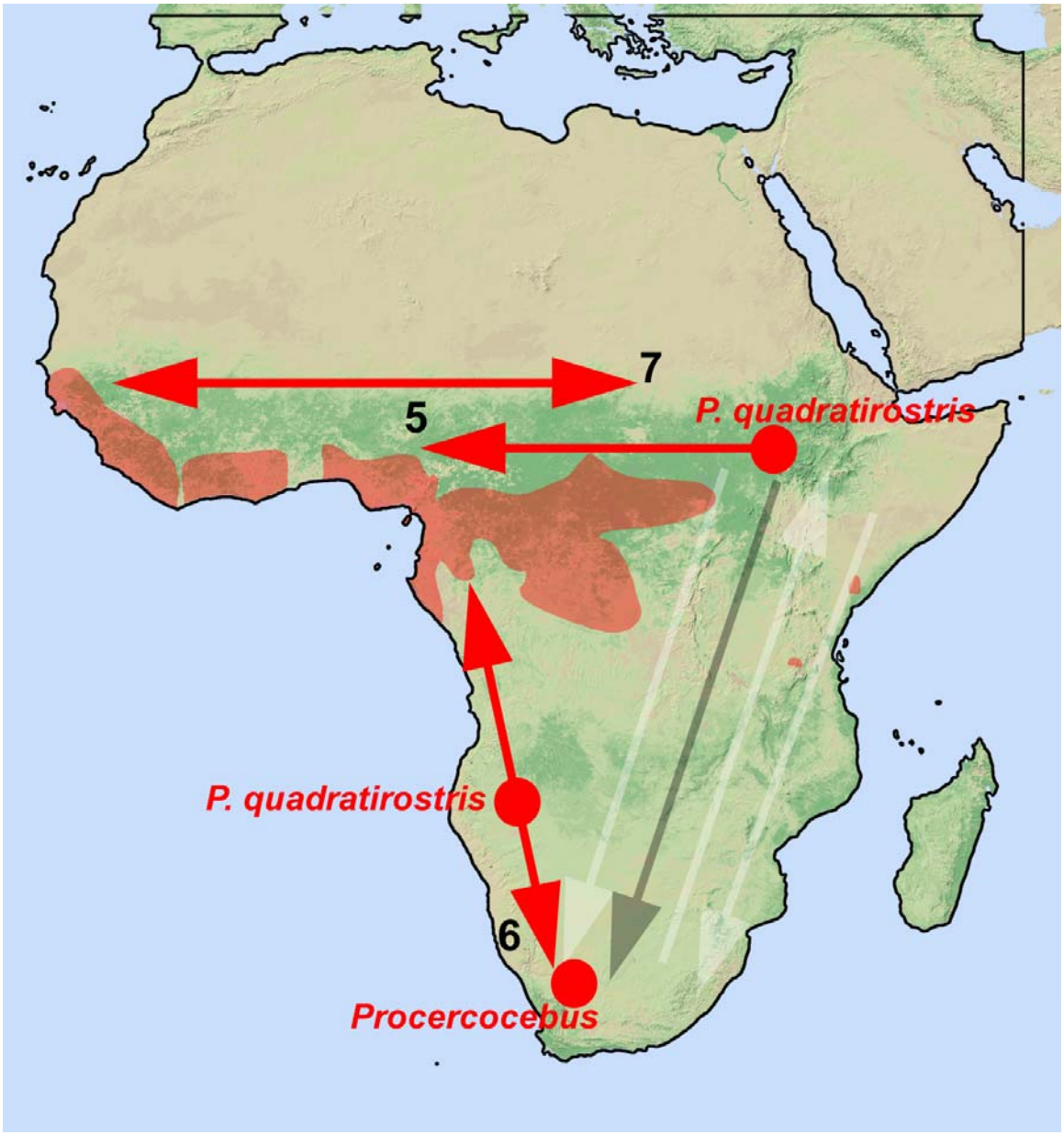

Figure 5.3

Table 5.1. Fossil Taxa/OTUs recognized and used in this study.

Fossil Taxon/OUT	Geographic Location	Character States Assigned	Temporal Duration	Source of Dates
Cercocebus	East Africa, Central Africa	0/3	~2.3 Ma - present	Tosi et al., 2003; this study
Dinopithecus ingens	South Africa	2	~2.0 - 1.5 Ma	Delson et al., 2000
Gorgopithecus major	South Africa	2	~1.8 - 1.5 Ma	Delson et al., 2000
Lophocebus	Central Africa	3	~2.5 Ma - present	Harrison and Harris, 1996; this study
Lophocebus cf. albigena	East Africa	0	~1.88 - 1.39 Ma	Frost, 2001a; Jablonski and Leakey, in press
Macaca	North Africa	1	~ 5.3 Ma - present	Delson et al., 2000
Mandrillus	West Africa	4	~3.6 Ma - present	Tosi et al., 2003; this study
Papio hamadryas	East Africa, South Africa, Central Africa, West Africa	0/2/3/4	~2.5 Ma - present	Delson, 1984; 1988; Delson et al., 2000
Papio izodi	South Africa	2	~2.5 - 1.5 Ma	Delson, 1984; 1988 Delson et al., 2000;
Papio quadratirostris (USNO)	East Africa	0	~3.5 - 3.35 Ma	Delson and Dean, 1993; Eck and Jablonski, 1984;
Papio quadratirostris (Omo)	East Africa	0	~2.5 - 2.3 Ma	Feibel et al., 1989; Delson et al., 2000

Papio quadratirostris (Angola)	South Africa, West Africa	2/4	~1.5 Ma	Delson, 2000; Pickford et al., 1992; 1994
Parapapio ado	East Africa	0	~4.1 - 2.6 Ma	Delson, 1984 Delson et al., 2000;
Parapapio broomi	South Africa	2	~3.0 - 2.5	Delson et al., 2000
Parapapio jonesi	East Africa, South Africa	0/2	~3.5 - 2.5 Ma	Delson et al., 2000 Frost, 2001a; Frost and Delson, 2002; Haile-Selassie et al., 2007
Parapapio lothagamensis	East Africa	0	7.91 - 5.5 Ma	Leakey et al., 1996; Leakey et al., 2003
Parapapio whitei	South Africa	2	~3.0 - 2.5 Ma	Delson et al., 2000
Pliopapio alemui	East Africa	0	4.4 - 4.2 Ma	Frost, 2001a; 2001b
Procercocebus antiquus	South Africa	2	~2.3 - 1.5 Ma	Delson, 1984; 1988; Delson et al., 2000; Gilbert, 2007; this study
Theropithecus baringensis	East Africa	0	~3.2 Ma	Delson and Dean, 1993;
Theropithecus brumpti	East Africa	0	~3.4 - 2.0 Ma	Delson and Dean, 1993; Delson et al., 2000 Leakey, pers. comm.
Theropithecus oswaldi	East Africa, South Africa	0/2	~ 3.4 Ma - 400 Ka	Delson and Dean, 1993; Eck, 1993; Frost, 2001a; 2007
Theropithecus gelada	East Africa	0	~3.4 Ma - present	this study

Victoriapithecus macinnesi	East Africa	0	~19 – 12.5 Ma	Benefit and McCrossin, 2002

Table 5.2. Geographic Region and Color Codes for Biogeographic Character States.

Character State(s) Assigned	Geographic Region	Color Code
0	East Africa	White
1	North Africa	Blue
2	South Africa	Green
3	Central Africa	Yellow
4	West Africa	Black

Notes: Also see Figure 1 and Table 1.

Table 5.3. Implied Biogeographic Dispersal Events During the African Plio-Pleistocene.

	Mammalian Dispersal Event	Hominin Dispersal Event	Papionin Dispersal Event
Dispersal	East Africa to South Africa	East Africa to South Africa	East Africa to South Africa
Time	~3.0 Ma	~3.5 - 3.0 Ma	~5.0 - 3.0 Ma
Period	*Canis*	*A. africanus*	*Parapapio* sp.
Taxa	*Cercopithecoides*		*Theropithecus oswaldi darti*
	Diceros		*Dinopithecus ingens*
	Metridiochoerus		
Dispersal			South Africa to East Africa
Time	X	X	~3.5 Ma
Period			*Parapapio jonesi*
Taxa			
Dispersal			East Africa - West Africa
Time			~3.4 - 2.3 Ma
Period	X	X	*Papio quadratirostris*
Taxa			*Mandrillus*
			Cercocebus

Dispersal	South Africa to East Africa	South Africa to East Africa	South Africa to East Africa
Time	~2.7 - 2.0 Ma	~2.7 - 2.0 Ma	~2.7 - 2.0 Ma
Period	*Cercopithecoides*	*Homo* ancestor	*Papio hamadryas**
Taxa	*Connochaetes*	*H. rudolfensis/H. ergaster*	
	Parmularius	ancestor	
	Tragelaphus	*H. habilis*	
	Antidorcus	*Paranthropus* ancestor	
		P. aethiopicus	
		P. boisei	
Dispersal		East Africa to South Africa	East Africa to South Africa
Time		~2.5 - 1.7 Ma	~2.5 - 1.5 Ma
Period		*P. robustus*	*Dinopithecus ingens*
Taxa	X	*H. habilis*	*Gorgopithecus major*
			Papio izodi
			Papio hamadryas robinsoni
			Papio quadratirostris
Dispersal			West Africa to South Africa
Time	X	X	~2.3-1.5 Ma
Period			*Procercocebus antiquus*
Taxa			*Papio quadratirostris*

Dispersal	East Africa to South Africa	East Africa to South Africa	East Africa to South Africa
Time	~1.8 - 1.5 Ma	~1.8 - 1.5 Ma	~1.8 - 1.5 Ma
Period	*Nyctereutes*	*H. habilis*	*Papio quadratirostris*
Taxa	*Equus*		
	Metridiochoerus		
	Kobus		
	Hippotragus		
	Tragelaphus		
	Hipparion		
Dispersal			East Africa to Central Africa
Time	X	X	~2. 5 - present
Period			*Lophocebus*
Taxa			*Papio hamadryas*
Dispersal			West Africa to Central Africa
Time	X	X	~2.3 - present
Period			*Cercocebus*
Taxa			

Notes: For each hypothesized dispersal event, all possibilities of taxa are listed. Some combinations of taxa or hypothesized dispersal events may be mutually exclusive, but insufficient evidence exists to eliminate certain possibilities at this time. Each taxon listed for

each dispersal event refers to that taxon or its immediate ancestor, unless otherwise noted; * refers to the listed taxon only. Hypothesized mammalian and hominin dispersal events taken from Turner and Wood (1993) and Strait and Wood (1999). See text for details.

Chapter 6

Conclusions

As its title implies, this dissertation set out to illuminate African papionin phylogenetic history and Plio-Pleistocene biogeography. Two different methodologies were employed in various phylogenetic analyses: cladistic analysis of more traditional quantitative and qualitative craniodental characters, and 3-D geometric morphometric multivariate techniques. Both techniques offered interesting results and raise questions and possibilities for future studies. However, in the context of the overall goals of this dissertation, I believe that the cladistic analyses offer a clearer hypothesis of papionin phylogenetic history with much greater degree and rationale of support.

Chapter 2 illustrated that when allometry is controlled for in phylogenetic analysis, trees derived from African papionin craniodental data are congruent with molecular trees. These suggest that two major clades exist among African papionins: *Cercocebus/ Mandrillus* and *Papio/Lophocebus/Theropithecus*. Whereas molecular data cannot resolve the relationships among these last three taxa, the morphological data analyzed here strongly support a sister relationship between *Papio* and *Lophocebus*.

Chapter 2 also highlighted the effect in phylogenetic analysis of dramatically different male and female phenotypes within taxa. When the sexes are analyzed separately, male morphologies perform better. Analysis of male craniodental data results in phylogenetic trees that are shorter and have higher CI, RI, RC and bootstrap values compared to analyses of female data. The superior performance of the male craniodental data set supports previous claims about the higher utility of male morphologies relative to female morphologies among highly sexually dimorphic primates (Fleagle and McGraw, 2002; Gilbert and Rossie, 2007). It is likely that the distinctive traits of papionin males are tied to sexual selection, and these are therefore phylogenetically informative because closely related taxa, by definition, must have shared a common mate recognition system more recently than distantly related taxa (Paterson, 1985; Gilbert and Rossie, 2007). In

addition, sexual selection in the form of mate competition is almost exclusive to males among catarrhine taxa. Similar types and levels of contest competition over females in closely related taxa would help explain the evolution of distinctive and phylogenetically informative male craniodental characters and their potential absence in female craniodental anatomy. In future studies of highly sexually dimorphic primate taxa, males and females should be separated for analysis, and particular attention should be paid to male morphologies, or whichever data set clearly displays higher CI, RI, RC, and bootstrap values.

In contrast to previous studies (e.g., Collard and O'Higgins, 2001; Collard and Wood, 2000; 2001; Singleton, 2002), analyses on highly sexually dimorphic taxa such as the papionin monkeys appear to be in error if they resort to sex-averaging methodology (see also Creel, 1986). Averaging together highly dimorphic phenotypes results in an "imaginary" phenotype, a phenotype that clearly does not exist in the biological world. Using this phenotype in analysis seems much less than optimal. Instead, when both sexes are included in phylogenetic analysis, the results of this dissertation advocates a combined-sex approach, whereby the sexes are coded separately and then male and female matrices are combined for parsimony or similar analysis. There are a number of reasons why combining male and female matrices that have been coded separately is the most appropriate and accurate portrayal of morphological information about a given taxon, particularly a sexually dimorphic one. First, the integrity of the separate male and female morphotypes is retained. Second, male and female morphotypes in sexually dimorphic taxa obviously have a genetic basis, which is included in this approach. Third, increasing the number of characters in phylogenetic analysis has been demonstrated to increase overall phylogenetic accuracy (e.g., Wiens, 2003a; 2003b; 2006). In this case, combining characters that have been scored separately for males and females allows for unique male and female character states that are phylogenetically informative to be sampled together during the analysis. This, in turn, potentially increases the strength and accuracy of the phylogenetic signal.

Chapter 3 combined the lessons learned from Chapter 2 and applies them in a combined-sex analysis of extant and fossil African papionin taxa. Given the high degree of confidence in the morphological data set used in this analysis, the resulting

phylogenetic trees from Chapter 3 represent the most comprehensive and best-supported hypotheses of African papionin phylogenetic history to date. Results suggest that *Parapapio*, *Pliopapio*, and *Dinopithecus* are stem African papionins. Crown Plio-Pleistocene African papionins include *Gorgopithecus*, *Lophocebus*, *Procercocebus*, and *Papio quadratirostris*. Notable phylogenetic conclusions include the following: *Papio quadratirostris*, as defined by Delson and Dean (1993), is reconstructed as the sister taxon to the clade containing *Mandrillus*, *Procercocebus*, and *Cercocebus*. *Theropithecus baringensis* is strongly supported as a primitive member of the genus *Theropithecus*, which is a primitive crown African papionin taxon. *Gorgopithecus* is closely related to *Papio* and *Lophocebus*. The origin of crown African papionins appears to be defined in part by the appearance of definitive maxillary fossae, a feature which may be tied to sexual selection since increased levels of sexual dimorphism also appear in crown papionin taxa. *Papio*, *Lophocebus*, and *Gorgopithecus* are united by the most extensive development of maxillary fossae among African papionin taxa.

The *Mandrillus/Cercocebus/Procercocebus/Papio quadratirostris* clade is defined by features such as upturned nuchal crests (especially in males), widely divergent temporal lines (especially in males), a shift in chewing-muscle forces onto the premolars, and a tendency to enlarge the premolars as an adaptation for hard-object food processing. The adaptive origins of the genus *Theropithecus* appear to be associated with a diet that required a shift in chewing emphasis onto the molar battery. This may, in turn, be associated with the evolution of distinctive *Theropithecus* morphological features such as the anterior union of the temporal lines, reversed Curve of Spee, and increased enamel infoldings.

Chapter 4 presented a 3-D morphometric analysis of the extant papionin basicranium. When the effects of allometry are eliminated by excluding size-correlated PC scores, phylogenetic analyses of papionin basicranial morphology are incongruent with recent molecular and morphological studies of African papionins. The addition of fossil taxa, noted to generally increase phylogenetic accuracy, results in phylogenetic hypotheses inconsistent with recent results of molecular and morphological studies of extant and fossil African papionins. These results suggest that important phylogenetic information is contained within the size-correlated PCs, and this information is being

discarded during the attempt to eliminate the effects of body size. The nature of principal components analyses, in particular the likely combination of many cladistic characters on individual PCs, effectively results in a character reduction that does not allow as fine-grained a phylogenetic analysis as cladistic studies. A direct comparison of the phylogenetic trees produced from 3-D geometric morphometrics of the basicranium to those produced from cladistic analysis of 33 basicranial characters demonstrates that male, female, sex-averaged, and combined-sex cladistic analyses of basicranial morphology, adjusted for allometry using the narrow allometric coding method, recover phylogenetic trees that are congruent with larger morphological data sets (Chapter 2) as well as molecular data (Table 6.1). Furthermore, these trees have high bootstrap support (see Table 6.1). These results support other studies indicating that the basicranium is a highly informative phylogenetic region (Lockwood et al., 2004; Cardini and Elton, 2008), but the shape analyses and the PCs that contain the morphological information are not fine-grained enough, include too much "noise", or do not capture the same details as a given set of cladistic characters. Future 3-D morphometric studies of phylogeny should focus on the development of methodologies to adjust for allometric effects.

Finally, Chapter 5 takes the phylogenetic trees produced in Chapter 3 and uses them to analyze African papionin biogeography compared to hominin taxa in the Plio-Pleistocene. African papionin Plio-Pleistocene dispersal patterns largely mirror those of early hominins and, in at least one case, oppose general mammalian trends as well. These results suggest that papionin and early hominin species are eurybiomic compared to the mammalian groups (e.g., bovids and micromammals) typically cited in major dispersal events.

In addition, African papionin monkeys appear to document a biogeographic connection between West and South Africa ~2.3 - 1.5 Ma. Future paleontological work may help determine if this faunal connection may have involved other mammalian taxa, including hominins. The *Cercocebus/Mandrillus* lineage is linked with a Plio-Pleistocene extension of forested environments from East Africa to West Africa and southward to Angola and South Africa. A basic geographic division since the Plio-Pleistocene appears to have separated the living mangabey taxa, *Cercocebus* and *Lophocebus*, with the oldest and most primitive *Cercocebus* populations having evolved

in West Africa and the oldest and most primitive populations of *Lophocebus* having evolved in East Africa. Subsequent to their origins, both mangabey groups dispersed in Central Africa where they now cohabitate extant forests.

To test the ideas and hypotheses put forth in this study, future work will depend on additional, and better preserved, fossil material (particularly male specimens) and, in some cases, clearer resolution of taxonomy. The taxonomic status of some specimens attributed to various *Parapapio* species, some of the Angolan specimens, some of the later Omo specimens, as well as undescribed Namibian material may alter our understanding of levels of variation in certain taxa, or result in the recognition of new taxa and therefore add new data to future phylogenetic studies. The addition of postcrania in future phylogenetic analyses would also be a potentially useful addition to the study presented here; however, such analyses will depend on associated postcrania being identified and/or assigned in the fossil record (e.g., Ciochon 1993; Elton, 2001). Among extant taxa, the newly named *Rungwecebus kipunji* (Jones et al., 2005; Davenport et al., 2006) will no doubt be important in clarifying the relationships among itself, *Papio*, *Lophocebus*, and *Theropithecus*. While more comprehensive 3-D geometric morphometric studies of the entire cranium may help shed light on phylogenetic relationships among taxa, given the incomplete nature of many fossil crania, the difficulty of adjusting for allometry in multivariate morphometric analyses, and the fact that some phylogenetically informative features are not easily digitized, I believe that comprehensive cladistic analyses of craniodental data will prove more informative in phylogenetic studies, at least in the case of the papionin monkeys.

Table 6.1. Summary of Most Parsimonious Phylogenetic Trees Produced From Exhaustive Searches In PAUP 4.10b With Bootstrap Support For Various Clades.

						Bootstrap Support, %	
Analysis	**Tree Length**	**CI**	**RI**	**RC**	**HI**	***Cercocebus Mandrillus***	***Papio/Lophocebus/Theropithecus***
Sex-Averaged	115	0.6261	0.4416	0.2765	0.3739	80%	90%
Males	79	0.6709	0.5439	0.3649	0.3291	82%	98%
Females	86	0.6279	0.4182	0.2626	0.3721	76%	71%
Combined-Sex	165	0.6485	0.4821	0.3127	0.3515	90%	99%

Notes: Study based on 33 basicranial characters. Characters included: C4, C10-C12, C14-C16, C19, C21, C25-C48. See Tables 1-2 in Chapter 2 for full description of these characters and character states.

References Cited

Barnicot, N.A., Wade, P.T., 1970. Protein structure and the systematics of Old World monkeys. In: Napier, J.R., Napier, P.H. (Eds.), Old World Monkeys: Evolution, Systematics, and Behavior. Academic Press, New York, pp. 29-56.

Barnicot, N.A., Hewett-Emmett, D., 1972. Red cell and serum proteins of *Cercocebus*, *Presbytis, Colobus* and certain other species. Folia Primatol. 17, 442-457.

Benefit, B.R., McCrossin, M.L., 1993. Facial anatomy of *Victoriapithecus* and its relevance to the ancestral cranial morphology of Old World monkeys and apes, Am. J. Phys. Anthropol. 92, pp. 329–370.

Benefit, B.R., McCrossin, M.L., 2002. The Victoriapithecidae, Cercopithecoidea. In: Hartwig, W.C. (Ed.), The Primate Fossil Record. Cambridge University Press, Cambridge, pp. 241-253.

Bloch, J., Silcox, M., 2001. New basicrania of Paleocene-Eocene *Ignacius*: Re-evaluation of the Plesiadapiform-Dermopteran link. Am. J. Phys. Anthropol. 116, 184-198.

Bookstein, F.L., 1989. "Size and shape": A comment on semantics. Syst. Zool. 38, 173-180.

Broom, R., 1940. The South African Pleistocene ceropithecid apes. Ann. Transvaal Mus. 20, 89-100.

Cardini, A., Elton, S. 2008. Does the skull carry a phylogenetic signal? Evolution and modularity in the guenons. Biological Journal of the Linnean Society 93, 813-834.

Chamberlain, A.T., 1987. A taxonomic review and phylogenetic analysis of *Homo habilis*. Ph. D. Dissertation, The University of Liverpool.

Ciochon, R.L., 1993. Evolution of the Cercopithecoid forelimb: phylogenetic and functional implications from morphometric analyses. Univ. Cal. Pub.Geo. Sci. 138, 1-251.

Collard, M., O'Higgins, P., 2001. Ontogeny and homoplasy in the papionin monkey face. Evol. Dev. 3, 322-331.

Collard, M., Wood, B.A., 2000. How reliable are human phylogenetic hypotheses? Proc. Natl. Acad. Sci. U.S.A. 97, 5003-5006.

Collard, M., Wood, B.A., 2001. Homoplasy and the early hominid masticatory system: inferences from analyses of extant hominoids and papionins. J. Hum. Evol. 41, 167-194.

Creel, N., 1986. Size and phylogeny in hominoid primates. Syst. Zool. 35: 81-99.

Cronin, J.E., Sarich, V.M., 1976. Molecular evidence for dual origin of mangabeys among Old World monkeys. Nature 260, 700-702.

Darroch, J.N., Mosimann, J.E., 1985. Canonical and principal components of shape. Biometrika 72, 241-252.

Davenport, T.R.B., Stanley, W.T., Sargis, E.J., De Luca, D.W., Mpunga, N.E., Machaga, S.J., Olson, L.E., 2006. A new genus of African monkey, *Rungwecebus*: morphology, ecology, and molecular phylogenetics. Science 312, 1378-1381.

Dechow, P.C., Singer, R., 1984. Additional fossil *Theropithecus* from Hopefield, South Africa: a comparison with other African sites and a reevaluation of its taxonomic status. Am. J. Phys. Anthropol. 63, 405-435.

Dean, M.C., Wood, B.A., 1981. Metrical analysis of the basicranium of extant hominoids and *Australopithecus*. Am. J. Phys. Anthropol. 54**,** 63–71.

Dean, M.C., Wood, B.A., 1982. Basicranial anatomy of Plio-Pleistocene hominids from East and South Africa. Am. J. Phys. Anthropol. 59, 157–174.

Delson, E., 1980. Fossil macaques, phyletic relationships and a scenario of deployment. In: Lindburg, D. G. (Ed.), Macaques: Studies in Ecology, Behavior and Evolution. Van Nostrand, New York, pp. 10-30.

Delson, E., 1984. Cercopithecid biochronology of the African Plio-Pleistocene: Correlation among eastern and southern hominid-bearing localities. Cour. Forsch. Inst. Senckenberg 89, 199-218.

Delson, E., 1988. Chronology of South African Australopith Site Units. In: Grine, F.E. (Ed.), Evolutionary History of the "Robust" Australopithecines. Aldine, New York, pp. 317-324.

Delson, E., 1993. *Theropithecus* fossils from Africa and India and the taxonomy of the genus. In: Jablonski, N.G. (Ed.), *Theropithecus*: The Rise and Fall of a Primate Genus. Cambridge University Press, Cambridge, pp. 157-189.

Delson, E ., Dean, D., 1993. Are *Papio baringensis* R. Leakey, 1969, and *P. quadratirostris* Iwamoto, 1982, species of *Papio* or *Theropithecus*? In: Jablonski, N.G. (Ed.), Theropithecus: The Rise and Fall of a Primate Genus. Cambridge University Press, Cambridge, pp. 157-189.

Delson, E., Terranova, C.J., Jungers, W.L., Sargis, E.J., Jablonski, N.G., Dechow, P.C., 2000a. Body mass in Cercopithecidae (Primates, Mammalia): estimation and scaling in extinct and extant taxa. Anthropol. Pap. Am. Mus. 83, 1-159.

Delson, E., Tattersall, I., van Couvering, J.A., Brooks, A.S. (Eds.), 2000b. Encyclopedia of Human Evolution and Prehistory. 2nd ed. Garland Publishing Inc., New York.

Disotell, T.R., 1994. Generic level relationships of the Papionini (Cercopithecoidea). Am J. Phys. Anthropol. 94, 47-57.

Disotell, T.R., 2000. Molecular systematics of the Cercopithecidae. In: Whitehead, P.F., Jolly, C.J. (Eds.): Old World Monkeys. Cambridge University Press, Cambridge, pp. 29-56.

Disotell, T.R., Raaum, R.L., 2002. Molecular timescale and gene tree incongruence in the guenons. In: eds. Glenn, M.E., Cords, M. (Eds.), The Guenons: Diversity and Adaptation in African Monkeys. Kluwer Academic/Plenum Publishers, New York, pp. 27-36.

Disotell, T.R., Honeycutt, R.L., Ruvulo, M., 1992. Mitochondrial DNA phylogeny of the Old-World monkey tribe Papionini. Mol. Biol. Evol. 9, 1-13.

Donoghue, M.J., Doyle, J.A., Gauthier, J., Kluge, A.G., Rowe, T. 1989. The Importance of Fossils in Phylogeny Reconstruction. Ann. Rev. Ecol. Syst. 20, 431-460.

Eck, G.G., Jablonski, N.G., 1984. A reassessment of the taxonomic status and phyletic relationships of *Papio baringensis* and *Papio quadratirostris.* Am. J. Phys. Anthropol. 65, 109-134.

Eck, G.G., Jablonski, N.G., 1987. The skull of *Theropithecus brumpti* compared with those of other species of the genus *Theropithecus*. In: Coppens, Y., Howell, F.C. (Eds.), Les Faunes Plio-Pleistocenes de la Basse Vallee de l'Omo (Ethiopie), Tome 3, Cercopithecidae de la Formation Shungura. Cahiers de Paleontologie, Editions du Centre National de la Recherche Scientifique, pp. 11-122.

Eck, G.G., 1993. *Theropithecus darti* from the Hadar Formation, Ethiopia. In: Jablonski, N.G. (Ed.), *Theropithecus*: The Rise and Fall of a Primate Genus. Cambridge University Press, Cambridge, pp.15-83.

Elton, S., 2001. Locomotor and habitat classification of cercopithecoid postcranial material from Sterkfontein Member 4, Bolt's Farm and Swartkrans Members 1 and 2, South Africa. Palaeont. Afr. 37, 115-126.

Feibel, C.S., Brown, F.H., McDougall, I., 1989. Stratigraphic context of fossil hominids from the Omo group deposits, northern Turkana Basin, Kenya and Ethiopia. Am. J. Phys. Anthropol. 78, 595-622.

Fleagle, J.G., 1999. Primate Adaptation and Evolution. Academic Press, New York.

Fleagle, J.G., McGraw, W.S., 1999. Skeletal and dental morphology supports diphyletic origin of baboons and mandrills. Proc. Natl. Acad. Sci. U.S.A. 96, 1157-1161.

Fleagle, J.G., McGraw, W.S., 2002. Skeletal and dental morphology of African papionins: unmasking a cryptic clade. J. Hum. Evol. 42, 267-292.

Fleagle, J.G., Gilbert, C.C., 2006. Biogeography and the primate fossil record: the role of tectonics, climate, and chance. In: Lehman, S., Fleagle, J.G. (Eds.), Primate Biogeography: Progress and Prospects. Springer, New York, pp. 375-418.

Fooden, J., 1975. Taxonomy and evolution of liontail and pigtail macaques (Primates: Cercopithecidae). Field. Zool. 67, 1–169.

Fourie, N.H., Lee-Thorp, J.A., Ackermann, R.R., 2008. Biogeochemical and craniometric investigation of dietary ecology, niche separation, and taxonomy of Plio-Pleistocene cercopithecoids from the Makapansgat Limeworks. Am. J. Phys. Anthropol.

Freedman, L., 1957. The fossil Cercopithecoidea of South Africa. Ann. Transvaal Mus. 23, 121-262.

Freedman, L., 1961. New cercopithecoids fossils, including a new species, from Taung, Cape Province, South Africa. Ann. S. Afr. Mus. 46, 1-14.

Freedman, L., 1962. Growth of muzzle length relative to calvaria length in *Papio*. Growth 26, 117-128.

Freedman, L., 1965. Fossil and subfossil primates from the limestone deposits at Taung, Bolt's Farm, and Witkrans, South Africa. Palaeont. Afr. 9, 19-48.

Freedman, L., Stenhouse, N.S., 1972. The *Parapapio* species of Sterkfontein, Transvaal, South Africa. Palaeont. Afr. 14, 93-111.

Frost, S.R., 2001a. Fossil Cercopithecidae of the Afar Depression, Ethiopia: species systematics and comparison to the Turkana Basin. Ph. D. Dissertation. The City University of New York, New York.

Frost, S.R., 2001b. New Early Pliocene Cercopithecidae (Mammalia: Primates) from Aramis, Middle Awash Valley, Ethiopia. Am. Mus. Nov. 3350, 1-36.

Frost, S.R., 2007. Fossil Cercopithecidae from the Middle Pleistocene Dawaitoli Formation, Middle Awash Valley, Afar Region, Ethiopia. Am. J. Phys. Anthropol. 134, 460-471.

Frost, S.R., and Delson, E., 2002. Fossil Cercopithecidae from the Hadar Formation and surrounding areas of the Afar Depression, Ethiopia. J. Hum. Evol. 43, 687-748.

Frost, S.R., Marcus, L., Bookstein, F., Reddy, C., Delson, E., 2003. Cranial allometry, phylogeography, and systematics of large-bodied papionins (Primates: Cercopithecinae) inferred from geometric morphometric analysis of landmark data. Anat. Rec. 275A, 1048-1072.

Gaffney, E.S., 1979. An introduction to the logic of phylogeny reconstruction. In: Cracraft, J., Eldredge, N. (Eds.), Phylogenetic Anlysis and Paleontology. Columbia University Press, New York, pp. 79-111.

Gatesy, J., O'Leary, M.A., 2001. Deciphering whale origins with molecules and fossils. Trends Ecol. Evol. 16, 562-570.

Gatesy, J., Amato, G., Norell, M., DeSalle, R., Hayashi, C., 2003. Combined support for wholesale taxic atavism in Gavailine Crocodylians. Syst. Biol. 52, 403-422.

Gauthier, J., Kluge, A., Row, T., 1988. Amniote phylogeny and the importance of fossils. Cladistics 4, 105-209.

Gear, J.H.S., 1926. A preliminary account of the baboon remains from Taungs. S. Afr. J. Sci. 23, 731-747.

Gilbert, C.C., 2007a. Craniomandibular morphology supporting the diphyletic origin of mangabeys and a new genus of the *Cercocebus/Mandrillus* clade, *Procercocebus*. J. Hum. Evol. 53, 69-102.

Gilbert, C.C., 2007b. Identification and description of the first *Theropithecus* (Primates: Cercopithecidae) material from Bolt's Farm, South Africa. Ann. Transvaal Mus. 44, 1-10.

Gilbert, C.C., Rossie, J.B., 2007. Congruence of molecules and morphology using a narrow allometric approach. Proc. Natl. Acad. Sci. U.S.A. 104, 11910-11914.

Grine, F.E., Hendey, Q.B., 1981. Earliest primate remains from South Africa. S. Afr. J. Sci. 77, 374-376.

Groves, C.P., 1978. Phylogenetic and population systematics of the mangabeys (Primates: Cercopithecoidea). Primates 19, 1-34.

Groves, C.P., 1989. A Theory of Human and Primate Evolution. Oxford University Press, Oxford.

Groves, C.P., 2000. The phylogeny of the Cercopithecoidea. In: Whitehead, P.F., Jolly, C.J. (Eds.), Old World Monkeys. Cambridge University Press, Cambridge, pp. 180-213.

Groves, C.P., 2001. Primate Taxonomy. Smithsonian Institution Press, Washington.

Grubb, P., 1978. Patterns of speciation in African mammals. Bull. Carnegie Mus. Nat. Hist. 6, 152-167.

Grubb, P., 1982. Refuges and dispersal in the speciation of African mammals. In: Prance, G.T. (Ed.), Biological Diversification in the Tropics. Columbia University Press, New York, pp. 537-553.

Haile-Selassie, Y., Deino, A., Saylor, B., Umer, M., Latimer, B., 2007. Preliminary geology and paleontology of new hominid-bearing localities in the central Afar region of Ethiopia. Anthropol. Sci. 115, 215-222.

Harris, E.E., 2000. Molecular systematics of the Old World monkey tribe Papionini: analysis of the total available genetic sequences. J. Hum. Evol. 38, 235-256.

Harris, E.E., Disotell, T.R., 1998. Nuclear gene trees and the phylogenetic relationships of the mangabeys (Primates: Papionini). Mol. Biol. Evol. 15, 892-900.

Harrison, T., Harris, E.E., 1996. Plio-Pleistocene cercopithecids from Kanam East, western Kenya. J. Hum. Evol. 30, 539-561.

Harvati, K., 2001. The Neanderthal problem: 3-D geometric morphometric models of cranial shape variation within and among species. Ph.D. Dissertation. The City University of New York.

Harvati, K., 2003. Quantitative analysis of Neanderthal temporal bone morphology using three-dimensional geometric morphometrics. Am. J. Phys. Anthropol. 120, 323-338.

Heaton, J.L., 2006. Taxonomy of the Sterkfontein fossil Cercopithecinae: the Papionini of Members 2 and 4 (Gauteng, South Africa). Ph. D. Dissertation, Indiana University, Bloomington.

Hennig, W., 1966. Phylogenetic Systematics. D. Dwight Davis and Rainer Zangerl, tr. University of Illinois Press, Urbana.

Hewett-Emmett, D., Cook, C.N., Barnicot, M.A., 1976. Old World monkey hemoglobins: Deciphering phylogeny from complex patterns of molecular evolution. In: Goodman, M., Tashian, R.E., Tashian, J.H., (Eds.): Molecular Anthropology: Genes and Proteins in the Evolutionary Ascent of the Primates. Plenum Press, New York, pp. 257-275.

Jablonski, N.G., 1994. New fossil cercopithecid remains from the Humpata Plateau, southern Angola. Am. J. Phys. Anthropol. 94, 435-464.

Jablonski, N.G., 2002. Fossil Old World monkeys: the late Neogene radiation. In: Hartwig, W.C. (Ed.), The Primate Fossil Record. Cambridge University Pres, Cambridge, pp. 255-299.

Jablonski, N.G., Leakey, M.G. (Eds.), in press. Koobi Fora Research Project, vol. 6: Monkeys. Memoir of the California Academy of Sciences, San Francisco.

Jolly, C.J., 1970. The seed-eaters: a new model of hominid differentiation based on a baboon analogy. Man 5, 5-26.

Jolly, C.J., 1972. The classification and natural history of *Theropithecus* (*Simopithecus*) (Andrews, 1916), baboons of the African Plio-Pleistocene. Bull. Brit. Mus. (Nat. Hist.) Geology 22, 1-122.

Jolly, C.J., 2001. A proper study for mankind: Analogies from the papionin monkeys and their implications for human evolution. Yearb. Phys. Anthropol. 44, 177-204.

Jones, T., Ehardt, C.L., Butynski, T.M., Davenport, T.R.B., Mpunga, N.E., Machaga, S.J., De Luca, D.W., 2005. The highland mangabey *Lophocebus kipunji*: a new species of African monkey. Science 308, 1161-1164.

Jungers, W.L., Falsetti, A.B., Wall, C.E., 1995. Shape, relative size, and size-adjustments in morphometrics. Yearb. Phys. Anthropol. 38, 137-161.

Kay, R.F., Ross, C.F., Williams, B.A., 1997. Anthropoid Origins. Science 275, 797-804.

Kay, R.F., Simons, E., Ross, J.L., 2008. The Basicranial Anatomy of African Eocene/Oligocene Anthropoids. Are There Any Clues for Platyrrhine Origins? In: Fleagle, J.G., Gilbert, C.C. (Eds.), Elwyn Simons: A Search for Origins. Springer, New York, pp. 125-158.

Leakey, M.G., 1993. Evolution of *Theropithecus* in the Turkana Basin. In: Jablonski, N.G. (Ed.), *Theropithecus*: The Rise and Fall of a Primate Genus. Cambridge University Press, Cambridge, pp. 85-123.

Leakey, M.G., Delson, E., 1987. Fossil Cercopithecidae from the Laetoli beds. In: ed. Leakey, M.D., Harris, J.M. (Eds.), *Laetoli: A Pliocene site in Northern Tanzania*. Clarendon Press, Oxford, pp. 91-107.

Leakey, M.G., Leakey, R.E.F., 1976. Further Cercopithecinae (Mammalia, Primates) from the Plio/Pleistocene of East Africa. In: Savage, R.J.G., Coryndon, S.C.

(Eds.), Fossil Vertebrates of Africa, vol. 4. Academic Press, London, pp. 121-146.

Leakey, M.G., Feibel, C.S., Bernor, R.L., Harris, J.M., Cerling, T.E., Stewart, K.M, Storrs, G.W., Walker, A., Werdelin, L., Winkler, A.J., 1996. Lothagam: a record of faunal change in the Late Miocene of East Africa. J. Vert. Paleontol. 16: 556-570.

Leakey, M.G., Teaford, M.F., Ward, C.V., 2003. Cercopithecidae from Lothagam. In: Leakey, M.G., Harris, J.M. (Eds.), Lothagam: The Dawn of Humanity in Eastern Africa. Columbia University Press, New York, pp. 201-248.

Leakey, R.E.F., 1969. New Cercopithecidae from the Chemeron Beds of Lake Baringo, Kenya. Fossil Vertebrates of Africa 1, 53-69.

Leigh, S.R., Shah, N.S., Buchanan, L.S., 2003. Ontogeny and phylogeny in papionin primates. J. Hum. Evol. 45, 285-316.

Lockwood, C.A., Fleagle, J.G., 1999. The Recognition and evaluation of homoplasy in primate and human Evolution. Yearb. Phys. Anthropol. 42, 189-232.

Lockwood, C.A., Kimbel, W.H., Lynch, J.M., 2004. Morphometrics and hominoid phylogeny: support for a chimpanzee-human clade and differentiation among great ape subspecies. Proc. Natl. Acad. Sci. U.S.A. 101, 4356-4360.

Lycett, S.J., Collard, M., 2005. Do homoiologies impede phylogenetic analyses of the fossil hominids? An assessment based on extant papionin craniodental morphology. J. Hum. Evol. 49, 618-642.

MacPhee, R.D.E., Cartmill, M., 1986. Basicranial structures and primate systematics. In: Swindler, D.R., Erwin, J. (Eds.), Comparative Primate Biology, Vol. 1: Systematics, Evolution, and Anatomy. Alan R. Liss, New York, pp. 219-275

Maddison, W. P., Maddison, D.R., 2006. Mesquite: a modular system for evolutionary analysis. Version 1.11 http://mesquiteproject.org

Maier, W., 1971. Two new skulls of *Parapapio antiquus* from Taung and a suggested phylogenetic arrangement of the genus *Parapapio*. Ann. S. Afr. Mus. 59, 1-16.

McGraw, W.S., Fleagle, J.G., 2006. Biogeography and evolution of the *Cercocebus-Mandrillus* clade: evidence from the face. In: Lehman, S., Fleagle, J.G. (Eds.), Primate Biogeography: Progress and Prospects. Springer, New York, pp. 201-224.

Morales, J.C., Melnick, D.J., 1998. Phylogenetic relationships of the macaques (Cercopithecidae: *Macaca*), as revealed by high resolution restriction site mapping of mitochondrial ribosomal genes. J. Hum. Evol. 34, 1-23.

Mosimann, J.E., 1970. Size allometry: size and shape variables with characterizations of the lognormal and generalized gamma distributions. J. Am. Stat. Assoc. 56, 930-945.

Mosimann, J.E., James, F.C., 1979. New statistical methods for allometry with application to Florida red-winged blackbirds. Evolution 33, 444-459.

Nadal-Roberts, M., Collard, M., 2005. Impact of methodological choices on assessments of the reliability of fossil primate phylogenetic hypotheses. Folia Primatol. 76, 207-221.

Napier, P.H., 1981. Catalogue of primates in the British Museum (Natural History) and elsewhere in the British Isles. Part II: family Cercopithecidae, subfamily Cercopithecinae. British Museum (Natural History), London.

Napier, P.H., 1985. Catalogue of primates in the British Museum (Natural History) and elsewhere in the British Isles. Part III: family Cercopithecidae, subfamily Colobinae. British Museum (Natural History), London.

Nelson, G., Platnick, N., 1981. Systematics and Biogeography: Cladistics and Vicariance. Columbia University Press, New York.

Newman, T.K., Jolly, C.J., Rogers, J., 2004. Mitochondrial phylogeny and systematics of baboons (*Papio*). Am. J. Phys. Anthropol. 124, 17-27.

O'Higgins, P., Jones, N., 1998. Facial growth in *Cercocebus torquatus*: an application of three-dimensional geometric morphometric techniques to the study of morphological variation. Journal of Anatomy 193, 251-272.

Paterson, H.E.H., 1985. The recognition concept of species. In: Vrba, E.S. (Ed.), Species and Speciation. Transvaal Museum Monograph 4, 21-29.

Pickford, M., Mein, P., Senut, B., 1992. Primate bearing Plio-Pleistocene cave deposits of Humpata, Southern Angola. Hum. Evol. 7, 17-33.

Pickford, M., Mein, P., Senut, B., 1994. Fossiliferous Neogene karst fillings in Angola, Botswana and Namibia. S. Afr. J. Sci. 90, 227-230.

Rae, T.C., 2008. Paranasal pheumatization in extant and fossil Cercopithecoidea. J. Hum. Evol. 54, 279-286.

Rae, T.C., Koppe, T., 2003. The term "lateral recess" and craniofacial pneumatization in Old World monkeys (Mammalia, Primates, Cercopithedoidea). J. Morphol. 258, 193-199.

Reed, K.E., 1997. Early hominid evolution and ecological change through the African Plio-Pleistocene. J. Hum. Evol. 32, 289-322

Rohlf, F.J., Sokal, R.R., 1995. Statistical Tables, Third Edition. W.H. Freeman and Co., New York.

Ross, C.F., 1994. The craniofacial evidence for anthropoid and tarsier relationships. In: Fleagle, J.G., Kay, R.F. (Eds.), Anthropoid Origins. Plenum Press, New York, pp. 469-548.

Ross, C.F., Williams, B.A., Kay, R.F., 1998. Phylogenetic analysis of anthropoid relationships. J. Hum. Evol. 35, 221-306.

Ross, C.F., Covert, H.H., 2000. The petrosal of *Omomys carteri* and the evolution of the primate basicranium. J. Hum. Evol. 39, 225-231.

Schrenk, F., Juwayeyi, Y.M., 1995. Paleobiogeography of the Malawi Rift: Age and vertebrate paleontology of the Chiwondo Beds, northern Malawi. J. Hum. Evol. 28, 37-57.

Scotland, R.W., Olmstead, R.G., Bennett, J.R., 2003. Phylogeny reconstruction: The role of morphology. Syst. Biol. 52, 539 – 548.

Singleton, M., 2002. Patterns of cranial shape variation in the Papionini (Primates: Cercopithecinae). J. Hum. Evol. 42, 547-578.

Smith, N.D., Turner, A.H., 2004. Morphology's role in phylogeny reconstruction: perspectives from paleontology. Syst. Biol. 54, 166-173.

Smith, R.J., 1984. Allometric scaling in comparative biology: problems of concept and method. Am. J. Physiol. 246, R152-R160.

Smith, R.J., Jungers, W.L., 1997. Body mass in comparative primatology. J. Hum. Evol. 32, 523-559.

Springer, M.S., Teeling, E.C., Madsen, O., Stanhope, M.J., de Jong, W.W., 2001. Integrated fossil and molecular data reconstruct bat echolocation. Proc. Natl. Acad. Sci. U.S.A. 98, 6241-6246.

Strait, D.S., 2001. Integration, phylogeny, and the hominid cranial base. Am, J.Phys. Anthropol. 114, 273-297.

Strait, D.S., Grine, F.E., Moniz, M.A., 1997. A reappraisal of early hominid phylogeny. J. Hum. Evol. 32, 17-82.

Strait, D.S., Grine, F.E., 2004. Inferring hominoid and early hominid phylogeny using craniodental characters: the role of fossil taxa. J. Hum. Evol. 47, 399-452.

Strait, D.S., Wood, B.A., 1999. Early hominid biogeography. Proc. Natl. Acad. Sci. U.S.A. 96, 9196 –9200.

Strasser, E., Delson, E., 1987. Cladistic analysis of cercopithecid relationships. J. Hum. Evol. 16, 81-99.

Swindler, D.R. 2002. Primate Dentition: An Introduction to the Teeth of Non-Human Primates. Cambrige University Press, Cambridge.

Swofford, D.L., 2001. PAUP 4.0b10. Sinauer Associates, Sunderland MA.

Szalay, F.S., Delson, E., 1979. Evolutionary History of the Primates. Academic Press, New York.

Thiele, K., 1993. The holy grail of the perfect character: the cladistic treatment of. morphometric data. Cladistics 9, 275-304.

Tosi, A.J., Morales, J.C., Melnick, D.J., 1999. Y-chromosome phylogeny of the macaques (Cercopithecidae: *Macaca*). Am. J. Phys. Anthropol. 28(Suppl.):266.

Tosi, A.J., Disotell, T.R., Morales, J.C., Melnick, D.J., 2003. Cercopithecine Y-chromosome data provide a test of competing morphological evolutionary hypotheses. Mol. Phylogenet. Evol. 27, 510-521.

Tosi, A.J., Detwiler, K.M, Disotell, T.R., 2003. X-chromosomal window into the evolutionary history of the guenons (Primates: Cercopithecini). Mol. Phylogenet. Evol. 36, 58-66.

Trevor-Jones, R., 1972. The ethmoid, the vomer and the palatine bones from the baboon skull. S. Afr. J. Sci., 68, 156–161.

Turner, A., Wood, B., 1993. Taxonomic and geographic diversity in robust australopithecines and other Plio-Pleistocene larger mammals. J. Hum. Evol. 24: 147-168.

Vrba, E.S., 1992. Mammals as a key to evolutionary theory. J. Mammol. 73: 1-28.

Wesselman, H.B., 1985. Fossil micromammals as indicators of climatic change about 2.4 Myr ago in the Omo valley, Ethiopia. S. Afr. J. Sci. 81: 260-261.

Wheeler, W.C., 1992. Extinction, sampling, and molecular phylogenetics. In: Novacek, M.J., Wheeler, Q.D. (Eds.), *Extinction & Phylogeny*. Columbia Press, New York, pp. 205-215.

Wiens, J.J., 2003a. Incomplete taxa, incomplete characters, and phylogenetic accuracy: is there a missing data problem? J. Vertebr. Paleontol. 23, 297-310.

Wiens, J.J., 2003b. Missing data, incomplete taxa, and phylogenetic accuracy. Syst. Biol. 52, 528-538.

Wiens, J.J., 2004. The role of morphological data in phylogeny reconstruction. Syst. Biol. 53, 653-661.

Wiens, J.J., 2006. Missing data and the design of phylogenetic analyses. J. Biomed. Inform. 39, 34-42.

Wiens, JJ., Fetzner, J.W., Parkinson, C.L., Reeder, T.W., 2005. Hylid frog phylogeny and sampling strategies for speciose clades. Syst. Biol. 54, 719-748.

Wood, B.A., 1991. Koobi Fora Research Project, Volume 4: Hominid Cranial Remains. Clarendon Press, Oxford.

Zwickl, D.J., Hillis, D.M., 2002. Increased taxon sampling greatly reduces phylogenetic error. Syst. Biol. 51, 588-598.